



Chen, Z. Q., Yang, H., Luo, M., Benton, M. J., Kaiho, K., Zhao, L., Huang, Y., Zhang, K., Fang, Y., Jiang, H., Qiu, H., Li, Y., Tu, C., Shi, L., Zhang, L., Feng, X., & Chen, L. (2015). Complete biotic and sedimentary records of the Permian-Triassic transition from Meishan section, South China: Ecologically assessing mass extinction and its aftermath. *Earth-Science Reviews*, 149, 67-107.
<https://doi.org/10.1016/j.earscirev.2014.10.005>

Peer reviewed version

License (if available):
CC BY-NC-ND

Link to published version (if available):
[10.1016/j.earscirev.2014.10.005](https://doi.org/10.1016/j.earscirev.2014.10.005)

[Link to publication record in Explore Bristol Research](#)
PDF-document

This is the accepted author manuscript (AAM). The final published version (version of record) is available online via Elsevier at <http://dx.doi.org/10.1016/j.earscirev.2014.10.005>. Please refer to any applicable terms of use of the publisher.

University of Bristol - Explore Bristol Research

General rights

This document is made available in accordance with publisher policies. Please cite only the published version using the reference above. Full terms of use are available:
<http://www.bristol.ac.uk/red/research-policy/pure/user-guides/ebr-terms/>

1 Complete biotic and sedimentary records of the Permian-Triassic
 2 transition from Meishan section, South China: ecologically
 3 assessing mass extinction and its aftermath

4

5 Zhong-Qiang Chen^{a,*}, Hao Yang^a, Mao Luo^b, Michael J. Benton^c, Kunio Kaiho^d, Laishi
 6 Zhao^e, Yuangeng Huang^a, Kexing Zhang^a, Yuheng Fang^a, Haishui Jiang^a, Huan Qiu^e,
 7 Yang Li^e, Chengyi Tu^a, Lei Shi^a, Lei Zhang^e, Xueqian Feng^a, Long Chen^a

8

9 ^a *State Key Laboratory of Biogeology and Environmental Geology, China University of*
 10 *Geosciences (Wuhan), Wuhan 430074, China*

11 ^b *School of Earth and Environment, The University of Western Australia, Crawley, WA*
 12 *3009, Australia*

13 ^c *School of Earth Sciences, University of Bristol, Bristol, BS8 1RJ, UK;*

14 ^d *Institute of Geology and Paleontology, Tohoku University, Sendai 980-8578, Japan;*

15 ^e *State Key Laboratory of Geological Processes and Mineral Resources, China University*
 16 *of Geosciences (Wuhan), Wuhan 430074, China*

17

18 * Corresponding author (Z.Q. Chen). *E-mail address:* zhong.qiang.chen@cug.edu.cn

19

20 **ABSTRACT**

21

22 The Meishan section, South China is the Global Stratotype Section and Point (GSSP) for
23 the Permian-Triassic boundary (PTB), and also is well known for the best record
24 demonstrating the Permian-Triassic mass extinction (PTME) all over the world. This
25 section has also been studied using multidisciplinary approaches to reveal the possible
26 causes for the greatest Phanerozoic biocrisis of life on Earth; many important scenarios
27 interpreting the great dying have been proposed on the basis of data from Meishan.
28 Nevertheless, debates on biotic extinction patterns and possible killers still continue. This
29 paper reviews all fossil and sedimentary records from the Permo-Triassic (P-Tr)
30 transition, based on previously published data and our newly obtained data from Meishan,
31 and assesses ecologically the PTME and its aftermath to determine the biotic response to
32 climatic and environmental extremes associated with the biocrisis. Eight updated
33 conodont zones: *C. yini*, *C. meishanensis*, *H. changxingensis*, *C. taylorae*, *H. parvus*, *I.*
34 *staeschei*, *I. isarcica*, and *C. planate* Zones are proposed for the PTB beds at Meishan.

35 Major turnover in fossil fragment contents and ichnodiversity occurs across the boundary
36 between Bed 24e-5 and Bed 24e-6, suggesting an extinction horizon in thin section. The
37 irregular surface in the middle of Bed 27 is re-interpreted as a firmground of
38 *Glossifungites* ichnofacies rather than the previously proposed submarine dissolution
39 surface or hardground surface. Both fossil fragment contents and ichnodiversity
40 underwent dramatic declines in Beds 25–26a, coinciding with metazoan mass extinction.
41 Fossil fragment content, ichnodiversity and all ichnofabric proxies (including burrow
42 size, tiering level, bioturbation level) indicate that the P-Tr ecologic crisis comprises two
43 discrete stages, coinciding with the first and second phases of the PTME in Meishan.
44 Ecologic crisis lagged behind biodiversity decline during the PTME. Pyrite framboid size
45 variations suggest that depositional redox condition was anoxic to euxinic in the latest
46 Changhsingian, became euxinic in Beds 25–26a, turned dysoxic in Bed 27, then varied
47 from euxinic to anoxic through most of the Griesbachian. The ~9 °C increase in seawater
48 surface temperature from Bed 24e to Bed 27 at Meishan seems to result in dramatic
49 declines in biodiversity and fossil fragment contents in Beds 25–26a, but had little effect
50 on all ecologic proxies. Both metazoans and infauna seem not to be affected by the
51 pre-extinction anoxic-euxinic condition. The anoxic event associated with the PTME

52 may have occurred in a much shorter period than previously thought and is only recorded
53 in Beds 25–26a at Meishan. Fossil fragment contents, ichnofaunas, ichnofabrics and
54 pyrite framboid size all show that no signs of oceanic acidification and anoxia existed in
55 Bed 27. The early Griesbachian anoxia may have resulted in rarity of ichnofauna and
56 metazoans in the lower Yinkeng Formation, in which the ichnofauna is characterized by
57 small, simple horizontal burrows of *Planolites*, and metazoan faunas are characterized by
58 low diversity, high abundance, opportunist-dominated communities. The rapid increase
59 of ~9 °C in sea-surface temperature and a short anoxia or acidification coincided with the
60 first-pulse biocrisis, while a prolonged and widespread anoxia probably due to a long
61 period of high seawater temperate condition may be crucial in mortality of most
62 organisms in the second-pulse PTME. Marine ecosystems started to recover, coupled
63 with environmental amelioration, in the late Griesbachian.

64

65 *Keywords:* mass extinction, Permian-Triassic, fossil fragment, trace fossils, redox
66 condition, Meishan section

67

68

69	Contents
70	1. Introduction
71	2. Biochronostratigraphy: an update
72	2.1. Biostratigraphy and correlations
73	2.2. Geochronology
74	2.3. Duration of key conodont zones across the P-Tr boundary
75	3. Microstratigraphy, fossil fragment contents and paleoenvironmental analysis of the
76	P-Tr transition
77	3.1. Bed 23
78	3.2. Bed 24
79	3.3. Bed 25
80	3.4. Bed 26
81	3.5. Bed 27
82	3.6. Bed 28
83	3.7. Beds 29-59
84	4. Biotic changeover through the P-Tr transition
85	4.1. Biodiversity variations over the P-Tr transition

86	4.2. Fossil fragment content variations through the P-Tr transition
87	4.3. Community structural changes of shelly faunas
88	5. Trace fossils and bioturbation
89	5.1. P-Tr ichnotaxa and their stratigraphic distributions at Meishan
90	5.1.1. Stratigraphic distributions of ichnoassemblages
91	5.1.2. Ichnofabric changes within Bed 27
92	5.2. Extent of bioturbation
93	5.3. Changeover of trace-fossil diversity over the P-Tr transition
94	5.4. Burrow size variations through the P-Tr transition
95	5.5. Trace fossil form and complexity
96	5.6. Infaunal tiering
97	6. Size variations of pyrite framboids and redox conditions over the P-Tr transition
98	7. Assessing ecologically PTME and its aftermath
99	7.1. Testing extinction patterns
100	7.2. Ecologic crisis lagging behind biodiversity drop at the PTME
101	7.3. Dramatic increase in seawater temperature and its consequences
102	7.4. Anoxic events and biotic response

103	7.4.1. Anoxic events
104	7.4.2. Biotic response
105	7.5. Testing extinction mechanisms7.6. Post-extinction amelioration of marine
106	ecosystems in late Griesbachian
107	8. Conclusions
108	
109	

110 **1. Introduction**

111

112 As the greatest biocrisis of life on Earth (Sepkoski, 1981), the Permian-Triassic
113 mass extinction (PTME) changed Earth's ecosystems fundamentally (Benton and
114 Twitchett, 2003; Erwin, 2006). After they had recovered, the marine ecosystems after the
115 PTME gave rise to the forerunners of modern-day ecosystems, both the Triassic and
116 modern ecosystems being comparable to each other in composition of functioning groups
117 and trophic structure (Chen and Benton, 2012). However, the causes of this enigmatic
118 biocrisis have long been disputed despite intense study, and the same is true of the
119 profoundly delayed recovery following the PTME (Erwin, 2001). Thus, studies of these
120 issues have enjoyed a surge in scientific interest in the past 30 years that shows no sign of
121 abating (Chen et al., 2014a).

122 Although this era-boundary crisis has been widely recognized in
123 Permian–Triassic boundary (PTB) sections around the world, many important
124 hypotheses have been proposed based on paleontological and experimental data sampled
125 from the Meishan section of Changhsing County, Zhejiang Province, east China (Fig. 1A;
126 Renne et al., 1995; Bowring et al., 1998; Jin et al., 2000; Yin et al., 2001, 2012; Kaiho et

127 al., 2001, 2006a, b; Mundil et al., 2001, 2004; Grice et al., 2005; Xie et al., 2005, 2007;
128 Riccardi et al., 2007; Wang and Visscher, 2007; Cao et al., 2009; Chen et al., 2009, 2010a;
129 Song et al., 2009, 2013a, b; Shen et al., 2011b; Huang et al., 2011; Wu et al., 2013; Wang
130 et al., 2014; Burgess et al., 2014; Fig. 1A). This section is the Global Stratotype Section
131 and Point (GSSP) for the PTB (Yin et al., 2001; Fig. 1C) and also well known for the best
132 record of both biotic and geochemical signals demonstrating the PTME all over the world.
133 Here, the exposures of the PTB beds are spectacular, extending about 2 km laterally along
134 the Meishan hill (Fig. 1E). The PTME has been well demonstrated by Jin et al. (2000),
135 whose study based on paleontological data from Meishan reveals that this extinction
136 event was abrupt and dramatic, with most Permian organisms being wiped out within a
137 very short interval, which was precisely calibrated to the base of Bed 25, a white clay bed,
138 in Meishan (Fig. 1B, D), while the PTB is placed at the middle of Bed 27, about 16-20 cm
139 above the base of Bed 25 in the same section (Yin et al., 2001; Fig. 1C). As such, the
140 biocrisis clearly pre-dated the PTB (Fig. 1D). The P-Tr ecologic crisis is also marked by a
141 pronounced negative carbon isotopic excursion (Xu and Yan, 1993; Jin et al., 2000;
142 Kaiho et al., 2001; Cao et al., 2002; Xie et al., 2005, 2007; Fig. 2) and is also associated
143 with an end-Permian sulfur event (Kaiho et al., 2006; Riccardi et al., 2006).

144 After Jin et al.'s (2000) influential study, which was largely based on fossil data
145 obtained in 1980s (i.e., Zhao et al., 1981; Sheng et al., 1984; Liao, 1984; Sheng et al.,
146 1987; Shi and Wang, 1987), abundant brachiopod and foraminifer faunas have been
147 detected from Beds 25–27, immediately above the PTME horizon in Meishan (Chen et al.,
148 2005a, 2006b; Song et al., 2007, 2009). Quantitative analysis of the updated foraminifer
149 data from Meishan revealed a two-stage extinction pattern near the P-Tr boundary (Song
150 et al., 2009), which agrees well with two distinct peaks of cyanobacteria, detected by
151 biomarker analysis from the same section, suggesting two extinction events
152 corresponding to Beds 25 and 28 (Xie et al., 2005). The two-stage extinction pattern is
153 also strengthened by extremely abundant benthic fossils obtained from a shallow
154 platform facies of the PTB section at Huangzhishan, about 40 km from Meishan (Chen et
155 al., 2009). However, Shen et al. (2011b) clarified an abrupt biotic decline in a short
156 interval equivalent to Beds 25–28 of Meishan based on quantitative analysis of fossil
157 records from Meishan and other PTB sections in South China. In contrast, Song et al.
158 (2013a) demonstrated nicely a two-stage extinction pattern for the P-Tr crisis based on
159 quantitative analysis of paleontological data derived from Meishan and a further six PTB
160 sections in South China. Thus, debate on whether the PTME was either a single crisis or

161 episodic extinctions still continues (Shen et al., 2011b; Song et al., 2013a; Wang et al.,
162 2014). Regardless of whether the extinction was single or a two-phase pattern, an
163 increasing number of faunas have been found in Beds 25-28 of Meishan and its
164 counterparts across all of South China, although this interval may just last 60 kyr
165 (Burgess et al., 2014).

166 In addition, a further extinction event resulting in depletion of Permian reefs in South
167 China was calibrated to the base of Bed 24e at Meishan (Yang et al., 1993). Yin et al.
168 (2007) re-documented biotic and geochemical signal changes across this horizon, which
169 is reinforced by several lines of evidence, including reduction in conodont sizes (Luo et
170 al., 2006), possible extinction of radiolarians in deep habitats and a negative shift in
171 organic carbon isotope values (Cao et al., 2009). To sum up, biotic variations based on
172 sound paleontology over the P-Tr transition have been far less studied in comparison with
173 the intense geochemical studies of this catastrophe in most PTB sections. Current,
174 updated fossil records from extensive PTB sections are crucial to reveal the true biotic
175 responses to these environmental crises.

176 As briefly summarized above, there have been great advances in research on the
177 PTME at Meishan in recent years. Multiple scenarios interpreting the causes of the P-Tr

178 biocrisis have been proposed based on experimental data sampled from this section.
179 Nevertheless, any reasonable models interpreting the P-Tr crisis need to be tested by
180 analysis of precise biotic extinction patterns and physiological reactions of victims and
181 survivors (Knoll et al., 2007). As a result, we herein document the updated, complete
182 fossil and sedimentary records, including microfacies, microfossils, body and trace
183 fossils, and pyrite framboids, throughout the P-Tr transition and attempt to test biotic
184 responses to various environmental and climatic catastrophes from the GSSP Meishan.

185

186 **2. Biochronostratigraphy: an update**

187

188 *2.1. Biostratigraphy and correlations*

189

190 After Yin et al.'s (2001) placement of the PTB at the base of Bed 27c, marked by
191 the first appearance datum (FAD) of the conodont *Hindeodus parvus*, Jiang et al. (2007)
192 established gondolellid and hindeodid conodont zones across the PTB in Meishan. The
193 former include the *Clarkina yini*, *C. meishanensis* and *C. taylorae* Zones, while the latter
194 comprise the *Hindeodus latidentatus*, *H. praeparvus*, *H. changxingensis*, *H. parvus*,

195 *Isarcicella staeschei*, and *I. isarcica* Zones (Jiang et al., 2007, fig. 2). Later, Zhang et al.
 196 (2009) integrated them as one conodont zonation series: *C. yini* Zone (Bed 24), *C.*
 197 *meishanensis* Zone (Bed 25), *H. changxingensis* Zone (Beds 26-27b), *H. parvus* Zone
 198 (Bed 27c), *I. staeschei* Zone (Beds 27d-28), *I. isarcica* Zone (Beds 29-51), and *C.*
 199 *tulongensis*-*C. planata* Zone (Beds 52-72, top of the Yinkeng Formation).
 200 Given that *C. taylorae* is confined to Bed 27a-28 in Meishan (Jiang et al., 2007;
 201 Zhang et al., 2009) and has also been widely reported from PTB beds around the world
 202 (Orchard et al., 1994; Orchard and Krystn, 1998; Nicoll et al., 2002; Algeo et al., 2012;
 203 Zhao et al., 2013b), the *C. taylorae* Zone is regarded as a discrete zone beneath the *H.*
 204 *parvus* Zone and retained for Bed 27a-b (Fig. 2). In addition, we have also re-examined
 205 stratigraphic distributions of some key conodont species based on previously published
 206 data and newly extracted specimens from Meishan. An updated conodont zonation is
 207 proposed for the P-Tr succession of the GSSP Meishan (Fig. 2). The new conodont zones,
 208 with their stratigraphic ranges in brackets, include *C. changxingensis* Zone (Beds 22-23),
 209 *C. yini* Zone (Bed 24), *C. meishanensis* Zone (Bed 25), *H. changxingensis* Zone (Bed 26),
 210 *C. taylorae* Zone (Bed 27a-b), *H. parvus* Zone (Bed 27c-d), *I. staeschei* Zone (Beds
 211 28-29a), *I. isarcica* Zone (Bed 29b), *C. planata* Zone (Beds 30-54), and *Neoclarkina*

212 *discreta* Zone (Bed 35 and above) (Fig. 2).

213 It is noteworthy that Yuan et al. (2014) confined the *C. changxingensis* Zone to
214 mid-Bed 10 to mid-Bed 22, *C. yini* Zone to mid-Bed 22 to Bed 24d, and *C. meishanensis*
215 Zone to Bed 24e to Bed 25. The first occurrence of the nominal species of these conodont
216 zones seems to be lower than they occurred in our samples. In particular, *C. meishanensis*
217 occurs in the so-called ‘white boundary clay’ bed and above strata in most PTB sections
218 in South China (Zhang et al., 2007; Jiang et al., 2007, 2011, Zhao et al., 2013b) and is
219 rarely present in the Permian bioclastic limestone. The *C. meishanensis* Zone is also
220 associated with a pronounced negative shifting excursion of carbon isotopes in most of
221 the PTB sections in South China. Accordingly, the bases of these Changhsingian
222 conodont zones remain tentative and need to be confirmed when additional conodont
223 samples are processed in future.

224 Other important findings from the PTB beds include restriction of *Isarcicella*
225 *peculiaris* to Bed 28 and the first occurrences of *Hindeodus eurypyge* and *Isarcicella*
226 *lobata* at the bases of Bed 27a and Bed 28, respectively (Jiang et al. 2007; fig. 2). These
227 species also have the potential to serve as key elements marking the PTB beds (Jiang et al.,
228 2007, 2011, 2014). Of these, *I. lobata*, confined to Beds 28-29 in Meishan, was proposed

229 as a distinct zone between the *H. parvus* and *I. staeschei* Zones in the southern Alps (Perri
230 and Farabegoli, 2003, 2012; Fig. 2). This species therefore occurred slightly earlier in the
231 southern Alps than in the GSSP Meishan. In the new conodont zonation, the *I. isarcica*
232 Zone is retained for Bed 29b, and thus has a much narrower stratigraphic range than
233 before. The *C. planata* Zone is newly proposed for Beds 30-54 and the *Neoclarkina*
234 *discreta* Zone for Bed 55 and higher strata in Meishan (Fig. 2) based on re-examination of
235 their stratigraphic distributions (Zhang et al., 2007, 2009).

236 The updated conodont zonation enables the PTB beds of Meishan to be
237 correlated precisely with their counterparts recorded elsewhere in the Tethys region, such
238 as North Italy, Iran, Germanic basin, and Spiti of Himalaya region (Fig. 2). The *H. parvus*,
239 *I. staeschei* and *I. isarcica* Zones have also been recognized in both Spiti and North Italy
240 (Fig. 2). Both *H. parvus* and *I. isarcica* Zones occur in the Abdadeh region, Iran (Korte et
241 al., 2004). Korte et al. (2004) also argued that there might be a hiatus between Beds 24e
242 and 25 because both the *C. iranica* and *C. hauschkei* Zones, between the *C. yini*-*C. zhang*
243 and *C. meishanensis*-*H. praeparvus* Zones, are absent in Meishan. *C. hauschkei* does
244 occur in Meishan, but shares the same stratigraphic range with both *C. yini* and *C. zhang*
245 in Bed 24 (Jiang et al., 2007, 2011). More importantly, no sedimentary gap has been

246 found in this interval in the GSSP Meishan (see below). The last occurrence of both *C.*
247 *yini* and *C. zhangii* has been calibrated to the top of Bed 24e (Yin et al., 2001; Zhang et al.,
248 2007; Jiang et al., 2007). The depositional succession between the *C. meishanensis* and *C.*
249 *yini* Zones shows no sign of a hiatus. Thus, both *C. hauschkei* and *C. iranica* either can be
250 recognized from the upper part of the *N. yini* Zone in the future, or do not occur due to
251 different biofacies controls (Korte et al., 2004).

252 Recognition and correlations of PTB beds in conodont-barren sections have long
253 remained problematic. Chen et al. (2009) established the bivalves *Claraia huzhouensis*-*C.*
254 *cf. bioni* and *Eumorphotis venetiana*-*Towapteria scythica*-*Pteria ussurica variabilis*
255 Assemblages from the PTB beds of both the Meishan and adjacent Huangzhishan
256 sections. The former is coeval with the *C. meishanensis* and *H. changxingensis* Zones of
257 the GSSP Meishan (Chen et al., 2009). The small, weakly costated *Claraia*-like species
258 “*Peribositra*” *baoqingensis* from Bed 26 of Meishan (Zhao et al., 1981) has been
259 re-assigned to *Claraia* (Chen, 2004). These primitive *Claraia* species from Meishan are
260 diagnostic of the *C. huzhouensis*-*C. cf. bioni* Assemblage and locate the PTME in the
261 shallow-water, conodont-barren PTB sections in South China (Chen et al., 2009). The
262 latter bivalve assemblage is contemporaneous with the *H. parvus* Zone in the

263 Huangzhishan section, pointing to an age of earliest Triassic (Chen et al., 2009). Both
264 *Claraia wangi* and *C. griesbachi* are also abundant in Beds 29b-54 in Meishan, and thus
265 form the *C. wangi*-*C. griesbachi* Assemblage (Chen et al., 2010a), which is coeval with
266 the *I. isarcica* and *C. planata* Zones (Fig. 2). The ammonoids *Rotodiscoceras*,
267 *Hypophiceras*, *Ophiceras*, and *Lytophiceras* characterize the assemblages from Beds
268 22-24, Beds 25-26, Beds 27-50, and Beds 51-55, respectively in Meishan (Fig. 2; Zhao et
269 al., 1984; Sheng et al., 1984; Yin et al., 2001; Chen et al., 2010a). Brachiopods are also
270 reasonably abundant in Beds 25-26, Bed 27 and Beds 51-55 of Meishan (Chen et al.,
271 2002, 2006b, 2007). They are assignable to the *Tethyochonetes liaoi* Assemblage (Beds
272 25-26), *Paryphella triquetra* Assemblage (Bed 27), and *Meishanorhynchia meishanensis*
273 Assemblage (Beds 51-55) (Chen et al., 2010a). Song et al. (2007, 2009) also reported
274 diverse foraminifers from the Changhsing and lowest Yinkeng Formations in Meishan,
275 but did not establish biozones. A palynological *Lundbladispora-Taeniaesporites*-
276 *Equisetosporites* Assemblage was established from Beds 33-53 of the Yinkeng
277 Formation (Zhang et al., 2007), which, therefore, correlates collectively with the
278 conodont *C. planata* Zone (Fig. 2).

279

280 2.2. Geochronology

281

282 In Meishan, volcanic ash beds are well exposed and conspicuous in the
283 uppermost Permian to Lower Triassic successions. In particular, Beds 25 and 28 near the
284 PTB have been dated by multiple research groups using various techniques (Table 1). The
285 most updated radiometric ages for Beds 25 and 28 are 251.941 ± 0.037 Ma and $251.880 \pm$
286 0.031 Ma, respectively (Burgess et al., 2014), which constrain the duration between those
287 two phases of the PTME (Song et al., 2013a) or the duration of the PTME (Shen et al.,
288 2011b; Wang et al., 2014) as 60 ka (Burgess et al., 2014). Burgess et al. (2014) have also
289 given updated estimates for sediment accumulation rates through the P-Tr transition,
290 which show that sedimentation rates of the Changhsing Formation decline towards the
291 end of the Permian, reach the lowest value during the time of extinction (Beds 25-28), and
292 then increase gently in the early Griesbachian (Beds 28-37) and steeply in the
293 early-middle Griesbachian (Beds 37-48) in Meishan (Burgess et al., 2014). In addition,
294 these authors estimated that the abrupt decline in $\delta^{13}\text{C}_{\text{carb}}$ in Bed 24e took place at
295 251.950 ± 0.042 Mya, while the FAD of *H. parvus* at the GSSP Meishan is at $251.902 \pm$
296 0.024 Mya (Burgess et al., 2014).

297

298 2.3. Duration of key conodont zones across the P-Tr boundary

299

300 At Meishan, intense high-precision dating of volcanic ash beds (Table 1) and
301 high resolution conodont zones (Fig. 2) allow reasonable estimates of the duration of
302 each conodont zone. The widespread *H. parvus* Zone is estimated to have lasted 16 ka
303 (Table 2), while the *C. meishanensis* Zone, the PTME marker, lasted 8 ka, which is much
304 shorter than previously thought. The last conodont zone prior to the PTME, the *C. yini*
305 Zone, may have lasted 28 ka (Table 2).

306

307 **3. Microstratigraphy, fossil fragment contents and paleoenvironmental analysis of**
308 **the P-Tr transition**

309

310 At Meishan, the P-Tr succession comprises the Changhsing and Yinkeng
311 Formations below and above. The former unit is a 41-m-thick carbonate succession
312 consisting of medium- to thin-bedded limestone, while the Yinkeng Formation is about
313 15 m thick and dominated by mudstone and muddy limestone in the lower part and

314 characterized by thin-bedded limestone in the upper part (Fig. 3). These two formations
315 have been frequently described (Zhao et al., 1981; Sheng et al., 1984, 1987; Yang et al.,
316 1987; Yin et al., 1996, 2001; Zhang et al., 2005). Cao and Zheng (2007) re-described the
317 Changhsing Formation (Beds 1-24) and recognized 247 natural, single layers, each 2 to
318 37 cm in thickness. Chen et al. (2007) gave an updated description for the Yinkeng
319 Formation (Beds 25-59), in which 183 natural layers are recognizable. In addition, Cao
320 and Shang (1998) conducted the first cm-scale stratigraphy, also termed
321 microstratigraphy, of the P-Tr boundary beds in Meishan. Since then, microstratigraphy
322 of the Beds 24-29 of the Meishan section has been intensely studied (Cao and Zheng,
323 2009; Zhao and Tong, 2010; Zheng et al., 2013).

324 The top two beds of the Changhsing Formation, Beds 23-24, record important
325 sedimentary and paleontological information just prior to the PTME, while most parts of
326 the Yinkeng Formation record the severe biotic extinction and its consequences. Thus,
327 microstratigraphy of the uppermost Changhsing Formation to Yinkeng Formation
328 succession (Beds 23-59) is summarized here in view of the previously published data and
329 our new observations in petrologic thin sections. These thin sections were sampled
330 almost continuously in Beds 24e to 29 and in a 20-cm-interval in Beds 22 to 24d of the

331 Changhsing Formation. The sampling interval is 0.5 m throughout Bed 30 to Bed 59 of
332 the Yinkeng Formation in the GSSP Meishan.

333 Point counting is a relatively quick method that quantifies the occurrence of skeletal
334 fragments of major fossil groups in different horizons under the microscope (Flügel, 1984;
335 Payne et al., 2006). However, care must be taken when using the point-counting method
336 because large shell fragments of some clades may bias counting results (Jacobsen et al.,
337 2011). As an alternative, Jacobsen et al. (2011) proposed the equal area approach to
338 quantify the occurrence of skeletal fragments in thin section. In order to eliminate biases
339 of counting areas, it is suggested that at least eight equal area fields of view ought to be
340 counted per thin section sample (Jacobsen et al., 2011). Similar to the equal area approach,
341 fragment percentage data of various clades from each thin section are estimated based on
342 the observation of 300 to 350 views under a magnification of $\times 50$ in one sample,
343 collected for microfacies analysis of the PTB beds. Then, percentages of various skeletal
344 components, micrite, cavities and undertermined particles (i.e., pyrites and other minerals)
345 from samples throughout Bed 22 to Bed 60 of Meishan were combined to yield the mean
346 abundance of each composition in each sample throughout the study succession (Table 3).

347

348 3.1. *Bed 23*

349

350 Bed 23 of the upper Changhsing Formation comprises dark gray thin-to
351 medium-bedded bioclastic limestone interbedded with thin-bedded muddy limestone and
352 siliceous mudstone layers. Small-scale wavy cross bedding is commonly present in the
353 bioclastic limestone, while horizontal stratification occurs in the muddy limestone and
354 siliceous mudstone (Fig. 4G, H). Grain bedding structures are also occasionally present in
355 the bioclastic limestone unit. The bioclastic limestone usually has a packstone to
356 grainstone texture. The former texture is very common, while a grainstone texture is also
357 occasionally present (Fig. 5C). This unit is usually strongly bioturbated in comparison
358 with the weakly bioturbated thin siliceous layers that are usually horizontally stratified
359 (Fig. 3). The autochthonous and allochthonous fossil assemblage is highly diverse and
360 dominated by foraminifers, crinoids, and brachiopods with minor constituents of
361 ostracods, echinoids, bryozoans, sponge spicules, calcareous sponges, gastropods,
362 radiolarians, and macroalgae (Fig. 6). The matrix comprises micrite (about 20-23%, Fig.
363 6). Cavities, pyrites and other undetermined particles are also commonly present (Table
364 3). The alternating occurrence of horizontal stratification and small-scale cross bedding

365 and/or grain-grading bedding structures indicates that Bed 23 was deposited on a
366 carbonate ramp between fair-weather wavebase and storm wavebase (Fig. 3; Zhang et al.,
367 2005).

368

369 3.2. *Bed 24*

370

371 Bed 24, the topmost unit of the Changhsing Formation, consists mainly of thin-
372 to medium-bedded bioclastic packstone rich in large ammonoids and other macrofossils
373 (Fig. 4E). This bed has attracted intense attentions in terms of fossil record and
374 sedimentary characterization because of its stratigraphic position just beneath the biotic
375 extinction horizon (base of Bed 25; Jin et al., 2000). Bed 24, 71-90 cm in thickness, is
376 usually labelled as Bed 24a-e (Yin et al., 1996) and consists of 14 layers, with the thinnest
377 being 2 cm thick (Cao and Zheng, 2007). The conodonts from Bed 24 belong to the
378 *Clarkina yini* Zone (Mei et al., 1998), which is distinct from the underlying *C.*
379 *changxingensis* Zone (Beds 22-23).

380 Bed 24a-c has similar petrographic features to Bed 23 (Figs. 5D, 6). The dark
381 organic-rich muddy limestone or siliceous mudstone, usually about 2 cm in thickness, has

382 well-developed horizontal stratifications and possesses packstone to micritic textures
383 with tiny, highly fragmented fossil skeletons of brachiopods and ostracods. These
384 horizontally stratified layers are usually weakly bioturbated. In contrast, the bioclastic
385 limestone unit, usually > 5cm thick, possesses small-scale wavy cross bedding and
386 bioclastic packstone to grainstone texture. These layers are also highly bioturbated
387 (Zheng et al., 2013). All skeletal components of Bed 23 also persist into Bed 24 (Fig. 6).
388 Accordingly, Bed 24a-c was likely deposited in the same environment as Bed 23.

389 Although Bed 24d has similar petrographic texture to Bed 24a-c (Fig. 6), the
390 presence of abundant fecal pellets and peloids characterizes the grain assemblage of Bed
391 24d. Fossil fragment contents in rocks from both Bed 24d and Bed 24a-c are also
392 comparable with one another (Fig. 6). In addition, burrows are commonly present near
393 the boundary between bioclastic limestone unit and organic-rich muddy limestone or
394 siliceous mudstone layer. Bed 24d yields abundant trace fossils (see Section 5).
395 Pronounced cross-bedding and vertical burrows characterize the upper part of Bed 24d
396 (Fig. 4J). The top of Bed 24d is, however, weakly bioturbated and characterized by
397 smooth cone-shaped surfaces, which was termed a hard-ground structure representing
398 interrupted or highly condensed deposits (Cao and Zheng, 2009). Cao and Zheng (2009)

399 regarded this irregular contact as a sequence boundary indicating a changeover interface
400 from lowermost level to rapid rise. The same contact, however, has been interpreted as an
401 erosional surface, serving as a sequence base of a 3rd-order depositional sequence
402 following a major fall in sea level (Zhang et al., 1997; Yin et al., 2014). This
403 interpretation is reinforced by the presence of a diverse shallow-water facies trace fossil
404 assemblage including vertical burrows of *Balanogossites* (Fig. 4J; see also Section 5).
405 Cao and Zheng (2007) have also noted that abundant burrows of *Planolites* and *Skolithos*
406 and mud-crack structures are present near the boundary between Beds 24d and 24e.
407 Accordingly, Bed 24d, overall, is inferred to have been deposited in the upper part of the
408 subtidal zone of a carbonate ramp (Fig. 3; Zhang et al., 1997).

409 The topmost 10 cm thick limestone of Bed 24 is labelled Bed 24e, which
410 consists of eight natural layers (Cao and Zheng, 2009) and these were sampled at six
411 horizons here (Bed 24e-1 to Bed 24e-6). Trace fossils occur near the irregular contact
412 between Beds 24d and 24e-1 (see Section 5). Bed 24e, except for the topmost 3 cm (24e-5,
413 24e-6), is a dark gray bioclastic packstone containing abundant fossil fragments of
414 foraminifers, brachiopods, and crinoids. Other fossil groups such as bryozoans,
415 gastropods, macroalgae, ostracods, calcareous sponges, and sponge spicules are also seen

416 in thin sections, which have no major difference from the underlying Bed 24d (Fig. 6).

417 The uneven top surface is always capped by several muddy laminae. Cylindrical, vertical

418 burrows, ranging from 0.1 to 0.5 cm in diameter and from 3.0 to 1.0 cm in length occur in

419 the upper bedding surface. Bed 24e saw a slight increase in lime mud in the matrix and

420 pyrite within the bed (see below). Bed 24e therefore was probably deposited in the

421 fair-weather wave action zone (Fig. 3) and was interpreted as a lowstand platform margin

422 wedge of a 3rd sequence (Zhang et al., 1997; Yin et al., 2014).

423 The topmost 2-3-cm-interval, labelled as Bed 24e-5 and 24e-6, is characterized

424 by relatively low contents of P and Ca and high Ni content (Kaiho et al., 2001, 2006b).

425 Bed 24e-5, about 1.0-1.1 cm in thickness, comprises bioclastic packstone and contains

426 abundant fossil fragments of foraminifers, crinoids, brachiopods, and ostracods.

427 Fragments of calcareous sponges, sponge spicules, gastropods, bryozoans and

428 macroalgae are also occasionally present, and these are comparable in major fossil

429 components with Beds 24e-1 to 24e-4 (Fig. 6). Moreover, abundant, reasonably large

430 horizontal burrows (*Planolites*) are densely packed on the surface of Bed 24e-6 (also see

431 Section 5).

432 The contact between Beds 24e-5 and 24e-6 is a laminated wavy lime layer (Fig.

433 7D). Bed 24e-6 is a 10- to 19-mm-thick bioclastic packstone and dominated by silica bars,
434 which were interpreted as sponge spicules (Kaiho et al., 2006). The elongate bars are
435 actually longitudinal outlines and the circular grains are cross sections of spicules (Fig.
436 7A-C). This identification is reinforced by the abundant isolated silicified sponge spicule
437 specimens extracted from Bed 24e-6 (Fig. 7E). Contrasting to the predominance of
438 sponge spicules, fragmentary contents of foraminifers, crinoids, echinoids and
439 brachiopods decline dramatically. The skeletal grain assemblage experienced a dramatic
440 reduction in both abundance and diversity across the contact between Beds 24e-5 and
441 24e-6 (Fig. 7E), to which the PTME was calibrated (Kaiho et al., 2006a).

442

443 3.3. *Bed 25*

444

445 This bed is the so-called “Boundary clay bed” or “White clay bed” (Zhao et al.,
446 1981; Sheng et al., 1984; Yang et al., 1987). Its thickness ranges from 2 cm to 6 cm
447 depending on the weathering intensity, the higher the intensity the thicker the bed. The
448 bed grades upward into Bed 26 as a consequence of a gradual increase in organic and
449 calcareous content and decrease in volcanic ash layers. The total thickness of these two

450 beds is around 10 cm.

451 The basal part of Bed 25 comprises a 0.1- to 0.2-mm-thick layer of greyish black
452 mudstone rich in Fe grains, termed Bed 25-1, which usually becomes a reddish
453 ferruginous layer capping the dark Bed 24e-6 and is conspicuous at outcrops in all
454 Meishan quarries owing to weathering. Previously, this Fe-rich layer was termed the
455 “pyrite lamina” layer (Wignall and Hallam, 1993; Shen et al., 2007) or Pyrite layer (Cao
456 and Zheng, 2009), based on the abundant pyrite-like grains visible at outcrops. Elemental
457 analysis shows that these Fe grains are either Fe-Ni grains (Kaiho et al., 2001, 2006b) or
458 goethites (Liang et al., 2002). Pyrite framboids are also commonly present in this layer
459 (Shen et al., 2007). In addition, Zheng et al. (2013) detected abundant irregular volcanic
460 glasses from this layer.

461 The reddish ferruginous surface of Bed 25-1, together with the absence of both
462 the *N. iranica* and *N. hauschkei* conodont zones, was considered as evidence indicating an
463 exposure surface and representing a hiatus (Korte et al., 2004). However, the presence of
464 marine fossils such as foraminifers and brachiopods (Rui et al., 1988; Yin et al., 2001) in
465 Bed 25 and abundant sponge spicules and other fossil fragments in Bed 24e-6 (Fig. 6)
466 indicates the absence of a paleo-exposure surface or an aerial hiatus. The absence of these

467 two conodont zones may relate to biofacies controls and cannot bracket a hiatus, as
468 discussed in Section 2.1.

469 The overlying thin layer (Bed 25-2), 0.3-1 mm thick, is dark yellowish orange,
470 and encompasses mainly gypsum and Fe (Table 4). The remaining part of Bed 25 (Layer
471 25-3, 2-4 cm thick; Kaiho et al., 2006b) is a light gray illite–montmorillonite–kaolinite
472 claystone (white clay) (Table 4). Gypsum and pyrite are very common in thin section. No
473 fossil fragments are seen in thin section (Fig. 5A). Marine fossils of conodonts,
474 foraminifers, ostracods and tiny brachiopods have been found from this bed, but are
475 always sparse (Rui et al., 1988; Jiang et al., 2007). Benthic carbonate skeletal fossils
476 diminished dramatically in this bed. Calcareous shells are often pyritized and attached
477 with crystals and framboidal pyrites on the surface (Rui et al., 1988). Conodonts from
478 Bed 25 are included in the *C. meishanensis* Zone (Fig. 2). Microspherules and β -type
479 quartz crystals are much more abundant in this bed than in other ash clay beds, and could
480 be products of acid volcanic eruptions (He et al., 1987). However, comparable
481 microsphaerules are also abundant in the background soils in Meishan and other PTB
482 sections in South China, suggesting that they may be the modern industrial products
483 rather than geological objects (Zhang et al., 2014). Both Hf-isotope and elemental

484 analysis of magmatic zircons suggests these ash clays near the PTB in South China may
485 have been sourced from volcanism taking place along the convergent continent margins
486 during the formation of the Pangea supercontinent (Gao et al., 2013).

487

488 3.4. Bed 26

489

490 Bed 26, the so-called “black clay bed” (Yang et al., 1987), comprises black shale,
491 4-6 cm in thickness. Nine pronounced yellow clay layers are interbedded in the black
492 shale. Horizontal laminae and pyrite are common. The clay layer is composed mainly of
493 montmorillonite–illite, which is similar to that of Bed 25 (Table 4). Fossil fragments are
494 very rare in most parts of this bed (Fig. 5B) except for the top 2-cm-interval where fossil
495 fragments are fairly abundant in calcareous nodules (Fig. 8), including foraminifers,
496 ostracods, echinoids, bryozoans, and brachiopods (Table 3; Figs. 6, 8). Microspherules
497 or/and α -quartz (in the form of β quartz pseudomorphs; He, 1981) are rich in the lower
498 part, but they may be the products of modern industry (Zhang et al., 2014). Various
499 burrowing systems are common in the upper part of Bed 26, from which Cao and Zheng
500 (2009, fig. 5b) identified *Chondrites*, *Planolites* and *Zoophycos*. The identification of the

501 last ichnogenus, however, is problematic based on insufficient information illustrated by
502 these authors. The upper part of the bed, Bed 26b, therefore is highly bioturbated (Fig. 3;
503 Cao and Zheng, 2009).

504 Skeletal fossils are rare but considerably diverse, including ammonoids,
505 brachiopods, bivalves, ostracods, and conodonts. Co-occurrence of the Triassic-type
506 faunas (i.e., *Otoceras*, *Claraia* and many conodont species) and Permian-type elements
507 (i.e., ammonoids *Pseudogastroceras* and *Xinodiscus*, and many brachiopods and
508 foraminifera) is particularly interesting. Brachiopods are small in size and thin-shelled,
509 and include species of *Orbicoiella*, *Preliissoryhnychia*, *Cathaysia*, *Paryphella*,
510 *Tethyochonetes*, and *Spinomarginifera* (Chen et al., 2006b; Chen and McNamara, 2006).

511 The presence of the relatively diverse fossil assemblage in the upper part of Bed 26
512 indicates the earliest re-colonization of epifauna on the barren soft substratum
513 immediately after volcanic eruption. Most of these shelly fossils are complete and well
514 preserved regardless of the delicacy of the skeleton. The change from Bed 26 to Bed 27 is
515 gradual and no boundary surface can be recognized. Crystal and framboidal pyrite are
516 concentrated in a discontinuous dark lamina with rich organics (Shen et al., 2007). The
517 slow sedimentation rate, and quiet and anoxic environment (Shen et al., 2007) suggest

518 that Bed 26 probably represents a semi-closed, low-energy subtidal zone (Fig. 3). The
519 succession of Beds 24e, 25 and 26, overall, shows that continuing fall of sea level through
520 Bed 24e turned to a rise in the upper part of Bed 26, with the lowest point of sea level
521 corresponding probably to the base of Bed 25 (Yin et al., 2014).

522

523 3.5. *Bed 27*

524

525 Bed 27 comprises biotic packstone to wackestone with occasionally micrite
526 texture and contains fairly abundant fossil skeletons and pyrite crystals throughout the
527 bed (see Section 6). Relatively complete shells of ostracodes, foraminifers and
528 thin-shelled brachiopods are reasonably abundant. This bed contains three major irregular
529 contact surfaces, termed hardground surfaces (Cao and Shang, 1998) and firmground
530 surfaces (Cao and Zheng, 2009), at various levels (Fig. 9). Of these, the first irregular
531 surface is rather pronounced, about 5 cm above the base of Bed 27 and near the boundary
532 between Beds 27a and 27b. The second occurs near the contact between Bed 27c and 27d,
533 while the third is not prominent and occurs within Bed 27d (Fig. 9). These ‘firmground’
534 surfaces divide Bed 27 into three depositional cycles, with each beginning with dark

535 muddy limestone and grading upwards into pale bioclastic limestone. Rich organic and
536 muddy laminae parallel to the bedding plane decrease upward from the base within each
537 cycle. The upper unit of each cycle was disturbed by repeated burrowings, which form
538 part of the firmground (see Section 5). Microscopic examination reveals that the dark,
539 early-lithified rock contains a minor percent of clay, rich organic shreds and bioclasts (Fig.
540 9; Table 4).

541 Microfossils in Bed 27 are much more abundant and diverse than previously
542 thought (Fig. 6). Of these, foraminifera are most abundant among all clades. Echinoids
543 are also remarkably abundant, although they cannot be identified beyond a certain
544 taxonomic level (Figs. 10-12). Bed 27a contains fossil skeletons of foraminifers,
545 ostracods, echinoids, and brachiopods (Fig. 10), which is similar in component
546 composition to Bed 26 (Fig. 6). Bed 27b comprises marls and clays in the lower part, in
547 which fossil fragments are very rare (Fig. 9). The remainder of Bed 27b yields a fossil
548 fragment abundance (FFA) composed mainly of foraminifers and brachiopods (Fig. 6).
549 Both Beds 27c and 27d contain much more abundant and diverse FFA than Bed 27b (Figs.
550 10-12), both of which are dominated by foraminifers, ostracods and brachiopods with
551 minor constituents of echinoids (Fig. 6).

552 It should be noted that Bed 27 is usually subdivided into four layers (Yin et al.,
553 2001). Cao and Zheng (2009), however, divided this bed into six layers (units) including a
554 stromatolite layer (Bed 27-5) and mudstone (Bed 27-6) in the upper part of Bed 27. Later,
555 Zheng et al. (2013) denied the existence of the stromatolite layer and divided Bed 27 into
556 five layers; no stromatolitic structures are seen in our thin sections either. Except for the
557 topmost 0.5 cm thick layer of carbonaceous mudstone, another four layers are similar to
558 those recognized by Yin et al. (2001). In addition, Cao and Zheng (2009) and Zheng et al.
559 (2013) interpreted the irregular surface separating Beds 27a and 27b (Fig. 9) as
560 firmground surface as a result of a rapid transgression. Here, we agree with the
561 firmground interpretation of these irregular surfaces within Bed 27 (Cao and Zheng, 2009;
562 Zheng et al., 2013) because of the presence of abundant burrows typical of the
563 *Glossifungites* ichnofacies (Seilacher, 1967) and distinct lithological interfaces, typically
564 dark muddy micrite overlain by light gray, coarser-grained bioclastic
565 packstone-wackestone, within Bed 27 (Fig. 9; see also Section 5). Firmgrounds of the
566 *Glossifungites* ichnofacies, also termed omission surfaces (Knaust, 1998), have been
567 extensively used in sequence stratigraphy to identify and characterize discontinuity
568 surfaces (Pemberton and Frey, 1985; MacEachern et al., 1992, 2007; Buatois and

569 Mángano, 2011). Within Bed 27, the unlined burrows penetrating into muddy limestone
570 are passively filled with coarser grains from the overlying stratum. This means that the
571 burrows remained open after the trace maker had left, thereby permitting bioclast grains
572 from subsequent depositional events to fill the open, stable burrows. Although the
573 majority of documented *Glossifungites* ichnofacies are from shallow-marine settings
574 (Knaust, 1998; Buatois and Mángano, 2011), this ichnofacies is also present in relatively
575 deep marine contexts, such as incision of submarine canyons during relative sea-level
576 falls (e.g. Dasgupta and Buatois, 2012) or autogenic erosional episodes by turbidity
577 currents and bottom currents (Savrda et al., 2001; Gérard and Bromley, 2008; Hubbard
578 and Shultz, 2008). As such, the *Glossifungites* ichnofacies from Bed 27 may represent an
579 omission surface, but cannot indicate a precise depositional environment for Bed 27.
580 Integration of lithofacies, paleoecologic and ichnofacies indicates that Bed 27 may have
581 been deposited on a carbonate ramp near the storm wave action zone (Fig. 3), as
582 suggested by Zhang et al. (1997; 2005).

583

584 3.6. Bed 28

585

586 Bed 28 comprises yellow claystone having similar composition to Bed 25 (Table
587 4), dominated by montmorillonite mixed with illite. Apart from conodonts (Jiang et al.,
588 2007), no other fossils have been recovered from this bed.

589

590 3.7. Beds 29-59

591

592 Bed 29 encompasses wackestone with rare foraminifer tests (Fig. 13). Pyrite is
593 commonly seen in thin section and pyrite content increases up-section. A minor omission
594 surface, equivalent to the erosional surface of Zhang et al. (2007) is developed in the
595 middle part of Bed 29 (Zhang et al., 2007). Fossil fragments are very rare and their
596 contents decrease upwards within the bed (Fig. 6; Table 3). Bed 30 is a marlstone, which
597 has a micritic texture and lacks any fossil fragments (Table 3). Both beds contain
598 laminated stratification and lack any cross bedding, indicating a low-energy environment.
599 Beds 29-30 therefore may have been deposited in the upper part of the offshore setting
600 that is below fair-weather wavebase (Chen et al., 2007).

601 Beds 31-51 are typified by alternating black shale, greenish gray mudstone, and
602 gray marlstone in the lower part, and interbeds of gray calcareous mudstone and pale

603 muddy limestone in its upper part. They are subdivided into 39 cm-scale cycles (Chen et
604 al., 2007; Fig. 3). In general, the lower unit of the cycle is characterized by black shale or
605 greenish mudstone rich in bivalve and ammonoid fossils (Fig. 4F, I), while the upper unit
606 is dominated by calcareous mudstone and marlstone. The mudstone-dominated cycles
607 are transitional to the marl-dominated cycles up-section, indicating a long-term
608 up-shallowing cycle (Chen et al., 2002, 2007; Tian et al., 2014). In addition to the
609 lithologic variation, Beds 31-34 are characterized by the calcareous mudstone and shale
610 where laminated stratifications are commonly preserved (Fig. 4C), while the upper part
611 of the formation (Beds 35-51) is typified by an increasing number of laminated marl beds
612 (Fig. 3). Fossil fragments occur occasionally in Beds 45, 50 and 51, characterized by
613 foraminifer and ostracod skeletons (Table 3; Fig. 6). Horizontal burrows of *Planolites* are
614 present in Beds 36-51, which also yield a few shell beds of bivalves (i.e., *Claraia*
615 *griesbachi*) and ammonoids (*Ophiceras* spp.) (Chen et al., 2007). This unit was
616 interpreted as the result of sedimentation relatively deep offshore (Fig. 3; Zhang et al.,
617 2005; Chen et al., 2007).

618 Beds 52-53 comprise alternations of shale and marlstone, yielding reasonably
619 abundant burrows of *Chondrites* and *Planolites*. Increasing fossil fragment content is

620 seen in both Beds 52 and 53, in which foraminifer, ostracod and echinoid shell fragments
621 are remarkable (Fig. 13), although they are definitely minority components in thin
622 section (Fig. 6; Table 3). Moreover, horizontal stratification is commonly present in both
623 shale and marlstone. These two beds were interpreted as the result of sedimentation in the
624 relatively deep offshore below storm wavebase (Chen et al., 2007).

625 Towards the top of the Yinkeng Formation, the succession (Beds 54-59) is
626 dominated by marl-dominated cycles. A thin- to medium-bedded marl is hummocky
627 cross-stratified (HCS; Fig. 4A, B, D) and often displays multidirectional tool marks on
628 its base, and horizons of loading and soft sediment deformation are very common (Chen
629 et al., 2002). Fossil fragments are reasonably abundant in Beds 54-59 (Fig. 13), although
630 they are still in the minority in thin section (Fig. 6; Table 3). Foraminifers, ostracod and
631 echinoids characterize their FFA (Fig. 6; Table 3). Trace fossils are also commonly
632 present in these beds, including *Planolites* isp. 2, *Treptichnus* sp., and *Thalassinoides* isp.
633 3. Moreover, the sedimentary structure HCS was interpreted as having been generated by
634 offshore storm currents. Beds 54-59 therefore may have been deposited offshore, near
635 storm wavebase (Chen et al., 2007).

636

637 **4. Biotic changeover through the P-Tr transition**

638

639 *4.1. Biodiversity variations over the P-Tr transition*

640

641 Comprehensive paleontological studies of the Meishan section were undertaken
642 in the 1980s (Zhao et al., 1981; Sheng et al., 1984; Yang et al., 1987; Shi and Chen, 1987).
643 The fossil record employed by Jin et al. (2000) to document the PTME pattern, which
644 shows an abrupt extinction calibrated to the base of Bed 25, was sourced mainly from
645 these studies. Since then, more diverse faunas and floras have been documented from
646 Meishan, including foraminifers (Song et al., 2007, 2009), radiolarians (He et al., 2005),
647 brachiopods (Chen et al., 2002, 2005a, 2006b; Li and Shen, 2008; Chen and Liao, 2009),
648 conodonts (Nicoll et al., 2002; Tong and Yang, 2004; Luo et al., 2006, 2008; Jiang et al.,
649 2007, 2008; Zhang et al., 2007, 2009; Yuan et al., 2014), ostracods (Crasquin et al., 2010;
650 Forel and Crasquin, 2011), palynolomorphs (Zhang et al., 2007), and arcritarchs (Li et al.,
651 2004). Additional macrofossils were collected throughout the upper Changhsing
652 Formation to the Yinkeng Formation. Several shelly fossil communities from Beds 24, 26,
653 27, 32, 40, and 53-55 were quantitatively analysed (Chen et al., 2010a).

654 Shen et al. (2011b) and Wang et al. (2014) demonstrated a steep decline zone of
655 species richness corresponding to the interval between Beds 25 and 28 in Meishan by a
656 means of quantitative analysis on fossil records from more than ten PTB sections
657 (including Meishan) from South China. In contrast, Song et al. (2013a) calculated species
658 richness of each layer marked in microstratigraphic analysis (Beds 24-29) based on the
659 updated fossil record mentioned above. Species richness of single layers experienced a
660 stepwise but minor decline within Bed 24. Two distinct declines in species richness were
661 well demonstrated and calibrated to Beds 25 and 28. The same pattern is also indicated in
662 seven PTB sections in South China (Song et al., 2013a). Above Bed 28, species richness
663 remains very low in the remaining part of the Yinkeng Formation.

664 Here, additional fossil specimens, primarily brachiopods, ammonoids and
665 bivalves, have been collected from Beds 24e, 26, 27 to document biotic turnover across
666 the PTB. Moreover, microfossils were observed in the petrologic thin sections used for
667 microfacies analysis (see Section 3). Of these, foraminifers are the most abundant skeletal
668 fragments among all clades. Most of these foraminifer tests, however, were illustrated by
669 Song et al. (2007, 2009), so the newly obtained fossil record does not affect the biotic
670 extinction pattern revealed by Song et al. (2013a).

671

672 *4.2. Fossil fragment content variations through the P-Tr transition*

673

674 The abundance and diversity of skeletal grains within the late Changhsingian
675 samples (Beds 22-24) is remarkably high. Skeletal grains from all sampled levels except
676 for the top 1-2 cm (Bed 24e-6) of Bed 24e comprise 68-74% of the total rock volume in
677 the uppermost Changhsing Formation (Fig. 14). Fossil fragment assemblages are
678 strikingly similar to one another in all sampled layers within the interval between Bed 22
679 and 24e-5, and each of these is dominated by foraminifers, crinoids and brachiopods.
680 Other major constituents include ostracods, bryozoans, sponge spicules, and macroalgae
681 (Fig. 14). Skeletal grains of gastropods, calcareous sponges and radiolarians are relatively
682 rare and absent in some horizons (Fig. 14).

683 It is noteworthy that FFAs do not appear to differ at all across the contact
684 between Beds 24d and 24e, although an omission surface, also a 3rd sequence boundary
685 (Zhang et al., 1997), separates these two layers (Zhang et al., 1997). In contrast, FFAs
686 experienced a dramatic reduction in diversity across a lime laminae layer between Beds
687 24e-5 and 24e-6 (Figs. 6, 14). Above this lamina layer (Fig. 7D), skeletal grains of Bed

688 24e-6 comprise about 60% of all rock in thin section in comparison with nearly 70% in
689 Beds 22-24e-5 (Fig. 14). The overwhelming majority of the FFA in Bed 24e-6 is sponge
690 spicules (35%) with minor constituents of foraminifers (8%), brachiopods (7%), crinoids
691 (6%), and echinoids (4%) (Table 3; Fig. 6). Furthermore, fusulinids disappeared forever
692 at this lamina (Kaiho et al., 2006b). The FFA experiences a loss of five major orders (i.e.,
693 ostracods, bryozoans, calcareous sponges, gastropods, and macroalgae) across the
694 boundary between Beds 24e-5 and 24e-6 (Figs. 6, 14). More importantly, this horizon
695 coincides with a pronounced negative carbon isotope excursion and a sulfur isotopic
696 excursion anomaly (Kaiho et al., 2006a, b), and thus marks the actual biotic extinction
697 horizon (Kaiho et al., 2006b).

698 Fossil fragment contents form a high plateau in both abundance and diversity,
699 comprising nearly 70% of total rock and including almost all skeletal clades recognized
700 from the Changshing Formation. They underwent a dramatic depletion in both abundance
701 and diversity in Beds 25-26a, which are nearly barren of skeletal grains (Fig. 14). This
702 severe depletion therefore is calibrated to the base of Bed 25, coinciding with the PTME
703 (Jin et al., 2000; Shen et al., 2011b) or the first phase of the PTME (Song et al., 2013a).
704 After the PTME, skeletal grains started to rebound in Bed 26b, the top 2-cm interval of

705 the bed and 8-10 cm above the base of Bed 25. Fossil fragments in Bed 26b, however,
706 comprise only 32% of all rock in comparison with nearly 70% before the PTME (Figs. 6,
707 14). The FFA in Bed 26b comprises mainly foraminifers, ostracods, brachiopods,
708 bryozoans, and echinoids (Fig. 7). Both foraminifers and echinoids are the most abundant
709 among all clades (Fig. 6). Of particular interest is the presence of both echinoids and
710 bryozoans, with bryozoans represented by fenestellid fragments. These two clades have
711 generally been believed to have gone extinct at the PTME (Sepkoski, 1981, 2002), but
712 instead they occur in the aftermath of the PTME at Meishan. Their body fossils were also
713 found in association with the *H. parvus* Zone in the neighbouring Huangzhishan section
714 of western Zhejiang Province (Chen et al., 2009).

715 Fossil fragment abundance remains almost same as in Bed 26b, comprising
716 nearly 31-38% through the entire Bed 27, except for Bed 27b, in which skeletal grains are
717 only 10% of all rock. Thus, fossil fragments rebounded and reached nearly half their
718 pre-extinction level with a major depletion occurring in mid-Bed 27 (Fig. 14). If
719 considering the FFA of the entire Bed 27, which contains elements of brachiopods,
720 bryozoans, foraminifers, and ostracods (Table 3), then recovery of FFA diversity in Bed
721 27 is marked by the re-appearance of 45.5% of all pre-extinction orders.

722 FFA experienced a major loss in Bed 29, down to less than 10% (Fig. 14). Fossil
723 fragments are absent in Beds 28-44. After rebounding in Bed 45, the skeletal grain
724 assemblage underwent a stepwise abundance recovery in Beds 50-51 and remained at a
725 relatively stable level, occupying nearly 16% of all rock in Beds 52-60. FFA diversity,
726 however, remains at a rather low level, with the re-appearance of only three orders:
727 foraminifera, ostracods and echinoids (Fig. 14).

728

729 4.3. Community structural changes of shelly faunas

730

731 The P-Tr shelly communities are characterized by a mixture of large-sized
732 ammonoids and small brachiopods in the uppermost Changhsing Formation and by
733 numerous shell beds in the Yinkeng Formation (Fig. 15). Chen et al. (2010a) recognized
734 six macrofossil communities from the uppermost Permian to lowest Triassic in Meishan,
735 including the *Rotodiscoceras* sp.–*Paracrithyris pigmaea* (R–P) Community (Bed 24),
736 *Tethyochonetes liaoi* (T) Community (Bed 26), *Paryphella triquetra*–*Tethyochonetes*
737 *liaoi* (P–T) Community (Bed 27), *Claraia griesbachi*–*Ophiceras* sp. (C–O) Community
738 (Bed 32), *Claraia wangi* (C) Community (Beds 40), and

739 *Meishanorhynchia-Lytosphericeras (M-L) Community (Beds 53-55).*

740 Several diversity indices (Shannon and Simpson indices and Dominance) are
741 usually employed to measure community structures. It should be noted that the Shannon
742 measures are the only standard diversity indices that generate meaningful independent
743 alpha and beta components when the community weights are unequal or sampling is
744 uneven (Jost, 2007). Dominance index (D) measures ‘evenness’ of the community from 0
745 to 1, 0 being the most even distribution amongst taxa. Simpson index = $1 - \text{Dominance}$
746 index, and values range from 0 (one taxon dominates the community completely) to 1 (all
747 taxa are equally present) (Hammer et al., 2001). Note that these diversity indices are
748 useful in estimating diversity but are not themselves measures of diversity. Their
749 numerical equivalent indicates changes of true diversity (Jost, 2007; Kosnik and Wagner,
750 2006). Conversion of both Shannon and Dominance indices to true diversities developed
751 by Jost (2006, 2007) is performed to indicate true diversity changes over the P-Tr
752 transition. In addition, the bias-corrected Simpson evenness index (Olszewski, 2004) is
753 also applied to estimate the evenness within and among communities examined here.
754 Detailed community structural indices are listed on Table 5.

755 The late Changhsingian *R-P* community has Shannon index (H) of 2.029, which

756 is slightly smaller than the same index of 2.796 for the Changhsingian brachiopod
 757 *Cathaysia–Martinia* (*C–M*) community reported from the Shaiwa Group of southern
 758 Guizhou Province, southwest China (Chen et al., 2006a), but is slightly larger than the
 759 same index of 1.879 for the Wuchiapingian brachiopod *Edriosteges*
 760 *poyangensis–Spinomarginifera lopingensis* (*E–S*) Community reported from the basal
 761 Lungtan Formation of the Daijiagou section, Chongqing city, southwest China (Chen et
 762 al., 2005b). Dominance of the *R–P* community, $D = 0.1519$, also lies between the same
 763 indices of the above Changhsingian and Wuchiapingian brachiopod communities, with D
 764 $= 0.07375$ and 0.178 , respectively (Chen et al., 2010b, table 4). It is also true for evenness
 765 of community (E) that the *R–P* community has E of 0.8453 , which lies between 0.9262
 766 and 0.822 , the values of E for the *C–M* and *E–S* communities, respectively (Chen et al.,
 767 2010b). Accordingly, the *R–P* community is typical of Late Permian shelly communities.
 768 In contrast, H values of all post-extinction communities, 1.47 , 1.565 , 0.7559 , 0 ,
 769 and 1.288 for the *T*, *P–T*, *C–O*, *C*, and *M–L* communities, respectively (Table 5) are much
 770 smaller than the same values of the Changhsingian and Wuchiapingian communities, $H =$
 771 2.796 and 1.879 , respectively. These post-extinction communities therefore are much less
 772 diverse than the pre-extinction communities of the Late Permian, indicating the severe

773 impact of the PTME on marine communities.

774 Changes in both standard diversity Shannon index [Exp (H)] and dominance

775 index (D') between neighboring pairs of communities show that major losses in diversity

776 coincide with the turnovers of the *R-P/T* and *P-T/ C-O* communities, losing 43.6% and

777 55.5% respectively. Similarly, standard diversity dominance (D') increases by 34% and

778 54%, respectively (Table 6). Thus, community structural collapse indicated by a decrease

779 in diversity, coupled with increase in dominance, coincides with two extinctions

780 bracketed at the bases of Beds 25 and 28 at Meishan (Song et al., 2013a). In addition, Exp

781 (H) value increases by 262.6% from the *C* to *M-L* communities, and also increases by

782 70%, coupled with a decrease of 15.2% in D' values, from the *C-O* to *M-L* communities,

783 suggesting an improvement in shelly community structures in Beds 53-55 at Meishan.

784 Structural improvement of the *M-L* community is also reinforced by comparison

785 between the *M-L* community and the Anisian *Madonia* sp.-*Rhaetina angustaeformis*

786 (*M-R*) Community, which marks the recovery of benthic communities in the Anisian

787 (Chen et al., 2010b). The Anisian community has H and D values of 2.051 and 0.1501

788 respectively (Chen et al., 2010b, table 4), but the same values for the *M-L* community are

789 H = 1.288 and D = 0.4379, respectively. Consequently, the *M-L* community embraces

790 much more improved diversity indices than other Griesbachian communities in Meishan,
791 but instead has a much lower diversity and higher dominance index than both
792 pre-extinction and recovery communities.

793

794 **5. Trace fossils and bioturbation**

795

796 At Meishan, Bottjer et al. (1988) made the first attempt to ecologically test the
797 PTME based on trace-fossil assemblages. These authors, however, could not collect
798 sufficient trace fossils because of restricted exposure at that time, but they noted that
799 ichnotaxa from the PTB beds are dominated by *Planolites* and *Chondrites*, which indicate
800 generally a poorly oxygenated environment (Bottjer et al., 1988). Later, Cao and Shang
801 (1998) reported a few ichnotaxa such as *Thalassinoides*, *Planolites* and *Skolithos* from
802 the PTB beds of Meishan, but *Skolithos* was later rejected by these authors (Cao and
803 Zheng, 2009; Zheng et al., 2013). Zhang and Tong (2010) also examined trace fossils
804 recorded in drilling cores through the P-Tr transition in Meishan. Although these authors
805 clarified that trace fossil evidence suggests two ecologic crises, coinciding with Beds
806 24e-27 and Beds 34-39, respectively (Zhang and Tong, 2010), the documented

807 ichnofossils are too few to support such a conclusion (see Section 7). As a result, several
808 lines of evidence show that trace fossils are reasonably abundant in the PTB beds in
809 Meishan. They however remain poorly understood owing to inadequate trace fossil
810 specimens.

811 Here, we document our observations at all PTB sites newly exposed during the
812 construction of the geological park in the GSSP Meishan in the 2000s, which uncovered
813 extensive fresh exposures along all the quarries (Fig. 1E). Abundant trace fossils were
814 collected from Beds 8-9 and 23-24 of the Changhsing Formation and Beds 26-27 and
815 35-57 of the Yinkeng Formation. The ichnofabric indices (ii, *sensu* Droser and Bottjer,
816 1986) and bedding plane bioturbation index (BPBI, Miller and Smail, 1997) throughout
817 the upper Changhsing Formation and entire Yinkeng Formation are also examined.

818

819 *5.1. P-Tr ichnotaxa and their stratigraphic distributions in Meishan*

820

821 *5.1.1. Stratigraphic distribution of ichnoassemblages*

822

823 A total of 17 ichnospecies in 13 ichnogenera and a problematic ichnotaxon have

824 been found in the P-Tr transition at Meishan (Figs. 16-18). Major characteristics,
825 stratigraphic distributions and interpretation of each ichnotaxon are tabulated here (Table
826 7). Trace fossils are distributed mainly in Beds 8-9 and Beds 23-24 of the Changhsing
827 Formation, and in Beds 27, 35-53, 55-57 of the Yinkeng Formation. Of these, the lower
828 Changhsing Formation (Beds 8-9) ichnoassemblage is dominated by relatively large
829 burrows of *Thalassinoides* isp. 1 (Fig. 16A, D) and resting traces of *Lockeia* isp. (Fig.
830 16F). *Paleophycus* isp. (Fig. 16B) is also commonly present in Beds 8-9.

831 The trace-fossil assemblage from Beds 23-24e is characterized by tree-like
832 traces of *Dendrorhaphie* isp. (Fig. 17F) and abundant burrows of problematic status. The
833 latter is represent by simple, straight, unbranched burrows (Fig. 17B-C), each originating
834 at a small, close end and extending distally to form a horn-shaped burrow with an open
835 distal end (Fig. 17B-C). Burrow diameters vary from 20-27 mm. Some burrows penetrate
836 the bedding at acute angles, and others are horizontally distributed on bedding planes.
837 The burrow has a distinct circular wall, about 2-5 mm thick. These burrows are preserved
838 in dark organic muddy limestone and filled with light-colored, coarse-grained sediments.
839 These morphologies suggest that this problematic form differs from all known ichnotaxa.

840 Another feature of the Bed 24 ichnoassemblage is the presence of abundant

841 ichnofossils near the contact between Beds 24d and 24e, including several distinct
842 burrowing ichnotaxa: *Balanoglossites triadicus*, *Taenidium* isp., *Thalassinoides* isp. 1,
843 and *Planolites* isp. 1. Of these, *Balanoglossites* is represented by vertical tubes (Fig. 16C)
844 that penetrate to a depth of 5-10 cm perpendicular to bedding. This ichnogenus occurs
845 usually at omission surfaces that served as sequence boundaries (i.e., Knaust, 1998).
846 These traces are preserved in limestone of the upper part of Bed 24d (Fig. 3). *Taenidium*
847 burrows (Fig. 16E, 17E) are also very common in Bed 24d-e, and they are usually
848 cylindrical, straight, unbranched, and backfilled. This ichnoassemblage as a whole
849 represents the *Balanoglossites* ichnofacies associated with the omission surface, as
850 described by Knaust (1998, 2004). In addition, horizontal burrows of *Planolites* isp. are
851 densely packed on top of Bed 24e (Fig. 17A, E), which is just beneath the base of Bed 25,
852 in which the PTME horizon is placed (Jin et al., 2000).

853 Abundant burrows were also found in association with an omission surface
854 within Bed 27. These burrows and the possible firmground surface have long remained
855 disputed, although several recent studies have addressed an ichnoassemblage of this bed
856 (Cao and Shang, 1998; Cao and Zheng, 2009; Zheng et al., 2013). Burrow systems
857 preserved in Bed 27 therefore are re-studied here (see below).

858 Beds 28-34 are barren of trace fossils. The remaining part of the lower Yinkeng
859 Formation (Beds 35-51) yields rare trace fossils, which are dominated by simple,
860 horizontal burrows of *Planolites* isp. 2 (Fig. 18A-B). Increasing numbers of ichnotaxa
861 occur in the upper Yinkeng Formation and are characterized by the presence of the
862 tree-like burrow system of *Chondrites* isp. (Bed 52; Fig. 18C) and relatively complicated
863 burrows of *Thalassinoides* isp. 3 (Fig. 18D-E) and *Treptichnus* isp. (Fig. 18G-H).

864

865 5.1.2. *Ichnofabric changes within Bed 27*

866

867 Within Bed 27, intensive burrowing on an omission surface, characteristic of the
868 *Glossifungites* ichnofacies, caused a pronounced relief on the firmground surface up to 3
869 cm high near the boundary between Beds 27a and 27b (Figs. 19-20). The firmground of
870 *Glossifungites* ichnofacies is partly covered by a faintly laminar black muddy limestone
871 that seems resistant to weathering. Highly irregular relief at the surface of the firmground
872 indicates that the solid rock was affected deep subsolution (Savrda, 1992). Trace fossils
873 increase upward to the contact between Beds 27c and 27d, which is overlain by finely
874 laminated muddy limestone (Bed 27d) again.

875 To reconstruct complete burrowing systems within Bed 27, one complete sample
876 of the bed (from base to top) was cut and separated into three blocks (Fig. 19). The
877 transverse view from three polished slabs shows the colonizing zonation (CZ) from base
878 to top of the bed by various ichnocoenoses within a 16-cm-thick unit (Fig. 20).

879 CZ I: This is a historical zone, a unit that is beyond the reach of even the deepest
880 burrows (Fig. 20). CZ I includes the first 2-3 cm of the lower part of Bed 27, which
881 comprises gray, calcareous mudstone to muddy limestone and is almost barren of trace
882 fossils. Minor bioturbation is also limited. Body fossils are scarce, except some small,
883 thin-bedded brachiopods and foraminifers. Pyrite framboids and crystals are relatively
884 rich and occur in both sediments and fossil shells (see Section 6).

885 CZ II: This is a transitional zone (Fig. 20), which is extremely heterogeneous
886 from the activity of deeper burrows (Savrda, 1992). Sediments in this zone were
887 semi-lithified to form a firmground substratum. Firmground sediments are dark-colored,
888 and are disrupted by passively filled burrows of an ichnoassemblage characteristic of the
889 *Glossifungites* ichnofacies. Representative ichnogenera include *Arenicolites*,
890 *Gastrochaenolites*, *Psilonichnus*, and *Thalassinoides*. Of these, *Arenicolites* comprises
891 vertical burrows that penetrate into the dark gray sediments. *Gastrochaenolites* comprises

892 tear-shaped borings, now filled with light gray, coarse-grained sediments in a
893 dark-colored firmground lime muddy substrate. This ichnogenus is commonly present in
894 the *Trypanites* ichnofacies as well (Wilson and Palmer, 1998; Benner and Ekdale, 2004).
895 The vertical cylindrical burrows of *Psilonichnus* are inclined, with bedding in the distal
896 end (Buatois and Mángano, 2011). *Thalassinoides* is typified by its Y-shaped ramification.
897 All these burrows have unlined walls and are filled with light gray-colored,
898 coarse-grained sediments of the overlying layer, indicating that these burrows were
899 passively filled.

900 CZ III: This is a very thin, highly condensed omission surface (Fig. 20), which is
901 characterized by some coarse-grained, reworked sediments that were generated by
902 frequent activity of wave currents. This omission surface is distinguished from the
903 underlying firmground ichnocoenosis of *Glossifungites* ichnofacies and overlying
904 softground ichnocoenosis of *Cruziana* ichnofacies (see below).

905 CZ IV: This is a mixed unit (Fig. 20), which is saturated with water and totally
906 homogenized by bioturbation. This unit, about 5 cm thick, yields ichnocoenoses
907 represented by minute burrows of *Diplocraterion* isp. and tear-shaped borings, which
908 resemble the vertical features of *Chondrites* and small *Planolites*. Owing to the soft

909 nature of substrate and intensive bioturbation, burrow boundaries and morphologies have
910 become blurred, making it difficult to identify them confidently to ichnogenus level. This
911 ichnoassemblage, together with the soft substrate, is characteristic of the softground
912 ichnocoenosis of *Cruziana* ichnofacies (Seilacher, 1977).

913 CZ V: This thin unit is devoid of bioturbation and comprises finely laminated
914 muddy layers (Fig. 20), which yield small pyrite framboids (see Section 6), indicating the
915 establishment of a quiet, low energy and probably reduced environment.

916

917 5.2. *Extent of bioturbation*

918

919 Ichnofabric indices (Droser and Bottjer, 1986) of the Upper Changhsing
920 Formation (Beds 22–24) are usually rather low (ii1-2) with several peaks reaching 3 (ii3)
921 except for the horizons near the boundary between Beds 24d and 24e (Fig. 3) that records
922 an ichnofabric index of 4 (ii4), but bioturbated strata are about 80% of the entire
923 measured units of the Changhsing Formation. Ichnofabric indices decrease to 2 (ii 2)
924 again at the upper part of Bed 24e, then increase to 3 (ii3) at the top of the bed. No
925 ichnofabrics are observed in Beds 25-26a. The ii value surges to 3 (ii3) in Beds 26b-27,

926 with 40% strata bioturbated. Beds 28-34 are void of ichnofabrics again. The ii value of
927 Beds 35-57 remains rather low (ii1) except for several peaks reaching 2 (ii2) in Beds 42,
928 46, 52-53, and 56-57 (Fig. 3). Only 15% of the examined units are bioturbated.
929 Accordingly, ichnofabric indices of the upper Changhsing Formation vary from 2 to 4
930 (ii2–4). Averagely 80% strata of the upper Changhsing Formation are significantly
931 bioturbated. Ichnofabric indices from Bed 27 remain relatively high (ii4), although only
932 40% strata are bioturbated. The remaining part of the lower Yinkeng Formation records a
933 rather low ii value (ii1) and no strata are significantly bioturbated. Ichnofabric indices in
934 the middle and upper parts of the Yinkeng Formation vary from 1 to 2 (ii1-2). On average,
935 15% of strata are significantly bioturbated.

936 In the upper Changhsing Formation, the two bedding planes in Bed 23
937 containing *Dendrorhaphis* isp. (Fig. 17F) and the problematic trace (Fig. 17D), show
938 coverage of 90% and thus indicate a BPBI of 5 (Fig. 3). The same BPBI value (ii 5) is also
939 estimated from two horizons of Beds 24d, containing *Taenidium* burrows. Bedding planes
940 from other horizons in the upper Changhsing Formation generally have bioturbation
941 coverage varying from 10% to 60%, indicating BPBI of 1-5. For the top bedding plane of
942 Bed 24e, just below the mass extinction horizon, containing *Planolites* (Fig. 17A, E) the

943 coverage was up to 90%, indicating a BPBI of 5. Beds 25-26a have the lowest BPBI, with
944 almost no bioturbation recorded. Several bedding planes from Beds 26b-27 show changes
945 in coverage from 20% to 40%, indicating a BPBI of 2-4. Bedding plane coverage in Beds
946 28-34 is generally rather low because bioturbation is broadly absent. Beds 35-51, overall,
947 have bioturbation coverage <10%, but some bedding planes containing *Planolites* show
948 coverage up to 20%, indicating a BPBI of 2. Another bedding plane containing
949 *Chondrites* has coverage up to 90%, indicating a BPBI of 5. In the upper Yinkeng
950 Formation, one bedding plane containing *Thalassinoides* shows coverage up to 20%,
951 indicating a BPBI of 2.

952

953 5.3. Changeover of trace-fossil diversity over the P-Tr transition

954

955 Ichnodiversity, represented by ichnogenic richness, decreased remarkably
956 over the P-Tr transition. Eight ichnogenera are commonly encountered in the uppermost
957 Changhsing Formation: *Balanoglossites*, *Dendrorhaphie*, *Lockeia*, *Paleophycus*,
958 *Planolites*, *Problematica*, *Taenidium*, and *Thalassinoides* (Fig. 21A). Only *Planolites* is
959 present at the top of Bed 24e, dropping to 87.5% in the upper part of Bed 24e. All

960 ichnotaxa disappear at the top of Bed 24e, coinciding with the PTME. As a consequence,
961 Beds 25-26a are barren of ichnotaxa. The ichnofauna rebounded in Bed 26b and
962 diversified in Bed 27, including seven ichnogenera: *Arenicolites*, *Diplocraterion*,
963 *Gastrochaenolites*, *Psilonichnus*, *Thalassinoides*, *Chondrites*, and *Planolites*. Of
964 particular interest is the presence of four vertically burrowing ichnogenera (*Arenicolites*,
965 *Diplocraterion*, *Gastrochaenolites*, *Psilonichnus*) and one relatively complicated
966 burrowing ichnogenus (*Thalassinoides*), implying that ichnodiversity almost reached the
967 pre-extinction level in Bed 27 (Fig. 21A). All ichnotaxa disappeared soon after (in Bed
968 28). As a consequence, Beds 28-34, ranging through conodont zones *I. isarcica* and *I.*
969 *planata* Zones, lack any ichnotaxa and remained poorly bioturbed (Fig. 3). The
970 post-extinction rebound of ichnotaxa is marked by the presence of *Planolites* in Bed 35.
971 Since then, ichnodiversity remained at a rather low level and did not increase until the
972 middle-late Griesbachian, which saw the rise of *Chondrites* in Bed 52. Although
973 *Chondrites* disappeared in the middle-late Griesbachian, the trace-fossil assemblage
974 slightly diversified and included *Planolites*, *Treptichnus* and *Thalassinoides*.
975 As a result, P-Tr ichnotaxa underwent two pronounced reductions in diversity
976 coinciding with the two episodes of PTME calibrated to the bases of Beds 25 and 28.

977 Ichnofaunas fell to their lowest diversity in the early Griesbachian, and experienced a
978 slow increase in diversity throughout the middle-late Griesbachian (Fig. 21A). However,
979 post-extinction trace-fossil diversity never returned to the pre-extinction level.

980

981 *5.4. Burrow size variations through the P-Tr transition*

982

983 Nine bedding planes were examined to determine the size distribution of burrow
984 diameters of *Arenicolites*, *Dendrorhaphé*, *Diplocraterion*, *Paleophycus*, *Planolites*,
985 *Problematica*, *Taenidium*, *Thalassinoides*, and *Treptichnus* (Fig. 22). Burrow size change
986 over the P-Tr transition is apparent, especially in *Planolites*, as well as other traces such
987 as *Balanoglossites*, *Chondrites*, *Dendrorhaphé*, *Taenidium*, *Thalassinoides*, *Treptichnus*,
988 and *Problematica* (Fig. 22). *Planolites* is distributed in ten horizons throughout the
989 uppermost Changhsingian to middle-upper Griesbachian, and thus is a good proxy for
990 size variation of trace fossils over the P-Tr transition. Mean diameters of the Changhsing
991 Formation *Planolites* burrows are 7 mm, 8.5 mm, and 5.5 mm, respectively from three
992 horizons, with maximum burrow diameter up to 9.2 mm (Fig. 22A). Burrow sizes
993 decrease remarkably across the boundary between Beds 24 and 25, the PTME horizon

994 (Fig. 1B), with mean burrow diameters of 1.7 mm and the greatest burrow diameter only
995 2.2 mm in Bed 27 (Fig. 22A). Burrow sizes of *Planolites* remain very small throughout
996 the early-middle Griesbachian and become larger by the late Griesbachian (Beds 54-57).
997 These late Griesbachian traces are still much smaller than their counterparts recorded in
998 the pre-extinction strata (Fig. 22A). Comparable size change over the P-Tr transition is
999 also demonstrated by both the greatest size and mean size of *Thalassinoides* from the
1000 same interval (Fig. 22B).

1001 Several other ichnotaxa in the uppermost Permian have mean and maximum
1002 diameters, such as *Balanoglossites* (4.6 mm, 6.4 mm), *Dendrorhipe* (12 mm, 17 mm),
1003 problematica (22 mm, 28 mm), and *Taenidium* (7.8-8.8 mm, 9.2 mm), that are obviously
1004 larger than that of those ichnotaxa confined to the lowest Triassic, i.e., *Chondrites* (2.8
1005 mm, 5.6 mm) and *Treptichnus* (6.3 mm, 6.3 mm) (Fig. 22C-D). When the measurements
1006 of all 273 burrows measured from the P-Tr strata of Meishan are combined, both mean
1007 and maximum diameters exhibit remarkable reduction across the boundary between Beds
1008 24 and 25 and remain very low values until Bed 27. The same values further decline from
1009 Bed 27 to Beds 28-34, and then undergo a stepwise increase through Beds 35-57 (Fig.
1010 21B)

Trace-fossil size variations over the P-Tr transition are consistent with figures from northern Italy (Twitchett, 1999; Twitchett and Barras, 2004) and South China (Chen et al., 2011). It should be noted that the Early Triassic *Planolites* traces are much smaller than their Changhsingian counterparts at Meishan (Fig. 22A), unlike the same traces elsewhere (Pruss and Bottjer, 2004). *Planolites* is supposed to be the least susceptible to mass extinction because this simple trace can be produced by a variety of organisms (Pruss and Bottjer, 2004). Accordingly, the Changhsingian *Planolites* and their Early Triassic counterparts may have been made by different organisms.

5.5. Trace fossil form and complexity

The Changhsing Formation trace fossils are morphologically diversified, and include simple, horizontal burrows (*Planolites*), vertical or oblique burrows (*Balanoglossites* and *Problematica*), resting traces (*Lockeia*), and complex forms (*Dendrorhape*, *Taenidium*, and *Thalassinoides*). They, however, disappear across the PTME horizon (base of Bed 25). Both *Planolites* and *Thalassinoides* rebound in Bed 27, but decrease markedly in size in comparison with their Changhsingian counterparts.

1028 *Thalassinoides* is also less complex than the same trace recorded in the Changhsingian.

1029 Complex forms, and resting and vertical traces of the Changhsingian (*Balanoglossites*,

1030 *Lockeia*, *Taenidium*, *Dendrorhipe*, and Problematica) vanish in Bed 27. Instead, the

1031 relatively complex burrow systems of the *Glossifungites* ichnofacies, i.e., *Arenicolites*,

1032 *Gastrochaenolites*, *Psilonichnus*, and *Thalassinoides*, characterize the ichnoassemblage

1033 in the lower part of Bed 27. Vertical burrows of *Diplocraterion*, together with *Chondrites*

1034 and *Planolites* also occur in the upper part of Bed 27. Accordingly, ichnotaxa recovered

1035 from the pre-extinction level are similar to those in Bed 27 in terms of complexity,

1036 although these burrows are much smaller than their counterparts elsewhere.

1037 Early Griesbachian traces are dominated by small, simple, horizontal burrows of

1038 *Planolites*, as reported elsewhere (Twitchett and Barras, 2004; Pruss and Bottjer, 2004;

1039 Fraiser and Bottjer, 2009; Chen et al., 2011, 2012). In the middle-late Griesbachian trace

1040 fossils become slightly more complex and are marked by the presence of *Chondrites*,

1041 *Thalassinoides* and *Treptichnus*, although these burrows are still very small. Nevertheless,

1042 these middle-late Griesbachian burrows are branched and form slightly complex

1043 networks, and thus are more complex than the *Planolites*-dominated ichnoassemblage in

1044 the early Griesbachian.

1045 As a result, trace-fossil complexity, reflecting behavioral complexity of the
1046 trace-makers, decreased dramatically during the PTME. Then, the trace-fossil
1047 assemblage shows an increase in complexity, varying from simple, horizontal traces (i.e.,
1048 *Planolites*) in the early Griesbachian to relatively complex traces (*Chondrites*,
1049 *Thalassinoides* and *Treptichnus*) in the middle-upper Griesbachian. In particular, the
1050 reappearance of *Thalassinoides* and *Treptichnus* probably implies increasing behavioral
1051 complexity that typically indicates the beginning of biotic recovery elsewhere (Twitchett
1052 and Barras, 2004).

1053

1054 5.6. Infaunal tiering

1055

1056 Levels of tiering above and below the sediment were greatly reduced after the
1057 PTME (Ausich and Bottjer, 1982, 2002). At Meishan, the change in infaunal tiering over
1058 the P-Tr transition is reflected by the penetration depth of burrows (Fig. 21C), which was
1059 measured in the field. Vertical burrows of the Changhsing Formation may extend a
1060 maximum depth of 10 cm into the sediment, indicating a rather deep tiering level (ii5). In
1061 contrast, burrows of *Planolites* and *Thalassinoides* recorded in Bed 27 may penetrate to <

1062 2 cm into the sediment. In particular, *Thalassinoides* commonly shows the second tiering
1063 level (ii2) (Bottjer and Droser, 1994). Early Griesbachian *Planolites* has burrows
1064 extending to a maximum depth of only 0.5 cm (Fig. 21C) indicating the lowest tiering
1065 level (ii1) (Bottjer and Droser, 1994). Thus, tiering fell to its minimum level in the early
1066 Griesbachian. An increase in tiering level during the middle Griesbachian is marked by
1067 the presence of *Chondrites*, an anoxic burrow system penetrating to a depth up to 1-2 cm
1068 and indicating the second tiering level (ii2) (Bottjer and Droser, 1994). The same tiering
1069 level is also reflected in upper Griesbachian *Thalassinoides* and *Treptichnus* burrows,
1070 which may extend to a maximum depth of 1-2 cm (Fig. 21C). Accordingly, the tiering
1071 level decreases significantly across the PTME horizon in Meishan, and then increases
1072 throughout the Griesbachian (Fig. 21C).

1073

1074 **6. Size variations of pyrite framboids and redox conditions over the P-Tr transition**

1075

1076 Pyrite is commonly present in the latest Changhsingian to Griesbachian rocks at
1077 Meishan (Wignall and Hallam, 1993), which is also confirmed by our observations of
1078 thin sections through the P-Tr transition at Meishan. Several pyrite-enriched beds have

1079 been treated as indications of anoxic conditions at Meishan (Wignall and Hallam, 1993).
1080 In particular, pyrite framboids, which are spherical aggregates of pyrite microcrystals, are
1081 rather abundant in these pyrite-enriched beds near the PTB at Meishan (Jiang et al., 2006;
1082 Shen et al., 2007). Pyrite framboids in ancient and modern sediments are interpreted as
1083 the result of redox conditions (e.g., Bond and Wignall, 2010), and these authors show that
1084 small framboids, usually 3-5 μm in diameter, indicate euxinic conditions (H_2S -bearing,
1085 O_2 -free bottom waters). Accordingly, pyrite framboids have been considered as one of
1086 the most important pieces of evidence indicating redox conditions over the P-Tr transition
1087 worldwide (Wignall et al., 1998, 2005; Jiang et al., 2006; Shen et al., 2007; Gorjan et al.,
1088 2007; Bond and Wignall, 2010; Algeo et al., 2011b).

1089 At Meishan, Jiang et al. (2006) reported that pyrite framboids are commonly
1090 present in all beds through the PTB (Beds 24-29), based on etched residues from bulk
1091 samples. Shen et al. (2007) also observed framboids *in situ* on polished blocks and etched
1092 residues. Both studies detected that framboids are abundant in Bed 25. Contrasting to
1093 Jiang et al.'s (2006) observation, Shen et al. (2007) found no pyrite framboids in Bed 27.
1094 However, unequal sampling in various beds near the PTB, for instance, 40 g each from
1095 Beds 25 and 26, but only 5 g each from Beds 24, 27, 28 and 29 may have biased their

1096 observation (Shen et al., 2007). Bed 27 comprises various lithologies from its base to top,
1097 which may have been deposited in different environments (Figs. 19-20). Thus, pyrite
1098 framboids may be absent in these bioturbated layers (i.e., CZs II, III-IV in Bed 24; Fig.
1099 20), but instead may occur in finely laminated layers without bioburbation (i.e., CZs I and
1100 V; Fig. 20).

1101 We have also observed pyrite framboids in continuous thin sections throughout
1102 Beds 24-30. We used a FEI Quanta 400 Scanning Electron Microscope (SEM) equipped
1103 with a GENESERS 2000 energy dispersive spectrometer (EDS) at the State Key
1104 Laboratory of Biogeology and Environmental Geology, China University of Geosciences,
1105 Wuhan, China. SEM images and EDS spectra were produced by the Zeiss VPSEM
1106 coupled with an energy dispersive X-ray spectrometer. We confirmed Jiang et al.'s (2006)
1107 observation that both pyrite framboids and crystals occur in Bed 27 on brachiopod shells
1108 and in foraminiferal tests and sediments (Fig. 23). In addition, we measured framboid
1109 sizes in samples from Beds 29-60 using the SEM. Pyrite framboids are abundant in
1110 samples from 17 horizons over the P-Tr transition (Fig. 24). The majority of framboid
1111 diameters in most measured beds are smaller than, or around 5 μm , except for Beds 28
1112 and 44, in which most framboids have diameters of 7-8 μm . Moreover, framboid

1113 diameters are concentrated in a narrow size range ($< 10\mu\text{m}$) in Beds 27, 28, 43, and 58. In
1114 contrast, they have a greater size range in Beds 24b, 24e, 25-26, 29-30, 39, 42, 49, 51-52
1115 and 56, with maximum diameter up to $20\mu\text{m}$ in Bed 51.

1116 Bond and Wignall (2010, table 1) proposed several characters, including
1117 framboid diameter and pyrite morphology, to determine redox conditions during
1118 deposition. In general, when framboids are small (mean diameters: $3\text{-}5\mu\text{m}$), abundant,
1119 with a narrow size range, and form the dominant pyrite fraction, they could have been
1120 deposited in euxinic condition (with a persistently sulfidic lower water column). If
1121 framboids are small (mean diameters: $4\text{-}6\mu\text{m}$), abundant, with a few, larger forms, and
1122 dominate the pyrite fraction, then they could have been deposited in anoxic condition
1123 (without oxygen in bottom waters for long periods). When framboids have mean
1124 diameters of $6\text{-}10\mu\text{m}$ and are moderately common, with a few, larger framboids together
1125 with some crystalline pyrite, they could have been deposited in lower dysoxic condition
1126 (with weakly oxygenated bottom waters). In upper dysoxic condition (with partial
1127 oxygen restriction in bottom waters) framboids are commonly to rarely present, with a
1128 broad range of sizes, only a small proportion of framboids $< 5\mu\text{m}$, and the majority of
1129 pyrite as crystals. In oxic condition (without oxygen restriction), no framboids are present,

1130 and pyrite crystals occur rarely.

1131 If these five criteria given by Bond and Wignall (2010) are followed, we can
1132 determine redox conditions over the P-Tr transition in Meishan. Bed 24 contains
1133 abundant framboids, usually around 5 μm in diameter with some larger framboids, and
1134 their size range is relatively broad, pointing to anoxic conditions. Framboids in Beds
1135 25-26 are usually 3-5 μm in diameter, a narrow size range, and no pyrite crystals are
1136 present, suggesting euxinic conditions (Fig. 25). Framboids from Bed 27 have a relatively
1137 large diameter and a broad size range (Fig. 24), and are also associated with some large
1138 pyrite crystals, pointing to a lower to upper dysoxic condition (Fig. 25). Pyrite framboids
1139 are moderately common in Bed 28 and have mean diameters of 8-9 μm , but no larger
1140 framboids and crystalline pyrite occur. Thus, Bed 28 is inferred to be deposited in a
1141 transitional zone between anoxic and lower dysoxic conditions based on the criteria
1142 determining redox conditions proposed by Bond and Wignall (2010). Redox conditions
1143 became euxinic soon after in Bed 29, in which framboids are very small (3-5 μm) and
1144 have a narrow size range, without pyrite crystals. It should be noted that no pyrite
1145 framboids were found in Beds 30-35, although a pronounced negative excursion of
1146 carbon isotopes (Xie et al., 2007) and environmental stress indicated by biomarker

1147 signals (Yin et al., 2012) occur in these beds. Framboids from Beds 39 and 42 indicate
1148 euxinic-anoxic transitional conditions in terms of diameter, size range and association
1149 with pyrite crystals. Framboids from Bed 43 are 4-6 μm in diameter, but have some larger
1150 forms and are also associated with some pronounced pyrite crystals, and thus indicate a
1151 lower to upper dysoxic condition. Then, redox conditions indicated by pyrite framboids
1152 changed to anoxic to euxinic transitional conditions. Surprisingly, framboids from Bed
1153 58 suggest euxinic condition, which coincides with the last negative excursion of carbon
1154 isotopes in the middle-late Griesbachian detected by Burgess et al. (2014).

1155

1156 **7. Assessing ecologically PTME and its aftermath**

1157

1158 *7.1. Testing ecologically extinction patterns*

1159

1160 The updated fossil record from Meishan shows two pronounced declines of
1161 species richness at the bases of Beds 25 and 28 (Song et al., 2013a; Fig. 26). Similarly,
1162 fossil fragment contents recorded in thin sections also show two distinct drops in both
1163 abundance and diversity corresponding to the top of Bed 24e and base of Bed 28 (Figs. 6,

1164 14). Further, ichnodiversity also declined within Beds 24 and 27. In Bed 24, trace fossils
1165 are rather abundant and comprise four distinct ichnogenera: *Balanoglossites*, *Planolites*,
1166 *Taenidium* and *Thalassinoides* in horizons near the boundary between Beds 24d and 24e,
1167 but only *Planolites* persisted into Bed 24e-6, in which relatively large burrows are
1168 densely packed, indicating a considerably high bioturbation level. All ichnotaxa
1169 disappeared in Beds 25-26a. Similarly, ichnotaxa decline from five ichnogenera
1170 (*Arenicolites*, *Gastrochaenolites*, *Planolites*, *Psilonichnus*, and *Thalassinoides*) in CZ II
1171 (Bed 27b) to three ichnogenera (*Diplocraterion*, *Chondrites* and *Planolites*) in CZ IV
1172 (Bed 27c), and then further declined and disappeared at the top of Bed 27d. Other proxies
1173 of trace fossils and bioturbation also show two pronounced declines corresponding to the
1174 bases of Beds 25 and 28. Clearly, the PTME ecologic crisis comprised two phases,
1175 coinciding with metazoan extinctions calibrated to the bases of Beds 25 and 28 (Song et
1176 al., 2013a).

1177 In addition, both fossil fragment contents and ichnodiversity show that a
1178 pronounced decline in diversity and abundance started at the stratal interval 10 to 19 mm
1179 below the top of Bed 24e. The boundary between Beds 24e-5 and 24e-6 is the most
1180 distinct eliminated horizon of skeletal fragment of major fossil groups, coinciding with

1181 end-Permian sulfur anomaly (Kaiho et al., 2006a) and the start of the negative
1182 end-Permian carbon isotopic excursion (Kaiho et al., 2009), and thus may indicate the
1183 PTME. Abundant sponge spicules above this event horizon indicate that they lasted in
1184 seawater for a while, although complete sponge fossils disappeared at the PTME event. It
1185 is therefore unlikely that the disappearance of calcareous fossils at the top of bed 24e-6
1186 was a result of an increase in the input of terrestrial material associated with the facies
1187 shift, as indicated by the lithologic shift from the limestone of Bed 24 to the claystone of
1188 Bed 25 and black shale of Bed 26. Instead, the extinction of calcareous biota and the
1189 associated environmental perturbation was most likely caused the lithologic change from
1190 limestone to mudstone. As a result, the sharp decline in biotic abundance and diversity
1191 10-19 mm below the top of Bed 24e may signal the first episode of the PTME previously
1192 inferred from statistical paleontological data (Song et al., 2013a).

1193

1194 7.2. *Ecologic collapse lagging behind biodiversity crisis during the PTME*

1195

1196 At Meishan, the Permian biota experienced a dramatic drop in diversity at the
1197 base of Bed 25, with 172 species (94%) being wiped out in Beds 25-26 and no

1198 pronounced reduction of species richness in Bed 28 (Jin et al., 2000). The updated fossil
1199 record obtained from Meishan shows that species richness was reduced by at least 79%
1200 across the boundary between Beds 24e and 25, compared to 65% loss in species richness
1201 across the boundary between Beds 27d and 28 (Song et al., 2013a). This means that
1202 marine animals suffered a more severe depletion in species richness in the first phase of
1203 the PTME than in the second phase of the same event (Fig. 26). The biodiversity decline
1204 pattern from Meishan is confirmed by the same pattern at a further seven PTB sections in
1205 South China (Song et al., 2013a). It should also be noted that generic richness declined by
1206 a similar magnitude, 85% and 82%, in the first and second phases of the PTME,
1207 respectively in Meishan, but both generic and species richness underwent a stepwise
1208 decline from the uppermost Changhsingian to lowest Griesbachian (Fig. 26).
1209 Consequently, biotic diversity suffered a larger loss in the first episode than in the second
1210 episode of the PTME in terms of the number of lost taxa. This pattern is reinforced by
1211 fossil fragment content variations across the PTME horizons. Fossil components usually
1212 occupy nearly 70% in all rock in strata below Bed 25, but only about 30% in Bed 27, and
1213 FFA lost nearly 60% in thin section (Fig. 14). Over the same period, 11 Permian orders
1214 declined to five orders in Bed 27, losing 54.5% in ordinal richness.

1215 Both the standard diversity Shannon index [Exp (H)] and dominance index (D')

1216 assess whether the shelly community possesses a healthy structure. Exp (H) values

1217 declined by 43.6% from the *R–P* to *T* communities, and 55.5% from the *P–T* to *C–O*

1218 communities, coinciding with the first and second phases of the PTME, respectively. This

1219 means that the shelly communities suffered a greater loss in community diversity in the

1220 second phase of the PTME than in the first phase. Similarly, standard diversity

1221 dominance (D') increases by 34% and 54% during the two pronounced drops in diversity,

1222 respectively (Table 6). This means that the shelly communities became more uneven after

1223 the second phase of the PTME than after the first phase. Thus, shelly communities

1224 underwent relatively more serious ecologic crisis in the second phase than in the first

1225 phase of the PTME. This observation is also reinforced by ichnofaunal variations and

1226 ichnofabric changes over the P-Tr transition in Meishan.

1227 The presence of seven ichnogenera in Bed 27 suggests that ichnogenic

1228 richness nearly recovered to the pre-extinction level, although there was a taxonomic loss

1229 in Beds 25-26a. In contrast, a more dramatic ichnofaunal loss occurred in the second

1230 phase of the PTME, corresponding to Bed 28. As a consequence, Beds 28-34 are barren

1231 of ichnotaxa. Thus, ichnofaunas suffered a more severe decline in the second phase of the

1232 PTME. This pattern is also strengthened by burrow size variations and tiering level
1233 changes, both of which remained relatively high in the Changhsingian, and experienced a
1234 stepwise decline through Beds 23-27, then fell to their lowest values in the early
1235 Griesbachian (Beds 28-34). Ichnofabric variation also shows that Bed 27 still remains
1236 highly bioturbated and yields rather complex burrow systems of the *Glossifungites*
1237 ichnofacies and *Cruziana* ichnofacies, which are commonly present in the pre-extinction
1238 period, thus showing the largest turnover at the base of Bed 28 rather than at the base of
1239 Bed 25. In contrast, ichnotaxa became very rare after the second phase of the PTME,
1240 although 2-3 ichnotaxa rebounded in the middle-late Griesbachian. Consequently, the
1241 greatest losses of ichnotaxa correspond to the top of Bed 27, simultaneous with the
1242 second phase of metazoan extinction in Meishan (Song et al., 2013a). This ichnodiversity
1243 drop coincides with a remarkable decrease in tiering level (Fig. 21) and burrowing
1244 intensity (Fig. 3). Ichnofabric indices recorded in the upper Changhsing Formation are
1245 rather high (ii4-5) (Fig. 3). Complex traces of both the *Glossifungites* and *Cruziana*
1246 ichnofacies recorded in Bed 27 (Figs. 19-20) also indicate a fairly high ichnofabric index
1247 (ii3-4). Consequently, there was not a sharp decrease, but a gradual decrease, in
1248 burrowing intensity (ii4-5 down to ii3-4) over the first phase of the PTME. This is in

1249 sharp contrast to the pronounced drop in biodiversity of metazoans in this phase of the
1250 PTME (Fig. 26), suggesting a gradual worsening in environmental conditions.

1251 In contrast, almost all of the complex traces of the *Glossifungites* and *Cruziana*
1252 ichnofacies disappeared in the second phase of the PTME. The early Griesbachian
1253 *Planolites* is confined to discrete horizons (ii1-2) separated by metres of unbioturbated
1254 sediment, and indicates a rather low ichnofabric index (ii1) (Fig. 3). A low ichnofabric
1255 index indicates an absence or rarity of burrowing infauna, which in turn implies a stressed
1256 environment immediately after the PTME (Chen et al., 2011). Accordingly, the great loss
1257 of burrowing infauna and associated environmental stress occur at the horizon between
1258 Beds 27 and 28. These facts imply that ecologic collapse of marine ecosystems
1259 post-dated the metazoan biodiversity crisis at Meishan.

1260 Contrasting to the two-stage extinction pattern (Song et al., 2013a), Shen et al.
1261 (2011b) and Wang et al. (2014) argued that the severest biodiversity declines fell in a
1262 short period equivalent to Beds 25-28 of Meishan, and there was one prolonged
1263 extinction rather than two discrete episodes. Indeed, Beds 25-28 represent a very short
1264 duration of about 60 ky (Burgess et al., 2014). However, all lines of evidence, including
1265 fossil fragment contents, and ichnofabric and community structural changes, show that

1266 the P-Tr ecologic crisis clearly comprises two pronounced steps, at the bases of Beds 25
1267 and 28 (Figs. 14, 21, 26). Nevertheless, whether the mass extinction occurred as one
1268 prolonged event or two pulses, all studies agree that Beds 25-28 of Meishan and their
1269 equivalents represent a critical period when the greatest biotic turnover of life on Earth
1270 took place in Meishan. During this critical turnover period, the ecologic crisis clearly
1271 lagged behind the diversity decline. As a result, the Meishan fossil record shows that the
1272 mass extinction started with a dramatic depletion of biodiversity and ended with a severe
1273 ecologic crisis.

1274

1275 *7.3. Dramatic increase in seawater surface temperature and its consequence*

1276

1277 Recent oxygen isotopic studies of conodont bioapatites reveal that sea surface
1278 temperature rose ~9 °C from Bed 24e to Bed 27a in Meishan (Joachimski et al., 2012;
1279 Sun et al., 2012; Fig. 26). However, the precise relationship between temperature
1280 increase and biotic extinction remains unclear owing to the lack of oxygen isotopic values
1281 from Bed 25, the base of which coincides with the PTME (Shen et al., 2011b) or the first
1282 phase of the PTME (Song et al., 2013a). The same is also true for the relationship

1283 between the temperature rise and the dramatic negative carbonate carbon isotopic
 1284 excursion (Fig. 26). The solution is to undertake more detailed study of conodont oxygen
 1285 isotopes of the PTB beds from less condensed sections than Meishan to evaluate whether
 1286 temperature change leads or lags the extinction (Burgess et al., 2014). Hinojosa et al.
 1287 (2012) found a negative shift in $\delta^{44/40}\text{Ca}$ of conodont bioapatite in the Great Bank of
 1288 Guizhou, South China during the same interval as temperature increase in Meishan. This
 1289 $\delta^{44/40}\text{Ca}$ excursion is also coupled with a major shift in $\delta^{13}\text{C}_{\text{carb}}$ composition from an
 1290 average of approximately +3.5‰ in the latest Permian to approximately –1‰ in the
 1291 earliest Triassic (Payne et al., 2004). The anomaly of $\delta^{44/40}\text{Ca}$ therefore was interpreted as
 1292 a consequence, in part, of acidification of the ocean. Thus, oceanic acidification in
 1293 platform areas of the Great Bank of Guizhou may have resulted from elevated seawater
 1294 temperature (Burgess et al., 2014). However, this ocean acidification seems not to have
 1295 spread to the Meishan area because rather abundant and diverse complex traces of both
 1296 *Glossifungites* and *Cruziana* ichnofacies occur in Bed 27 (Figs. 19-20), although
 1297 calcareous skeletons decreased significantly in Beds 25-28 (Fig. 14).
 1298 Previously, the irregular surface occurring in the middle of Bed 27 at Meishan
 1299 was interpreted as a submarine dissolution surface, explained by a regional ocean

1300 acidification in South China (Payne et al., 2007, but see Wignall et al., 2009). This
1301 pronounced irregular surface, however, was re-interpreted as a distinct firmground
1302 surface, on which abundant complex traces of *Glossifungites* ichnofacies occur (see
1303 Section 3.5). Firmgrounds of *Glossifungites* ichnofacies are usually characteristic of
1304 initial transgression, and such horizons are usually employed to define sequence
1305 boundaries (Buatois and Mángano, 2011). Thus, no sign of acidification is recorded in
1306 Bed 27 in Meishan.

1307 Another potential consequence of elevated temperature is intensified chemical
1308 weathering (Sheldon, 2006) and consequent increased physical erosion of soils on land
1309 (Sephton et al., 2005; Xie et al., 2007), or a combination of these processes. These
1310 processes are also indicated by the increased chemical index of alteration (CIA) profile
1311 immediately after the first phase of the PTME (Bed 25; Fig. 26). It should be noted that
1312 the CIA value was calculated as $\text{Al}_2\text{O}_3/(\text{Al}_2\text{O}_3+\text{K}_2\text{O}+\text{Na}_2\text{O})$ (Zhao et al., 2013a), a
1313 modification of the original CIA equation (Nesbitt and Young, 1982). Increased chemical
1314 weathering during the PTME and its aftermath is also mirrored by the Eu/Eu* profile of
1315 conodont bioapatites (Zhao et al., 2013a). The latter rare-earth elemental (REE) proxy is a
1316 useful tracer of sediment provenance because fractionation between Eu^{+2} and Eu^{+3} does

1317 not occur under Earth-surface conditions (Elderfield and Greaves, 1982). Eu^{+2} tends to
1318 become segregated into feldspar during magmatic differentiation, resulting in Eu/Eu^*
1319 values >1.0 in the crystal fraction and <1.0 in the residual fluid (Zhao et al., 2013a).
1320 Eu/Eu^* ratios >1.0 are characteristic of magmas from lower crustal or mantle sources
1321 where substantial feldspar crystallization has taken place (Condie, 2001). Although the
1322 REE “fingerprint” of the ash-rich clastics is reflected by both CIA and Eu/Eu^* profiles
1323 that match one another throughout P-Tr transition in Meishan (Fig. 26) and these ash beds
1324 near the PTB likely sourced from regional convergent continent marginal volcanisms
1325 (Gao et al., 2013, 2014), the shift toward Eu/Eu^* values of 1.0–1.5 in Bed 24e,
1326 immediately preceding the PTME, may be evidence of a transient influx of volcanic
1327 material with a lower crustal or mantle source. Zhao et al. (2013a) argued that these
1328 mantle-sourced ash fingerprints indicated by Eu/Eu^* values could be the product of the
1329 Siberian trap eruption (Reichow et al., 2009). Thus, this volcanic eruption could have
1330 caused the severe biocrisis and rapid increase in sea-surface temperature occurring
1331 ~20-80 kyr later following the estimate of maximum and minimum sedimentation rates
1332 given by Burgess et al. (2014).

1333 Burgess et al. (2014) also estimated the rate of temperature rise in Beds 25-28 as

1334 an ~ 1 °C increase per 6,000 y, which is comparable with the rate and magnitude of the
1335 increase at the Paleocene–Eocene Thermal Maximum (Zeebe et al., 2009) and
1336 Pleistocene/Holocene postglacial warming (~ 2 °C/5 ka) (Lea et al., 2000). However, this
1337 estimate of the rate of temperature rise needs to be cautious because no temperature data
1338 is available from Bed 25 and the temperature rise spans Beds 24e-27 (Sun et al., 2012).
1339 To sum up, although the killing mechanism of the ~ 9 °C increase of seawater surface
1340 temperature on organisms remains unclear, this rapid temperature increase coincides with
1341 biotic turnover and ecologic collapse during the PTME at Meishan. Nevertheless, the
1342 elevated temperature seems to have had little effect on ichnofaunas and ichnofabrics, as
1343 indicated by abundant ichnofaunas living in the firmground of the *Glossifungites*
1344 ichnofacies (Bed 27), but instead resulted in dramatic losses of fossil skeletons in
1345 sediments (Fig. 14).

1346 In addition, Sun et al. (2012) reported the acme of high seawater temperatures
1347 occurred in the late Griesbachian, corresponding to the upper *I. isarcica* Zone and lower
1348 *C. planata* Zone (Sun et al., 2012, fig. 2), which range from Beds 48-54. These two zones
1349 are amended herein (Fig. 2) and are equivalent to the upper part of *C. planata* Zone in the
1350 revised conodont zonation (Fig. 2). This acme of high temperature postdates the second

1351 negative shift excursion of carbon isotopes of Xie et al. (2007) and includes the second
1352 negative shifting excursion of carbon isotopes of Burgess et al. (2014). Surprisingly, this
1353 interval saw an increase in biodiversity (Chen et al., 2002, 2007), ichnological
1354 amelioration and bioturbation (Fig. 3). Accordingly, the acme of high temperature has
1355 little effect on faunas.

1356

1357 *7.4. Anoxic events and biotic response*

1358

1359 *7.4.1. Anoxic events* At Meishan, Wignall and Hallam (1993) recognized an anoxic
1360 event associated with the PTME, but considered that the greatest acme of anoxia, coupled
1361 with a maximum flooding event, occurs in the lower Yinkeng Formation. Wignall and
1362 Twitchett (2002) believed that the oxygen-deficient waters spread into exceedingly
1363 shallow settings near the PTB in the Tethys regions (i.e., South China). More recently,
1364 multiple geochemical signals indicate the existence of anoxic to euxinic conditions
1365 before, during and after the PTME at Meishan.

1366 An exceptional increase in sea surface temperature is also believed to be

1367 synchronous with the flooding of shelf areas with anoxic and euxinic waters during the

1368 P-Tr transition (Sun et al., 2012). Both extremely high values of total organic content
1369 (TOC) (Yin et al., 2012) and reduced sizes of pyrite framboids (Fig. 26) indicate euxinic
1370 to anoxic condition in Beds 25-26, coinciding with the PTME. However, pyrite
1371 framboids from Bed 27 are generally larger than $5\ \mu\text{m}$ in diameter with abundant crystals
1372 and thus indicate the upper part of dysoxic conditions (Fig. 25). Moreover, high
1373 bioturbation levels are also observed in upper part of Bed 26 and multiple layers of Bed
1374 27. Thus, a euxinic to anoxic condition was probably limited only to Beds 25-26a, which
1375 is less than 20 ka based on duration estimate of conodont zones from these beds (Table 2),
1376 a much shorter period than previously thought. The anoxic condition of the water column
1377 is also reflected by the abrupt increase of Ce/Ce^* values of conodont bioapatite from
1378 $\sim 0.7\text{--}0.8$ in Beds 23-24 to $0.9\text{--}1.1$ in Beds 25-27b (Zhao et al., 2013a; Fig. 26). Values of
1379 $0.7\text{--}1.0$ are sustained through Beds 27c to 30, above which Ce/Ce^* decreases to $0.5\text{--}0.7$.
1380 It should be noted that Ce/Ce^* ratios derived from Bed 27a-d are not totally in accordance
1381 with size analysis of pyrite framboids, which shows that Bed 27a-d may represent redox
1382 conditions ranging from anoxia to upper level of dysoxia (Fig. 25). Although Ce/Ce^*
1383 values from Meishan may have been biased by the fingerprint of clay input, Ce/Ce^*
1384 values of $0.9\text{--}1.1$ indicate an anoxic depositional system (Zhao et al., 2013a; Shen et al.,

1385 2012). This inference is consistent with the results of earlier studies documenting anoxia
1386 around the PTME in South China PTB sections (Grice et al., 2005; Algeo et al., 2007;
1387 Shen et al., 2007; Cao et al., 2009; Bond and Wignall, 2010; Luo et al., 2010) and
1388 globally (Algeo et al., 2010, 2011b; Brennecka et al., 2011).

1389 Euxinic condition may have occurred prior to the PTME in Meishan, i.e., Beds
1390 22-24, demonstrated by the anomaly of sulfur isotopes (Shen et al., 2011a) and various
1391 biomarker signals in Beds 22-24 (Grice et al., 2005; Cao et al., 2009; Luo et al., 2010,
1392 2011). Algeo et al. (2011a) also interpreted the anoxic and euxinic conditions as a result
1393 of an expansion of the oxygen minimum zone (OMZ) in the water column over the P-Tr
1394 transition. These authors considered that the OMZ may have expanded prior to the PTME
1395 in Meishan.

1396 A post-extinction reduced condition is also indicated by a pronounced negative
1397 excursion of carbon isotopes in Beds 34-36 (Xie et al., 2007; Luo et al., 2010; Fig. 26),
1398 coupled with an increase in TOC and terrestrial input indicated by various biomarker
1399 signals (Yin et al., 2012), and elevated contents of CO₂ (Fraiser and Bottjer, 2007). The
1400 CIA profile slightly increases in Beds 34-36, indicating elevated chemical weathering on
1401 land, which is consistent with the increased TOC and terrestrial input (Yin et al., 2012). In

1402 addition, conodont bioapatite from Beds 33–39 generally yields lower Ce/Ce* ratios
1403 (0.4–0.7) that may indicate an oxic to suboxic depositional environment. Conodont
1404 bioapatite Ce, however, was probably derived mainly from detrital clay minerals and
1405 taken up during diagenesis, as indicated by other REE proxies (Zhao et al., 2013). If so,
1406 the observed Ce/Ce* ratios only reflect the REE composition of the source clays (Zhao et
1407 al., 2013a).

1408 Alternatively, size variations of pyrite framboids indicate that Beds 27–29 record
1409 a dramatic redox change from upper dysoxic to euxinic conditions (Fig. 25). A euxinic to
1410 anoxic condition prevailed throughout Bed 29 to Bed 42 (Fig. 25). The combination of
1411 mean size of framboids and presence of both larger framboids and crystal pyrites
1412 indicates Bed 43 may be deposited in a lower to upper dysoxic condition. If a redox
1413 interpretation is warranted, then this pattern suggests that the anoxic episode following
1414 the PTME in Meishan lasted a relatively long duration, probably ~50 kyr. Moreover,
1415 mean sizes and morphologies of framboids from Beds 44–58 also generally reflect an
1416 anoxic to euxinic condition, which, however, is not supported by various ichnological
1417 proxies.

1418

1419 7.4.2. *Biotic response*

1420

1421 The pre-extinction anoxic to euxinic conditions are generally supported by the
1422 presence of abundant small pyrite framboids, 3-5 μm in diameter, in Beds 23-24 (Figs.
1423 23-24). However, biodiversity of metazoans remains very stable, with 64-78 species in
1424 34-44 genera in each layer through Beds 24a to 24e (Fig. 26). Bed 24 contains 82 species
1425 in 47 genera, and there are similar numbers in Bed 23 (Jin et al., 2000). Thus, no major
1426 losses in species and generic richness are recognizable in Beds 23-24. Fossil fragment
1427 contents are almost the same in each layer through Beds 22-24, except for the top 1-2 cm
1428 of Bed 24e, in which there is a pronounced loss in fossil components across the boundary
1429 between Beds 24e-5 and 24e-6 (Figs. 6, 14). Fossil fragment contents fell by >16% in thin
1430 section from Beds 24e-5 to 24e-6. The FFA of Bed 24e-5 comprises 10 major fossil
1431 groups that are commonly present in all Permian limestones, but five clades, ostracods,
1432 bryozoans, calcareous sponges, gastropods, and macroalgae, disappeared, losing 50%,
1433 across this boundary (Figs. 6, 14). The FFA of Bed 24e-6 is dominated by sponge spicules
1434 (35%) and thus has a high dominance and low diversity and evenness, in contrast to the
1435 low dominance, high diversity/evenness FFA in Bed 24e-5 (Fig. 6). Furthermore, the last

1436 occurrence of Permian fusulinids was also bracketed to the base of Bed 24e-6 (Kaiho et
1437 al., 2006b).

1438 Ichnodiversity also declined significantly across the boundary between Beds
1439 24e-5 and 24e-6 (Fig. 21A). These relatively complex or vertical burrows such as
1440 *Balanoglossites* and *Thalassinoides*, which usually occur in oxygenated settings,
1441 disappeared at the base of Bed 24e-6. Instead, only simple, horizontal burrows of
1442 *Planolites* occur in Bed 24e-6. Ichnofabrics, however, do not exhibit a major change
1443 across the same boundary (Fig. 3), with abundant *Planolites* burrows being densely
1444 packed on the surface of Bed 24e-6. However, most geochemical studies do not have such
1445 a high sampling intensity, and thus neglected this boundary.

1446 Both metazoan biodiversity and fossil fragment contents experienced dramatic
1447 declines in Beds 25-26a. Other ecologic measures, such as community structures,
1448 ichnodiversity, burrow size, tiering level, and ichnofabric variation, also indicate an
1449 ecologic crisis in Beds 25-26a, coinciding with the anoxia indicated by both pyrite
1450 framboid sizes and various geochemical signals (Fig. 26). However, the metazoan fauna
1451 from Bed 27 is rather abundant and diverse, including 66 species in 34 genera (Song et al.,
1452 2013a). Both community structural indices and fossil fragment contents indicate that

1453 metazoans had recovered well in Bed 27. The presence of abundant complex burrows in
1454 Bed 27 indicates the infaunal proliferation in the firmground of *Glossifungites*
1455 ichnofacies (Fig. 20). The occasional occurrence of pyrite framboids in Bed 27 may
1456 indicate a very short period of anoxic condition, but Bed 27, as a whole, represents a
1457 dysoxic to oxic condition in which benthos and infaunas proliferated.

1458 By contrast, all data, including the low ichnodiversity (only *Planolites*), small
1459 burrow size, low trace complexity, low ichnofabric from Beds 29-51 indices and low
1460 tiering level as well as low-diversity metazoans (Chen et al., 2007, 2010a), support the
1461 view that anoxic conditions may have prevailed throughout the early Griesbachian in
1462 Meishan (Wignall and Hallam, 1993; Xie et al., 2007; Yin et al., 2012). Of these, Beds
1463 29-34 are barren of trace fossils and bioturbation. This is supported by trace fossil size,
1464 which is also regarded as a proxy for paleoenvironmental conditions (Twitchett, 1999;
1465 Pruss and Bottjer, 2004). In general, small-sized traces are usually found in poorly
1466 oxygenated sediments (Savrda and Bottjer, 1987) or brackish environments (Pemberton
1467 et al., 1982; Buatois et al., 2005) or habitats with low nutrient supply (Jumars and
1468 Wheatcroft, 1989). Thus small traces are characteristic of stressed environments
1469 (Twitchett, 1999; Pruss and Bottjer, 2004). The dramatic size reduction of trace fossils

1470 after the PTME indicates environmental stresses associated with the PTME, and the small
1471 sizes of Early Triassic traces suggest prolonged environmental stress following the event
1472 (Bottjer et al., 2008).

1473

1474 *7.5. Testing extinction mechanisms*

1475 Multiple scenarios have been proposed to interpret the killing mechanisms of the
1476 PTME, including widespread anoxia, hypercapnia, massive volcanic eruption, global
1477 warming, ocean acidification, and increased sediment flux (Erwin, 2006; Knoll et al.,
1478 2007; Clapham and Payne, 2011; Algeo and Twitchett, 2010; Algeo et al., 2011a;
1479 Joachimski et al., 2012; Sun et al., 2012; Burgess et al., 2014; Song et al., 2014). However,
1480 the true causes of this biocrisis still remain unclear due to the incomplete record of
1481 evidence supporting any of these alternatives.

1482 Recently, Song et al. (2013a) suggested that different extinction mechanisms
1483 may have driven each of these two pulses given their differences in biodiversity and
1484 ecologic losses. These authors considered that anoxia may be related to the first-pulse
1485 losses of biota, but played a crucial role in the second-pulse biocrisis (Song et al., 2013a).
1486 Elevated sea-surface temperature not only resulted in the spread of anoxia but also killed

1487 directly shallow-water taxa, while the anoxia killed the deep-water organisms (Song et al.,
1488 2014). However, extinction and survival selectivity of various fossil groups is more
1489 complicated than previously thought (i.e., Song et al., 2013a, 2014). This is because
1490 various elements of the same clade may have different lifestyles. For instance, the P-Tr
1491 brachiopods have six types of lifestyles based on attachment modes on the substratum:
1492 burrowing, body cementation, pedicle attaching on substratum, body spines anchoring on
1493 substratum, pedicle attaching on objects, and clasping spines on other shells/or objects
1494 (Chen et al., 2006a, 2011b). These brachiopods having the last two types of attachment
1495 modes behaviour like nektons. Moreover, some shallow-water elements were also able to
1496 survive in deep niches during the latest Permian (Chen et al., 2006a). It is also true for the
1497 P-Tr bivalves that embrace several lifestyles (Huang et al., 2014). Accordingly, our high
1498 resolution comprehensive analyses of biodiversity, community structural, fossil fragment,
1499 ichnological, and redox condition changes associated with these two discrete events
1500 allow an evaluation of the proposed kill mechanisms for these two ecologic crises.

1501 Most of the Permian brachiopods became extinct in the first extinction. The
1502 survivors are dominated by chonetids or chonetid-like productids or small, thin-shelled
1503 spiriferids/rhynchonellids that usually have attachment modes of clasping spines on other

1504 shells/or objects or pedicle-attaching on other shells or objects (Chen et al., 2005a,
1505 2011b). These survivors attached their bodies on some float objects (i.e., other shells and
1506 algae) suspending above the seafloor (Chen et al., 2005a, 2011b), and thus provided
1507 brachiopods higher adaptability surviving the deleterious environments, i.e., increased
1508 acidity of precipitation (Wignall, 2007), large-scale marine acidification (Clapham and
1509 Payne, 2011) and widespread anoxia (Wignall and Twitchett, 2002; Payne and Clapham,
1510 2012) during the first biocrisis. Inarticulated brachiopods i.e., lingulids also survived this
1511 event, although having a burrowing lifestyle. This is because lingulids are able to survive
1512 in poorly oxygenated waters due to having respiratory pigment acting the function to
1513 transport oxygen or to store oxygen within the body tissues under anoxic conditions or
1514 during cessation of respiration (Williams et al., 1997).

1515 Similarly, Huang et al. (2014) argued that the anoxia or acidification may have
1516 impacted seriously on bivalve's extinction and survival selectivity during the first
1517 extinction based on ecologic analysis of the P-Tr bivalves. As a result, both brachiopod's
1518 and bivalve's evidence indicates that anoxia impacted clearly by in the first-pulse
1519 biocrisis (Chen et al., 2011b; Huang et al., 2014). The acidification associated with this
1520 extinction cannot be excluded (Clapham and Payne, 2011; Hinojosa et al., 2012). The

1521 anoxia or acidification, however, lasted a very short duration, ~30 ka, as discussed above.

1522 Furthermore, a rapid increase of about ~9°C of sea-surface temperature (within a
1523 period of ~30 ka) across Beds 24e-27a (Sun et al., 2012) must have facilitated respiratory
1524 frequency and accelerated oxygen consumption of most brachiopods and become lethal
1525 to brachiopods, and thus causes mortality, regardless their shallower or deeper habitats
1526 (Chen et al., 2014b in this volume). The rapidly elevated seawater temperature also
1527 coincides with the first dramatic losses of body fossil biodiversity and fossil fragments as
1528 well as moderate losses of ichnodiversity and community diversity, and a moderate
1529 decrease in bioturbation, tiering levels of infaunas and burrow sizes.

1530 However, marine ecosystems seem not to have collapsed completely during the
1531 first-pulse crisis (Chen and Benton, 2012), some organisms survived the short
1532 environmental and climatic devastation. Thus, both biodiversity and ichnodiversity, and
1533 all of ichnological and community structural measures rebounded rapidly in Bed 27a-d
1534 (Fig. 26).

1535 Like the first extinction, the second-pulse biocrisis is also associated with a clay
1536 bed (Bed 28), in which pyrite framboids indicate a lower dysoxic to anoxic condition (Fig.
1537 25). However, the redox condition became euxinic soon after and is indicated by

1538 framboids obtained from the base of Bed 29. Thus, a dramatic change from upper dysoxic
1539 to oxic condition in Bed 27 to euxinic condition in basal Bed 29 indicates an
1540 anoxia/euxinia coincided with the 2nd biocrisis, which is followed by a long period of
1541 euxinic to anoxic conditions, which was probably driven by a relatively long (>62 ka)
1542 acme of high temperature (up to 35-37°C) in earliest Griesbachian. Accordingly, both
1543 epifaunal and infaunal ecosystems collapsed after suffering such a long period of lethally
1544 hot seawater temperature and widespread anoxia in earliest Triassic oceans (Fig. 26).
1545 This is reinforced by the replacement of free-lying brachiopod-dominated communities
1546 in Bed 27 with nekton-dominated communities in Beds 31-37 (Chen et al., 2010a) and
1547 Beds 28-34 barren of bioturbation and ichnofossils (Figs. 3, 26). As stated above, these
1548 surviving brachiopods yielded from Beds 26-27 should have enhanced resistant ability to
1549 anoxic or acidified water mass near seafloor because they survived from the first-pulse
1550 crisis. The morality of the free-lying brachiopods in the second-pulse crisis is probably
1551 due to the loss of other shells or float algae, on which the brachiopods attach using either
1552 pedicle or clasping spines.
1553 Accordingly, the killing mechanisms for these two extinction events near the PTB seem
1554 not to be fundamentally different from one another, although no sign of acidification has

1555 been reported in the second phase of the PTME. However, a short anoxia or acidification
1556 probably caused by a rapid increase in seawater temperature may have played an
1557 important role in the first-pulse biocrisis, while the long-lasting and widespread anoxia
1558 induced by a long period of high temperature condition may have killed most organisms
1559 in the second-pulse crisis.

1560 *7.6. Post-extinction amelioration of marine ecosystems in late Griesbachian*

1561

1562 Post-extinction benthic communities did not appear to return to normal until the
1563 early Middle Triassic (Chen and Benton, 2012). The deleterious environment that
1564 prevailed in early Triassic oceans may be largely responsible for this long-delayed
1565 recovery (Bottjer et al., 2008). In particular, Early Triassic carbon isotopic records show
1566 several negative excursions that indicate sharp global warming (Payne et al., 2004), and
1567 these coincide with diversity drops. Furthermore, intrinsic relationships between
1568 organisms and ecosystem structures may also have slowed down biotic recovery
1569 following the PTME (Chen and Benton, 2012). Recent studies show that the biotic
1570 recovery process may be mirrored by stepwise establishment of trophic structures of
1571 marine ecosystems throughout Olenekian-Anisian interval (Chen and Benton, 2012).

1572 However, biotic recovery may occur earlier in oxygenated environments (Twitchett et al.,
1573 2004; Beatty et al., 2008; Zonneveld et al., 2010). As a result, Early Triassic marine
1574 environments were not always deleterious globally. Chen et al. (2007) also detected that
1575 marine environments had greatly ameliorated during the late Griesbachian in Meishan.
1576 The sea-floor recuperation, including shallowing water depth, increasing oxygenation
1577 and oceanic productivity, coincides with an increase in benthic biodiversity, signalling
1578 that ecologic and environmental restoration might have initiated in the late Griesbachian
1579 (Chen et al., 2002, 2007).

1580 The example of elevated recovery of the benthic community in late
1581 Griesbachian at Meishan is also strengthened by community structural changes and
1582 ichnofabric variation through the PTB to late Griesbachian. The Exp (H) value increases
1583 by 262.6% from the *C* to *M–L* communities, and also increases 70%, coupled with a
1584 decrease of 15.2% in *D'* values, from the *C–O* to *M–L* communities, suggesting an
1585 improvement in shelly community structures in the upper Yinkeng Formation at Meishan
1586 (Chen et al., 2002, 2007).

1587 Trace fossils and ichnofabrics documented here also show that the late
1588 Griesbachian trace-fossil assemblage is marked by significant increases in ichnodiversity,

1589 burrow size, trace complexity, tiering level, and bioturbation level, in comparison with
1590 early Griesbachian ichnoassemblages, although they did not achieve Changhsingian
1591 levels (Fig. 21). Thus, the Meishan trace fossils, together with increasing diversity in the
1592 shelly community, sedimentary structures (HCS), up-shallowing sedimentary cycle and
1593 geochemical proxies (Chen et al., 2007), suggest that biotic recovery recorded in the
1594 upper Yinkeng Formation may be categorized as recovery stage 2 (*sensu* Twitchett, 2006),
1595 and also mark the return of parts of the meso-consumer functioning group within the
1596 ecosystem trophic structure, which usually occurs in the Spathian around the world (Chen
1597 and Benton, 2012).

1598

1599 **8. Conclusions**

1600

1601 Updated conodont biostratigraphy allows the establishment of eight conodont
1602 zones from the latest Changhsingian to early Griesbachian at Meishan, the *C. yini*, *C.*
1603 *meishanensis*, *H. changxingensis*, *C. taylorae*, *H. parvus*, *I. staeschei*, *I. isarcica*, and *C.*
1604 *planate* zones. Microstratigraphic analysis shows that a major turnover in fossil fragment
1605 contents and ichnodiversity occurs across the boundary between Beds 24e-5 and 24e-6,

1606 suggesting the actual mass extinction horizon in thin section. Bed 27 contains a
1607 firmground of *Glossifungites* ichnofacies rather than the previously proposed submarine
1608 dissolution surface or hardground surface. Fossil fragment contents show a dramatic
1609 decline in both fossil component percentage and assemblage diversity in Beds 25-26a,
1610 coinciding with metazoan mass extinction. Fossil fragment content, ichnodiversity and
1611 all ichnofabric proxies (including burrow size, tiering level, and bioturbation level)
1612 throughout the uppermost Changhsing to Yinkeng formations indicate that the P-Tr
1613 ecologic crisis comprises two discrete stages, coinciding with the first and second phases
1614 of the PTME, in support of a proposed two-stage extinction pattern of metazoans over the
1615 P-Tr transition. The PTME was of short duration, lasting about 60 kyr. A biodiversity
1616 crisis indicates the start of the extinction interval, but its end is marked by the ecologic
1617 collapse of ecosystems. Thus, the ecologic crisis lagged behind the biodiversity decline
1618 during the PTME. Pyrite framboid size variations suggest that the depositional redox
1619 condition was anoxic to euxinic in the latest Changhsingian, became euxinic in Beds
1620 25-26a, turned to be dyoxic in Bed 27, then varied from euxinic to anoxic through most of
1621 the Griesbachian. Although metazoan biodiversity and fossil fragment contents show
1622 dramatic declines, coinciding with a ~9 °C increase in seawater surface temperature, from

1623 Bed 24e to Bed 27 in Meishan, all ecologic proxies show much smaller effects from the
1624 elevated seawater temperature. Bed 27 contains abundant infauna and shows no signs of
1625 ocean acidification. Pre-extinction anoxic-euxinic conditions had little effect on both
1626 metazoans and infauna. The anoxic event associated with the PTME may have lasted for
1627 much less time than previously thought, and is limited to Beds 25-26a at Meishan. Fossil
1628 fragment contents, ichnofaunas, ichnofabrics and pyrite framboid size all show that
1629 anoxic conditions did not exist in Bed 27. Early Griesbachian anoxia is possible, and may
1630 have caused the rarity of ichnofaunas and metazoans in the lower Yinkeng Formation.
1631 The ichnofauna is characterized by small, simple horizontal burrows of *Planolites*, while
1632 metazoan faunas are characterized by low diversity, high abundance,
1633 opportunist-dominated communities. The killing mechanisms for these two extinction
1634 events near the PTB similar to one another. A rapid increase of ~9 °C in seawater
1635 temperature and its inducing short anoxia or acidification may have played an important
1636 role in the first-pulse biocrisis, while the long-time and widespread anoxia probably
1637 caused by long-time high temperature condition may have resulted in mortality of most
1638 organisms in the second-pulse crisis. Initial recovery of marine ecosystems coupled with
1639 environmental amelioration occurred in the late Griesbachian, marking the return of parts

1640 of the meso-consumer functioning group.

1641

1642 **Acknowledgements**

1643

1644 We thank J. Tong for help in the field and H.J. Song for discussion on foraminiferal
1645 taxonomy of collections from the PTB beds in Meishan. This work was supported by the
1646 973 Program and China 111 Program. It is a contribution to IGCPs 572 and 630.

1647

1648 **References**

- 1649 Algeo, T.J., Twitchett, R.J., 2010. Anomalous Early Triassic sediment fluxes due to
1650 elevated weathering rates and their biological consequences. *Geology* 38,
1651 1023–1026.
- 1652 Algeo, T.J., Chen, Z.Q., Fraiser, M.L., Twitchett, R.J., 2011a. Terrestrial-marine
1653 teleconnections in the collapse and rebuilding of Early Triassic marine ecosystems.
1654 *Palaeogeography, Palaeoclimatology, Palaeoecology* 308, 1–11.
- 1655 Algeo, T.J., Hannigan, R., Rowe, H., Brookfield, M., Baud, A., Krystyn, L., Ellwood,
1656 B.B., 2007. Sequencing events across the Permian–Triassic boundary, Guryul

- 1657 Ravine (Kashmir, India). *Palaeogeography, Palaeoclimatology, Palaeoecology* 252,
1658 328–346.
- 1659 Algeo, T.J., Henderson, C.M., Ellwood, B., Rowe, H., Elswich, E., Bates, S., Lyons, T.,
1660 Hower, J.C., Smith, C., Maynard, B., Hays, L.E., Summons, R.E., Fulton, J.,
1661 Freeman, K.H., 2012. Evidence for a diachronous late Permian marine crisis from
1662 the Canadian Arctic region. *Geological Society of America Bulletin* 124,
1663 1424–1448.
- 1664 Algeo, T.J., Hinnov, L., Moser, J., Maynard, J.B., Elswich, E., Kuwahara, K., Sano, H.,
1665 2010. Changes in productivity and redox conditions in the Panthalassic Ocean during
1666 the latest Permian. *Geology* 38, 187–190.
- 1667 Algeo, T.J., Kuwahara, K., Sano, H., Bates, S., Lyons, T., Elswich, E., Hinnov, L.,
1668 Ellwood, B., Moser, J., Maynard, J.B., 2011b. Spatial variation in sediment fluxes,
1669 redox conditions, and productivity in the Permian–Triassic Panthalassic Ocean.
1670 *Palaeogeography, Palaeoclimatology, Palaeoecology* 308, 65–83.
- 1671 Ausich, W.I., Bottjer, D.J., 2002. Sessile invertebrates. In: Briggs, D.E.G., Crowther, P.R.
1672 (eds.), *Palaeobiology II*. Blackwell Science, Oxford, pp. 384–386.
- 1673 Baldwin, C.T., McCave, I.N., 1999. Bioturbation in an active deep-sea area: Implications

- 1674 for models of trace fossil tiering. *Palaios* 14, 375-388.
- 1675 Beatty, T.W., Zonneveld, J.-P., Henderson, C.M., 2008. Anomalously diverse Early
- 1676 Triassic ichnofossil assemblages in northwest Pangea: a case for a shallow-marine
- 1677 habitable zone. *Geology* 36, 771–774.
- 1678 Benner, J.S., Ekdale, A.A., 2004. Macroborings (*Gastrochaenolites*) in Lower
- 1679 Ordovician Hardgrounds of Utah: Sedimentologic, Paleoecologic, and Evolutionary
- 1680 Implications. *Palaios* 19, 543–550.
- 1681 Benton, M.J., Twitchett, R.J., 2003. How to kill (almost) all life: the end-Permian
- 1682 extinction event. *Trends in Ecology and Evolution* 18, 358–365.
- 1683 Bond, D.P.G., Wignall, P.B., 2010. Pyrite framboid study of marine Permian–Triassic
- 1684 boundary sections: a complex anoxic event and its relationship to contemporaneous
- 1685 mass extinction. *Geological Society of America Bulletin* 122, 1265–1279.
- 1686 Bottjer, D.J., Droser, M.L., Jablonski, D., 1988. Fine-scale resolution of mass extinction
- 1687 events: Trace fossil evidence from the Permian-Triassic boundary in South China.
- 1688 *Geological Society of America, Abstracts with Programs* 20, p. A106.
- 1689 Bottjer, D.J., Clapham, M.E., Frasier, M.L., Powers, C.M., 2008. Understanding
- 1690 mechanisms for the end-Permian mass extinction and the protracted Early Triassic

1691 aftermath and recovery. *GSA Today* 18, 4–10.

1692 Bowring, S.A., Erwin, D.H., Jin, Y.G., Martin, M.W., David, E.K., Wang, W., 1998.

1693 U/Pb zircon geochronology and tempo of the end-Permian mass extinction. *Science*

1694 280, 1039–1045.

1695 Brennecka, G.A., Herrmann, A.D., Algeo, T.J., Anbar, A.D., 2011. Rapid expansion of

1696 oceanic anoxia immediately before the end-Permian mass extinction. *Proceedings of*

1697 the National Academy of Sciences, U.S.A. 108, 17631–17634.

1698 Bromley, R.G., 1996. *Trace Fossils: Biology, Taphonomy and Applications* (2nd edition).

1699 Chapman & Hall, London, 361 pp.

1700 Bromley, R.G., Ekdale, A.A., 1984. *Chondrites*: a trace fossil indicator of anoxia in

1701 sediments. *Science* 224, 872-874.

1702 Buatois, L.A., Mángano, M.G., 2011. *Ichnology: Organism-Substrate Interactions in*

1703 Space and Time. Cambridge University Press, New York. 1–358.

1704 Buatois, L.A., Gingras, M.K., MacEachern, J., Mangano, M.G., Zonneveld, J.P.,

1705 Pemberton, S.G., Netto, R.G., Martin, A., 2005. Colonization of brackish-water

1706 systems through time: Evidence from the trace-fossil record. *Palaios* 20, 321-347.

1707 Burgess, S.D., Bowring, S., Shen, Z.Q., 2014. High-precision timeline for Earth's most

- 1708 severe extinction. *Proceedings of National Academy of Sciences, U.S.A.* 111,
1709 3316–3321.
- 1710 Cao, C.Q., Shang, Q.H., 1998. Microstratigraphy of Permo-Triassic transitional sequence
1711 of the Meishan section, Zhejiang, China. *Palaeoworld* 9, 147-152.
- 1712 Cao, C.Q., Zheng, Q.F., 2007. High-resolution lithostratigraphy of the Changhsingian
1713 stage in Meishan section, Zhejiang. *Journal of Stratigraphy* 31, 14-22.
- 1714 Cao C Q, Zheng Q F. 2009. Geological event sequences of the Permian-Triassic
1715 transition recorded in the microfacies in Meishan section. *Science China Series*
1716 *D-Earth Sciences* 52, 1529–1536
- 1717 Cao, C.Q., Wang, W., Jin, Y., 2002. Carbon isotope excursions across the
1718 Permian-Triassic boundary in the Meishan section, Zhejiang Province, China.
1719 *Chinese Science Bulletin* 47, 1125-1129.
- 1720 Cao, C., Love, G.D., Hays, L.E., Wang, W., Shen, S., Summons, R.E., 2009.
1721 Biogeochemical evidence for euxinic oceans and ecological disturbance presaging
1722 the end-Permian mass extinction event. *Earth and Planetary Science Letters* 281,
1723 188–201.
- 1724 Chen, J., Chen, Z.Q., Tong, J.N., 2010b. Palaeoecology and taphonomy of two

- 1725 brachiopod shell beds from the Anisian (Middle Triassic) of Guizhou, Southwest
- 1726 China: recovery of benthic communities from the end-Permian mass extinction.
- 1727 *Global and Planetary Change* 73, 149-160.
- 1728 Chen, J., Chen, Z.Q., Tong, J., 2011b. Environmental determinants and ecologic
- 1729 selectivity of benthic faunas from nearshore to bathyal zones in the end-Permian
- 1730 mass extinction: brachiopod evidence from South China. *Palaeogeography,*
- 1731 *Palaeoclimatology, Palaeoecology* 308, 84-97.
- 1732 Chen, J.H., 2004. Macroevolution of bivalves after the end-Permian mass extinction in
- 1733 South China. In: Rong, J.Y., Fong, Z.J. (eds), *Biotic mass extinction and*
- 1734 *recovery—evidence from Palaeozoic and Triassic of South China*. China University
- 1735 of Science & Technology Press, Hefei. pp. 647–700.
- 1736 Chen, Z.Q., Benton, M.J., 2012. The timing and pattern of biotic recovery following the
- 1737 end-Permian mass extinction. *Nature Geoscience* 5, 375–383.
- 1738 Chen, Z.Q., Liao, Z.T., 2009. Brachiopod faunas across the Wuchiapingian-
- 1739 Changhsingian (Late Permian) boundary at the stratotype section and subsurface of
- 1740 Changxing area, South China. *Neues Jahrbuch für Geologie und Paläontologie* 254,
- 1741 315–335.

- 1742 Chen, Z.Q., McNamara, K.J., 2006. End-Permian extinction and subsequent recovery of
1743 the Ophiuroidea (Echinodermata). *Palaeogeography, Palaeoclimatology,*
1744 *Palaeoecology* 236, 321–344.
- 1745 Chen, Z.Q., Algeo, T.J., Bottjer, D.J., 2014a. Global review of the Permian–Triassic mass
1746 extinction and subsequent recovery: Part I. *Earth-Science Reviews* 137, 1–5.
- 1747 Chen, Z.Q., Campi, M., Shi, G.R., Kaiho, K., 2005b. Post-extinction brachiopod faunas
1748 from the Late Permian Wuchiapingian coal series of South China. *Acta*
1749 *Palaeontologica Polonica* 50, 343–363.
- 1750 Chen, Z.Q., Fraiser, M.L., Bolton, C., 2012. Early Triassic trace fossils from Gondwana
1751 Interior Sea: Implication for ecosystem recovery following the end-Permian mass
1752 extinction in south high-latitude region. *Gondwana Research* 22, 238–255.
- 1753 Chen, Z.Q., Kaiho, K., George, A.D., 2005a. Survival strategies of brachiopod faunas
1754 from the end-Permian mass extinction. *Palaeogeography, Palaeoclimatology,*
1755 *Palaeoecology* 224, 232–269.
- 1756 Chen, Z.Q., Kaiho, K., George, A.D., Tong, J., 2006b. Survival brachiopod faunas of the
1757 end-Permian mass extinction from northern Italy and south China. *Geological*
1758 *Magazine* 143, 301–327.

- 1759 Chen, Z.Q., Shi, G.R., Kaiho, K., 2002. A new genus of rhynchonellid brachiopod from
1760 the Lower Triassic of South China and implications for timing the recovery of
1761 Brachiopoda after the end-Permian mass extinction. *Palaeontology* 45, 149-164.
- 1762 Chen, Z.Q., Shi, G.R., Yang, F.Q., Gao, Y.Q., Tong, J.N., Peng, Y.Q., 2006a. An
1763 ecologically mixed brachiopod fauna from Changhsingian deep-water basin of South
1764 China: consequence of end-Permian global warming. *Lethaia* 39, 79–90.
- 1765 Chen, Z.Q., Tong, J.N., Fraiser, M.L., 2011a. Trace fossil evidence for restoration of
1766 marine ecosystems following the end-Permian mass extinction in the Lower Yangtze
1767 region, South China. *Palaeogeography, Palaeoclimatology, Palaeoecology* 299,
1768 449–474.
- 1769 Chen, Z.Q., Tong, J.N., Liao, Z.T., Chen, J., 2010a. Structural changes of marine
1770 communities over the Permian–Triassic transition: ecologically assessing the
1771 end-Permian mass extinction and its aftermath. *Global and Planetary Change* 73,
1772 123–140.
- 1773 Chen, Z.Q., Tong, J., Zhang, K., Yang, H., Liao, Z., Song, H., Chen, J., 2009.
1774 Environmental and biotic turnover across Permian–Triassic boundary from shallow
1775 carbonate platform in western Zhejiang, South China. *Australian Journal of Earth*

- 1776 Sciences 56, 775–797.
- 1777 Chen, Z.Q., Tong, J., Kaiho, K., Kawahata, H., 2007. Onset of biotic and environmental
- 1778 recovery from the end-Permian mass extinction within 1-2 million years: A case
- 1779 study of the Lower Triassic of the Meishan section, South China. *Palaeogeography,*
- 1780 *Palaeoclimatology, Palaeoecology* 252, 176-187.
- 1781 Chen, Z.Q., Wang, J.L., Yang, H., Tu, C.Y., Polov, Y., He, W.H., 2014b. Permian-Triassic
- 1782 evolutionary dynamics of the Brachiopoda: paleobiogeography,
- 1783 extinction-survival-recovery, latitudinal diversity gradients, body size variations,
- 1784 and longevity changes. *Earth-Science Reviews* (under review, in this volume).
- 1785 Claoue-Long, J.C., Zhang, Z.C., Ma, G.G. and Du, S.H., 1991. The age of the
- 1786 Permian-Triassic boundary. *Earth and Planetary Science Letters* 105, 182–190.
- 1787 Clapham, M., Payne, J., 2011. Acidification, anoxia, and extinction: a multiple logistic
- 1788 regression analysis of extinction selectivity during the Middle and Late Permian.
- 1789 *Geology* 39, 1059–1062.
- 1790 Condie, K.C., 2001. *Mantle Plumes and Their Record in Earth History*. Cambridge
- 1791 University Press, Cambridge. 306 pp.
- 1792 Crasquin, S., Forel, M.B., Feng, Q.L., Yuan, A.H., Baudin, F., Collin, P.Y., 2010.

- 1793 Ostracods (Crustacea) through the Permian-Triassic boundary in South China: the
- 1794 Meishan stratotype (Zhejiang Province). *Journal of Systematic Palaeontology* 8,
- 1795 331-370.
- 1796 Dasgupta, S., Buatois, L.A., 2012. Unusual occurrence and stratigraphic significance of
- 1797 the *Glossifungites* ichnofacies in a submarine paleo-canyon — Example from a
- 1798 Pliocene shelf-edge delta, Southeast Trinidad. *Sedimentary Geology* 269-270,
- 1799 69-77.
- 1800 Droser, M.L., Bottjer, D.J., 1986. A semiquantitative field classification of ichnofabric.
- 1801 *Journal of Sedimentary Petrology* 56, 558-559.
- 1802 Ekdale, A.A., Bromley, R.G., 2001. A day and a night in the life of a cleft-foot clam:
- 1803 *Protovirgularia-Lockeia-Lophoctenium*. *Lethaia* 34, 119-124.
- 1804 Ekdale, A.A., Bromley, R.G., 2003. Paleoethologic interpretation of complex
- 1805 *Thalassinoides* in shallow-marine limestone, Lower Ordovician, southern Sweden.
- 1806 *Palaeogeography, Palaeoclimatology, Palaeoecology* 192, 221-227.
- 1807 Elderfield, H., Greaves, M.J., 1982. The rare earth elements in seawater. *Nature* 296,
- 1808 214–219.
- 1809 Erwin, D.H., 2001. Lessons from the past: biotic recoveries from mass extinctions.

- 1810 Proceedings of the National Academy of Sciences, U.S.A. 98, 5399–5403.
- 1811 Erwin, D.H., 2006. How Life on Earth Nearly Ended 250 Million Years Ago. Princeton
- 1812 University Press, Princeton, 306 pp.
- 1813 Farabegoli, E., Perri, M.C., 2012. Millennial physical events and the end-Permian mass
- 1814 mortality in the western Palaeotethys: timing and primary causes. In: Talent, J.A.
- 1815 (ed.), Earth and Life, International Year of Planet Earth, Springer, London, pp.
- 1816 719-758.
- 1817 Flugel, E., 1982. Microfacies Analysis of Limestone, Springer, New York, 663 pp.
- 1818 Forel, M.-B., Crasquin, S., 2011. Lower Triassic ostracods (Crustacea) from the Meishan
- 1819 section, Permian-Triassic boundary GSSP (Zhejiang Province, South China). Journal
- 1820 of Systematic Palaeontology 9, 455-466.
- 1821 Fraiser, M.L., Bottjer, D.J., 2007. Elevated atmospheric CO₂ and the delayed biotic
- 1822 recovery from the end-Permian mass extinction. Palaeogeography,
- 1823 Palaeoclimatology, Palaeoecology 252, 164–175.
- 1824 Fraiser, M.L., Bottjer, D.J., 2009. Opportunistic behavior of invertebrate marine
- 1825 tracemakers during the Early Triassic aftermath of the end-Permian mass extinction.
- 1826 Australian Journal of Earth Sciences 56, 841–857.

- 1827 Gao, Q.L., Zhang, N., Xia, W.C., Feng, Q.L., Chen, Z.Q., Zheng, J.P., Griffin, W.L.,
- 1828 O'Reilly, S.Y., Pearson, N.J., Wang, G.Q., Wu, S., Zhong, W.L., Sun, X.F., 2013.
- 1829 Origin of volcanic ash beds across the Permian-Triassic boundary, Daxiakou, South
- 1830 China: Petrology and U-Pb age, trace elements and Hf-isotope composition of zircon.
- 1831 Chemical Geology 360-361, 41-53.
- 1832 Gao, Q.L., Chen, Z.Q., Zhang, N., Xia, W.C., Wang, G.Q., Jiang, T.F., Xia, X.F., 2014.
- 1833 Ages, trace elements and Hf-isotopic compositions of zircon from claystones around
- 1834 the Permian-Triassic boundary in the Zunyi section, South China: implications for
- 1835 nature and tectonic setting of the volcanism. Journal of Earth Sciences 26 (in press).
- 1836 Gorjan, P., Kaiho, K., Kakegawa, T., Niitsuma, S., Chen, Z.Q., Kajiwarra, Y., Nicora, A.,
- 1837 2007. Paleoredox, biotic and sulfur-isotopic changes associated with the
- 1838 end-Permian mass extinction in the western Tethys. Chemical Geology 244,
- 1839 483-492.
- 1840 Gouramis, C., Webb, J.A., Warren, A.A., 2003. Fluviodeltaic sedimentology and
- 1841 ichnology of part of the Silurian Grampians Group, western Victoria. Australian
- 1842 Journal of Earth Sciences 50, 811-825.
- 1843 Grice, K., Cao, C., Love, G.D., Bottcher, M.E., Twitchett, R.J., Grosjean, E., Summons,

- 1844 R.E., Turgeon, S.C., Dunning, W., Jin, Y., 2005. Photic zone euxinia during the
- 1845 Permian-Triassic superanoxic event. *Science* 307, 706-709
- 1846 Hammer, O., Harper, D.A.T., Ryan, P.D., 2001. PAST: palaeontological statistics
- 1847 software package for education and data analysis. *Palaeontologia Electronica* 4, 1–9.
- 1848 Häntzschel, W., 1975. Trace fossils and problematica. In: Teichert, C. (ed.), *Treatise of*
- 1849 *Invertebrate Paleontology* (2nd Edition), Part W, Miscellanea, Supp 1. University of
- 1850 Kansas and Geological Society of America, Lawrence, Kansas, 269 pp.
- 1851 He, J.W., 1981. Clay minerals in the Changhsingian stratotype section and the basal part
- 1852 of Yinkeng Formation, with reference to the Permo-Triassic boundary (in Chinese).
- 1853 *Journal of Stratigraphy* 5, 197–206
- 1854 He, J.W., Rui, L., Chai, Z.F., 1987. The latest Permian and earliest Triassic volcanic
- 1855 activities in the Meishan area of Changxing, Zhejiang. *Journal of Stratigraphy* 11,
- 1856 194–199.
- 1857 He, W., Feng, Q., Gu, S., Jin, Y., 2005. Changxingian (Upper Permian) Radiolarian fauna
- 1858 from Meishan D section, Changxing, Zhejiang, China, and its possible
- 1859 paleoecological significance. *Journal of Paleontology* 79, 209–218.
- 1860 Hinojosa, J.L., Brown, S.T., Chen, J., DePaolo, D.J., Paytan, A., Shen, S.Z., Payne, J.L.,

1861 2012. Evidence for end-Permian ocean acidification from calcium isotopes in
1862 biogenic apatite. *Geology* 40, 743-746.

1863 Huang, C.J., Tong, J.N., Hinnov, L., Chen, Z.Q., 2011. Did the great dying of life take
1864 700 ky? Evidence from global astronomical correlation of the Permian-Triassic
1865 boundary interval. *Geology* 39, 779-782.

1866 Huang, Y.F., Tong, J.N., Fraiser, M.L., Chen, Z.Q., 2014. Extinction patterns among
1867 bivalves in South China during the Permian-Triassic crisis. *Palaeogeography,*
1868 *Palaeoclimatology, Palaeoecology* 399, 78-88.

1869 Hubbard, S.M., Shultz, M.R., 2008. Deep burrows in submarine fan-channel deposits of
1870 the Cerro Toro Formation (Cretaceous), Chilean Patagonia: implications for
1871 firmground development and colonization in the deep sea. *Palaios* 23, 223–232.

1872 Jacobsen, N., Twitchett, R.J., Krystyn, L., 2011. Palaeoecological methods for assessing
1873 marine ecosystem recovery following the Late Permian mass extinction event.
1874 *Palaeogeography, Palaeoclimatology, Palaeoecology* 308, 200–212.

1875 Jiang, H.S., Lai, X., Luo, G., Aldridge, R., Zhang, K., Wignall, P.B., 2007. Restudy of
1876 conodont zonation and evolution across the P/T boundary at Meishan section,
1877 Changxing, Zhejiang, China. *Global and Planetary Change* 55, 39-55.

- 1878 Jiang, H.S., Aldridge, R.J., Lai, X.L., Sun, Y.D., Luo, G.M., 2008. Observations on the
1879 surface microreticulation of platform elements of *Neogondolella* (Conodonta) from
1880 the Upper Permian, Meishan, China. *Lethaia* 41, 263-274.
- 1881 Jiang, H.S., Lai, X.L., Sun, Y.D., Wignall, P.B., Liu, J., Yan, C., 2014. Permian-Triassic
1882 conodonts from Dajiang (Guizhou, South China) and their implication for the age of
1883 microbialite deposition in the aftermath of the end-Permian mass extinction. *Journal*
1884 *of Earth Science* 25, 413-430.
- 1885 Jiang, H.S., Lai, X.L., Yan, C.B., Aldridge, R.J., Wignall, P., Sun, Y.D., 2011. Revised
1886 conodont zonation and conodont evolution across the Permian-Triassic boundary at
1887 the Shangsi section, Guangyuan, Sichuan, South China. *Global and Planetary Change*,
1888 77, 103-115,
- 1889 Jiang, Y., Tang, Y., Dai, S., Zou, X., Qian, H., Zhou, G., 2006. Pyrites and sulfur isotopic
1890 composition near the Permian-Triassic boundary in Meishan. *Zhejiang. Acta*
1891 *Geologica Sinica* 80, 1202-1207.
- 1892 Jin, Y., Wang, Y., Wang, W., Shang, Q., Cao, C., Erwin, D.H., 2000. Pattern of marine
1893 mass extinction near the Permian-Triassic boundary in South China. *Science* 289,
1894 432-436.

- 1895 Joachimski, M.M., Lai, X., Shen, S., Jiang, H., Luo, G., Chen, B., Chen, J., Sun, Y., 2012.
- 1896 Climate warming in the latest Permian and the Permian–Triassic mass extinction.
- 1897 Geology 40, 195–198.
- 1898 Jost, L., 2006. Entropy and diversity. *Oikos* 113, 363–375.
- 1899 Jost, L., 2007. Partitioning diversity into independent alpha and beta components.
- 1900 Ecology 88, 2427–2439.
- 1901 Jumars, P.A., Wheatcroft, R.A., 1989. Responses of benthos to changing food quality and
- 1902 quantity with a focus of deposit feeding and bioturbation. In: Berger, W.H., Smetacek,
- 1903 V.S., Wefer, G., (eds.), *Productivity in the Ocean: Past and Present*. Wiley, Chichester,
- 1904 pp. 235-253.
- 1905 Kaiho, K., Chen, Z.Q., Miura, Y., Kawahata, H., Kajiwar, Y., Sato, H., 2006b. Close-up
- 1906 of the end-Permian mass extinction horizon recorded in the Meishan section, South
- 1907 China: Sedimentary, elemental, and biotic characterization with a negative shift of
- 1908 sulfate sulfur isotope ratio. *Palaeogeography, Palaeoclimatology, Palaeoecology* 239,
- 1909 396-405.
- 1910 Kaiho, K., Kajiwar, Y., Chen, Z.Q., Gorjan, P., 2006a. A sulfur isotope event at the end
- 1911 of the Permian. *Chemical Geology* 235, 33-47

- 1912 Kaiho, K., Chen, Z.Q., Sawada, K., 2009. Possible causes for a negative shift of stable
1913 carbon isotope ratio before, during, and after the end-Permian mass extinction in
1914 Meishan, South China. *Australian Journal of Earth Sciences* 56, 799-808.
- 1915 Kaiho, K., Kajiwarra, Y., Nakano, T., Miura, Y., Chen, Z.Q., Shi, G.R., 2001. End-Permian
1916 catastrophe by a bolide impact: evidence of a gigantic release of sulfur from the
1917 mantle. *Geology* 29, 815-818.
- 1918 Keighley, D.G., Pickeril, P.K., 1994. The ichnogenus *Beaconites* and its distinction from
1919 *Ancorichnus* and *Taenidium*. *Palaeontology* 37, 305-337.
- 1920 Knaust, D., 1998. Trace fossils and ichnofabrics on the Lower Muschelkalk carbonate
1921 ramp (Triassic) of Germany: tool for high-resolution sequence stratigraphy.
1922 *Geologische Rundschau* 87, 21-31.
- 1923 Knaust, D., 2004. Cambro–Ordovician trace fossils from the SW Norwegian Caledonides.
1924 *Geological Journal* 39, 1–24.
- 1925 Knoll, A.H., Bambach, R.K., Oayne, J.L., Pruss, S., Fischer, W.W., 2007.
1926 Paleophysiology and end-Permian mass extinction. *Earth and Planetary Science*
1927 *Letters* 256, 295–313.
- 1928 Korte, C., Kozur, H., Joachimski, M.M., Strauss, H., Veizer, J., Schwark, L., 2004a.

- 1929 Carbon, sulfur, oxygen and strontium isotope records, organic geochemistry and
- 1930 biostratigraphy across the Permian/Triassic boundary in Abadeh, Iran. *International*
- 1931 *Journal of Earth Sciences* 93, 565–581
- 1932 Kosnik, M.A., Wagner, P.J., 2006. Effects of taxon abundance distributions on expected
- 1933 numbers of sampled taxa. *Evolutionary Ecology Research* 8, 195–211.
- 1934 Kozur, H., 2007. Biostratigraphy and event stratigraphy in Iran around the
- 1935 Permian–Triassic Boundary (PTB): Implications for the causes of the PTB biotic
- 1936 crisis. *Global and Planetary Change* 55, 155–176.
- 1937 Lea, D.W., Pak, D.K., Spero, H.J., 2000. Climate impact of late quaternary equatorial
- 1938 pacific sea surface temperature variations. *Science* 289, 1719–1724.
- 1939 Li, J., Cao, C.Q., Servais, T., Zhu, Y.H., 2004. Later Permian acritarchs from Meishan
- 1940 (SE China) in the context of Permian palaeobiogeography and palaeoecology. *Neues*
- 1941 *Jahrbuch für Geologie und Paläontologie, Monatshefte* 7, 427–448.
- 1942 Li, W.Z., Shen, S.Z., 2008. Lopingian (Late Permian) brachiopods around the
- 1943 Wuchiapingian-Changhsingian boundary at the Meishan sections C and D,
- 1944 Changxing, South China. *Geobios* 41, 307–320.
- 1945 Liang H., 2002, End-Permian catastrophic event of marine acidification by hydrated

- 1946 sulfuric acid: Mineralogical evidence from Meishan section of South China:
- 1947 Chinese Science Bulletin 47, 1393-1397.
- 1948 Liao, Z.T., 1984. New genera and species of Late Permian and earliest Triassic
- 1949 brachiopods from Jiangsu, Zhejiang and Anhui Provinces. Acta Palaeontologica
- 1950 Sinica 23, 276–285.
- 1951 Luo, G.M., Lai, X.L., Jiang, H.S., Zhang, K.X., 2006. Size variation of the end Permian
- 1952 conodont *Neogondolella* at Meishan section, Changxing, Zhejiang and its
- 1953 significance. Science in China, Series D 49, 337–347.
- 1954 Luo, G.M., Lai, X.L., Shi, G.R., Jiang, H.S., Yin, H.F., Xie, S.C., Tong, J.N., Zhang,
- 1955 K.X., He, W.H., Wignall, P.B., 2008. Size variation of conodont elements of the
- 1956 *Hindeodus-Isarciciella* clade during the Permian-Triassic transition in South China
- 1957 and its implication for mass extinction. Palaeogeography, Palaeoclimatology,
- 1958 Palaeoecology 264, 176-187.
- 1959 Luo, G.M., Huang, J.H., Xie, S.C., Wignall, P.B., Tang, X.Y., Huang, X.Y., Yin, H.F.,
- 1960 2010. Relationships between carbon isotope evolution and variation of microbes
- 1961 during the Permian-Triassic transition at Meishan section, South China. International
- 1962 Journal of Earth Sciences 99, 775-784.

- 1963 Luo, G.M., Wang, Y.B., Yang, H., Algeo, T.J., Kump, L., Huang, J.H., Xie, S.C., 2011.
- 1964 Stepwise and large-magnitude negative shift in delta C-13 (carb) preceded the main
- 1965 marine mass extinction of the Permian-Triassic crisis interval. *Palaeogeography,*
- 1966 *Palaeoclimatology, Palaeoecology* 299, 70-82.
- 1967 MacEachern, J.A., Raychaudhuri, I., Pemberton, S.G., 1992. Stratigraphic applications of
- 1968 the *Glossifungites* ichnofacies: delineating discontinuities in the rock record. In:
- 1969 Pemberton, S.G. (ed.), *Applications of Ichnology to Petroleum Exploration: A Core*
- 1970 *Workshop: SEPM Core Workshop No. 17*, pp. 169–198 Tulsa, USA.
- 1971 MacEachern, J.A., Bann, K.L., Pemberton, S.G., Gingras, M.K., 2007. The ichnofacies
- 1972 paradigm: high-resolution paleoenvironmental interpretation of the rock record. In:
- 1973 MacEachern, J.A., Bann, K.L., Gingras, M.K., Pemberton, S.G. (eds), *Applied*
- 1974 *Ichnology: SEPM Short Course Notes No. 52*, pp. 27–64. Tulsa, USA.
- 1975 Mei, S.L., Zhang, K.X., Wardlaw, B.R., 1998. A refined succession of Changhsingian and
- 1976 Griesbachian neogondolellid conodonts from the Meishan section, candidate of the
- 1977 Global Stratotype Section and Point of the Permian-Triassic boundary.
- 1978 *Palaeogeography, Palaeoclimatology, Palaeoecology* 143, 213-226.
- 1979 Miller, M.F., Smail, S.E., 1997. A semiquantitative method for evaluating bioturbation

- 1980 on bedding planes. *Palaios* 12, 391–396.
- 1981 Mundil, R., Metcalfe, I., Ludwig, K.R., Renne, P.R., Oberli, F., Nicoll, R.S., 2001.
- 1982 Timing of the Permian–Triassic biotic crisis: implications from new zircon U/Pb age
- 1983 data (and their limitations). *Earth and Planetary Science Letters* 187, 131–145.
- 1984 Mundil, R., Ludwig, K.R., Metcalfe, I., Renne, P.R., 2004. Age and timing of the Permian
- 1985 mass extinctions: U/Pb dating of closed-system zircons. *Science* 305, 1760–1763.
- 1986 Myrow, P.M., 1995. *Thalassinoides* and the enigma of early Paleozoic open-framework
- 1987 burrow systems. *Palaios* 10, 58–74.
- 1988 Nicoll, R.S., Metcalfe, I., Wang, C.Y., 2002. New species of the conodont genus
- 1989 *Hindeodus* and conodont biostratigraphy of the Permian–Triassic boundary interval.
- 1990 *Journal of Asian Earth Sciences* 20, 609–631.
- 1991 Olszewski, T.D., 2004. A unified mathematical framework for the measurement of
- 1992 richness and evenness within and among multiple communities. *Oikos* 104,
- 1993 377–378.
- 1994 Orchard, M.J., Krystyn, L., 1998. Conodonts of the lowermost Triassic of Spiti, and new
- 1995 zonation based on *Neogondolella* successions. *Rivista Italiana di Paleontologia e*
- 1996 *Stratigrafia* 104, 341–368.

- 1997 Orchard, M.J., Nassichuk, W.W., Rui, L., 1994. Conodonts from the Lower Griesbachian
- 1998 *Otoceras latilobatum* bed of Selong, Tibet and the position of the Permian–Triassic
- 1999 boundary. Canadian Society of Petroleum Geologists, Proceedings of Pangea
- 2000 Conference, Memoir 17, 823–843.
- 2001 Payne, J.L., Clapham, M.E., 2012. End-Permian mass extinction in the oceans: An
- 2002 ancient analog for the twenty-first century? Annual Reviews of Earth and Planetary
- 2003 Sciences 40, 89–111.
- 2004 Payne, J.L., Lehrmann, D.J., Wei, J.Y., Orchard, M.J., Schrag, D.P., Knoll, A.H., 2004.
- 2005 Large perturbations of the carbon cycle during recovery from the end-Permian
- 2006 extinction. Science 205, 505-509.
- 2007 Payne, J.L., Lehrmann, D.J., Wei, J., Knoll, A.H., 2006. The pattern and timing of biotic
- 2008 recovery from the end-Permian extinction on the Great Bank of Guizhou, Guizhou
- 2009 Province, China. Palaios 21, 63–85.
- 2010 Payne, J.L., Lehrmann, D.J., Follett, D., Seibel, M., Kump, L.R., Riccardi, A., Altiner, D.,
- 2011 Sano, H., Wei, J., 2007. Erosional truncation of uppermost Permian shallow-marine
- 2012 carbonates and implications for Permian–Triassic boundary events. Geological
- 2013 Society of America, Bulletin 119, 771–784.

- 2014 Pemberton, S.G., Frey, R.W., 1985. The *Glossifungites* ichnofacies: modern examples
2015 from the Georgia coast, USA. In: Curran, H.A., (ed.), Biogenic Structures: Their Use
2016 in Interpreting Depositional Environments: SEPM Special Publication, 35, pp.
2017 237–259, Tulsa, USA.
- 2018 Pemberton, S.G., Flach, P.D., Mossop, G.D., 1982. Trace fossils from the Athabasca Oil
2019 Sands, Alberta, Canada. Science 217, 825-827.
- 2020 Pemberton, S.G., MacEachern, J.A., Saunders, T., 2004. Stratigraphic applications of
2021 substratespecific ichnofacies: delineating discontinuities in the fossil record. In:
2022 McIlroy, D. (ed.), The Application of Ichnology to Palaeoenvironmental and
2023 Stratigraphic Analysis: Geological Society of London, Special Publication, 228,
2024 29–62.
- 2025 Perri, M.C., Farabegoli, E., 2003. Conodonts across the Permian–Triassic boundary in
2026 the Southern Alps. Courier Forschungsinstitute Senckenberg 245, 281–313.
- 2027 Pruss, S.B., Bottjer, D.J., 2004. Early Triassic fossils of the western United States and
2028 their implications for prolonged environmental stress from the end-Permian mass
2029 extinction. Palaios 19, 551-564.
- 2030 Reichow, M.K., Pringle, M.S., Al'Mukhamedov, A.I., Allen, M.B., Andreichev, V.L.,

2031 Buslov, M.M., Davies, C.E., Fedoseev, G.S., Fitton, J.G., Inger, S., Medvedev, A.Y.,
 2032 Mitchell, C., Puchkov, V.N., Safanova, I.Y., Scott, R.A., Saunders, A.D., 2009. The
 2033 timing and extent of the eruption of the Siberian Traps large igneous province:
 2034 implications for the end-Permian environmental crisis. *Earth and Planetary Sciences*
 2035 *Letters* 277, 9–20.

2036 Renne, P.R., Black, M.T., Zheng, Z.C., Richards, M.A., Basu, A.R., 1995. Synchrony
 2037 and causal relations between Permian–Triassic boundary crisis and Siberian flood
 2038 volcanism. *Science* 269, 1413–1416.

2039 Renne, P.R., Mundil, R., Balco, G., Min, K., Ludwig, K.R., 2010. Joint determination of
 2040 ^{40}K decay constants and $^{40}\text{Ar}^*/^{40}\text{K}$ for the Fish Canyon sanidine standard, and
 2041 improved accuracy for $^{40}\text{Ar}/^{39}\text{Ar}$ geochronology. *Geochimica et Cosmochimica*
 2042 *Acta* 74, 5349–5367.

2043 Riccardi, A., Arthur, M.A., Kump, L.R., 2006. Sulfur isotopic evidence for chemocline
 2044 upward excursions during the end-Permian mass extinction. *Geochimica et*
 2045 *Cosmochimica Acta* 70, 5740–5752.

2046 Rindsberg, A.K., Kopaska-Merkel, D.C., 2005. *Treptichnus* and *Arenicolites* from the
 2047 Steven C. Minkin Paleozoic footprint Site (Langsettian, Alabama, USA). In: Buta,

- 2048 R.J., Rindsberg, A.K., Kopaska-Merkel, D.C., (eds.), *Pennsylvanian Footprints in*
 2049 *the Black Warrior Basin of Alabama: Monograph, 1. Alabama Paleontological*
 2050 *Society*, pp. 121–141.
- 2051 Rui, L., He, J., Chen, C., Wang, Y., 1988. Discovery of fossil animals from the basal clay
 2052 of Permian–Triassic boundary in the Meishan area of Changxing, Zhejiang and its
 2053 significance. *Journal of Stratigraphy* 12, 48–52.
- 2054 Savrda, C.E., 1992. Trace fossils and benthic oxygenation. In: Maples, C.G., West, R.R.
 2055 (eds), *Trace Fossils, Short Courses in Paleontology 5*. University of Tennessee Press,
 2056 Knoxville pp. 172–196.
- 2057 Savrda, C.E., Bottjer, D.J., 1987. The exaerobic zone, a new oxygen-deficient marine
 2058 biofacies. *Nature* 327, 54–56.
- 2059 Savrda, C.E., Browning, J.V., Krawinkel, H., Hesselbo, S.P., 2001. Firmground
 2060 ichnofabrics in deep-water sequence stratigraphy, Tertiary clinoform-toe deposits,
 2061 New Jersey slope. *Palaios* 16, 294–305.
- 2062 Seilacher, A. 1967. Bathymetry of trace fossils. *Marine Geology* 5, 413–428.
- 2063 Seilacher, A. 1977. Pattern analysis of *Paleodictyon* and related trace fossils. In: Crimes,
 2064 T.P., Harper, J.C. (eds.), *Trace Fossils 2. Geological Journal Special Issue No. 9*,

- 2065 289-334.
- 2066 Seilacher, A., 2007. Trace Fossil Analysis. Springer, Berlin. 226 pp.
- 2067 Sephton, M.A., Looy, C.V., Brinkhuis, H., Wignall, P.B., de Leeuw, J.W., Visscher, H.,
- 2068 2005. Catastrophic soil erosion during the end-Permian biotic crisis. *Geology* 33,
- 2069 941–944.
- 2070 Sepkoski Jr., J.J., 1982. A Compendium of Fossil Marine Families: Milwaukee Public
- 2071 Museum Contributions in Biology and Geology, 51, p. 125.
- 2072 Sepkoski Jr., J.J., 2002. A Compendium of Fossil Marine Animal Genera: *Bulletin of*
- 2073 *American Paleontology* 363, 1-563.
- 2074 Sheldon, N.D., 2006. Abrupt chemical weathering increase across the Permian–Triassic
- 2075 boundary. *Palaeogeography, Palaeoclimatology, Palaeoecology* 231, 315–321.
- 2076 Shen, J., Algeo, T.J., Zhou, L., Feng, Q., Yu, J., Ellwood, B., 2012. Volcanic
- 2077 perturbations of the marine environment in South China preceding the latest Permian
- 2078 mass extinction and their biotic effects. *Geobiology* 10, 82-103.
- 2079 Shen, S.Z., James L. Crowley, J.L., Wang, Y., Bowring, S.A., Erwin, D.H., Sadler, P.M.,
- 2080 Cao, C.Q., Rothman, D.H., Henderson, C.M., Ramezani, J., Zhang, H., Shen, Y.A.,
- 2081 Wang, X.D., Wang, W., Mu, L., Li, W.Z., Tang, Y.G., Liu, X.L., Liu, L.J., Zeng, Y.,

- 2082 Jiang, Y.F., Jin, Y.G., 2011b. Calibrating the end-Permian mass extinction. *Science*
- 2083 9, 1367-1372,
- 2084 Shen, W.J., Lin, Y.T., Xu, L., Li, J. F., Wu, Y.S., Sun, Y.G., 2007. Pyrite framboids in the
- 2085 Permian-Triassic boundary section at Meishan, China: Evidence for dysoxic
- 2086 deposition. *Palaeogeography, Palaeoclimatology, Palaeoecology* 253, 323-331.
- 2087 Shen, Y.A., Farquhar, J., Zhang, H., Masterson, A., Zhang, T., Wing, B.A., 2011a.
- 2088 Multiple S-isotopic evidence for episodic shoaling of anoxic water during Late
- 2089 Permian mass extinction. *Nature Communications* 2, 210e.
- 2090 Sheng, J., Chen, C., Wang, Y., Rui, L., Liao, Z., Bando, Y., Ishii, K., Nakazawa, K.,
- 2091 Nakamura, K., 1984. Permian–Triassic boundary in Middle and Eastern Tethys.
- 2092 *Journal of Faculty of Science, Hokkaido University* 21, 133–181.
- 2093 Sheng, J.Z., Chen, C.Z., Wang, Y.G., Rui, L., Liao, Z.T., He, J.W., Jiang, N.Y., Wang,
- 2094 C.Y., 1987. New evidence on the Permian and Triassic boundary of Jiangsu,
- 2095 Zhejiang and Anhui. In: Nanjing Institute of Geology and Palaeontology, Academia
- 2096 Sinica (ed.), *Stratigraphy and Palaeontology of Systemic Boundaries in China*.
- 2097 Permian–Triassic Boundary (1). Nanjing University Press, Nanjing, pp. 1–21
- 2098 Shi, C., Chen, D., 1987. The Changhsingian ostracodes from Meishan, Changxing,

- 2099 Zhejiang. In: Nanjing Institute of Geology and Palaeontology, Academia Sinica (Ed.),
- 2100 Stratigraphy and Palaeontology of systemic boundaries in China. Permian-Triassic
- 2101 boundary (1). Nanjing University Press, Nanjing, pp. 23-80.
- 2102 Song, H., Tong, J., Chen, Z.Q., 2009. Two episodes of foraminiferal extinction near the
- 2103 Permian–Triassic boundary at the Meishan section, South China. Australian Journal
- 2104 of Earth Sciences 56, 765–773.
- 2105 Song, H., Tong, J., Zhang, K., Wang, Q., Chen, Z.Q., 2007. Foraminiferal survivors from
- 2106 the Permian–Triassic mass extinction in the Meishan section, South China.
- 2107 Palaeoworld 16, 105–119.
- 2108 Song, H.J., Wignall, P.B., Tong, J.N., Yin, H.F., 2013a. Two pulses of extinction during
- 2109 the Permian-Triassic crisis. Nature Geoscience 6, 52-56.
- 2110 Song, H.J., Wignall, P.B., Chu, D.L., Tong, J.N., Sun, Y.D., Song, H.Y., He, W.H., Tian,
- 2111 L., 2014. Anoxia/High temperature double whammy during the Permian-Triassic
- 2112 marine crisis and its aftermath. Scientific Reports 4, 4132.
- 2113 Song, H.Y., Tong, J.N., Algeo, T.J., Horacek, M., Qiu, H.O., Song, H.J., Tian, L., Chen,
- 2114 Z.Q., 2013b. Large vertical $\delta^{13}\text{C}$ gradients in Early Triassic seas of the South China
- 2115 craton: Implications for oceanographic changes related to Siberian Traps volcanism.

- 2116 Global and Planetary Change 105, 7–20.
- 2117 Sun, Y.D., Joachimski, M.M., Wignall, P.B., Yan, C.B., Chen, Y.L., Jiang, H.S., Wang,
2118 L., Lai, X.L., 2012. Lethally hot temperatures during the Early Triassic greenhouse.
2119 Science 338, 366–370.
- 2120 Tian, S.F., Chen, Z.Q., Huang, C.J., 2014. Orbital forcing and sea-level changes in the
2121 earliest Triassic of the Meishan section, South China. Journal of Earth Science 25,
2122 64–73.
- 2123 Tong, J.N., Yang, Y., 1998. Advance in the study of the Lower Triassic conodonts at
2124 Meishan section, Changxing, Zhejiang Province. Chinese Science Bulletin 43,
2125 1350–1353.
- 2126 Twitchett, R.J., 1999. Palaeoenvironments and faunal recovery after the end-Permian
2127 mass extinction. Palaeogeography, Palaeoclimatology, Palaeoecology 154, 27–37.
- 2128 Twitchett, R.J., 2006. The palaeoclimatology, palaeoecology and palaeoenvironmental
2129 analysis of mass extinction events. Palaeogeography, Palaeoclimatology,
2130 Palaeoecology 232, 190–213.
- 2131 Twitchett, R.J., Barras, C.G., 2004. Trace fossils in the aftermath of mass extinction
2132 events. In: McIlroy, D. (Ed.), Application of Ichnology to Palaeoenvironmental and

2133 Stratigraphic Analysis. Geological Society of London, Special Publication 228, pp.

2134 395-415.

2135 Twitchett, R.J., Krystyn, L., Baud, A., Wheeley, J.R., Richoz, S., 2004. Rapid marine

2136 recovery after the end-Permian mass-extinction event in the absence of marine

2137 anoxia. *Geology* 32, 805-808.

2138 Wang, C., Visscher, H., 2007. Abundance anomalies of aromatic biomarkers in the

2139 Permian–Triassic boundary section at Meishan, China—evidence of end-Permian

2140 terrestrial ecosystem collapse. *Palaeogeography, Palaeoclimatology, Palaeoecology*

2141 252, 291–303.

2142 Wang, Y., Sadler, P.M., Shen, S.Z., Erwin, D.H., Zhang, Y.C., Wang, X.D., Wang, W.,

2143 Crowley, J.L., Henderson, C.M., 2014. Quantifying the process and abruptness of the

2144 end-Permian mass extinction. *Paleobiology* 40, 113-129.

2145 Wignall, P.B., 2007. The end-Permian mass extinction—how bad did it get? *Geobiology*

2146 5, 303–309.

2147 Wignall, P.B., Hallam, A., 1993. Griesbachian (earliest Triassic) palaeoenvironmental

2148 changes in the Salt Range, Pakistan and southeast China and their bearing on the

2149 Permo–Triassic mass extinction. *Palaeogeography, Palaeoclimatology,*

- 2150 Palaeoecology 102, 215-37.
- 2151 Wignall, P.B., Twitchett, R.J., 2002. Extent, duration and nature of the Permian-Triassic
 2152 superanoxic event. Geological Society of America, Special Paper 356, 395-413.
- 2153 Wignall, P.B., Morante, R., Newton, R., 1998. The Permo–Triassic transition in
 2154 Spitsbergen; $\delta^{34}\text{S}$ chemostratigraphy, Fe and S geochemistry, facies, fauna and
 2155 trace fossils. Geological Magazine 135, 47-62.
- 2156 Wignall, P.B., Newton, R., Brookfield, M.E., 2005. Pyrite framboid evidence for
 2157 oxygen-poor deposition during the Permian–Triassic crisis in Kashmir.
- 2158 Palaeogeography, Palaeoclimatology, Palaeoecology 216, 183–188.
- 2159 Wignall, P.B., Kershaw, S., Collin, P.Y., Crasquin-Soleau, S., 2009. Comment: erosional
 2160 truncation of uppermost Permian shallow-marine carbonates and implications for
 2161 Permian–Triassic boundary events. Geological Society of America, Bulletin 121,
 2162 954–956.
- 2163 Williams, A., James, M.A., Emig, C.C., Mackay, S., Rhodes, M.C., Cohen, B.L.,
 2164 Gawthrop, A.B., Peck, L.S., Curry, G.B., Ansell, A.D., Cusack, M., Walton, D.,
 2165 Brunton, C.H.C., MacKinnon, D.I., Richardson, J.R., 1997. Treatise on Invertebrate
 2166 Paleontology Part H, Brachiopoda, Revised, Volume 1: Introduction. The Geological

2167 Society of America and The University of Kansas, Boulder, Colorado and Lawrence,
 2168 Kansas, 539 pp.

2169 Wilson, M.A., Palmer, T.J., 1998. The earliest *Gastrochaenolites* (Early Pennsylvanian,
 2170 Arkansas, USA): an upper Paleozoic bivalve boring? *Journal of Paleontology*, 72,
 2171 769–772.

2172 Wu, H.C., Zhang, S.H., Hinnov, L.A., Jiang, G.Q., Feng, Q.L., Li, H.Y., Yang, T.S., 2013.
 2173 Time-calibrated Milankovitch cycles for the Late Permian. *Nature Communications*
 2174 4, 2452.

2175 Xie, S.C., Pancost, R.D., Yin, H.F., Wang, H.M., Evershed, R.P., 2005. Two episodes of
 2176 microbial change coupled with Permo/Triassic faunal mass extinction. *Nature* 343,
 2177 494–497.

2178 Xie, S., Pancost, R.D., Huang, J., Wignall, P.B., Yu, J., Tang, X., Chen, L., Huang, X.,
 2179 Lai, X., 2007. Changes in the global carbon cycle occurred as two episodes during
 2180 the Permian–Triassic crisis. *Geology* 35, 1083–1086.

2181 Xu, D.Y., Yan, Z., 1993. Carbon-isotope iridium event markers near the Permian-Triassic
 2182 boundary in the Meishan section, Zhejiang Province, China. *Palaeogeography*,
 2183 *Palaeoclimatology, Palaeoecology* 104, 171–176.

- 2184 Yang, W., Jiang, N., 1981. Sedimentary features and microfacies of the Changhsing
2185 Formation and Permian-Triassic boundary. *Bulletins of the Nanjing Institute of*
2186 *Geology and Palaeontology, Academia Sinica* 2, 113-133.
- 2187 Yang, Z., Yin, H., Wu, S., Yang, F., Ding, M., Xu, G., 1987. Permian-Triassic boundary
2188 stratigraphy and fauna of South China. Ministry of Geology and Mineral Resources,
2189 People's Republic of China, Geological Memoirs Series 2, Number 6. Geological
2190 Publishing House, Beijing, 379 pp.
- 2191 Yang, Z., Wu, S., Yin, H., Xu, G., Zhang, K., Bi, X., 1993. Permo-Triassic events of South
2192 China. Geological Publishing House, Beijing, 153 pp.
- 2193 Yin, H., Ding, M., Zhang, K., Tong, J., Yang, F., Lai, X., 1995. Dongwuan-Indosinian
2194 (Late Permian-Middle Triassic) Ecostratigraphy of the Yangtze Region and its
2195 Margins. Science Press, Beijing, 338 pp.
- 2196 Yin, H., Zhang, K., Tong, J., Yang, Z., Wu, S., 2001. The Global Stratotype Section and
2197 Point (GSSP) of the Permian-Triassic Boundary. *Episodes* 24(2), 102-114.
- 2198 Yin, H., Sweet, W.C., Glenister, B.F., Kotlyar, G., Kozur, H., Newell, N.D., Sheng, J.,
2199 Yang, Z. and Zakharov, Y.D., 1996, Recommendation of the Meishan section as
2200 Global Stratotype Section and Point for basal boundary of Triassic System:

- 2201 Newsletter on Stratigraphy 34, 81–108.
- 2202 Yin, H.F., Feng, Q.L., Lai, X.L., Baud, A., Tong, J.N., 2007. The protracted
- 2203 Permo-Triassic crisis and multi-episode extinction around the Permian-Triassic
- 2204 boundary. *Global and Planetary Change* 55, 1-20.
- 2205 Yin, H.F., Huang, S.J., Zhang, K.X., Hansen, H.J., Yang, F.Q., Ding, M.H., Bie, X.M.,
- 2206 1992, The effects of volcanism on the Permo-Triassic mass extinction in South
- 2207 China, *in* Sweet, W.C., Yang, Z.Y, Dickins, J.M., Yin, H.F. (eds), *Permo-Triassic*
- 2208 *Events in the Eastern Tethys*. Cambridge, UK, Cambridge University Press, p.
- 2209 169-174.
- 2210 Yin, H.F., Xie, S., Luo, G., Algeo, T.J., Zhang, K., 2012. Two episodes of environmental
- 2211 change at the Permian-Triassic boundary of the GSSP section Meishan.
- 2212 *Earth-Science Reviews* 115, 163-172.
- 2213 Yin, H.F., Jiang, H.S., Xia, W.C., Feng, Q.L., Zhang, N., Shen, J., 2014. The end-Permian
- 2214 regression in South China and its implication on mass extinction. *Earth-Science*
- 2215 *Reviews* 137, 19-33.
- 2216 Yuan, D.X., Shen, S.Z., Henderson, C.M., Chen, J., Zhang, H., Feng, H.Z., 2014. Revised
- 2217 conodont-based integrated high-resolution timescale for the Changhsingian Stage

- 2218 and end-Permian extinction interval at the Meishan sections, South China. *Lithos*
- 2219 204, 220-245.
- 2220 Zeebe, R.E., Zachos, J.C., Dickens, G.R., 2009. Carbon dioxide forcing alone insufficient
- 2221 to explain Palaeocene–Eocene thermal maximum warming. *Nature Geoscience* 2,
- 2222 576–580.
- 2223 Zhang, H., Shen, S.Z., Cao, C.Q., Zheng, Q.F., 2014. Origins of microspherules from the
- 2224 Permian-Triassic boundary event layers in South China. *Lithos* 204, 246-257.
- 2225 Zhang, K.X., Lai, X.L., Tong, J.N., Jiang, H.S., 2009. Progresses on study of conodont
- 2226 sequence for the GSSP section at Meishan, Changxing, Zhejiang Province, South
- 2227 China. *Acta Palaeontologica Sinica* 48, 485-495.
- 2228 Zhang, K.X., Tong, J.N., Shi, G.R., Lai, L.X., Peng, Y.Q., Yu, J.X., He, W., Jin, Y.L.,
- 2229 2007. Early Triassic conodont-palynological biostratigraphy of the Meishan D
- 2230 section in Changxing, Zhejiang Province, South China. *Palaeogeography,*
- 2231 *Palaeoclimatology, Palaeoecology* 252, 4–23
- 2232 Zhang, K.X., Tong, J.N., Yin, H.F., Wu, S.B., 1997. Sequence stratigraphy of the
- 2233 Permian-Triassic boundary section of Changxing, Zhejiang, Southern China. *Acta*
- 2234 *Geologica Sinica* 71, 90-103.

- 2235 Zhang, K.X., Tong, J.N., Hou, G.J., Wu, S.B., Zhu, Y.H., Lin, Q.X., 2005. Regional
- 2236 Geological report, the People's Republic of China (Meishanzhen Map H50E006023,
- 2237 Changxingian Map, H50E006024, Scale:1:50000). University of Geosciences Press,
- 2238 264 pp., Wuhan, China.
- 2239 Zhao, J., Sheng, J., Yao, Z., Liang, X., Chen, C., Rui, L., Liao, Z., 1981. The
- 2240 Changhsingian and Permian-Triassic boundary of South China, Bulletin of the
- 2241 Nanjing Institute of Geology and Palaeontology, Academia Sinica 2, 1-95.
- 2242 Zhao, X.M., Tong, J.N., 2010. Two episodic changes of trace fossils through the
- 2243 Permian-Triassic transition in the Meishan section cores, Zhejiang Province, Science
- 2244 China, Earth Science 40, 1241-1249.
- 2245 Zheng, Q.F., Cao, C.Q., Zhang, M.Y., 2013. Sedimentary features of the Permian-Triassic
- 2246 boundary sequence of the Meishan section in Changxing County, Zhejiang Province.
- 2247 Science China, Earth Sciences 56, 956-969.
- 2248 Zhao, L., Chen, Y., Chen, Z.Q., Cao, L., 2013b. Uppermost Permian to Lower Triassic
- 2249 conodont zonation from Three Gorges area, South China. Palaios 28, 523-540.
- 2250 Zhao, L., Chen, Z.Q., Algeo, T.J., Chen, J., Chen, Y., Tong, J., Gao, S., Zhou, L., Hu, Z.,
- 2251 Liu, Y., 2013a. Rare-earth element patterns in conodont albid crowns: Evidence for

2252 massive inputs of volcanic ash during the latest Permian biocrisis? Global and
 2253 Planetary Change 105, 135-151.

2254 Zonneveld, J.-P., Gingras, M.K., Beatty, T.W., 2010. Diverse ichnofossil assemblage
 2255 following the P–T mass extinction, Lower Triassic, Alberta and British Columbia,
 2256 Canada: evidence for shallow marine refugia on the northwestern coast of Pangaea.
 2257 Palaios 25, 368–392.

2258

2259

2260 **Figure captions**

2261

2262 **Fig. 1.** The GSSP for the Permian-Triassic boundary at Meishan, Changxing county,
 2263 northwestern Zhejiang Province, east China. A, location of the Meishan section. B,
 2264 close-up of the white volcanic ash bed (Bed 25) in Meishan. C, geopark of the GSSP
 2265 Meishan showing GSSP position at the Meishan section D. D, the P-Tr boundary beds
 2266 showing biostratigraphic boundary through the mid-Bed 27 and the mass extinction
 2267 horizon at the base of Bed 25. E, outcrop of the P-Tr boundary beds and Yinkeng
 2268 Formation along strike on the Meishan hill from the geopark section.

2269 **Fig. 2.** Biostratigraphy of the P-Tr transition at the Meishan section with the updated
 2270 conodont zones and correlations with ammonoid, bivalve, brachiopod and microfloral
 2271 assemblages from Meishan as well as conodont zones from North Italy, Iran and
 2272 Germany, and India. Note that the updated conodont zonation is revised from those
 2273 documented by Jiang et al. (2007) and Zhang et al. (2009) and our new observations.
 2274 White arrows indicate that conodont zones extend to horizons below Bed 22 of Meishan
 2275 and its equivalents.

2276 **Fig. 3.** P-Tr succession exposed in the GSSP Meishan showing lithology, facies types,
 2277 depositional environments, stratigraphic distributions of trace fossils, and bioturbation
 2278 levels. Ichnofabric indices (ii: Droser and Bottjer, 1986) are assessed as 1 to 6, indicating
 2279 bioturbation from lowest to highest levels. Bedding plane bioturbation index (bpbi) is
 2280 evaluated based on bedding plane coverage of burrows (Miller and Smail, 1997). Facies
 2281 symbols: om = offshore mudstone facies, bs = basinal black shale facies, ow = offshore
 2282 wackestone facies, os = offshore siltstone facies; ew = epeiric sea wackestone facies,
 2283 HCS = hummocky cross stratification, hb = horizontal bedding. Depositional
 2284 environment (DE): ns = nearshore, fw = fair-weather wave base, sw = subtidal zone to
 2285 fair-weather wave base, swb = storm wavebase.

2286 **Fig. 4.** Lithology and fossils from the exposure of the P-Tr transition in Meishan. A-B, D,
 2287 field photograph, polished surface and microphotograph showing hummocky
 2288 cross-stratified (HCS) muddy limestone (Bed 54), upper Yinkeng Formation; pen is 15
 2289 cm long; scale bars are 2 cm. C, pale mudstone and calcareous mudstone (Bed 41)
 2290 showing horizontal stratification, lower Yinkeng Formation; pen is 15 cm long. E, F, I,
 2291 ammonoid fossils across the P-Tr boundary with large ammonoid shell (E) in Bed 24e of
 2292 the Changhsing Formation contrasting to small shells (F, I) recorded in the middle and
 2293 upper Yinkeng Formation; coins are 1.5 cm in diameter; scale bar is 1 cm. G, dark
 2294 thin-bedded limestone interbedded with bioclastic limestone bands, Bed 24e; pen is 10
 2295 cm long. H, irregular contact between Beds 24d and 24e; cross-bedding is pronounced in
 2296 the uppermost Bed 24d; scale bar is 1 cm. J, vertical burrow of *Balanoglossites* in the
 2297 upper part of Bed 24d; scale bar is 1.5 cm.

2298 **Fig.5.** Microfacies and fossil fragment assemblages from Beds 23-26, upper Changhsing
 2299 Formation. A, microphotograph of claystone, Bed 25. B, microphotograph showing
 2300 horizontal laminae (black arrow) of black shale, Bed 26. C, bioclastic packstone of Bed
 2301 23a showing brachiopod (b), crinoid (c), and ostracod (o) fragments. D, bioclastic
 2302 packstone of Bed 24c showing abundant foraminifer (f), brachiopod (b), crinoid (c),

2303 ostracod (o) and other fragments.

2304 **Fig. 6.** Pie diagrams showing percentage of major components in all rocks sampled from
2305 Beds 22-60 in Meishan. Detailed fossil fragment contents (%) of each sample are
2306 tabulated in Table 3. Component symbols: 1 = foraminifers, 2 = ostracods, 3 = crinoids, 4
2307 = echinoids, 5 = brachiopods, 6 = bryozoans, 7 = sponge spicules, 8 = calcareous sponges,
2308 9 = gastropods, 10 = radiolarians, 11 = macroalgae, 12 = micrites, 13 = cavities, 14 =
2309 other particles (fecal pellets, peloids, pyrites and undetermined particles).

2310 **Fig.7.** Microfacies across the boundary between Beds 24e-5 and 24e-6. A, transverse
2311 view of one sponge spicule. B-C, cross-section view of sponge spicules. D,
2312 microphotograph showing the laminated horizon separating bioclastic layer (Bed 24e-5)
2313 from the overlying sponge spicule-rich layer (Bed 24e-6). E, SEM image of one isolated
2314 specimen of a sponge spicule. B-C, scale bars are both 50 μ m; E, Scale bar is 40 μ m.

2315 **Fig. 8.** Microfacies and fossil fragment assemblages from Bed 26b, 8-10 cm above the
2316 base of Bed 25. A, microphotograph showing foraminifer (f), bryozoan (bry), echinoid
2317 (e), and brachiopod (bra) fragments. B, microphotograph showing ostracod (o), echinoid
2318 (e), and brachiopod (bra) fragments. C, microphotograph showing brachiopod (bra) and
2319 echinoid (e) fragments. D, microphotograph showing bryozoan (bry) and brachiopod (bra)

2320 fragments. E, microphotograph showing foraminifer (f) and echinoid (e) fragments. F,
 2321 microphotograph showing brachiopod (bra) and foraminifer (f) fragments. G,
 2322 microphotograph showing foraminifer (f) and echinoid (e) fragments. H,
 2323 microphotograph showing bryozoan (bry) and foraminifer (f) fragments. I,
 2324 microphotograph showing foraminifer (f) and echinoid (e) fragments. J,
 2325 microphotograph showing foraminifer (f) fragments. K, microphotograph showing
 2326 bryozoan (bry) and echinoid (e) fragments. L, microphotograph showing foraminifer (f)
 2327 and echinoid (e) fragments. All scale bars are all 100 μm .
 2328 **Fig. 9.** Polished surface of Bed 27 and its microfacies features. A, polished surface
 2329 showing the entire bed is subdivided into four parts (labelled a, b, c, d) by two sets of
 2330 pronounced irregular surfaces, in which burrows (red arrows) are commonly present. B,
 2331 microphotograph of the basal part of Bed 27a, 11-13 cm above the base of Bed 25,
 2332 showing foraminifer (f) and brachiopod (bra) fragments. C, microphotograph of the
 2333 upper part of Bed 27a, 13-15 cm above the base of Bed 25, showing foraminifers (f) and
 2334 other fossil fragments. D, microphotograph of the lower part of Bed 27b, 15-17 cm above
 2335 the base of Bed 25, showing claystone-dominated texture. E, microphotograph of the
 2336 upper part of Bed 27b, 18-20 cm above the base of Bed 25, showing echinoid (e) and

2337 other fossil fragments. F, microphotograph of the upper part of Bed 27c, 21-23 cm above
 2338 the base of Bed 25, showing abundant foraminifer (f), echinoid (e) and brachiopod (bra)
 2339 fragments. G, microphotograph of Bed 27d, 23-28 cm above the base of Bed 25, showing
 2340 abundant ostracod (o), foraminifer (f), echinoid (e), and other fragments. H,
 2341 microphotograph of the upper part of Bed 26b, 8-10 cm above the base of Bed 25,
 2342 showing abundant foraminifer (f) and other fossil fragments.

2343 **Fig. 10.** Bioclastic packstone to wackestone showing various fossil fragments from Bed
 2344 27a, 13-15 cm above the base of Bed 25. A, foraminifer (f). B, brachiopod (bra) and other
 2345 fragments. C, foraminifer (f), echinoid (e) and other undetermined fragments. D,
 2346 foraminifer (f). E, foraminifer (f). F, foraminifer (f), brachiopod (b) and other
 2347 undetermined fragments. G, I-K, foraminifer tests. H, echinoid (e) fragment. Scale bars
 2348 are all 50 μm .

2349 **Fig. 11.** Bioclastic packstone and various fossil fragments from Bed 27c, 21-23 cm above
 2350 the base of Bed 25. A, foraminifer (f) and brachiopod (bra) fragments. B, foraminifer
 2351 *Frodina permica* test. C, echinoid (e) and brachiopod (b) fragments; D, bryozoan (bry) ,
 2352 foraminifer (f) and other undetermined fragments. E, foraminifer (f) *Nodosinelloides*
 2353 *netschajewi* test and echinoid (e) fragments. F, foraminifer test of *Hemigordius* sp. G,

2354 brachiopod (bra) fragment. H, bryozoan (bry) fragment. I, foraminifer (f) *Hemigordius* sp.
2355 test. J, foraminiferal (f) fragment. K, echinoid (e) and foraminifer (f) fragments. L-M,
2356 echinoid fragments. Scale bars are all 50 μ m.

2357 **Fig. 12.** Bioclastic packstone to wackestone showing various fossil fragments from Bed
2358 27d, 23-28 cm above the base of Bed 25. A, foraminifer test of *Nodosinelloides* sp. B,
2359 brachiopod (b), foraminifer (f), and echinoid (e) fragments. C-D, foraminifer tests of
2360 *Nodosinelloides* sp. and *Nodosaria* sp., respectively. E, brachiopod (bra), foraminifer (f),
2361 and other fragments. F, echinoid fragment. G, sponge spicule. H, foraminiferal fragment
2362 of *Tuberitina maljavkini*. I, echinoid fragment. J, brachiopod (bra) and sponge spicule (ss);
2363 K, foraminifer test of *Nodosinelloides* sp. L, foraminifer *Nodosinelloides aequiampila* and
2364 brachiopod (bra) fragments. M, foraminifer (f) fragment. N, ostracod (o), foraminifer (f),
2365 and echinoid (e) fragments. O, brachiopod (bra) and echinoid (e) fragments; P,
2366 brachiopod (bra) and echinod (e) fragments. B, scale bar is 100 μ m; F-G, scale bars are
2367 20 μ m; other scale bars are all 50 μ m.

2368 **Fig. 13.** Microfacies and fossil fragment assemblage from strata of Bed 29 and above. A,
2369 bioclastic wackestone with ostracod (o) and brachiopod (bra) fragments, Bed 29. B,
2370 bioclastic wackestone with brachiopod (bra) and ostracod (o) fragments, Bed 29. C,

2371 echinoid fragment, Bed 53. D, ostracods test, Bed 52. F, ostracod test, Bed 53. I, K, M,
 2372 ostracods tests, Bed 54. N, ostracods test, Bed 55. P-R, ostracod tests, Beds 56, 57 and 58,
 2373 respectively. E, foraminifer fragment, Bed 29. J, L, foraminifer fragments, Beds 52 and
 2374 53, respectively. G, foraminifer *Nodosaria* sp., Bed 56. H, foraminifer *Nodosaria*
 2375 *rostrata* Trifonova, Bed 56. O, micrite containing pyrite particles (black) and tiny tubes
 2376 (t), Bed 44. Scale bars are all 50 μ m.

2377 **Fig. 14.** Fossil fragment distributions over the P-Tr transition (Beds 22-60) in Meishan.

2378 Vertical axis represents percentage of various fossil fragments in all rock.

2379 **Fig. 15.** Shell beds from the Yinkeng Formation in Meishan. A, *Claraia* concentrations

2380 (white arrows) from Bed 40; scale bar is 1 cm; B, shell concretions of *Claraia griesbachi*

2381 (c) and *Ophiceras* sp. (o) of the *O-P* community from Bed 32; coin is 1.5 cm in diameter;

2382 C, shell concretions of *Claraia griesbachi* from Bed 35; coin is 1.5 cm in diameter; D,

2383 shell concretions of *Claraia wangi* of the *C* community from Bed 40; coin is 1.5 cm in

2384 diameter; E, shell concretions of *Claraia griesbachi* from Bed 36; coin is 1.5 cm in

2385 diameter; F, shell concretions of *Meishanorhynchia* (m), *Lytophiceras* (ly) and

2386 ophiceratid (o) of the *M-L* community from Bed 55; Scale bar is 4 mm.

2387 **Fig. 16.** Trace fossils from the Changhsing Formation of the Meishan section. A, D,

2388 *Thalassinoides* sp. 1 on base of Bed 8; coin is 1.5 cm; B, *Paleophycus* isp. from Bed 9;
2389 scale bar is 1 cm; C, *Balanoglossites triadicus* from Bed 24d; coin is 1.5 cm in diameter;
2390 E, *Taenidium* isp. from upper surface of Bed 24d; coin is 1.5 cm in diameter; F, *Lockeia*
2391 isp. on the upper surface of Bed 9; coin is 1.5 cm in diameter.

2392 **Fig. 17.** Trace fossils from the Changhsing Formation (Beds23-24) continued. A, E,
2393 horizontal burrows of *Planolites* isp. 1 from upper surface of Bed 24e-6; USB is 2 cm
2394 long; B-C, problematica from upper surface of Bed 23; Coins are 1.5 cm in diameter; D,
2395 *Taenidium* isp. from upper surface of Bed 24e; Coin is 1.5 cm in diameter; F,
2396 *Dendrorhaphe* isp. from upper surface of Bed 23; Coin is 1.5 cm in diameter.

2397 **Fig. 18.** Trace fossils from the Yinkeng Formation. A-B, F, *Planolites* from upper
2398 surfaces of Bed 36, 41, and 56, respectively; coins are 1.5 cm, 2 cm and 1.5 cm in
2399 diameter, respectively; C, *Chondrites* isp. on upper surface of Bed 52; Coin is 1.5 cm in
2400 diameter; D-E, *Thalassionoides* isp. 3 from upper surfaces of Bed 53 and 56, respectively;
2401 coins are 1.5 in diameter; G-H, sketch reconstruction and trace of *Treptichnus* isp. on
2402 upper surface of Bed 57; coin is 1.5 cm in diameter.

2403 **Fig. 19.** Polished slabs and sketches showing the successions of trace-fossil assemblages
2404 in Bed 27. A–C, vertical cross section of Bed 27 showing the ichnofabric change from a

2405 firmground ichnocoenoses of *Glossifungites* ichnofacies in the lower to a softground
2406 ichnocoenose in the upper. Note these three sample blocks (A-C) were cut from one
2407 complete sample of Bed 27. D-F, portraits of blocks A-C, respectively. Ar. = *Arenicolites*
2408 isp., Ch. = *Chondrites* isp. 1, Ga. = *Gastrochaenolites* isp., Pa. = *Planolites* isp. 2, Ps. =
2409 *Psilonichnus*; isp., Th. = *Thalassinoides* isp. 2.

2410 **Fig. 20.** Polished surface and its portrait of Bed 27 showing burrow systems in
2411 firmground of the *Glossifungites* ichnofacies and vertical colonization by ichnofaunas on
2412 different substrates. A, polished slab across the entire Bed 27 (from base to top). B, sketch
2413 reconstruction showing ichnofabrics manifested in Fig. 25A. C, cartoon reconstruction
2414 showing the generalized colonization zonation of ichnofaunas. For abbreviations of
2415 ichnotaxon names see caption of Fig. 19.

2416 **Fig. 21.** Trace fossil evolution at Meishan. A, ichnodiversity change throughout the
2417 uppermost Changhsingian to Griesbachian in Meishan. B, burrow size variations (in
2418 mean diameter and maximum diameter) over the P-Tr transition. C, tiering level change
2419 through the P-Tr transition.

2420 **Fig. 22.** Burrow sizes of selected ichnogenera through the P-Tr transition. A, burrow size
2421 variation of *Planolites* through the P-Tr transition. B, burrow size variation of

2422 *Thalassinoides* through the P-Tr transition. C, burrow sizes of both *Dendrorhapse* and
2423 problematic trace from the upper Changhsing Formation. D, burrow sizes of
2424 *Balanoglossites*, *Taenidium*, *Chondrites*, and *Treptichnus* from the P-Tr transition in
2425 Meishan.

2426 **Fig. 23.** Pyrite framboids and crystals preserved on fossil skeletons and in sediments of
2427 Bed 27. A-C, pyrite crystals (white arrows) on brachiopod shells of *Paryphella*. D-E,
2428 pyrite crystals (white arrows) preserved in sediments and foraminiferal test; scale bars are
2429 40 μm ; F-G, pyrite crystals (white arrows) preserved in foraminiferal tests; scale bars are
2430 all 40 μm . H, L, SEM images showing pyrite framboids preserved on brachiopod shells
2431 of Bed 27; I-K, pyrite framboids preserved in sediments of Bed 27; M-N, EDS results
2432 showing mineral composition of framboids of Fig. 23L and Fig. 23J, respectively.

2433 **Fig. 24.** Sizes of pyrite framboids from 17 horizons through the P-Tr transition in
2434 Meishan. MD = mean diameter, SD = standard derivation, N = Number of framboid
2435 grains.

2436 **Fig. 25.** Redox conditions indicated by pyrite framboid sizes through the P-Tr transition
2437 at Meishan. Two SEM images show morphologies of pyrite framboids from Bed 24 (left)
2438 and Bed 39 (right). PTB = Permo-Triassic boundary; PTME = Permo-Triassic mass

2439 extinction.

2440 **Fig. 26.** Composite figure showing exceptionally increased seawater surface temperature,
2441 carbon isotopic excursion, Chemical index of alternation (CIA) and Eu/Eu* profiles,
2442 through the P-Tr transition at Meishan. Total organic content (TOC) and Ce/Ce* profiles,
2443 framboid size variation, specific and generic richness variations, and community
2444 structural changes indicated by true diversity index (Exp (H)) and dominance (D) through
2445 the P-Tr transition in Meishan. Note: seawater temperature data after Joachimski et al.
2446 (2012) and Sun et al. (2012); CIA value is calculated using published data by Zhang et al.
2447 (2005); Carbon isotopic excursion after Burgess et al. (2014); Eu/Eu* and Ce/Ce* values
2448 after Zhao et al. (2013a). TOC profile after Yin et al. (2012). Framboid size data from this
2449 study. Detailed bioturbation data see Fig. 3; II = Ichnofabric indices; BPBI = Bedding
2450 plane bioturbation index. Datum source of burrow diameters sees Fig. 24. More details of
2451 fossil fragment contents see Fig. 14. Species and genus richness data after Song et al.
2452 (2013a). Community structure data from Chen et al. (2010a).

2453

2454 **Table captions**

2455

2456 Table 1. Radiometric ages obtained from the P-Tr succession at the GSSP Meishan (in
2457 Ma).

2458 Table 2. Key conodont zones with their durations across the PTB in Meishan.

2459 Table 3. Percentage of major components in all rocks sampled from Beds 22-60 in
2460 Meishan.

2461 Table 4. X-ray diffraction (XRD) data of the PTB beds at Meishan (sourced from Liang,
2462 2002).

2463 Table 5. Structural indices of the latest Permian to earliest Triassic shelly communities
2464 from Meishan (Chen et al., 2010a).

2465 Table 6. Major indices showing community structural changes over the P-Tr transition in
2466 Meishan

2467 Table 7. Characteristics of major trace fossils from the uppermost Permian to lowest
2468 Triassic in Meishan
2469

Complete biotic and sedimentary records of the Permian-Triassic transition from Meishan section, South China: ecologically assessing mass extinction and its aftermath

Zhong-Qiang Chen^{a,*}, Hao Yang^a, Mao Luo^b, Michael J. Benton^c, Kunio Kaiho^d, Laishi Zhao^e, Yuangeng Huang^a, Kexing Zhang^a, Yuheng Fang^a, Haishui Jiang^a, Huan Qiu^c, Yang Li^c, Chengyi Tu^a, Lei Shi^a, Lei Zhang^c, Xueqian Feng^a, Long Chen^a

^a *State Key Laboratory of Biogeology and Environmental Geology, China University of Geosciences (Wuhan), Wuhan 430074, China*

^b *School of Earth and Environment, The University of Western Australia, Crawley, WA 3009, Australia*

^c *School of Earth Sciences, University of Bristol, Bristol, BS8 1RJ, UK;*

^d *Institute of Geology and Paleontology, Tohoku University, Sendai 980-8578, Japan;*

^e *State Key Laboratory of Geological Processes and Mineral Resources, China University of Geosciences (Wuhan), Wuhan 430074, China*

* Corresponding author (Z.Q. Chen). *E-mail address:* zhong.qiang.chen@cug.edu.cn

ABSTRACT

The Meishan section, South China is the Global Stratotype Section and Point (GSSP) for the Permian-Triassic boundary (PTB), and also is well known for the best record demonstrating the Permian-Triassic mass extinction (PTME) all over the world. This section has also been studied using multidisciplinary approaches to reveal the possible causes for the greatest Phanerozoic biocrisis of life on Earth; many important scenarios interpreting the great dying have been proposed on the basis of data from Meishan.

Nevertheless, ~~hot~~ debates on biotic extinction patterns and possible killers still continue.

This paper reviews all fossil and sedimentary records from the Permo-Triassic (P-Tr) transition, based on previously published data and our newly obtained data from Meishan, and assesses ecologically the PTME and its aftermath to determine the biotic response to climatic and environmental extremes associated with the biocrisis. Eight updated conodont zones: *C. yini*, *C. meishanensis*, *H. ~~Changhsingensis~~changxingensis*, *C. taylorae*, *H. parvus*, *I. staeschei*, *I. isarcica*, and *C. planate* Zones are proposed for the

35 PTB beds at Meishan. Major turnover in fossil fragment contents and ichnodiversity
36 occurs across the boundary between Bed 24e-5 and Bed 24e-6, suggesting an extinction
37 horizon in thin section. The irregular surface in the middle of Bed 27 is re-interpreted as a
38 firmground of *Glossifungites* ichnofacies rather than the previously proposed submarine
39 ~~solution~~dissolution surface or hardground surface. Both fossil fragment contents and
40 ichnodiversity underwent dramatic declines in Beds 25–26a, coinciding with metazoan
41 mass extinction. Fossil fragment content, ichnodiversity and all ichnofabric proxies
42 (including burrow size, tiering level, bioturbation level) indicate that the P-Tr ecologic
43 crisis comprises two discrete stages, coinciding with the first and second phases of the
44 PTME in Meishan. Ecologic crisis lagged behind biodiversity decline during the PTME.
45 Pyrite framboid size variations suggest that depositional redox condition was anoxic to
46 euxinic in the latest Changhsingian, became euxinic in Beds 25–26a, turned dysoxic in
47 Bed 27, then varied from euxinic to anoxic through most of the Griesbachian. The ~~~10~~
48 9°C increase in seawater surface temperature from Bed 24e to Bed 27 at Meishan seems
49 to result in dramatic declines in biodiversity and fossil fragment contents in Beds 25–26a,
50 but had little effect on all ecologic proxies. Both metazoans and infauna seem not to be
51 affected by the pre-extinction anoxic-euxinic condition. The anoxic event associated with

the PTME may have occurred in a much shorter period than previously thought and is only recorded in Beds 25–26a at Meishan. Fossil fragment contents, ichnofaunas, ichnofabrics and pyrite framboid size all show that no signs of oceanic acidification and anoxia existed in Bed 27. The early Griesbachian anoxia may have resulted in rarity of ichnofauna and metazoans in the lower Yinkeng Formation, in which the ichnofauna is characterized by small, simple horizontal burrows of *Planolites*, and metazoan faunas are characterized by low diversity, high abundance, opportunist-dominated communities.

The rapid increase of ~9 °C in sea-surface temperature and a short anoxia or acidification coincided with the first-pulse biocrisis, while a prolonged and widespread anoxia probably due to a long period of high seawater temperate condition may be crucial in morality of most organisms in the second-pulse PTME. Marine ecosystems started to recover, coupled with environmental amelioration, in the late Griesbachian.

Keywords: mass extinction, Permian-Triassic, fossil fragment, trace fossils, redox condition, Meishan section

69	Contents
70	1. Introduction
71	2. Biochronostratigraphy: an update
72	2.1. Biostratigraphy and correlations
73	2.2. Geochronology
74	2.3. Duration of key conodont zones across the P-Tr boundary
75	3. Microstratigraphy, fossil fragment contents and paleoenvironmental analysis of the
76	P-Tr transition
77	3.1. Bed 23
78	3.2. Bed 24
79	3.3. Bed 25
80	3.4. Bed 26
81	3.5. Bed 27
82	3.6. Bed 28
83	3.7. Beds 29-59
84	4. Biotic changeover through the P-Tr transition
85	4.1. Biodiversity variations over the P-Tr transition

86	4.2. Fossil fragment content variations through the P-Tr transition
87	4.3. Community structural changes of shelly faunas
88	5. Trace fossils and bioturbation
89	5.1. P-Tr ichnotaxa and their stratigraphic distributions at Meishan
90	5.1.1. Stratigraphic distributions of ichnoassemblages
91	5.1.2. Ichnofabric changes within Bed 27
92	5.2. Extent of bioturbation
93	5.3. Changeover of trace-fossil diversity over the P-Tr transition
94	5.4. Burrow size variations through the P-Tr transition
95	5.5. Trace fossil form and complexity
96	5.6. Infaunal tiering
97	6. Size variations of pyrite framboids and redox conditions over the P-Tr transition
98	7. Assessing ecologically PTME and its aftermath
99	7.1. Testing extinction patterns
100	7.2. Ecologic crisis lagging behind biodiversity drop at the PTME
101	7.3. Dramatic increase in seawater temperature and its consequences
102	7.4. Anoxic events <u>and biotic response</u>

103

7.4.1. Anoxic events

104

7.4.2. Biotic response

105

7.5. Testing extinction mechanisms and biotic response

106

7.5.6. Post-extinction amelioration of marine ecosystems in late Griesbachian

107

8. Conclusions

108

109

Formatted: Indent: Left 2.36 ch, First line: 2 ch

Formatted: Font: Not Italic

1. Introduction

As the greatest biocrisis of life on Earth (Sepkoski, 1981), the Permian-Triassic mass extinction (PTME) changed Earth's ecosystems fundamentally (Benton and Twitchett, 2003; Erwin, 2006). After they had recovered, the marine ecosystems after the PTME gave rise to the forerunners of modern-day ecosystems, both the Triassic and modern ecosystems being comparable to each other in composition of functioning groups and trophic structure (Chen and Benton, 2012). However, the causes of this enigmatic biocrisis have long been disputed despite intense study, and the same is true of the profoundly delayed recovery following the PTME (Erwin, 2001). Thus, studies of these issues have enjoyed a surge in scientific interest in the past 30 years that shows no sign of abating (Chen et al., 2014a).

Although this era-boundary crisis has been widely recognized in Permian–Triassic boundary (PTB) sections around the world, many important hypotheses have been proposed based on paleontological and experimental data sampled from the Meishan section of Changhsing County, Zhejiang Province, east China (Fig. 1A; Renne et al., 1995; Bowring et al., 1998; Jin et al., 2000; Yin et al., 2001, 2012; Kaiho et

127 al., 2001, 2006a, b; Mundil et al., 2001, 2004; Grice et al., 2005; Xie et al., 2005, 2007;
128 Riccardi et al., 2007; Wang and Visscher, 2007; Cao et al., 2009; Chen et al., 2009, 2010a;
129 Song et al., 2009, 2013[a,b](#); Shen et al., 2011b; Huang et al., 2011; Wu et al., 2013; Wang
130 et al., 2014; Burgess et al., 2014; Fig. 1A). This section is the Global Stratotype Section
131 and Point (GSSP) for the PTB (Yin et al., 2001; Fig. 1C) and also well known for the best
132 record of both biotic and geochemical signals demonstrating the PTME all over the world.
133 Here, the exposures of the PTB beds are spectacular, extending about 2 km laterally along
134 the Meishan hill (Fig. 1E). The PTME has been well demonstrated by Jin et al. (2000),
135 whose study based on paleontological data from Meishan reveals that this extinction
136 event was abrupt and dramatic, with most Permian organisms being wiped out within a
137 very short interval, which was precisely calibrated to the base of Bed 25, a white clay bed,
138 in Meishan (Fig. 1B, D), while the PTB is placed at the middle of Bed 27, about 16-20 cm
139 above the base of Bed 25 in the same section (Yin et al., 2001; Fig. 1C). As such, the
140 biocrisis clearly pre-dated the PTB (Fig. 1D). The P-Tr ecologic crisis is also marked by a
141 pronounced negative carbon isotopic excursion (Xu and Yan, 1993; Jin et al., 2000;
142 Kaiho et al., 2001; Cao et al., 2002; Xie et al., 2005, 2007; Fig. 2) and is also associated
143 with an end-Permian sulfur event (Kaiho et al., 2006; Riccardi et al., 2006).

After Jin et al.'s (2000) influential study, which was largely based on fossil data obtained in 1980s (i.e., Zhao et al., 1981; Sheng et al., 1984; Liao, 1984; Sheng et al., 1987; Shi and Wang, 1987), abundant brachiopod and foraminifer faunas have been detected from Beds 25–27, immediately above the PTME horizon in Meishan (Chen et al., 2005a, 2006b; Song et al., 2007, 2009). Quantitative analysis of the updated foraminifer data from Meishan revealed a two-stage extinction pattern near the P-Tr boundary (Song et al., 2009), which agrees well with two distinct peaks of cyanobacteria, detected by biomarker analysis from the same section, suggesting two extinction events corresponding to Beds 25 and 28 (Xie et al., 2005). The two-stage extinction pattern is also strengthened by extremely abundant benthic fossils obtained from a shallow platform facies of the PTB section at Huangzhishan, about 40 km from Meishan (Chen et al., 2009). However, Shen et al. (2011b) clarified an abrupt biotic decline in a short interval equivalent to Beds 25–28 of Meishan based on quantitative analysis of fossil records from Meishan and other PTB sections in South China. In contrast, Song et al. (2013a) demonstrated nicely a two-stage extinction pattern for the P-Tr crisis based on quantitative analysis of paleontological data derived from Meishan and a further six PTB sections in South China. Thus, debate on whether the PTME was either a single crisis or

episodic extinctions still continues (Shen et al., 2011b; Song et al., 2013a; Wang et al., 2014). Regardless of whether the extinction was single or a two-phase pattern, an increasing number of faunas have been found in Beds 25-28 of Meishan and its counterparts across all of South China, although this interval may just last 60 kyr (Burgess et al., 2014).

In addition, a further extinction event resulting in depletion of Permian reefs in South China was calibrated to the base of Bed 24e at Meishan (Yang et al., 1993). Yin et al. (2007) re-documented biotic and geochemical signal changes across this horizon, which is reinforced by several lines of evidence, including reduction in conodont sizes (Luo et al., 2006), possible extinction of radiolarians in deep habitats and a negative shift in organic carbon isotope values (Cao et al., 2009). To sum up, biotic variations based on sound paleontology over the P-Tr transition have been far less studied in comparison with the intense geochemical studies of this catastrophe in most PTB sections. Current, updated fossil records from extensive PTB sections are crucial to reveal the true biotic responses to these environmental crises.

As briefly summarized above, there have been great advances in research on the PTME at Meishan in recent years. Multiple scenarios interpreting the causes of the P-Tr

biocrisis have been proposed based on experimental data sampled from this section. Nevertheless, any reasonable models interpreting the P-Tr crisis need to be tested by analysis of precise biotic extinction patterns and physiological reactions of victims and survivors (Knoll et al., 2007). As a result, we herein document the updated, complete fossil and sedimentary records, including microfacies, microfossils, body and trace fossils, and pyrite framboids, throughout the P-Tr transition and attempt to test biotic responses to various environmental and climatic catastrophes from the GSSP Meishan.

2. Biochronostratigraphy: an update

2.1. Biostratigraphy and correlations

After Yin et al.'s (2001) placement of the PTB at the base of Bed 27c, marked by the first appearance datum (FAD) of the conodont *Hindeodus parvus*, Jiang et al. (2007) established gondolellid and hindeodid conodont zones across the PTB in Meishan. The former include the *Clarkina yini*, *C. meishanensis* and *C. taylorae* Zones, while the latter comprise the *Hindeodus latidentatus*, *H. praeparvus*, *H. ~~Changhsingensis~~changxingensis*,

H. parvus, ~~*Isarcicella*~~-*staeschei*, and *I. isarcica* Zones (Jiang et al., 2007, fig. 2). Later, Zhang et al. (2009) integrated them as one conodont zonation series: *C. yini* Zone (Bed 24), *C. meishanensis* Zone (Bed 25), *H. ~~Changhsingensis~~-changxingensis* Zone (Beds 26-27b), *H. parvus* Zone (Bed 27c), *I. staeschei* Zone (Beds 27d-28), *I. isarcica* Zone (Beds 29-51), and *C. tulongensis*-*C. planata* Zone (Beds 52-72, top of the Yinkeng Formation).

Given that *C. taylorae* is confined to Bed 27a-28 in Meishan (Jiang et al., 2007; Zhang et al., 2009) and has also been widely reported from PTB beds around the world (Orchard et al., 1994; Orchard and Krystn, 1998; Nicoll et al., 2002; Algeo et al., 2012; Zhao et al., 2013^b), the *C. taylorae* Zone is regarded as a discrete zone beneath the *H. parvus* Zone and retained for Bed 27a-b (Fig. 2). In addition, we have also re-examined stratigraphic distributions of some key conodont species based on previously published data and newly extracted specimens from Meishan. An updated conodont zonation is proposed for the P-Tr succession of the GSSP Meishan (Fig. 2). The new conodont zones,

with their stratigraphic ranges in brackets, include *C. ~~Changhsingensis~~-changxingensis* Zone (Beds 22-23), *C. yini* Zone (Bed 24), *C. meishanensis* Zone (Bed 25), *H. ~~Changhsingensis~~-changxingensis* Zone (Bed 26), *C. taylorae* Zone (Bed 27a-b), *H.*

parvus Zone (Bed 27c-d), *I. staeyschei* Zone (Beds 28-29a), *I. isarcica* Zone (Bed 29b), *C. planata* Zone (Beds 30-54), and *Neoclarkina discreta* Zone (Bed 35 and above) (Fig. 2).

It is noteworthy that Yuan et al. (2014) confined the *C. changxingensis* Zone to mid-Bed 10 to mid-Bed 22, *C. yini* Zone to mid-Bed 22 to Bed 24d, and *C. meishanensis* Zone to Bed 24e to Bed 25. The first occurrence of the nominal species of these conodont zones seems to be lower than they occurred in our samples. In particular, *C. meishanensis* occurs in the so-called ‘white boundary clay’ bed and above strata in most PTB sections in South China (Zhang et al., 2007; Jiang et al., 2007, 2011, Zhao et al., 2013b) and is rarely present in the Permian bioclastic limestone. The *C. meishanensis* Zone is also associated with a pronounced negative shifting excursion of carbon isotopes in most of the PTB sections in South China. Accordingly, the bases of these Changhsingian conodont zones remain tentative and need to be confirmed when additional conodont samples are processed in future.

Other important findings from the PTB beds include restriction of *Isarcicella-peculiaris* to Bed 28 and the first occurrences of *Hindeodus eurypyge* and *Isarcicella-lobata* at the bases of Bed 27a and Bed 28, respectively (Jiang et al. 2007; fig. 2). These species also have the potential to serve as key elements marking the PTB beds (Jiang et al.,

229 [2007, 2011, 2014](#)). Of these, *I. lobata*, confined to Beds 28-29 in Meishan, was proposed
230 as a distinct zone between the *H. parvus* and *I. staeschei* Zones in the southern Alps (Perri
231 and Farabegoli, 2003, 2012; Fig. 2). This species therefore occurred slightly earlier in the
232 southern Alps than in the GSSP Meishan. In the new conodont zonation, the *I. isarcica*
233 Zone is retained for Bed 29b, and thus has a much narrower stratigraphic range than
234 before. The *C. planata* Zone is newly proposed for Beds 30-54 and the *Neoclarkina*
235 *discreta* Zone for Bed 55 and higher strata in Meishan (Fig. 2) based on re-examination of
236 their stratigraphic distributions (Zhang et al., 2007, 2009).

237 The updated conodont zonation enables the PTB beds of Meishan to be
238 correlated precisely with their counterparts recorded elsewhere in the Tethys region, such
239 as North Italy, Iran, Germanic basin, and Spiti of Himalaya region (Fig. 2). The *H. parvus*,
240 *I. staeschei* and *I. isarcica* Zones have also been recognized in both Spiti and North Italy
241 (Fig. 2). Both *H. parvus* and *I. isarcica* Zones occur in the Abdadeh region, Iran (Korte et
242 al., 2004). Korte et al. (2004) also argued that there might be a hiatus between Beds 24e
243 and 25 because both the *C. iranica* and *C. hauschkei* Zones, between the *C. yini*-*C. zhangi*
244 and *C. meishanensis*-*H. praeparvus* Zones, are absent in Meishan. *C. hauschkei* does
245 occur in Meishan, but shares the same stratigraphic range with both [AC](#). *yini* and [AC](#).

246 *zhang* in Bed 24 (Jiang et al., 2007, 2011). More importantly, no sedimentary gap has
247 been found in this interval in the GSSP Meishan (see below). The last occurrence of both
248 *C. yini* and *C. zhang* has been calibrated to the top of Bed 24e (Yin et al., 2001; Zhang et
249 al., 2007; Jiang et al., 2007). The depositional succession between the *C. meishanensis*
250 and *C. yini* Zones shows no sign of a hiatus. Thus, both *NC. hauschkei* and *NC. iranica*
251 either can be recognized from the upper part of the *N. yini* Zone in the future, or do not
252 occur due to different biofacies controls (Korte et al., 2004).

253 Recognition and correlations of PTB beds in conodont-barren sections have long
254 remained problematic. Chen et al. (2009) established the bivalves *Claraia huzhouensis*-*C.*
255 *cf. bioni* and *Eumorphotis venetiana*-*Towapteria scythica*-*Pteria ussurica variabilis*
256 Assemblages from the PTB beds of both the Meishan and adjacent Huangzhishan
257 sections. The former is coeval with the *C. meishanensis* and *H. Changhsingensis*
258 *changxingensis* Zones of the GSSP Meishan (Chen et al., 2009). The small, weakly
259 costated *Claraia*-like species “*Peribositra*” *baoqingensis* from Bed 26 of Meishan (Zhao
260 et al., 1981) has been re-assigned to *Claraia* (Chen, 2004). These primitive *Claraia*
261 species from Meishan are diagnostic of the *C. huzhouensis*-*C. cf. bioni* Assemblage and
262 locate the PTME in the shallow-water, conodont-barren PTB sections in South China

(Chen et al., 2009). The latter bivalve assemblage is contemporaneous with the *H. parvus* Zone in the Huangzhishan section, pointing to an age of earliest Triassic (Chen et al., 2009). Both *Claraia wangi* and *C. griesbachi* are also ~~very~~ abundant in Beds 29b-54 in Meishan, and thus form the *C. wangi*-*C. griesbachi* Assemblage (Chen et al., 2010a), which is coeval with the *I. isarcica* and *C. planata* Zones (Fig. 2). The ammonoids *Rotodiscoceras*, *Hypophiceras*, *Ophiceras*, and *Lytrophiceras* characterize the assemblages from Beds 22-24, Beds 25-26, Beds 27-50, and Beds 51-55, respectively in Meishan (Fig. 2; Zhao et al., 1984; Sheng et al., 1984; Yin et al., 2001; Chen et al., 2010a). Brachiopods are also reasonably abundant in Beds 25-26, Bed 27 and Beds 51-55 of Meishan (Chen et al., 2002, 2006b, 2007). They are assignable to the *Tethyochonetes liaoi* Assemblage (Beds 25-26), *Paryphella triquetra* Assemblage (Bed 27), and *Meishanorhynchia meishanensis* Assemblage (Beds 51-55) (Chen et al., 2010a). Song et al. (2007, 2009) also reported diverse foraminifers from the Changhsing and lowest Yinkeng Formations in Meishan, but did not establish biozones. A palynological *Lundbladispota-Taeniaesporites-Equisetosporites* Assemblage was established from Beds 33-53 of the Yinkeng Formation (Zhang et al., 2007), which, therefore, correlates collectively with the conodont *C. planata* Zone (Fig. 2).

2.2. Geochronology

In Meishan, volcanic ash beds are well exposed and conspicuous in the uppermost Permian to Lower Triassic successions. In particular, Beds 25 and 28 near the PTB have been dated by multiple research groups using various techniques (Table 1). The most updated radiometric ages for Beds 25 and 28 are 251.941 ± 0.037 Ma and 251.880 ± 0.031 Ma, respectively (Burgess et al., 2014), which constrain the duration between those two phases of the PTME (Song et al., 2013a) or the duration of the PTME (Shen et al., 2011b; Wang et al., 2014) as 60 ka (Burgess et al., 2014). Burgess et al. (2014) have also given updated estimates for sediment accumulation rates through the P-Tr transition, which show that sedimentation rates of the Changhsing Formation decline towards the end of the Permian, reach the lowest value during the time of extinction (Beds 25-28), and then increase gently in the early Griesbachian (Beds 28-37) and steeply in the early-middle Griesbachian (Beds 37-48) in Meishan (Burgess et al., 2014). In addition, these authors estimated that the abrupt decline in $\delta^{13}\text{C}_{\text{carb}}$ in Bed 24e took place at 251.950 ± 0.042 Mya, while the FAD of *H. parvus* at the GSSP Meishan is at $251.902 \pm$

0.024 Mya (Burgess et al., 2014).

2.3. Duration of key conodont zones across the P-Tr boundary

At Meishan, intense high-precision dating of volcanic ash beds (Table 1) and high resolution conodont zones (Fig. 2) allow reasonable estimates of the duration of each conodont zone. The widespread *H. parvus* Zone is estimated to have lasted 16 ka (Table 2), while the *C. meishanensis* Zone, the PTME marker, lasted 8 ka, which is much shorter than previously thought. The last conodont zone prior to the PTME, the *C. yini* Zone, may have lasted 28 ka (Table 2).

3. Microstratigraphy, fossil fragment contents and paleoenvironmental analysis of the P-Tr transition

At Meishan, the P-Tr succession comprises the Changhsing and Yinkeng Formations below and above. The former unit is a 41-m-thick carbonate succession consisting of medium- to thin-bedded limestone, while the Yinkeng Formation is about

15 m thick and dominated by mudstone and muddy limestone in the lower part and characterized by thin-bedded limestone in the upper part (Fig. 3). These two formations have been frequently described (Zhao et al., 1981; Sheng et al., 1984, 1987; Yang et al., 1987; Yin et al., 1996, 2001; Zhang et al., 2005). Cao and Zheng (2007) re-described the Changhsing Formation (Beds 1-24) and recognized 247 natural, single layers, each 2 to 37 cm in thickness. Chen et al. (2007) gave an updated description for the Yinkeng Formation (Beds 25-59), in which 183 natural layers are recognizable. In addition, Cao and Shang (1998) conducted the first cm-scale stratigraphy, also termed microstratigraphy, of the P-Tr boundary beds in Meishan. Since then, Microstratigraphy of the PTB beds (Beds 24-29) of the Meishan section has also been intensely studied (~~Cao and Shang, 1998;~~ Cao and Zheng, 2009; Zhao and Tong, 2010; Zheng et al., 2013).

The top two beds of the Changhsing Formation, Beds 23-24, record important sedimentary and paleontological information just prior to the PTME, while most parts of the Yinkeng Formation record the severe biotic extinction and its consequences. Thus, microstratigraphy of the uppermost Changhsing Formation to Yinkeng Formation succession (Beds 23-59) is summarized here in view of the previously published data and

331 our new observations in petrologic thin sections. These thin sections were sampled
332 almost continuously in Beds 24e to 29 and in a 20-cm-interval in Beds 22 to 24d of the
333 Changhsing Formation. The sampling interval is 0.5 m throughout Bed 30 to Bed 59 of
334 the Yinkeng Formation in the GSSP Meishan.

335 ~~In addition, p~~Point counting is a relatively quick method that quantifies the
336 occurrence of skeletal fragments of major fossil groups in different horizons under the
337 microscope (Flügel, 1984; Payne et al., 2006). However, care must be taken when using
338 the point-counting method because large shell fragments of some clades may bias
339 counting results (Jacobsen et al., 2011). As an alternative, Jacobsen et al. (2011) proposed
340 the equal area approach to quantify the occurrence of skeletal fragments in thin section. In
341 order to eliminate biases of counting areas, it is suggested that at least eight equal area
342 fields of view ought to be counted per thin section sample (Jacobsen et al., 2011). Similar
343 to the equal area approach, fragment percentage data of various clades from each thin
344 section are estimated based on the observation of 300 to 350 views under a magnification
345 of $\times 50$ in one sample, collected for microfacies analysis of the PTB beds. Then,
346 percentages of various skeletal components, micrite, cavities and undertermined particles
347 (i.e., pyrites and other minerals) from samples throughout Bed 22 to Bed 60 of Meishan

were combined to yield the mean abundance of each composition in each sample

throughout the study succession (Table 3).

3.1. Bed 23

Bed 23 of the upper Changhsing Formation comprises dark gray thin-to medium-bedded bioclastic limestone interbedded with thin-bedded muddy limestone and siliceous mudstone layers. Small-scale wavy cross bedding is commonly present in the bioclastic limestone, while horizontal stratification occurs in the muddy limestone and siliceous mudstone (Fig. 4G, H). Grain-grading bedding structures are also occasionally present in the bioclastic limestone unit. The bioclastic limestone usually has a packstone to grainstone texture. The former texture is very common, while a grainstone texture is also occasionally present (Fig. 5C). This unit is usually strongly bioturbated in comparison with the weakly bioturbated thin siliceous layers that are usually horizontally stratified (Fig. 3). The autochthonous and allochthonous fossil assemblage is highly diverse and dominated by foraminifers, crinoids, and brachiopods with minor constituents of ostracods, echinoids, bryozoans, sponge spicules, calcareous sponges,

gastropods, radiolarians, and macroalgae (Fig. 6). The matrix comprises micrite (about 20-23%, Fig. 6). Cavities, pyrites and other undetermined particles are also commonly present (Table 3). The alternating occurrence of horizontal stratification and small-scale cross bedding and/or grain-grading bedding structures indicates that Bed 23 was deposited on a carbonate ramp between fair-weather wavebase and storm wavebase (Fig. 3; Zhang et al., 2005).

3.2. Bed 24

Bed 24, the topmost unit of the Changhsing Formation, consists mainly of thin- to medium-bedded bioclastic packstone rich in large ammonoids and other macrofossils (Fig. 4E). This bed has attracted intense attentions in terms of fossil record and sedimentary characterization because of its stratigraphic position just beneath the biotic extinction horizon (base of Bed 25; Jin et al., 2000). Bed 24, 71-90 cm in thickness, is usually labelled as Bed 24a-e (Yin et al., 1996) and consists of 14 layers, with the thinnest being 2 cm thick (Cao and Zheng, 2007). The conodonts from Bed 24 belong to the *Clarkina yini* Zone (Mei et al., 1998), which is distinct from the underlying *Clarkina*.

Formatted: Font: Not Italic

~~Changhsingensis-changxingensis~~ Zone (Beds 22-23).

Bed 24a-c has similar petrographic features to Bed 23 (Figs. 5D, 6). The dark organic-rich muddy limestone or siliceous mudstone, usually ~~less than 1~~ about 2 cm in thickness, has well-developed horizontal stratifications and possesses packstone to micritic textures with tiny, highly fragmented fossil skeletons of brachiopods and ostracods. These horizontally stratified layers are usually weakly bioturbated. In contrast, the bioclastic limestone unit, usually > 5cm thick, possesses small-scale wavy cross bedding and bioclastic packstone to grainstone texture. These layers are also highly bioturbated (Zheng et al., 2013). All skeletal components of Bed 23 also persist into Bed 24 (Fig. 6). Accordingly, Bed 24a-c was likely deposited in the same environment as Bed 23.

Although Bed 24d has similar petrographic texture to Bed 24a-c (Fig. 6), the presence of abundant fecal pellets and peloids characterizes the grain assemblage of Bed 24d. Fossil fragment contents in rocks from both Bed 24d and Bed 24a-c are also comparable with one another (Fig. 6). In addition, burrows are commonly present near the boundary between bioclastic limestone unit and organic-rich muddy limestone or siliceous mudstone layer. Bed 24d yields abundant trace fossils (see Section 5).

399 Pronounced cross-bedding and vertical burrows characterize the upper part of Bed 24d
400 (Fig. 4J). The top of Bed 24d is, however, weakly bioturbated and characterized by
401 smooth cone-shaped surfaces, which was termed a hard-ground structure representing
402 interrupted or highly condensed deposits (Cao and Zheng, 2009). Cao and Zheng (2009)
403 regarded this irregular contact as a sequence boundary indicating a changeover interface
404 from lowermost level to rapid rise. The same contact, however, has been interpreted as an
405 erosional surface, serving as a sequence base of a 3rd-order depositional sequence
406 following a major fall in sea level (Zhang et al., 1997; Yin et al., 2014). This
407 interpretation is reinforced by the presence of a diverse shallow-water facies trace fossil
408 assemblage including vertical burrows of *Balanogossites* (Fig. 4J; see also Section 5).
409 Cao and Zheng (2007) have also noted that abundant burrows of *Planolites* and *Skolithos*
410 and mud-crack structures are present near the boundary between Beds 24d and 24e.
411 Accordingly, Bed 24d, overall, is inferred to have been deposited in the upper part of the
412 subtidal zone of a carbonate ramp (Fig. 3; Zhang et al., 1997).

413 The topmost 10 cm thick limestone of Bed 24 is labelled Bed 24e, which
414 consists of eight natural layers (Cao and Zheng, 2009) and these were sampled at six
415 horizons here (Bed 24e-1 to Bed 24e-6). Trace fossils occur near the irregular contact

416 between Beds 24d and 24e-1 (see Section 5). Bed 24e, except for the topmost 3 cm (24e-5,
417 24e-6), is a dark gray bioclastic packstone containing abundant fossil fragments of
418 foraminifers, brachiopods, and crinoids. Other fossil groups such as bryozoans,
419 gastropods, macroalgae, ostracods, calcareous sponges, and sponge spicules are also seen
420 in thin sections, which have no major difference from the underlying Bed 24d (Fig. 6).
421 The uneven top surface is always capped by several muddy laminae. Cylindrical, ~~straight,~~
422 vertical burrows, ranging from 0.1 to 0.5 cm in diameter and from 3.0 to 1.0 cm in length
423 occur in the ~~lateral margin of the upper natural bedding~~ surface. Bed 24e saw a slight
424 increase in lime mud in the matrix and pyrite within the bed (see below). Bed 24e
425 therefore was probably deposited in the fair-weather wave action zone (Fig. 3) and was
426 interpreted as a lowstand platform margin wedge of a 3rd sequence (Zhang et al., 1997;
427 Yin et al., 2014).

428 The topmost 2-3-cm-interval, labelled as Bed 24e-5 and 24e-6, is characterized
429 by relatively low contents of P and Ca and high Ni content (Kaiho et al., 2001, 2006b).
430 Bed 24e-5, about 1.0-1.1 cm in thickness, comprises bioclastic packstone and contains
431 ~~very~~ abundant fossil fragments of foraminifers, crinoids, brachiopods, and ostracods.
432 Fragments of calcareous sponges, sponge spicules, gastropods, bryozoans and

macroalgae are also occasionally present, and these are comparable in major fossil components with Beds 24e-1 to 24e-4 (Fig. 6). Moreover, abundant, reasonably large horizontal burrows (*Planolites*) are densely packed on the surface of Bed 24e-6 (also see Section 5).

The contact between Beds 24e-5 and 24e-6 is a laminated wavy lime layer (Fig. 7D). Bed 24e-6 is a 10- to 19-mm-thick bioclastic packstone and dominated by silica bars, which were interpreted as sponge spicules (Kaiho et al., 2006). The elongate bars are actually longitudinal outlines and the circular grains are cross sections of spicules (Fig. 7A-C). This identification is reinforced by the abundant isolated silicified sponge spicule specimens extracted from Bed 24e-6 (Fig. 7E). Contrasting to the predominance of sponge spicules, fragmentary contents of foraminifers, crinoids, echinoids and brachiopods decline dramatically. The skeletal grain assemblage experienced a dramatic reduction in both abundance and diversity across the contact between Beds 24e-5 and 24e-6 (Fig. 7E), to which the PTME was calibrated (Kaiho et al., 2006a).

3.3. Bed 25

450 This bed is the so-called “Boundary clay bed” or “White clay bed” (Zhao et al.,
451 1981; Sheng et al., 1984; Yang et al., 1987). Its thickness ranges from 2 cm to 6 cm
452 depending on the weathering intensity, the higher the intensity the thicker the bed. The
453 bed grades upward into Bed 26 as a consequence of a gradual increase in organic and
454 calcareous content and decrease in volcanic ash layers. The total thickness of these two
455 beds is around 10 cm.

456 The basal part of Bed 25 comprises a 0.1- to 0.2-mm-thick layer of ~~grayish~~
457 greyish black mudstone rich in Fe grains, termed Bed 25-1, which usually becomes a
458 reddish ferruginous layer capping the dark Bed 24e-6 and is conspicuous at outcrops in all
459 Meishan quarries owing to weathering. Previously, this Fe-rich layer was termed the
460 “pyrite lamina” layer (Wignall and Hallam, 1993; Shen et al., 2007) or Pyrite layer (Cao
461 and Zheng, 2009), based on the abundant pyrite-like grains visible at outcrops. Elemental
462 analysis shows that these Fe grains are either Fe-Ni grains (Kaiho et al., 2001, 2006b) or
463 goethites (Liang et al., 2002). Pyrite framboids are also commonly present in this layer
464 (Shen et al., 2007). In addition, Zheng et al. (2013) detected abundant irregular volcanic
465 glasses from this layer.

466 The reddish ferruginous surface of Bed 25-1, together with the absence of both

the *N. iranica* and *N. hauschkei* conodont zones, was considered as evidence indicating an exposure surface and representing a hiatus (Korte et al., 2004). However, the presence of marine fossils such as foraminifers and brachiopods (Rui et al., 1988; Yin et al., 2001) in Bed 25 and abundant sponge spicules and other fossil fragments in Bed 24e-6 (Fig. 6) indicates the absence of a paleo-exposure surface or an aerial hiatus. The absence of these two conodont zones may relate to biofacies controls and cannot bracket a hiatus, as discussed in Section 2.1.

The overlying thin layer (Bed 25-2), 0.3-1 mm thick, is dark yellowish orange, and encompasses mainly gypsum and Fe (Table 4). The remaining part of Bed 25 (Layer 25-3, 2-4 cm thick; Kaiho et al., 2006b) is a light gray illite–montmorillonite–kaolinite claystone (white clay) (Table 4). Gypsum and pyrite are very common in thin section. No fossil fragments are seen in thin section (Fig. 5A). Marine fossils of conodonts, foraminifers, ostracods and tiny brachiopods have been found from this bed, but are always sparse (Rui et al., 1988; Jiang et al., 2007). Benthic carbonate skeletal fossils diminished dramatically in this bed. Calcareous shells are often pyritized and attached with crystals and framboidal pyrites on the surface (Rui et al., 1988). Conodonts from Bed 25 are included in the *C. meishanensis* Zone (Fig. 2). Microspherules and β -type

484 quartz crystals are much more abundant in this bed than in other ash clay beds, and could
485 be products of acid volcanic eruptions (He et al., 1987). However, comparable
486 | microsphaerules are also ~~very~~ abundant in the background soils in Meishan and other
487 PTB sections in South China, suggesting that they may be the modern industrial products
488 rather than geological objects (Zhang et al., 2014). Both Hf-isotope and elemental
489 analysis of magmatic zircons suggests these ash clays near the PTB in South China may
490 have been sourced from volcanism taking place along the convergent continent margins
491 during the formation of the Pangea supercontinent (Gao et al., 2013).

492

493 3.4. Bed 26

494

495 Bed 26, the so-called “black clay bed” (Yang et al., 1987), comprises black shale,
496 4-6 cm in thickness. Nine pronounced yellow clay layers are interbedded in the black
497 shale. Horizontal laminae and pyrite are common. The clay layer is composed mainly of
498 montmorillonite–illite, which is similar to that of Bed 25 (Table 4). Fossil fragments are
499 very rare in most parts of this bed (Fig. 5B) except for the top 2-cm-interval where fossil
500 fragments are fairly abundant in calcareous nodules (Fig. 8), including foraminifers,

501 ostracods, echinoids, bryozoans, and brachiopods (Table 3; Figs. 6, 8). Microspherules
502 or/and α -quartz (in the form of β quartz pseudomorphs; He, 1981) are rich in the lower
503 part, but they may be the products of modern industry (Zhang et al., 2014). Various
504 burrowing systems are common in the upper part of Bed 26, from which Cao and Zheng
505 (2009, fig. 5b) identified *Chondrites*, *Planolites* and *Zoophycos*. The identification of the
506 last ichnogenus, however, is problematic based on insufficient information illustrated by
507 these authors. The upper part of the bed, Bed 26b, therefore is highly bioturbated (Fig. 3;
508 Cao and Zheng, 2009).

509 Skeletal fossils are rare but considerably diverse, including ammonoids,
510 brachiopods, bivalves, ostracods, and conodonts. Co-occurrence of the Triassic-type
511 faunas (i.e., *Otoceras*, *Claraia* and many conodont species) and Permian-type elements
512 (i.e., ammonoids *Pseudogastroceras* and *Xinodiscus*, and many brachiopods and
513 foraminifera) is particularly interesting. Brachiopods are small in size and thin-shelled,
514 and include species of *Orbicoiella*, *Preliassoryhynchia*, *Cathaysia*, *Paryphella*,
515 *Tethyochonetes*, and *Spinomarginifera* (Chen et al., 2006b; Chen and McNamara, 2006).
516 The presence of the relatively diverse fossil assemblage in the upper part of Bed 26
517 indicates the earliest re-colonization of epifauna on the barren soft substratum

immediately after volcanic eruption. Most of these shelly fossils are complete and well preserved regardless of the delicacy of the skeleton. The change from Bed 26 to Bed 27 is gradual and no boundary surface can be recognized. Crystal and framboidal pyrite are concentrated in a discontinuous dark lamina with rich organics (Shen et al., 2007). The slow sedimentation rate, and quiet and anoxic environment (Shen et al., 2007) suggest that Bed 26 probably represents a semi-closed, low-energy subtidal zone (Fig. 3). The succession of Beds 24e, 25 and 26, overall, shows that continuing fall of sea level through Bed 24e turned to a rise in the upper part of Bed 26, with the lowest point of sea level corresponding probably to the base of Bed 25 (Yin et al., 2014).

3.5. Bed 27

Bed 27 comprises biotic packstone to wackestone with occasionally micrite texture and contains fairly abundant fossil skeletons and pyrite crystals throughout the bed (see Section 6). Relatively complete shells of ostracodes, foraminifers and thin-shelled brachiopods are reasonably abundant. This bed contains three major irregular contact surfaces, termed hardground surfaces (Cao and Shang, 1998) and firmground

535 surfaces (Cao and Zheng, 2009), at various levels (Fig. 9). Of these, the first irregular
536 surface is rather pronounced, about 5 cm above the base of Bed 27 and near the boundary
537 between Beds 27a and 27b. The second occurs near the contact between Bed 27c and 27d,
538 while the third is not prominent and occurs within Bed 27d (Fig. 9). These ‘firmground’
539 surfaces divide Bed 27 into three depositional cycles, with each beginning with dark
540 muddy limestone and grading upwards into pale bioclastic limestone. Rich organic and
541 muddy laminae parallel to the bedding plane decrease upward from the base within each
542 cycle. The upper unit of each cycle was disturbed by repeated burrowings, which form
543 part of the firmground (see Section 5). Microscopic examination reveals that the dark,
544 early-lithified rock contains a minor percent of clay, rich organic shreds and bioclasts (Fig.
545 9; Table 4).

546 Microfossils in Bed 27 are much more abundant and diverse than previously
547 thought (Fig. 6). Of these, foraminifera are most abundant among all clades. Echinoids
548 are also remarkably abundant, although they cannot be identified beyond a certain
549 taxonomic level (Figs. 10-12). Bed 27a contains fossil skeletons of foraminifers,
550 ostracods, echinoids, and brachiopods (Fig. 10), which is similar in component
551 composition to Bed 26 (Fig. 6). Bed 27b comprises marls and clays in the lower part, in

which fossil fragments are very rare (Fig. 9). The remainder of Bed 27b yields a fossil fragment abundance (FFA) composed mainly of foraminifers and brachiopods (Fig. 6). Both Beds 27c and 27d contain much more abundant and diverse FFA than Bed 27b (Figs. 10-12), both of which are dominated by foraminifers, ostracods and brachiopods with minor constituents of echinoids (Fig. 6).

It should be noted that Bed 27 is usually subdivided into four layers (Yin et al., 2001). Cao and Zheng (2009), however, divided this bed into six layers (units) including a stromatolite layer (Bed 27-5) and mudstone (Bed 27-6) in the upper part of Bed 27. Later, Zheng et al. (2013) denied the existence of the stromatolite layer and divided Bed 27 into five layers; no stromatolitic structures are seen in our thin sections either. Except for the topmost 0.5 cm thick layer of carbonaceous mudstone, another four layers are similar to those recognized by Yin et al. (2001). In addition, Cao and Zheng (2009) and Zheng et al. (2013) interpreted the irregular surface separating Beds 27a and 27b (Fig. 9) as firmground surface as a result of a rapid transgression. Here, we agree with the firmground interpretation of these irregular surfaces within Bed 27 (Cao and Zheng, 2009; Zheng et al., 2013) because of the presence of abundant burrows typical of the *Glossifungites* ichnofacies (Seilacher, 1967) and distinct lithological interfaces, typically

569 dark muddy micrite overlain by light gray, coarser-grained bioclastic
570 packstone-wackestone, within Bed 27 (Fig. 9; see also Section 5). Firmgrounds of the
571 *Glossifungites* ichnofacies, also termed omission surfaces (Knaust, 1998), have been
572 extensively used in sequence stratigraphy to identify and characterize discontinuity
573 surfaces (Pemberton and Frey, 1985; MacEachern et al., 1992, 2007; Buatois and
574 Mángano, 2011). Within Bed 27, the unlined burrows penetrating into muddy limestone
575 are passively filled with coarser grains from the overlying stratum. This means that the
576 burrows remained open after the trace maker had left, thereby permitting bioclast grains
577 from subsequent depositional events to fill the open, stable burrows. Although the
578 majority of documented *Glossifungites* ichnofacies are from shallow-marine settings
579 (Knaust, 1998; Buatois and Mángano, 2011), this ichnofacies is also present in relatively
580 deep marine contexts, such as incision of submarine canyons during relative sea-level
581 falls (e.g. Dasgupta and Buatois, 2012) or autogenic erosional episodes by turbidity
582 currents and bottom currents (Savrda et al., 2001; Gérard and Bromley, 2008; Hubbard
583 and Shultz, 2008). As such, the *Glossifungites* ichnofacies from Bed 27 may represent an
584 omission surface, but cannot indicate a precise depositional environment for Bed 27.
585 Integration of lithofacies, paleoecologic and ichnofacies indicates that Bed 27 may have

been deposited on a carbonate ramp near the storm wave action zone (Fig. 3), as suggested by Zhang et al. (1997; 2005).

3.6. Bed 28

Bed 28 comprises yellow claystone having similar composition to Bed 25 (Table 4), dominated by montmorillonite mixed with illite. Apart from conodonts (Jiang et al., 2007), no other fossils have been recovered from this bed.

3.7. Beds 29-59

Bed 29 encompasses wackestone with rare foraminifer tests (Fig. 13). Pyrite is commonly seen in thin section and pyrite content increases up-section. A minor omission surface, equivalent to the erosional surface of Zhang et al. (2007) is developed in the middle part of Bed 29 (Zhang et al., 2007). Fossil fragments are very rare and their contents decrease upwards within the bed (Fig. 6; Table 3). Bed 30 is a marlstone, which has a ~~wackestone to~~ micritic texture and lacks any fossil fragments (Table 3). Both beds

603 contain laminated stratification and lack any cross bedding, indicating a low-energy
604 environment. Beds 29-30 therefore may have been deposited in the upper part of the
605 offshore setting that is below fair-weather wavebase (Chen et al., 2007).

606 Beds 31-51 are typified by alternating black shale, greenish gray mudstone, and
607 gray marlstone in the lower part, and interbeds of gray calcareous mudstone and pale
608 muddy limestone in its upper part. They are subdivided into 39 cm-scale cycles (Chen et
609 al., 2007; Fig. 3). In general, the lower unit of the cycle is characterized by black shale or
610 greenish mudstone rich in bivalve and ammonoid fossils (Fig. 4F, I), while the upper unit
611 is dominated by calcareous mudstone and marlstone. The mudstone-dominated cycles
612 are transitional to the marl-dominated cycles up-section, indicating a long-term
613 up-shallowing cycle (Chen et al., 2002, 2007; Tian et al., 2014). In addition to the
614 lithologic variation, Beds 31-34 are characterized by the calcareous mudstone and shale
615 where laminated stratifications are commonly preserved (Fig. 4C), while the upper part
616 of the formation (Beds 35-51) is typified by an increasing number of laminated marl beds
617 (Fig. 3). Fossil fragments occur occasionally in Beds 45, 50 and 51, characterized by
618 foraminifer and ostracod skeletons (Table 3; Fig. 6). Horizontal burrows of *Planolites* are
619 present in Beds 36-51, which also yield a few shell beds of bivalves (i.e., *Claraia*

620 *griesbachi*) and ammonoids (*Ophiceras* spp.) (Chen et al., 2007). This unit was
621 interpreted as the result of sedimentation relatively deep offshore (Fig. 3; Zhang et al.,
622 2005; Chen et al., 2007).

623 Beds 52-53 comprise alternations of shale and marlstone, yielding reasonably
624 abundant burrows of *Chondrites* and *Planolites*. Increasing fossil fragment content is
625 seen in both Beds 52 and 53, in which foraminifer, ostracod and echinoid shell fragments
626 are remarkable (Fig. 13), although they are definitely minority components in thin
627 section (Fig. 6; Table 3). Moreover, horizontal stratification is commonly present in both
628 shale and marlstone. These two beds were interpreted as the result of sedimentation in the
629 relatively deep offshore below storm wavebase (Chen et al., 2007).

630 Towards the top of the Yinkeng Formation, the succession (Beds 54-59) is
631 dominated by marl-dominated cycles. A thin- to medium-bedded marl is hummocky
632 cross-stratified (HCS; Fig. 4A, B, D) and often displays multidirectional tool marks on
633 its base, and horizons of loading and soft sediment deformation are very common (Chen
634 et al., 2002). Fossil fragments are reasonably abundant in Beds 54-59 (Fig. 13), although
635 they are still in the minority in thin section (Fig. 6; Table 3). Foraminifers, ostracod and
636 echinoids characterize their FFA (Fig. 6; Table 3). Trace fossils are also commonly

Formatted: Font: Italic

Formatted: Font: Italic

Formatted: Font: Italic

present in these beds, including *Planolites isp.*, *Treptichnus sp.*, and *Thalassinoides isp.*

3. Of these Moreover, the sedimentary structure HCS was interpreted as having been

generated by offshore storm currents. Beds 54-59 therefore may have been deposited

offshore, near storm wavebase (Chen et al., 2007).

4. Biotic changeover through the P-Tr transition

4.1. Biodiversity variations over the P-Tr transition

Comprehensive paleontological studies of the Meishan section were undertaken

in the 1980s (Zhao et al., 1981; Sheng et al., 1984; Yang et al., 1987; Shi and Chen, 1987).

The fossil record employed by Jin et al. (2000) to document the PTME pattern, which

shows an abrupt extinction calibrated to the base of Bed 25, was sourced mainly from

these studies. Since then, more diverse faunas and floras have been documented from

Meishan, including foraminifers (Song et al., 2007, 2009), radiolarians (He et al., 2005),

brachiopods (Chen et al., 2002, 2005a, 2006b; Li and Shen, 2008; Chen and Liao, 2009),

conodonts (Nicoll et al., 2002; Tong and Yang, 2004; Luo et al., 2006, 2008; Jiang et al.,

654 2007, 2008; Zhang et al., 2007, 2009; Yuan et al., 2014), ostracods (Crasquin et al., 2010;
655 Forel and Crasquin, 2011), palynolomorphs (Zhang et al., 2007), and arcritarchs (Li et al.,
656 2004). Additional macrofossils were collected throughout the upper Changhsing
657 Formation to the Yinkeng Formation. Several shelly fossil communities from Beds 24, 26,
658 27, 32, 40, and 53-55 were quantitatively analysed (Chen et al., 2010a).

659 Shen et al. (2011b) and Wang et al. (2014) demonstrated a steep decline zone of
660 species richness corresponding to the interval between Beds 25 and 28 in Meishan by a
661 means of quantitative analysis on fossil records from more than ten PTB sections
662 (including Meishan) from South China. In contrast, Song et al. (2013a) calculated species
663 richness of each layer marked in microstratigraphic analysis (Beds 24-29) based on the
664 updated fossil record mentioned above. Species richness of single layers experienced a
665 stepwise but minor decline within Bed 24. Two distinct declines in species richness were
666 well demonstrated and calibrated to Beds 25 and 28. The same pattern is also indicated in
667 seven PTB sections in South China (Song et al., 2013a). Above Bed 28, species richness
668 remains very low in the remaining part of the Yinkeng Formation.

669 Here, additional fossil specimens, primarily brachiopods, ammonoids and
670 bivalves, have been collected from Beds 24e, 26, 27 to document biotic turnover across

the PTB. Moreover, microfossils were observed in the petrologic thin sections used for microfacies analysis (see Section 3). Of these, foraminifers are the most abundant skeletal fragments among all clades. Most of these foraminifer tests, however, were illustrated by Song et al. (2007, 2009), so the newly obtained fossil record does not affect the biotic extinction pattern revealed by Song et al. (2013a).

4.2. Fossil fragment content variations through the P-Tr transition

The abundance and diversity of skeletal grains within the late Changhsingian samples (Beds 22-24) is remarkably high. Skeletal grains from all sampled levels except for the top 1-2 cm (Bed 24e-6) of Bed 24e comprise 68-74% of the total rock volume in the uppermost Changhsing Formation (Fig. 14). Fossil fragment assemblages are strikingly similar to one another in all sampled layers within the interval between Bed 22 and 24e-5, and each of these is dominated by foraminifers, crinoids and brachiopods. Other major constituents include ostracods, bryozoans, sponge spicules, and macroalgae (Fig. 14). Skeletal grains of gastropods, calcareous sponges and radiolarians are relatively rare and absent in some horizons (Fig. 14).

It is noteworthy that FFAs do not appear to differ at all across the contact between Beds 24d and 24e, although an omission surface, also a 3rd sequence boundary (Zhang et al., 1997), separates these two layers (Zhang et al., 1997). In contrast, FFAs experienced a dramatic reduction in diversity across a lime laminae layer between Beds 24e-5 and 24e-6 (Figs. 6, 14). Above this lamina layer (Fig. 7D), skeletal grains of Bed 24e-6 comprise about 60% of all rock in thin section in comparison with nearly 70% in Beds 22-24e-5 (Fig. 14). The overwhelming majority of the FFA in Bed 24e-6 is sponge spicules (35%) with minor constituents of foraminifers (8%), brachiopods (7%), crinoids (6%), and echinoids (4%) (Table 3; Fig. 6). Furthermore, fusulinids disappeared forever at this lamina (Kaiho et al., 2006b). The FFA experiences a loss of five major orders (i.e., ostracods, bryozoans, calcareous sponges, gastropods, and macroalgae) across the boundary between Beds 24e-5 and 24e-6 (Figs. 6, 14). More importantly, this horizon coincides with a pronounced negative carbon isotope excursion and a sulfur isotopic excursion anomaly (Kaiho et al., 2006a, b), and thus marks the actual biotic extinction horizon (Kaiho et al., 2006b).

Fossil fragment contents form a high plateau in both abundance and diversity, comprising nearly 70% of total rock and including almost all skeletal clades recognized

from the Changshing Formation. They underwent a dramatic depletion in both abundance and diversity in Beds 25-26a, which are nearly barren of skeletal grains (Fig. 14). This severe depletion therefore is calibrated to the base of Bed 25, coinciding with the PTME (Jin et al., 2000; Shen et al., 2011b) or the ~~main phase~~first phase of the PTME (Song et al., 2013a). After the PTME, skeletal grains started to rebound in Bed 26b, the top 2-cm interval of the bed and 8-10 cm above the base of Bed 25. Fossil fragments in Bed 26b, however, comprise only 32% of all rock in comparison with nearly 70% before the PTME (Figs. 6, 14). The FFA in Bed 26b comprises mainly foraminifers, ostracods, brachiopods, bryozoans, and echinoids (Fig. 7). Both foraminifers and echinoids are the most abundant among all clades (Fig. 6). Of particular interest is the presence of both echinoids and bryozoans, with bryozoans represented by fenestellid fragments. These two clades have generally been believed to have gone extinct at the PTME (Sepkoski, 1981, 2002), but instead they occur in the aftermath of the PTME at Meishan. Their body fossils were also found in association with the *H. parvus* Zone in the neighbouring Huangzhishan section of western Zhejiang Province (Chen et al., 2009).

Fossil fragment abundance remains almost same as in Bed 26b, comprising nearly 31-38% through the entire Bed 27, except for Bed 27b, in which skeletal grains are

only 10% of all rock. Thus, fossil fragments rebounded and reached nearly half their pre-extinction level with a major depletion occurring in mid-Bed 27 (Fig. 14). If considering the FFA of the entire Bed 27, which contains elements of brachiopods, bryozoans, foraminifers, and ostracods (Table 3), then ~~Recovery~~ recovery of FFA diversity in Bed 27 is marked by the re-appearance of 45.5% of all pre-extinction orders (Table 3).

FFA experienced a major loss in Bed 29, down to less than 10% (Fig. 14). Fossil fragments are absent in Beds 28-44. After rebounding in Bed 45, the skeletal grain assemblage underwent a stepwise abundance recovery in Beds 50-51 and remained at a relatively stable level, occupying nearly 16% of all rock in Beds 52-60. FFA diversity, however, remains at a rather low level, with the re-appearance of only three orders: foraminifera, ostracods and echinoids (Fig. 14).

4.3. Community structural changes of shelly faunas

The P-Tr shelly communities are characterized by a mixture of large-sized ammonoids and small brachiopods in the uppermost Changhsing Formation and by

739 numerous shell beds in the Yinkeng Formation (Fig. 15). Chen et al. (2010a) recognized
740 six macrofossil communities from the uppermost Permian to lowest Triassic in Meishan,
741 including the *Rotodiscoceras* sp.–*Paracrithyris pigmaea* (*R–P*) Community (Bed 24),
742 *Tethyochonetes liaoi* (*T*) Community (Bed 26), *Paryphella triquetra*–*Tethyochonetes*
743 *liaoi* (*P–T*) Community (Bed 27), *Claraia griesbachi*–*Ophiceras* sp. (*C–O*) Community
744 (Bed 32), *Claraia wangi* (*C*) Community (Beds 40), and
745 *Meishanorhynchia*–*Lytophiceras* (*M–L*) Community (Beds 53–55).

746 Several diversity indices (Shannon and Simpson indices and Dominance) are
747 usually employed to measure community structures. It should be noted that the Shannon
748 measures are the only standard diversity indices that generate meaningful independent
749 alpha and beta components when the community weights are unequal or sampling is
750 uneven (Jost, 2007). Dominance index (*D*) measures ‘evenness’ of the community from 0
751 to 1, 0 being the most even distribution amongst taxa. Simpson index = $1 - \text{Dominance}$
752 index, and values range from 0 (one taxon dominates the community completely) to 1 (all
753 taxa are equally present) (Hammer et al., 2001). Note that these diversity indices are
754 useful in estimating diversity but are not themselves measures of diversity. Their
755 numerical equivalent indicates changes of true diversity (Jost, 2007; Kosnik and Wagner,

2006). Conversion of both Shannon and Dominance indices to true diversities developed by Jost (2006, 2007) is performed to indicate true diversity changes over the P-Tr transition. In addition, the bias-corrected Simpson evenness index (Olszewski, 2004) is also applied to estimate the evenness within and among communities examined here. Detailed community structural indices are listed on Table 5.

The late Changhsingian *R-P* community has Shannon index (H) of 2.029, which is slightly smaller than the same index of 2.796 for the Changhsingian brachiopod *Cathaysia-Martinia* (*C-M*) community reported from the Shaiwa Group of southern Guizhou Province, southwest China (Chen et al., 2006a), but is slightly larger than the same index of 1.879 for the Wuchiapingian brachiopod *Edriostege* *poyangensis-Spinomarginifera lopingensis* (*E-S*) Community reported from the basal Lungtan Formation of the Daijiagou section, Chongqing city, southwest China (Chen et al., 2005b). Dominance of the *R-P* community, $D = 0.1519$, also lies between the same indices of the above Changhsingian and Wuchiapingian brachiopod communities, with $D = 0.07375$ and 0.178 , respectively (Chen et al., 2010b, table 4). It is also true for evenness of community (E) that the *R-P* community has E of 0.8453, which lies between 0.9262 and 0.822, the values of E for the *C-M* and *E-S* communities, respectively (Chen et al.,

2010b). Accordingly, the *R-P* community is typical of Late Permian shelly communities.

In contrast, *H* values of all post-extinction communities, 1.47, 1.565, 0.7559, 0, and 1.288 for the *T*, *P-T*, *C-O*, *C*, and *M-L* communities, respectively (Table 5) are much smaller than the same values of the Changhsingian and Wuchiapingian communities, *H* = 2.796 and 1.879, respectively. These post-extinction communities therefore are much less diverse than the pre-extinction communities of the Late Permian, indicating the severe impact of the PTME on marine communities.

Changes in both standard diversity Shannon index [*Exp* (*H*)] and dominance index (*D'*) between neighboring pairs of communities show that major losses in diversity coincide with the turnovers of the *R-P/T* and *P-T/ C-O* communities, losing 43.6% and 55.5% respectively. Similarly, standard diversity dominance (*D'*) increases by 34% and 54%, respectively (Table 6). Thus, community structural collapse indicated by a decrease in diversity, coupled with increase in dominance, coincides with two extinctions bracketed at the bases of Beds 25 and 28 at Meishan (Song et al., 2013a). In addition, *Exp* (*H*) value increases by 262.6% from the *C* to *M-L* communities, and also increases by 70%, coupled with a decrease of 15.2% in *D'* values, from the *C-O* to *M-L* communities, suggesting an improvement in shelly community structures in Beds 53-55 at Meishan.

Structural improvement of the *M-L* community is also reinforced by comparison between the *M-L* community and the Anisian *Madonia* sp.–*Rhaetina angustaeformis* (*M-R*) Community, which marks the recovery of benthic communities in the Anisian (Chen et al., 2010b). The Anisian community has H and D values of 2.051 and 0.1501 respectively (Chen et al., 2010b, table 4), but the same values for the *M-L* community are H = 1.288 and D = 0.4379, respectively. Consequently, the *M-L* community embraces much more improved diversity indices than other Griesbachian communities in Meishan, but instead has a much lower diversity and higher dominance index than both pre-extinction and recovery communities.

5. Trace fossils and bioturbation

At Meishan, Bottjer et al. (1988) made the first attempt to ecologically test the PTME based on trace-fossil assemblages. These authors, however, could not collect sufficient trace fossils because of restricted exposure at that time, but they noted that ichnotaxa from the PTB beds are dominated by *Planolites* and *Chondrites*, which indicate generally a poorly oxygenated environment (Bottjer et al., 1988). Later, Cao and Shang

807 (1998) reported a few ichnotaxa such as *Thalassinoides*, *Planolites* and *Skolithos* from
808 the PTB beds of Meishan, but *Skolithos* was later rejected by these authors (Cao and
809 Zheng, 2009; Zheng et al., 2013). Zhang and Tong (2010) also examined trace fossils
810 recorded in drilling cores through the P-Tr transition in Meishan. Although these authors
811 clarified that trace fossil evidence suggests two ecologic crises, coinciding with Beds
812 24e-27 and Beds 34-39, respectively (Zhang and Tong, 2010), the documented
813 ichnofossils are too few to support such a conclusion (see Section 7). As a result, several
814 lines of evidence show that trace fossils are reasonably abundant in the PTB beds in
815 Meishan. They however remain poorly understood owing to inadequate trace fossil
816 specimens.

817 Here, we document our observations at all PTB sites newly exposed during the
818 construction of the geological park in the GSSP Meishan in the 2000s, which uncovered
819 extensive fresh exposures along all the quarries (Fig. 1E). Abundant trace fossils were
820 collected from Beds 8-9 and 23-24 of the Changhsing Formation and Beds 26-27 and
821 35-57 of the Yinkeng Formation. The ichnofabric indices (ii, *sensu* Droser and Bottjer,
822 1986) and bedding plane bioturbation index (BPBI, Miller and Smail, 1997) throughout
823 the upper Changhsing Formation and entire Yinkeng Formation are also examined.

5.1. *P-Tr ichnotaxa and their stratigraphic distributions in Meishan*

5.1.1. *Stratigraphic distribution of ichnoassemblages*

A total of 17 ichnospecies in 13 ichnogenera and a problematic ichnotaxon have been found in the P-Tr transition at Meishan (Figs. 16-18). Major characteristics, stratigraphic distributions and interpretation of each ichnotaxon are tabulated here (Table 7). Trace fossils are distributed mainly in Beds 8-9 and Beds 23-24 of the Changhsing Formation, and in Beds 27, 35-53, 55-57 of the Yinkeng Formation. Of these, the lower Changhsing Formation (Beds 8-9) ichnoassemblage is dominated by relatively large burrows of *Thalassinoides* isp. 1 (Fig. 16A, D) and resting traces of *Lockeia* isp. (Fig. 16F). *Paleophycus* isp. (Fig. 16B) is also commonly present in Beds 8-9.

The trace-fossil assemblage from Beds 23-24e is characterized by tree-like traces of *Dendrorhaphe* isp. (Fig. 17F) and abundant burrows of problematic status. The latter is represented by simple, straight, unbranched burrows (Fig. 17B-C), each originating at a small, close end and extending distally to form a horn-shaped burrow with an open

841 distal end (Fig. 17B-C). Burrow diameters vary from 20-27 mm. Some burrows penetrate
842 the bedding at acute angles, and others are horizontally distributed on bedding planes.
843 The burrow has a distinct circular wall, about 2-5 mm thick. These burrows are preserved
844 in dark organic muddy limestone and filled with light-colored, coarse-grained sediments.
845 These morphologies suggest that this problematic form differs from all known ichnotaxa.

846 Another feature of the Bed 24 ichnoassemblage is the presence of abundant
847 ichnofossils near the contact between Beds 24d and 24e, including several distinct
848 burrowing ichnotaxa: *Balanoglossites triadicus*, *Taenidium* isp., *Thalassinoides* isp. 1,
849 and *Planolites* isp. 1. Of these, *Balanoglossites* is represented by vertical tubes (Fig. 16C)
850 that penetrate to a depth of 5-10 cm perpendicular to bedding. This ichnogenus occurs
851 usually at omission surfaces that served as sequence boundaries (i.e., Knaust, 1998).
852 These traces are preserved in limestone of the upper part of Bed 24d (Fig. 3). *Taenidium*
853 burrows (Fig. 16E, 17E) are also very common in Bed 24d-e, and they are usually
854 cylindrical, straight, unbranched, and backfilled. This ichnoassemblage as a whole
855 represents the *Balanoglossites* ichnofacies associated with the omission surface, as
856 described by Knaust (1998, 2004). In addition, horizontal burrows of *Planolites* isp. are
857 densely packed on top of Bed 24e (Fig. 17A, E), which is just beneath the base of Bed 25,

in which the PTME horizon is placed (Jin et al., 2000).

Abundant burrows were also found in association with an omission surface within Bed 27. These burrows and the possible firmground surface have long remained disputed, although several recent studies have addressed an ichnoassemblage of this bed (Cao and Shang, 1998; Cao and Zheng, 2009; Zheng et al., 2013). Burrow systems preserved in Bed 27 therefore are re-studied here (see below).

Beds 28-34 are barren of trace fossils. The remaining part of the lower Yinkeng Formation (Beds 35-51) yields rare trace fossils, which are dominated by simple, horizontal burrows of *Planolites* isp. 2 (Fig. 18A-B). Increasing numbers of ichnotaxa occur in the upper Yinkeng Formation and are characterized by the presence of the tree-like burrow system of *Chondrites* isp. (Bed 52; Fig. 18C) and relatively complicated burrows of *Thalassinoides* isp. 3 (Fig. 18D-E) and *Treptichnus* isp. (Fig. 18G-H).

5.1.2. Ichnofabric changes within Bed 27

Within Bed 27, intensive burrowing on an omission surface, characteristic of the *Glossifungites* ichnofacies, caused a pronounced relief on the firmground surface up to 3

875 cm high near the boundary between Beds 27a and 27b (Figs. 19-20). The firmground of
876 *Glossifungites* ichnofacies is partly covered by a faintly laminar black muddy limestone
877 that seems resistant to weathering. Highly irregular relief at the surface of the firmground
878 indicates that the solid rock was affected deep subsolution (Savrda, 1992). Trace fossils
879 increase upward to the contact between Beds 27c and 27d, which is overlain by finely
880 laminated muddy limestone (Bed 27d) again.

881 To reconstruct complete burrowing systems within Bed 27, one complete sample
882 of the bed (from base to top) was cut and separated into three blocks (Fig. 19). The
883 transverse view from three polished slabs shows the colonizing zonation (CZ) from base
884 to top of the bed by various ichnocoenoses within a 16-cm-thick unit (Fig. 20).

885 CZ I: This is a historical zone, a unit that is beyond the reach of even the deepest
886 burrows (Fig. 20). CZ I includes the first 2-3 cm of the lower part of Bed 27, which
887 comprises gray, calcareous mudstone to muddy limestone and is almost barren of trace
888 fossils. Minor bioturbation is also limited. Body fossils are scarce, except some small,
889 thin-bedded brachiopods and foraminifers. Pyrite framboids and crystals are relatively
890 rich and occur in both sediments and fossil shells (see Section 6).

891 CZ II: This is a transitional zone (Fig. 20), which is extremely heterogeneous

892 from the activity of deeper burrows (Savrda, 1992). Sediments in this zone were
893 semi-lithified to form a firmground substratum. Firmground sediments are dark-colored,
894 and are disrupted by passively filled burrows of an ichnoassemblage characteristic of the
895 *Glossifungites* ichnofacies. Representative ichnogenera include *Arenicolites*,
896 *Gastrochaenolites*, *Psilonichnus*, and *Thalassinoides*. Of these, *Arenicolites* comprises
897 vertical burrows that penetrate into the dark gray sediments. *Gastrochaenolites* comprises
898 tear-shaped borings, now filled with light gray, coarse-grained sediments in a
899 dark-colored firmground lime muddy substrate. This ichnogenus is commonly present in
900 the *Trypanites* ichnofacies as well (Wilson and Palmer, 1998; Benner and Ekdale, 2004).
901 The vertical cylindrical burrows of *Psilonichnus* are inclined, with bedding in the distal
902 end (Buatois and Mángano, 2011). *Thalassinoides* is typified by its Y-shaped ramification.
903 All these burrows have unlined walls and are filled with light gray-colored,
904 coarse-grained sediments of the overlying layer, indicating that these burrows were
905 passively filled.

906 CZ III: This is a very thin, highly condensed omission surface (Fig. 20), which is
907 characterized by some coarse-grained, reworked sediments that were generated by
908 frequent activity of wave currents. This omission surface is distinguished from the

underlying firmground ichnocoenosis of *Glossifungites* ichnofacies and overlying softground ichnocoenosis of *Cruziana* ichnofacies (see below).

CZ IV: This is a mixed unit (Fig. 20), which is saturated with water and totally homogenized by bioturbation. This unit, about 5 cm thick, yields ichnocoenoses represented by minute burrows of *Diplocraterion* isp. and tear-shaped borings, which resemble the vertical features of *Chondrites* and small *Planolites*. Owing to the soft nature of substrate and intensive bioturbation, burrow boundaries and morphologies have become blurred, making it difficult to identify them confidently to ichnogenus level. This ichnoassemblage, together with the soft substrate, is characteristic of the softground ichnocoenosis of *Cruziana* ichnofacies (Seilacher, 1977).

CZ V: This thin unit is devoid of bioturbation and comprises finely laminated muddy layers (Fig. 20), which yield small pyrite framboids (see Section 6), indicating the establishment of a quiet, low energy and probably reduced environment.

5.2. Extent of bioturbation

Ichnofabric indices (Droser and Bottjer, 1986) of the Upper Changhsing

926 Formation (Beds 22–24) are usually rather low (ii1-2) with several peaks reaching 3 (ii3)
927 except for the horizons near the boundary between Beds 24d and 24e (Fig. 3) that records
928 an ichnofabric index of 4 (ii4), but bioturbated strata are about 80% of the entire
929 measured units of the Changhsing Formation. Ichnofabric indices decrease to 2 (ii 2)
930 again at the upper part of Bed 24e, then increase to 3 (ii3) at the top of the bed. No
931 ichnofabrics are observed in Beds 25-26a. The ii value surges to 3 (ii3) in Beds 26b-27,
932 with 40% strata bioturbated. Beds 28-34 are void of ichnofabrics again. The ii value of
933 Beds 35-57 remains rather low (ii1) except for several peaks reaching 2 (ii2) in Beds 42,
934 46, 52-53, and 56-57 (Fig. 3). Only 15% of the examined units are bioturbated.
935 Accordingly, ichnofabric indices of the upper Changhsing Formation vary from 2 to 4
936 (ii2–4). Averagely 80% strata of the upper Changhsing Formation are significantly
937 bioturbated. Ichnofabric indices from Bed 27 remain relatively high (ii4), although only
938 40% strata are bioturbated. The remaining part of the lower Yinkeng Formation records a
939 rather low ii value (ii1) and no strata are significantly bioturbated. Ichnofabric indices in
940 the middle and upper parts of the Yinkeng Formation vary from 1 to 2 (ii1-2). On average,
941 15% of strata are significantly bioturbated.

942 In the upper Changhsing Formation, the two bedding planes in Bed 23

943 containing *Dendrorhaphis* isp. (Fig. 17F) and the problematic trace (Fig. 17D), show
944 coverage of 90% and thus indicate a BPBI of 5 (Fig. 3). The same BPBI value (ii 5) is also
945 estimated from two horizons of Beds 24d, containing *Taenidium* burrows. Bedding planes
946 from other horizons in the upper Changhsing Formation generally have bioturbation
947 coverage varying from 10% to 60%, indicating BPBI of 1-5. For the top bedding plane of
948 Bed 24e, just below the mass extinction horizon, containing *Planolites* (Fig. 17A, E) the
949 coverage was up to 90%, indicating a BPBI of 5. Beds 25-26a have the lowest BPBI, with
950 almost no bioturbation recorded. Several bedding planes from Beds 26b-27 show changes
951 in coverage from 20% to 40%, indicating a BPBI of 2-4. Bedding plane coverage in Beds
952 28-34 is generally rather low because bioturbation is broadly absent. Beds 35-51, overall,
953 have bioturbation coverage <10%, but some bedding planes containing *Planolites* show
954 coverage up to 20%, indicating a BPBI of 2. Another bedding plane containing
955 *Chondrites* has coverage up to 90%, indicating a BPBI of 5. In the upper Yinkeng
956 Formation, one bedding plane containing *Thalassinoides* shows coverage up to 20%,
957 indicating a BPBI of 2.

958

959 5.3. Changeover of trace-fossil diversity over the P-Tr transition

960

961 Ichnodiversity, represented by ichnogenic richness, decreased remarkably
962 over the P-Tr transition. Eight ichnogenera are commonly encountered in the uppermost
963 Changhsing Formation: *Balanoglossites*, *Dendrorhaphie*, *Lockeia*, *Paleophycus*,
964 *Planolites*, *Problematica*, *Taenidium*, and *Thalassinoides* (Fig. 21A). Only *Planolites* is
965 present at the top of Bed 24e, dropping to 87.5% in the upper part of Bed 24e. All
966 ichnotaxa disappear at the top of Bed 24e, coinciding with the PTME. As a consequence,
967 Beds 25-26a are barren of ichnotaxa. The ichnofauna rebounded in Bed 26b and
968 diversified in Bed 27, including seven ichnogenera: *Arenicolites*, *Diplocraterion*,
969 *Gastrochaenolites*, *Psilonichnus*, *Thalassinoides*, *Chondrites*, and *Planolites*. Of
970 particular interest is the presence of four vertically burrowing ichnogenera (*Arenicolites*,
971 *Diplocraterion*, *Gastrochaenolites*, *Psilonichnus*) and one relatively complicated
972 burrowing ichnogenus (*Thalassinoides*), implying that ichnodiversity almost reached the
973 pre-extinction level in Bed 27 (Fig. 21A). All ichnotaxa disappeared soon after (in Bed
974 28). As a consequence, Beds 28-34, ranging through conodont zones *I. isarcica* and *I.*
975 *planata* Zones, lack any ichnotaxa and remained poorly bioturbed (Fig. 3).The
976 post-extinction rebound of ichnotaxa is marked by the presence of *Planolites* in Bed 35.

Since then, ichnodiversity remained at a rather low level and did not increase until the middle-late Griesbachian, which saw the rise of *Chondrites* in Bed 52. Although *Chondrites* disappeared in the middle-late Griesbachian, the trace-fossil assemblage slightly diversified and included *Planolites*, *Treptichnus* and *Thalassinoides*.

As a result, P-Tr ichnotaxa underwent two pronounced reductions in diversity coinciding with the two episodes of PTME calibrated to the bases of Beds 25 and 28. Ichnofaunas fell to their lowest diversity in the early Griesbachian, and experienced a slow increase in diversity throughout the middle-late Griesbachian (Fig. 21A). However, post-extinction trace-fossil diversity never returned to the pre-extinction level.

5.4. Burrow size variations through the P-Tr transition

Nine bedding planes were examined to determine the size distribution of burrow diameters of *Arenicolites*, *Dendrorhaphé*, *Diplocraterion*, *Paleophycus*, *Planolites*, *Problematica*, *Taenidium*, *Thalassinoides*, and *Treptichnus* (Fig. 22). Burrow size change over the P-Tr transition is apparent, especially in *Planolites*, as well as other traces such as *Balanoglossites*, *Chondrites*, *Dendrorhaphé*, *Taenidium*, *Thalassinoides*, *Treptichnus*,

994 and Problematica (Fig. 22). *Planolites* is distributed in ten horizons throughout the
995 uppermost Changhsingian to middle-upper Griesbachian, and thus is a good proxy for
996 size variation of trace fossils over the P-Tr transition. Mean diameters of the Changhsing
997 Formation *Planolites* burrows are 7 mm, 8.5 mm, and 5.5 mm, respectively from three
998 horizons, with maximum burrow diameter up to 9.2 mm (Fig. 22A). Burrow sizes
999 decrease remarkably across the boundary between Beds 24 and 25, the PTME horizon
1000 (Fig. 1B), with mean burrow diameters of 1.7 mm and the greatest burrow diameter only
1001 2.2 mm in Bed 27 (Fig. 22A). Burrow sizes of *Planolites* remain very small throughout
1002 the early-middle Griesbachian and become larger by the late Griesbachian (Beds 54-57).
1003 These late Griesbachian traces are still much smaller than their counterparts recorded in
1004 the pre-extinction strata (Fig. 22A). Comparable size change over the P-Tr transition is
1005 also demonstrated by both the greatest size and mean size of *Thalassinoides* from the
1006 same interval (Fig. 22B).

1007 Several other ichnotaxa in the uppermost Permian have mean and maximum
1008 diameters, such as *Balanoglossites* (4.6 mm, 6.4 mm), *Dendrorhipe* (12 mm, 17 mm),
1009 problematica (22 mm, 28 mm), and *Taenidium* (7.8-8.8 mm, 9.2 mm), that are obviously
1010 larger than that of those ichnotaxa confined to the lowest Triassic, i.e., *Chondrites* (2.8

mm, 5.6 mm) and *Treptichnus* (6.3 mm, 6.3 mm) (Fig. 22C-D). When the measurements of all 273 burrows measured from the P-Tr strata of Meishan are combined, both mean and maximum diameters exhibit remarkable reduction across the boundary between Beds 24 and 25 and remain very low values until Bed 27. The same values further decline from Bed 27 to Beds 28-34, and then undergo a stepwise increase through Beds 35-57 (Fig. 21B)

Trace-fossil size variations over the P-Tr transition are consistent with figures from northern Italy (Twitchett, 1999; Twitchett and Barras, 2004) and South China (Chen et al., 2011). It should be noted that the Early Triassic *Planolites* traces are much smaller than their Changhsingian counterparts at Meishan (Fig. 22A), unlike the same traces elsewhere (Pruss and Bottjer, 2004). *Planolites* is supposed to be the least susceptible to mass extinction because this simple trace can be produced by a variety of organisms (Pruss and Bottjer, 2004). Accordingly, the Changhsingian *Planolites* and their Early Triassic counterparts may have been made by different organisms.

5.5. Trace fossil form and complexity

1028 The Changhsing Formation trace fossils are morphologically diversified, and
 1029 include simple, horizontal burrows (*Planolites*), vertical or oblique burrows
 1030 (*Balanoglossites* and Problematica), resting traces (*Lockeia*), and complex forms
 1031 (*Dendrorhape*, *Taenidium*, and *Thalassinoides*). They, however, disappear across the
 1032 PTME horizon (base of Bed 25). Both *Planolites* and *Thalassinoides* rebound in Bed 27,
 1033 but decrease markedly in size in comparison with their Changhsingian counterparts.
 1034 *Thalassinoides* is also less complex than the same trace recorded in the Changhsingian.
 1035 Complex forms, and resting and vertical traces of the Changhsingian (*Balanoglossites*,
 1036 *Lockeia*, *Taenidium*, *Dendrorhape*, and Problematica) vanish in Bed 27. Instead, the
 1037 relatively complex burrow systems of the *Glossifungites* ichnofacies, i.e., *Arenicolites*,
 1038 *Gastrochaenolites*, *Psilonichnus*, and *Thalassinoides*, characterize the ichnoassemblage
 1039 in the lower part of Bed 27. Vertical burrows of *Diplocraterion*, together with *Chondrites*
 1040 and *Planolites* also occur in the upper part of Bed 27. Accordingly, ichnotaxa recovered
 1041 from the pre-extinction level are similar to those in Bed 27 in terms of complexity,
 1042 although these burrows are much smaller than their counterparts elsewhere.
 1043 Early Griesbachian traces are dominated by small, simple, horizontal burrows of
 1044 *Planolites*, as reported elsewhere (Twitchett and Barras, 2004; Pruss and Bottjer, 2004;

Fraiser and Bottjer, 2009; Chen et al., 2011, 2012). In the middle-late Griesbachian trace fossils become slightly more complex and are marked by the presence of *Chondrites*, *Thalassinoides* and *Treptichnus*, although these burrows are still very small. Nevertheless, these middle-late Griesbachian burrows are branched and form slightly complex networks, and thus are more complex than the *Planolites*-dominated ichnoassemblage in the early Griesbachian.

As a result, trace-fossil complexity, reflecting behavioral complexity of the trace-makers, decreased dramatically during the PTME. Then, the trace-fossil assemblage shows an increase in complexity, varying from simple, horizontal traces (i.e., *Planolites*) in the early Griesbachian to relatively complex traces (*Chondrites*, *Thalassinoides* and *Treptichnus*) in the middle-upper Griesbachian. In particular, the reappearance of *Thalassinoides* and *Treptichnus* probably implies increasing behavioral complexity that typically indicates the beginning of biotic recovery elsewhere (Twitchett and Barras, 2004).

5.6. Infaunal tiering

1062 Levels of tiering above and below the sediment were greatly reduced after the
1063 PTME (Ausich and Bottjer, 1982, 2002). At Meishan, the change in infaunal tiering over
1064 the P-Tr transition is reflected by the penetration depth of burrows (Fig. 21C), which was
1065 measured in the field. Vertical burrows of the Changhsing Formation may extend a
1066 maximum depth of 10 cm into the sediment, indicating a rather deep tiering level (ii5). In
1067 contrast, burrows of *Planolites* and *Thalassinoides* recorded in Bed 27 may penetrate to <
1068 2 cm into the sediment. In particular, *Thalassinoides* commonly shows the second tiering
1069 level (ii2) (Bottjer and Droser, 1994). Early Griesbachian *Planolites* has burrows
1070 extending to a maximum depth of only 0.5 cm (Fig. 21C) indicating the lowest tiering
1071 level (ii1) (Bottjer and Droser, 1994). Thus, tiering fell to its minimum level in the early
1072 Griesbachian. An increase in tiering level during the middle Griesbachian is marked by
1073 the presence of *Chondrites*, an anoxic burrow system penetrating to a depth up to 1-2 cm
1074 and indicating the second tiering level (ii2) (Bottjer and Droser, 1994). The same tiering
1075 level is also reflected in upper Griesbachian *Thalassinoides* and *Treptichnus* burrows,
1076 which may extend to a maximum depth of 1-2 cm (Fig. 21C). Accordingly, the tiering
1077 level decreases significantly across the PTME horizon in Meishan, and then increases
1078 throughout the Griesbachian (Fig. 21C).

1079

1080 **6. Size variations of pyrite framboids and redox conditions over the P-Tr transition**

1081

1082 Pyrite is ~~rather~~ commonly present in the latest Changhsingian to Griesbachian
1083 rocks at Meishan (Wignall and Hallam, 1993), which is also confirmed by our
1084 observations of thin sections through the P-Tr transition at Meishan. Several
1085 pyrite-enriched beds have been treated as indications of anoxic conditions at Meishan
1086 (Wignall and Hallam, 1993). In particular, pyrite framboids, which are spherical
1087 aggregates of pyrite microcrystals, are rather abundant in these pyrite-enriched beds near
1088 the PTB at Meishan (Jiang et al., 2006; Shen et al., 2007). Pyrite framboids in ancient and
1089 modern sediments are interpreted as the result of redox conditions (e.g., Bond and
1090 Wignall, 2010), and these authors show that small framboids, usually 3-5 µm in diameter,
1091 indicate euxinic conditions (H₂S-bearing, O₂-free bottom waters). Accordingly, pyrite
1092 framboids have been considered as one of the most important pieces of evidence
1093 indicating redox conditions over the P-Tr transition worldwide (Wignall et al., 1998,
1094 2005; Jiang et al., 2006; Shen et al., 2007; Gorjan et al., 2007; Bond and Wignall, 2010;
1095 Algeo et al., 2011b).

At Meishan, Jiang et al. (2006) reported that pyrite framboids are ~~very~~ commonly present in all beds through the PTB (Beds 24-29), based on etched residues from bulk samples. Shen et al. (2007) also observed framboids *in situ* on polished blocks and etched residues. Both studies detected that framboids are ~~very~~ abundant in Bed 25. Contrasting to Jiang et al.'s (2006) observation, Shen et al. (2007) found no pyrite framboids in Bed 27. However, unequal sampling in various beds near the PTB, for instance, 40 g each from Beds 25 and 26, but only 5 g each from Beds 24, 27, 28 and 29 may have biased their observation (Shen et al., 2007). Bed 27 comprises various lithologies from its base to top, which may have been deposited in different environments (Figs. 19-20). Thus, pyrite framboids may be ~~rare~~ absent in these bioturbated layers (i.e., CZs II, III-IV in Bed 24; Fig. 20), but instead may occur in finely laminated layers without bioburbation (i.e., CZs I and ~~IV~~; Fig. 20).

We have also observed pyrite framboids in continuous thin sections throughout Beds 24-30. We used a FEI Quanta 400 Scanning Electron Microscope (SEM) equipped with a GENESERS 2000 energy dispersive spectrometer (EDS) at the State Key Laboratory of Biogeology and Environmental Geology, China University of Geosciences, Wuhan, China. SEM images and EDS spectra were produced by the Zeiss VPSEM

1113 coupled with an energy dispersive X-ray spectrometer. We confirmed Jiang et al.'s (2006)
1114 observation that both pyrite framboids and crystals occur in Bed 27 on brachiopod shells
1115 and in foraminiferal tests and sediments (Fig. 23). In addition, we measured framboid
1116 sizes in samples from Beds 29-60 using the SEM. Pyrite framboids are ~~very~~ abundant in
1117 samples from 17 horizons over the P-Tr transition (Fig. 24). The majority of framboid
1118 diameters in most measured beds are smaller than, or around 5 μm , except for Beds 28
1119 and 44, in which most framboids have diameters of 7-8 μm . Moreover, framboid
1120 diameters are concentrated in a narrow size range ($< 10\mu\text{m}$) in Beds 27, 28, 43, and 58. In
1121 contrast, they have a greater size range in Beds 24b, 24e, 25-26, 29-30, 39, 42, 49, 51-52
1122 and 56, with maximum diameter up to 20 μm in Bed 51.

1123 Bond and Wignall (2010, table 1) proposed several characters, including
1124 framboid diameter and pyrite morphology, to determine redox conditions during
1125 deposition. In general, when framboids are small (mean diameters: 3-5 μm), abundant,
1126 with a narrow size range, and form the dominant pyrite fraction, they could have been
1127 deposited in euxinic condition (with a persistently sulfidic lower water column). If
1128 framboids are small (mean diameters: 4-6 μm), abundant, with a few, larger forms, and
1129 dominate the pyrite fraction, then they could have been deposited in anoxic condition

1130 (without oxygen in bottom waters for long periods). When framboids have mean
1131 diameters of 6-10 μm and are moderately common, with a few, larger framboids together
1132 with some crystalline pyrite, they could have been deposited in lower dysoxic condition
1133 (with weakly oxygenated bottom waters). In upper dysoxic condition (with partial
1134 oxygen restriction in bottom waters) framboids are commonly to rarely present, with a
1135 broad range of sizes, only a small proportion of framboids $< 5\mu\text{m}$, and the majority of
1136 pyrite as crystals. In oxic condition (without oxygen restriction), no framboids are present,
1137 and pyrite crystals occur rarely.

1138 If these five criteria given by Bond and Wignall (2010) are followed, we can
1139 determine redox conditions over the P-Tr transition in Meishan. Bed 24 contains
1140 abundant framboids, usually around 5 μm in diameter with some larger framboids, and
1141 their size range is relatively broad, pointing to anoxic conditions. Framboids in Beds
1142 25-26 are usually 3-5 μm in diameter, a narrow size range, and no pyrite crystals are
1143 present, suggesting euxinic conditions (Fig. 25). Framboids from Bed 27 have a relatively
1144 large diameter and a broad size range (Fig. 24), and are also associated with some large
1145 pyrite crystals, pointing to a lower to upper dysoxic condition (Fig. 25). Pyrite framboids
1146 are moderately common in Bed 28 and have mean diameters of 8-9 μm , but no larger

framboids and crystalline pyrite occur. Thus, Bed 28 is inferred to be deposited in a
transitional zone between anoxic and lower dysoxic conditions based on the criteria
determining redox conditions proposed by Bond and Wignall (2010). Redox conditions
became euxinic soon after in Bed 29, in which framboids are very small (3-5 μm) and
have a narrow size range, without pyrite crystals. It should be noted that no pyrite
framboids were found in Beds 30-35, although a pronounced negative excursion of
carbon isotopes (Xie et al., 2007) and environmental stress indicated by biomarker
signals (Yin et al., 2012) occur in these beds. Framboids from Beds 39 and 42 indicate
euxinic-anoxic transitional conditions in terms of diameter, size range and association
with pyrite crystals. Framboids from Bed 43 are ~~64-106~~ μm in diameter, but have some
larger forms and are also associated with some pronounced pyrite crystals, and thus
indicate a lower to upper dysoxic condition. Then, redox conditions indicated by pyrite
framboids changed to anoxic to euxinic transitional conditions. Surprisingly, framboids
from Bed 58 suggest euxinic condition, which coincides with the last negative excursion
of carbon isotopes in the middle-late Griesbachian detected by Burgess et al. (2014).

7. Assessing ecologically PTME and its aftermath

7.1. Testing ecologically extinction patterns

The updated fossil record from Meishan shows two pronounced declines of species richness at the bases of Beds 25 and 28 (Song et al., 2013a; Fig. 26). Similarly, fossil fragment contents recorded in thin sections also show two distinct drops in both abundance and diversity corresponding to the top of Bed 24e and base of Bed 28 (Figs. 6, 14). Further, ichnodiversity also declined within Beds 24 and 27. In Bed 24, trace fossils are rather abundant and comprise four distinct ichnogenera: *Balanoglossites*, *Planolites*, *Taenidium* and *Thalassinoides* in horizons near the boundary between Beds 24d and 24e, but only *Planolites* persisted into Bed 24e-6, in which relatively large burrows are densely packed, indicating a considerably high bioturbation level. All ichnotaxa disappeared in Beds 25-26a. Similarly, ichnotaxa decline from five ichnogenera (*Arenicolites*, *Gastrochaenolites*, *Planolites*, *Psilonichnus*, and *Thalassinoides*) in CZ II (Bed 27b) to three ichnogenera (*Diplocraterion*, *Chondrites* and *Planolites*) in CZ IV (Bed 27c), and then further declined and disappeared at the top of Bed 27d. Other proxies of trace fossils and bioturbation also show two pronounced declines corresponding to the

bases of Beds 25 and 28. Clearly, the PTME ecologic crisis comprised two phases, coinciding with metazoan extinctions calibrated to the bases of Beds 25 and 28 (Song et al., 2013a).

In addition, both fossil fragment contents and ichnodiversity show that a pronounced decline in diversity and abundance started at the stratal interval 10 to 19 mm below the top of Bed 24e. The boundary between Beds 24e-5 and 24e-6 is the most distinct eliminated horizon of skeletal fragment of major fossil groups, coinciding with end-Permian sulfur anomaly (Kaiho et al., 2006a) and the start of the negative end-Permian carbon isotopic excursion (Kaiho et al., 2009), and thus may indicate the PTME. Abundant sponge spicules above this event horizon indicate that they lasted in seawater for a while, although complete sponge fossils disappeared at the PTME event. It is therefore unlikely that the disappearance of calcareous fossils at the top of bed 24e-6 was a result of an increase in the input of terrestrial material associated with the facies shift, as indicated by the lithologic shift from the limestone of Bed 24 to the claystone of Bed 25 and black shale of Bed 26. Instead, the extinction of calcareous biota and the associated environmental perturbation was most likely caused the lithologic change from limestone to mudstone. As a result, the sharp decline in biotic abundance and diversity

10-19 mm below the top of Bed 24e may signal the first episode of the PTME previously
inferred from statistical paleontological data (Song et al., 2013a).

7.2. Ecologic collapse lagging behind biodiversity crisis during the PTME

At Meishan, the Permian biota experienced a dramatic drop in diversity at the base of Bed 25, with 172 species (94%) being wiped out in Beds 25-26 and no pronounced reduction of species richness in Bed 28 (Jin et al., 2000). The updated fossil record obtained from Meishan shows that species richness was reduced by at least 79% across the boundary between Beds 24e and 25, compared to 65% loss in species richness across the boundary between Beds 27d and 28 (Song et al., 2013a). This means that marine animals suffered a more severe depletion in species richness in the first phase of the PTME than in the second phase of the same event (Fig. 26). The biodiversity decline pattern from Meishan is confirmed by the same pattern at a further seven PTB sections in South China (Song et al., 2013a). It should also be noted that generic richness declined by a similar magnitude, 85% and 82%, in the first and second phases of the PTME, respectively in Meishan, but both generic and species richness underwent a stepwise

1215 decline from the uppermost Changhsingian to lowest Griesbachian (Fig. 26).
1216 Consequently, biotic diversity suffered a larger loss in the first episode than in the second
1217 episode of the PTME in terms of the number of lost taxa. This pattern is reinforced by
1218 fossil fragment content variations across the PTME horizons. Fossil components usually
1219 occupy nearly 70% in all rock in strata below Bed 25, but only about 30% in Bed 27, and
1220 FFA lost nearly 60% in thin section (Fig. 14). Over the same period, 11 Permian orders
1221 declined to five orders in Bed 27, losing 54.5% in ordinal richness.

1222 Both the standard diversity Shannon index [Exp (H)] and dominance index (D')
1223 assess whether the shelly community possesses a healthy structure. Exp (H) values
1224 declined by 43.6% from the *R-P* to *T* communities, and 55.5% from the *P-T* to *C-O*
1225 communities, coinciding with the first and second phases of the PTME, respectively. This
1226 means that the shelly communities suffered a greater loss in community diversity in the
1227 second phase of the PTME than in the first phase. Similarly, standard diversity
1228 dominance (D') increases by 34% and 54% during the two pronounced drops in diversity,
1229 respectively (Table 6). This means that the shelly communities became more uneven after
1230 the second phase of the PTME than after the first phase. Thus, shelly communities
1231 underwent relatively more serious ecologic crisis in the second phase than in the first

phase of the PTME. This observation is also reinforced by ichnofaunal variations and ichnofabric changes over the P-Tr transition in Meishan.

The presence of seven ichnogenera in Bed 27 suggests that ichnogenic richness nearly recovered to the pre-extinction level, although there was a taxonomic loss in Beds 25-26a. In contrast, a more dramatic ichnofaunal loss occurred in the second phase of the PTME, corresponding to Bed 28. As a consequence, Beds 28-34 are barren of ichnotaxa. Thus, ichnofaunas suffered a more severe decline in the second phase of the PTME. This pattern is also strengthened by burrow size variations and tiering level changes, both of which remained relatively high in the Changhsingian, and experienced a stepwise decline through Beds 23-27, then fell to their lowest values in the early Griesbachian (Beds 28-34). Ichnofabric variation also shows that Bed 27 still remains highly bioturbated and yields rather complex burrow systems of the *Glossifungites* ichnofacies and *Cruziana* ichnofacies, which are commonly present in the pre-extinction period, thus showing the largest turnover at the base of Bed 28 rather than at the base of Bed 25. In contrast, ichnotaxa became very rare after the second phase of the PTME, although 2-3 ichnotaxa rebounded in the middle-late Griesbachian. Consequently, the greatest losses of ichnotaxa correspond to the top of Bed 27, simultaneous with the

second phase of metazoan extinction in Meishan (Song et al., 2013a). This ichnodiversity drop coincides with a remarkable decrease in tiering level (Fig. 21) and burrowing intensity (Fig. 3). Ichnofabric indices recorded in the upper Changhsing Formation are rather high (ii4-5) (Fig. 3). Complex traces of both the *Glossifungites* and *Cruziana* ichnofacies recorded in Bed 27 (Figs. 19-20) also indicate a fairly high ichnofabric index (ii3-4). Consequently, there was not a sharp decrease, but a gradual decrease, in burrowing intensity (ii4-5 down to ii3-4) over the first phase of the PTME. This is in sharp contrast to the pronounced drop in biodiversity of metazoans in this phase of the PTME (Fig. 26), suggesting a gradual worsening in environmental conditions.

In contrast, almost all of the complex traces of the *Glossifungites* and *Cruziana* ichnofacies disappeared in the second phase of the PTME. The early Griesbachian *Planolites* is confined to discrete horizons (ii1-2) separated by metres of unbioturbated sediment, and indicates a rather low ichnofabric index (ii1) (Fig. 3). A low ichnofabric index indicates an absence or rarity of burrowing infauna, which in turn implies a stressed environment immediately after the PTME (Chen et al., 2011). Accordingly, the great loss of burrowing infauna and associated environmental stress occur at the horizon between Beds 27 and 28. These facts imply that ecologic collapse of marine ecosystems

post-dated the metazoan biodiversity crisis at Meishan.

Contrasting to the two-stage extinction pattern (Song et al., 2013^a), Shen et al. (2011b) and Wang et al. (2014) argued that the severest biodiversity declines fell in a short period equivalent to Beds 25-28 of Meishan, and there was one prolonged extinction rather than two discrete episodes. Indeed, Beds 25-28 represent a very short duration of about 60 ky (Burgess et al., 2014). However, all lines of evidence, including fossil fragment contents, and ichnofabric and community structural changes, show that the P-Tr ecologic crisis clearly comprises two pronounced steps, at the bases of Beds 25 and 28 (Figs. 14, 21, 26). Nevertheless, whether the mass extinction occurred as one prolonged event or two pulses, all studies agree that Beds 25-28 of Meishan and their equivalents represent a critical period when the greatest biotic turnover of life on Earth took place in Meishan. During this critical turnover period, the ecologic crisis clearly lagged behind the diversity decline. As a result, the Meishan fossil record shows that the mass extinction started with a dramatic depletion of biodiversity and ended with a severe ecologic crisis.

7.3. Dramatic increase in seawater surface temperature and its consequence

1283

1284 Recent oxygen isotopic studies of conodont bioapatites reveal that sea surface
1285 | temperature rose ~~~940~~ °C from Bed 24e to Bed 27~~a~~ in Meishan (Joachimski et al., 2012;
1286 | Sun et al., 2012; Fig. 26). However, the precise relationship between temperature
1287 | increase and biotic extinction remains unclear owing to the lack of oxygen isotopic values
1288 | from Bed 25, the base of which coincides with the PTME (Shen et al., 2011b) or the first
1289 | phase of the PTME (Song et al., 2013~~a~~). The same is also true for the relationship
1290 | between the temperature rise and the dramatic negative carbonate carbon isotopic
1291 | excursion (Fig. 26). The solution is to undertake more detailed study of conodont oxygen
1292 | isotopes of the PTB beds from less condensed sections than Meishan to evaluate whether
1293 | temperature change leads or lags the extinction (Burgess et al., 2014).

1294 Hinojosa et al. (2012) found a negative shift in $\delta^{44/40}\text{Ca}$ of conodont bioapatite in
1295 | the Great Bank of Guizhou, South China during the same interval as temperature increase
1296 | in Meishan. This $\delta^{44/40}\text{Ca}$ excursion is also coupled with a major shift in $\delta^{13}\text{C}_{\text{carb}}$
1297 | composition from an average of approximately +3.5‰ in the latest Permian to
1298 | approximately -1‰ in the earliest Triassic (Payne et al., 2004). The anomaly of $\delta^{44/40}\text{Ca}$
1299 | therefore was interpreted as a consequence, in part, of acidification of the ocean. Thus,

1300 oceanic acidification in platform areas of the Great Bank of Guizhou may have resulted
1301 from elevated seawater temperature (Burgess et al., 2014). However, this ocean
1302 acidification seems not [to](#) have spread to the Meishan area because rather abundant and
1303 diverse complex traces of both *Glossifungites* and *Cruziana* ichnofacies occur in Bed 27
1304 (Figs. 19-20), although calcareous skeletons decreased significantly in Beds 25-28 (Fig.
1305 14).

1306 Previously, the irregular surface occurring in the middle of Bed 27 at Meishan
1307 was interpreted as a submarine ~~solution~~[dissolution](#) surface, explained by a regional ocean
1308 acidification in South China (Payne et al., 2007, but see Wignall et al., 2009). This
1309 pronounced irregular surface, however, was re-interpreted as a distinct firmground
1310 surface, on which abundant complex traces of *Glossifungites* ichnofacies occur (see
1311 Section 3.5). Firmgrounds of *Glossifungites* ichnofacies are usually characteristic of
1312 initial transgression, and such horizons are usually employed to define sequence
1313 boundaries (Buatois and Mángano, 2011). Thus, no sign of acidification is recorded in
1314 Bed 27 ~~at-in~~ Meishan.

1315 Another potential consequence of elevated temperature is intensified chemical
1316 weathering (Sheldon, 2006) and consequent increased physical erosion of soils on land

1317 (Sephton et al., 2005; Xie et al., 2007), or a combination of these processes. These
 1318 processes are also indicated by the increased chemical index of alteration (CIA) profile
 1319 immediately after the first phase of the PTME (Bed 25; Fig. 26). It should be noted that
 1320 the CIA value was calculated as $\text{Al}_2\text{O}_3/(\text{Al}_2\text{O}_3+\text{K}_2\text{O}+\text{Na}_2\text{O})$ (Zhao et al., 2013a), a
 1321 modification of the original CIA equation (Nesbitt and Young, 1982). Increased chemical
 1322 weathering during the PTME and its aftermath is also mirrored by the Eu/Eu* profile of
 1323 conodont bioapatites (Zhao et al., 2013a). The latter rare-earth elemental (REE) proxy is a
 1324 useful tracer of sediment provenance because fractionation between Eu^{+2} and Eu^{+3} does
 1325 not occur under Earth-surface conditions (Elderfield and Greaves, 1982). Eu^{+2} tends to
 1326 become segregated into feldspar during magmatic differentiation, resulting in Eu/Eu*
 1327 values >1.0 in the crystal fraction and <1.0 in the residual fluid (Zhao et al., 2013a).
 1328 Eu/Eu* ratios >1.0 are characteristic of magmas from lower crustal or mantle sources
 1329 where substantial feldspar crystallization has taken place (Condie, 2001). Although the
 1330 REE “fingerprint” of the ash-rich clastics is reflected by both CIA and Eu/Eu* profiles
 1331 that match one another throughout P-Tr transition in Meishan (Fig. 26) and these ash beds
 1332 near the PTB likely sourced from regional convergent continent marginal volcanisms
 1333 (Gao et al., 2013, 2014), the shift toward Eu/Eu* values of 1.0–1.5 in Bed 24e,

Formatted

1334 immediately preceding the PTME, may be evidence of a transient influx of volcanic
1335 material with a lower crustal or mantle source. Zhao et al. (2013^a) argued that these
1336 mantle-sourced ash fingerprints indicated by Eu/Eu* values could be the product of the
1337 Siberian trap eruption (Reichow et al., 2009). Thus, this volcanic eruption could have
1338 caused the severe biocrisis and rapid increase in sea-surface temperature occurring ~20-
1339 kyr and 80 kyr later, respectively following the estimate of maximum and minimum
1340 sedimentation rates given by Burgess et al. (2014).
1341 ~~In addition,~~ Burgess et al. (2014) also estimated the rate of temperature rise in
1342 Beds 25-28 as an ~1 °C increase per 6,000 y, which is comparable with the rate and
1343 magnitude of the increase at the Paleocene–Eocene Thermal Maximum (Zeebe et al.,
1344 2009) and Pleistocene/Holocene postglacial warming (~2 °C/5 ka) (Lea et al., 2000).
1345 However, this estimation of the rate of temperature rise needs to be cautious because no
1346 temperature data is available from Bed 25 and the temperature rise spans Beds 24e-27
1347 (Sun et al., 2012). To sum up~~Accordingly~~, although the killing mechanism of the ~~~10~~
1348 9 °C increase of seawater surface temperature on organisms remains unclear, this rapid
1349 temperature increase coincides with biotic turnover and ecologic collapse during the
1350 PTME at Meishan. Nevertheless, the elevated temperature seems to have had little effect

1351 on ichnofaunas and ichnofabrics, as indicated by abundant ichnofaunas living in the
1352 firmground of the *Glossifungites* ichnofacies (Bed 27), but instead resulted in dramatic
1353 losses of fossil skeletons in sediments (Fig. 14).

1354 In addition, Sun et al. (2012) reported the acme of high seawater temperatures
1355 occurred in the late Griesbachian, corresponding to the upper *I. jsarcica* Zone and lower
1356 *C. planata* Zone (Sun et al., 2012, fig. 2), which range from Beds 48-54. These two zones
1357 are amended herein (Fig. 2) and are equivalent to the upper part of *C. planata* Zone in the
1358 revised conodont zonation (Fig. 2). This acme of high temperature postdates the second
1359 negative shift excursion of carbon isotopes of Xie et al. (2007) and includes the second
1360 negative shifting excursion of carbon isotopes of Burgess et al. (2014). Surprisingly, this
1361 interval saw an increase in biodiversity (Chen et al., 2002, 2007), ichnological
1362 amoraliation and bioturbation (Fig. 3). Accordingly, the acme of high temperature has
1363 little effect on faunas.

1364

1365 7.4. Anoxic events ~~and biotic response~~ ~~and biotic response~~

1366

1367 ~~7.4.1. Anoxic events~~ 7.4.1. Anoxic events

Formatted: Font: Italic

Formatted: Font: Italic

Formatted: Font: Italic

Formatted: Font: Italic

Formatted: Font: Italic

Formatted: Font: Italic

At Meishan, Wignall and Hallam (1993) recognized an anoxic event associated with the PTME, but considered that the greatest acme of anoxia, coupled with a maximum flooding event, occurs in the lower Yinkeng Formation. Wignall and Twitchett (2002) believed that the oxygen-deficient waters spread into exceedingly shallow settings near the PTB in the Tethys regions (i.e., South China). More recently, multiple geochemical signals indicate the existence of anoxic to euxinic conditions before, during and after the PTME at Meishan.

An exceptional increase in sea surface temperature is also believed to be synchronous with the flooding of shelf areas with anoxic and euxinic waters during the P-Tr transition (Sun et al., 2012). Both extremely high values of total organic content (TOC) (Yin et al., 2012) and reduced sizes of pyrite framboids (Fig. 26) indicate euxinic to anoxic condition in Beds 25-26, coinciding with the PTME. However, pyrite framboids from Bed 27 are generally larger than 5 μm in diameter with abundant crystals and thus indicate the upper part of dysoxic conditions (Fig. 25). Moreover, high bioturbation levels are also observed in upper part of Bed 26 and multiple layers of Bed 27. Thus, a euxinic to anoxic condition was probably limited only to Beds 25-26, which is less than 20 ka based on duration estimate of conodont zones from these beds (Table 2),

1385 a much shorter period than previously thought. The anoxic condition of the water column
1386 is also reflected by the abrupt increase of Ce/Ce* values of conodont bioapatite from
1387 ~0.7–0.8 in Beds 23–24 to 0.9–1.1 in Beds 25–27**b** (Zhao et al., 2013**a**; Fig. 26). Values of
1388 0.7–1.0 are sustained through Beds 27**c** to 30, above which Ce/Ce* decreases to 0.5–0.7.
1389 It should be noted that Ce/Ce* ratios derived from Bed 27a-d are not totally in accordance
1390 with size analysis of pyrite framboids, which shows that Bed 27a-d may represent redox
1391 conditions ranging from anoxia to upper level of dysoxia (Fig. 25). Although Ce/Ce*
1392 values from Meishan may have been biased by the fingerprint of clay input, Ce/Ce*
1393 values of 0.9–1.1 indicate an anoxic depositional system (Zhao et al., 2013**a**; Shen et al.,
1394 2012). This inference is consistent with the results of earlier studies documenting anoxia
1395 around the PTME in South China PTB sections (Grice et al., 2005; Algeo et al., 2007;
1396 Shen et al., 2007; Cao et al., 2009; Bond and Wignall, 2010; Luo et al., 2010) and
1397 globally (Algeo et al., 2010, 2011b; Brennecka et al., 2011).

1398 Euxinic condition may have occurred prior to the PTME in Meishan, i.e., Beds
1399 22–24, demonstrated by the anomaly of sulfur isotopes (Shen et al., 2011a) and various
1400 biomarker signals in Beds 22–24 (Grice et al., 2005; Cao et al., 2009; Luo et al., 2010,
1401 2011). Algeo et al. (2011a) also interpreted the anoxic and euxinic conditions as a result

Formatted: Not Highlight

of an expansion of the ~~oxygen~~ minimum ~~oxygen~~-zone (OMZ) in the water column over the P-Tr transition. These authors considered that the OMZ may have expanded prior to the PTME in Meishan.

A post-extinction reduced condition is also indicated by a pronounced negative excursion of carbon isotopes in Beds 34-36 (Xie et al., 2007; Luo et al., 2010; Fig. 26), coupled with an increase in TOC and terrestrial input indicated by various biomarker signals (Yin et al., 2012), and elevated contents of CO₂ (Fraiser and Bottjer, 2007). The CIA profile slightly increases in Beds 34-36, indicating elevated chemical weathering on land, which is consistent with the increased TOC and terrestrial input (Yin et al., 2012).

~~However~~In addition, ~~conodont bioapatite from~~ Beds 33-39 generally yields lower Ce/Ce* ratios (0.4-0.7) that may indicate an oxic to suboxic depositional environment.

~~Conodont bioapatite Ce, however, was probably derived mainly from detrital clay minerals and taken up during diagenesis, as indicated by other REE proxies (Zhao et al., 2013). If so, the observed Ce/Ce* ratios only reflect the REE composition of the source clays (Zhao et al., 2013a).~~

~~Alternatively, size variations of pyrite framboids indicate that Beds 27-29 record a dramatic redox change from upper dysoxic to euxinic conditions (Fig. 25). A euxinic to~~

Formatted: Don't adjust space between Latin and Asian text, Don't adjust space between Asian text and numbers

Formatted

Formatted

Formatted: Font: (Default) Times New Roman, 12 pt

Formatted: Font: (Default) Times New Roman, 12 pt

Formatted: Font: (Default) Times New Roman, 12 pt

Formatted: Font: (Default) Times New Roman, 12 pt

Formatted

Formatted

Formatted: Indent: First line: 1.5 cm, Don't adjust space between Latin and Asian text, Don't adjust space between Asian text and numbers

anoxic condition prevailed throughout Bed 29 to Bed 42 (Fig. 25). The combination of
mean size of framboids and presence of both larger framboids and crystal pyrites
indicates Bed 43 may be deposited in a lower to upper dysoxic condition. If a redox
interpretation is warranted, then this pattern suggests that the anoxic episode following
the PTME ~~at in~~ Meishan ~~had lasted~~ a relatively ~~short~~ long duration, probably ~~no more~~
~~than~~ ~50 kyr. Moreover, mean sizes and morphologies of framboids from Beds 44-58
also generally reflect an anoxic to euxinic condition, which, however, is not supported by
various ichnological proxies.

7.4.24.2. Biotic response

The pre-extinction anoxic to euxinic conditions are generally supported by the
presence of abundant small pyrite framboids, 3-5 μm in diameter, in Beds 23-24 (Figs.
23-24). However, biodiversity of metazoans remains very stable, with 64-78 species in
34-44 genera in each layer through Beds 24a to 24e (Fig. 26). Bed 24 contains 82 species
in 47 genera, and there are similar numbers in Bed 23 (Jin et al., 2000). Thus, no major
losses in species and generic richness are recognizable in Beds 23-24. Fossil fragment

1436 contents are almost the same in each layer through Beds 22-24, except for the top 1-2 cm
1437 of Bed 24e, in which there is a pronounced loss in fossil components across the boundary
1438 between Beds 24e-5 and 24e-6 (Figs. 6, 14). Fossil fragment contents fell by >16% in thin
1439 section from Beds 24e-5 to 24e-6. The FFA of Bed 24e-5 comprises 10 major [fossil](#)
1440 [groups](#) ~~orders~~ that are commonly present in all Permian limestones, but five ~~orders~~ [clades](#),
1441 ostracods, bryozoans, calcareous sponges, gastropods, and macroalgae, disappeared,
1442 losing 50%, across this boundary (Figs. 6, 14). The FFA of Bed 24e-6 is dominated by
1443 sponge spicules (35%) and thus has a high dominance and low diversity and evenness, in
1444 contrast to the low dominance, high diversity/evenness FFA in Bed 24e-5 (Fig. 6).
1445 Furthermore, the last occurrence of Permian fusulinids was also bracketed to the base of
1446 Bed 24e-6 (Kaiho et al., 2006b).

1447 Ichnodiversity also declined significantly across the boundary between Beds
1448 24e-5 and 24e-6 (Fig. 21A). These relatively complex or vertical burrows such as
1449 *Balanoglossites* and *Thalassinoides*, which usually occur in oxygenated settings,
1450 disappeared at the base of Bed 24e-6. Instead, only simple, horizontal burrows of
1451 *Planolites* occur in Bed 24e-6. Ichnofabrics, however, do not exhibit a major change
1452 across the same boundary (Fig. 3), with abundant *Planolites* burrows being densely

packed on the surface of Bed 24e-6. However, most geochemical studies do not have such a high sampling intensity, and thus neglected this boundary.

Both metazoan biodiversity and fossil fragment contents experienced dramatic declines in Beds 25-26a. Other ecologic measures, such as community structures, ichnodiversity, burrow size, tiering level, and ichnofabric variation, also indicate an ecologic crisis in Beds 25-26a, coinciding with the anoxia indicated by both pyrite framboid sizes and various geochemical signals (Fig. 26). However, the metazoan fauna from Bed 27 is rather abundant and diverse, including 66 species in 34 genera (Song et al., 2013a). Both community structural indices and fossil fragment contents indicate that metazoans had recovered well in Bed 27. The presence of abundant complex burrows in Bed 27 indicates ~~that the infaunal~~ was little affected by the anoxic event and proliferated proliferation in the firmground of *Glossifungites* ichnofacies (Fig. 20). The occasional occurrence of pyrite framboids in Bed 27 may indicate a very short period of anoxic condition, but Bed 27, as a whole, represents a dysoxic to oxic condition in which benthos and infaunas proliferated.

By contrast, all data, including the low ichnodiversity (only *Planolites*), small burrow size, low trace complexity, low ichnofabric from Beds 29-51 indices and low

Formatted: Indent: First line: 0 cm

1470 tiering level as well as low-diversity metazoans (Chen et al., 2007, 2010a), support the
1471 view that anoxic conditions may have prevailed throughout the early Griesbachian in
1472 Meishan (Wignall and Hallam, 1993; Xie et al., 2007; Yin et al., 2012). Of these, Beds
1473 29-34 are barren of trace fossils and bioturbation. This is supported by trace fossil size,
1474 which is also regarded as a proxy for paleoenvironmental conditions (Twitchett, 1999;
1475 Pruss and Bottjer, 2004). In general, small-sized traces are usually found in poorly
1476 oxygenated sediments (Savrda and Bottjer, 1987) or brackish environments (Pemberton
1477 et al., 1982; Buatois et al., 2005) or habitats with low nutrient supply (Jumars and
1478 Wheatcroft, 1989). Thus small traces are characteristic of stressed environments
1479 (Twitchett, 1999; Pruss and Bottjer, 2004). The dramatic size reduction of trace fossils
1480 after the PTME indicates environmental stresses associated with the PTME, and the small
1481 sizes of Early Triassic traces suggest prolonged environmental stress following the event
1482 (Bottjer et al., 2008).

1484 7.5. Testing extinction mechanisms

1485 Multiple scenarios have been proposed to interpret the killing mechanisms of the
1486 PTME, including widespread anoxia, hypercapnia, massive volcanic eruption, global

Formatted: Indent: First line: 0.42 cm

Formatted: Font: Italic

Formatted: Font: Italic

Formatted: Indent: First line: 0 cm

Formatted: Indent: First line: 1.5 cm, Line spacing: Double

Formatted: Font: (Default) Times New Roman, 12 pt

Formatted: Font: (Default) Times New Roman, 12 pt

Formatted: Font: (Default) Times New Roman, 12 pt

Formatted: Font: (Default) Times New Roman, 12 pt

Formatted: Font: (Default) Times New Roman, 12 pt

Formatted: Font: (Default) Times New Roman, 12 pt

Formatted: Font: (Default) Times New Roman, 12 pt

1487 warming, ocean acidification, and increased sediment flux (Erwin, 2006; Knoll et al.,
1488 2007; Clapham and Payne, 2011; Algeo and Twitchett, 2010; Algeo et al., 2011a;
1489 Joachimski et al., 2012; Sun et al., 2012; Burgess et al., 2014; Song et al., 2014). However,
1490 the true causes of this biocrisis still remain unclear due to the incomplete record of
1491 evidence supporting any of these alternatives,

1492 Recently, Song et al. (2013a) suggested that different extinction mechanisms
1493 may have driven each of these two pulses given their differences in biodiversity and
1494 ecologic losses. These authors considered that anoxia may be related to the first-pulse
1495 losses of biota, but played a crucial role in the second-pulse biocrisis (Song et al., 2013a).
1496 Elevated sea-surface temperature not only resulted in the spread of anoxia but also killed
1497 directly shallow-water taxa, while the anoxia killed the deep-water organisms (Song et al.,
1498 2014). However, extinction and survival selectivity of various fossil groups is more
1499 complicated than previously thought (i.e., Song et al., 2013a, 2014). This is because
1500 various elements of the same clade may have different lifestyles. For instance, the P-Tr
1501 brachiopods have six types of lifestyles based on attachment modes on the substratum:
1502 burrowing, body cementation, pedicle attaching on substratum, body spines anchoring on
1503 substratum, pedicle attaching on objects, and clasping spines on other shells/or objects

Formatted: Font: (Default) Times New Roman, 12 pt

Formatted: Font: (Default) Times New Roman, 12 pt

Formatted: Font: (Default) Times New Roman, 12 pt

Formatted: Font: (Default) Times New Roman, 12 pt

Formatted

Formatted: Font: Times New Roman

Formatted

Formatted: Font: Times New Roman

Formatted: Font: Times New Roman

Formatted: Font: Times New Roman

Formatted

Formatted

Formatted

Formatted

Formatted

Formatted

Formatted: Font: Times New Roman

1504 (Chen et al., 2006a, 2011b). These brachiopods having the last two types of attachment
 1505 modes behaviour like nektons. Moreover, some shallow-water elements were also able to
 1506 survive in deep niches during the latest Permian (Chen et al., 2006a). It is also true for the
 1507 P-Tr bivalves that embrace several lifestyles (Huang et al., 2014). Accordingly, our high
 1508 resolution comprehensive analyses of biodiversity, community structural, fossil fragment,
 1509 ichnological, and redox condition changes associated with these two discrete events
 1510 allow an evaluation of the proposed kill mechanisms for these two ecologic crises.
 1511 Most of the Permian brachiopods became extinct in the first extinction. The
 1512 survivors are dominated by chonetids or chonetid-like productids or small, thin-shelled
 1513 spiriferids/rhynchonellids that usually have attachment modes of clasping spines on other
 1514 shells/or objects or pedicle-attaching on other shells or objects (Chen et al., 2005a,
 1515 2011b). These survivors attached their bodies on some float objects (i.e., other shells and
 1516 algae) suspending above the seafloor (Chen et al., 2005a, 2011b), and thus provided
 1517 brachiopods higher adaptability surviving the deleterious environments, i.e., increased
 1518 acidity of precipitation (Wignall, 2007), large-scale marine acidification (Clapham and
 1519 Payne, 2011) and widespread anoxia (Wignall and Twitchett, 2002; Payne and Clapham,
 1520 2012) during the first biocrisis. Inarticulated brachiopods i.e., lingulids also survived this

Formatted: Font: Times New Roman

Formatted: Font: Times New Roman

Formatted: Font: Times New Roman

Formatted: Font: Times New Roman

Formatted: Font: Times New Roman

Formatted: Font: Times New Roman

Formatted

Formatted

Formatted

Formatted

Formatted

Formatted

Formatted

Formatted: Font: (Default) Times New Roman, 12 pt

Formatted

Formatted: Font: (Default) Times New Roman, 12 pt

Formatted: Font: (Default) Times New Roman, 12 pt

Formatted: Font: (Default) Times New Roman, 12 pt

Formatted: Font: (Default) Times New Roman, 12 pt

Formatted: Font: (Default) Times New Roman, 12 pt

Formatted

1521 event, although having a burrowing lifestyle. This is because linguils are able to survive
1522 in poorly oxygenated waters due to having respiratory pigment acting the function to
1523 transport oxygen or to store oxygen within the body tissues under anoxic conditions or
1524 during cessation of respiration (Williams et al., 1997).

1525 Similarly, Huang et al. (2014) argued that the anoxia or acidification may have
1526 impacted seriously on bivalve's extinction and survival selectivity during the first
1527 extinction based on ecologic analysis of the P-Tr bivalves. As a result, both brachiopod's
1528 and bivalve's evidence indicates that anoxia impacted clearly by in the first-pulse
1529 biocrisis (Chen et al., 2011b; Huang et al., 2014). The acidification associated with this
1530 extinction cannot be excluded (Clapham and Payne, 2011; Hinojosa et al., 2012). The
1531 anoxia or acidification, however, lasted a very short duration, ~30 ka, as discussed above.

1532 Furthermore, a rapid increase of about ~9°C of sea-surface temperature (within a
1533 period of ~30 ka) across Beds 24e-27a (Sun et al., 2012) must have facilitated respiratory
1534 frequency and accelerated oxygen consumption of most brachiopods and become lethal
1535 to brachiopods, and thus causes mortality, regardless their shallower or deeper habitats
1536 (Chen et al., 2014b in this volume). The rapidly elevated seawater temperature also
1537 coincides with the first dramatic losses of body fossil biodiversity and fossil fragments as

Formatted: Indent: First line: 1.5 cm,
Line spacing: Double

well as moderate losses of ichnodiversity and community diversity, and a moderate decrease in bioturbation, tiering levels of infaunas and burrow sizes.

However, marine ecosystems seem not to have collapsed completely during the first-pulse crisis (Chen and Benton, 2012), some organisms survived the short environmental and climatic devastation. Thus, both biodiversity and ichnodiversity, and all of ichnological and community structural measures rebounded rapidly in Bed 27a-d (Fig. 26).

Like the first extinction, the second-pulse biocrisis is also associated with a clay bed (Bed 28), in which pyrite framboids indicate a lower dysoxic to anoxic condition (Fig. 25). However, the redox condition became euxinic soon after and is indicated by framboids obtained from the base of Bed 29. Thus, a dramatic change from upper dysoxic to oxic condition in Bed 27 to euxinic condition in basal Bed 29 indicates an anoxia/euxinia coincided with the 2nd biocrisis, which is followed by a long period of euxinic to anoxic conditions, which was probably driven by a relatively long (>62 ka) acme of high temperature (up to 35-37°C) in earliest Griesbachian. Accordingly, both epifaunal and infaunal ecosystems collapsed after suffering such a long period of lethally hot seawater temperature and widespread anoxia in earliest Triassic oceans (Fig. 26).

Formatted: Indent: First line: 1 cm,
Line spacing: Double

Formatted: Superscript

This is reinforced by the replacement of free-lying brachiopod-dominated communities in Bed 27 with nekton-dominated communities in Beds 31-37 (Chen et al., 2010a) and Beds 28-34 barren of bioturbation and ichnofossils (Figs. 3, 26). As stated above, these surviving brachiopods yielded from Beds 26-27 should have enhanced resistant ability to anoxic or acidified water mass near seafloor because they survived from the first-pulse crisis. The mortality of the free-lying brachiopods in the second-pulse crisis is probably due to the loss of other shells or float algae, on which the brachiopods attach using either pedicle or clasping spines.

Accordingly, the killing mechanisms for these two extinction events near the PTB seem not to be fundamentally different from one another, although no sign of acidification has been reported in the second phase of the PTME. However, a short anoxia or acidification probably caused by a rapid increase in seawater temperature may have played an important role in the first-pulse biocrisis, while the long-lasting and widespread anoxia induced by a long period of high temperature condition may have killed most organisms in the second-pulse crisis.

Formatted: Normal, Indent: First line: 1.5 cm, Line spacing: Double, Don't adjust space between Latin and Asian text, Don't adjust space between Asian text and numbers

7.56. Post-extinction amelioration of marine ecosystems in late Griesbachian

1572

1573 Post-extinction benthic communities did not appear to return to normal until the
1574 early Middle Triassic (Chen and Benton, 2012). The deleterious environment that
1575 prevailed in early Triassic oceans may be largely responsible for this long-delayed
1576 recovery (Bottjer et al., 2008). In particular, Early Triassic carbon isotopic records show
1577 several negative excursions that indicate sharp global warming (Payne et al., 2004), and
1578 these coincide with diversity drops. Furthermore, intrinsic relationships between
1579 organisms and ecosystem structures may also have slowed down biotic recovery
1580 following the PTME (Chen and Benton, 2012). Recent studies show that the biotic
1581 recovery process may be mirrored by stepwise establishment of trophic structures of
1582 marine ecosystems throughout Olenekian-Anisian interval (Chen and Benton, 2012).
1583 However, biotic recovery may occur earlier in oxygenated environments (Twitchett et al.,
1584 2004; Beatty et al., 2008; Zonneveld et al., 2010). As a result, Early Triassic marine
1585 environments were not always deleterious globally. Chen et al. (2007) also detected that
1586 marine environments had greatly ameliorated during the late Griesbachian in Meishan.
1587 The sea-floor recuperation, including shallowing water depth, increasing oxygenation
1588 and oceanic productivity, coincides with an increase in benthic biodiversity, signalling

that ecologic and environmental restoration might have initiated in the late Griesbachian (Chen et al., 2002, 2007).

The example of elevated recovery of the benthic community in late Griesbachian at Meishan is also strengthened by community structural changes and ichnofabric variation through the PTB to late Griesbachian. The Exp (H) value increases by 262.6% from the *C* to *M–L* communities, and also increases 70%, coupled with a decrease of 15.2% in *D'* values, from the *C–O* to *M–L* communities, suggesting an improvement in shelly community structures in the upper Yinkeng Formation at Meishan (Chen et al., 2002, 2007).

Trace fossils and ichnofabrics documented here also show that the late Griesbachian trace-fossil assemblage is marked by significant increases in ichnodiversity, burrow size, trace complexity, tiering level, and bioturbation level, in comparison with early Griesbachian ichnoassemblages, although they did not achieve Changhsingian levels (Fig. 21). Thus, the Meishan trace fossils, together with increasing diversity in the shelly community, sedimentary structures (HCS), up-shallowing sedimentary cycle and geochemical proxies (Chen et al., 2007), suggest that biotic recovery recorded in the upper Yinkeng Formation may be categorized as recovery stage 2 (*sensu* Twitchett, 2006),

and also mark the return of parts of the meso-consumer functioning group within the ecosystem trophic structure, which usually occurs in the Spathian around the world (Chen and Benton, 2012).

8. Conclusions

Updated conodont biostratigraphy allows the establishment of eight conodont zones from the latest Changhsingian to early Griesbachian at Meishan, the *C. yini*, *C. meishanensis*, *H. ~~changhsingensis~~changxingensis*, *C. taylorae*, *H. parvus*, *I. staeschei*, *I. isarcica*, and *C. planate* zones. Microstratigraphic analysis shows that a major turnover in fossil fragment contents and ichnodiversity occurs across the boundary between Beds 24e-5 and 24e-6, suggesting the actual mass extinction horizon in thin section. Bed 27 contains a firmground of *Glossifungites* ichnofacies rather than the previously proposed submarine ~~solution~~dissolution surface or hardground surface. Fossil fragment contents show a dramatic decline in both fossil component percentage and assemblage diversity in Beds 25-26a, coinciding with metazoan mass extinction. Fossil fragment content, ichnodiversity and all ichnofabric proxies (including burrow size, tiering level, and

1623 bioturbation level) throughout the uppermost Changhsing to Yinkeng formations indicate
1624 that the P-Tr ecologic crisis comprises two discrete stages, coinciding with the first and
1625 second phases of the PTME, in support of a proposed two-stage extinction pattern of
1626 metazoans over the P-Tr transition. The PTME was of short duration, lasting about 60 kyr.
1627 A biodiversity crisis indicates the start of the extinction interval, but its end is marked by
1628 the ecologic collapse of ecosystems. Thus, the ecologic crisis lagged behind the
1629 biodiversity decline during the PTME. Pyrite framboid size variations suggest that the
1630 depositional redox condition was anoxic to euxinic in the latest Changhsingian, became
1631 euxinic in Beds 25-26a, turned to be dyoxic in Bed 27, then varied from euxinic to anoxic
1632 through most of the Griesbachian. Although metazoan biodiversity and fossil fragment
1633 contents show dramatic declines, coinciding with a ~~~10~~~9 °C increase in seawater surface
1634 temperature, from Bed 24e to Bed 27 in Meishan, all ecologic proxies show much smaller
1635 effects from the elevated seawater temperature. Bed 27 contains abundant infauna and
1636 shows no signs of ocean acidification. Pre-extinction anoxic-euxinic conditions had little
1637 effect on both metazoans and infauna. The anoxic event associated with the PTME may
1638 have lasted for much less time than previously thought, and is limited to Beds 25-26a at
1639 Meishan. Fossil fragment contents, ichnofaunas, ichnofabrics and pyrite framboid size all

1640 show that anoxic conditions did not exist in Bed 27. Early Griesbachian anoxia is possible,
1641 and may have caused the rarity of ichnofaunas and metazoans in the lower Yinkeng
1642 Formation. The ichnofauna is characterized by small, simple horizontal burrows of
1643 *Planolites*, while metazoan faunas are characterized by low diversity, high abundance,
1644 opportunist-dominated communities. The killing mechanisms for these two extinction
1645 events near the PTB similar to one another. A rapid increase of ~9[°]C in seawater
1646 temperature and its inducing short anoxia or acidification may have played an important
1647 role in the first-pulse biocrisis, while the long-time and widespread anoxia probably
1648 caused by long-time high temperature condition may have resulted in mortality of most
1649 organisms in the second-pulse crisis. Initial recovery of marine ecosystems coupled with
1650 environmental amelioration occurred in the late Griesbachian, marking the return of parts
1651 of the meso-consumer functioning group.

1652

1653 Acknowledgements

1654

1655 We thank J. Tong for help in the field and H.J. Song for discussion on foraminiferal
1656 taxonomy of collections from the PTB beds in Meishan. This work was supported by the

Formatted: Superscript

1657 973 Program and China 111 Program. It is a contribution to IGCPs 572 and 630.

1658

1659 **References**

1660

1661 Algeo, T.J., Twitchett, R.J., 2010. [Anomalous Early Triassic sediment fluxes due to](#)

1662 [elevated weathering rates and their biological consequences](#). *Geology* 38,

1663 [1023–1026](#).

1664 Algeo, T.J., Chen, Z.Q., Fraiser, M.L., Twitchett, R.J., 2011a. Terrestrial-marine

1665 teleconnections in the collapse and rebuilding of Early Triassic marine ecosystems.

1666 *Palaeogeography, Palaeoclimatology, Palaeoecology* 308, 1–11.

1667 Algeo, T.J., Hannigan, R., Rowe, H., Brookfield, M., Baud, A., Krystyn, L., Ellwood,

1668 B.B., 2007. Sequencing events across the Permian–Triassic boundary, Guryul

1669 Ravine (Kashmir, India). *Palaeogeography, Palaeoclimatology, Palaeoecology* 252,

1670 328–346.

1671 Algeo, T.J., Henderson, C.M., Ellwood, B., Rowe, H., Elswich, E., Bates, S., Lyons, T.,

1672 Hower, J.C., Smith, C., Maynard, B., Hays, L.E., Summons, R.E., Fulton, J.,

1673 Freeman, K.H., 2012. Evidence for a diachronous late Permian marine crisis from

Formatted: Indent: Left: 0 cm,
Hanging: 1.77 ch, First line: -1.77 ch

Formatted: Font: (Default) Times
New Roman, 12 pt

Formatted: Indent: Left: 0 cm,
Hanging: 1.77 ch

Formatted

Formatted: Font: (Default) Times
New Roman, 12 pt

Formatted: Font: (Default) Times
New Roman, 12 pt

Formatted: Font: (Default) Times
New Roman, 12 pt

Formatted

1674 the Canadian Arctic region. Geological Society of America Bulletin 124,
1675 1424–1448.

1676 Algeo, T.J., Hinnov, L., Moser, J., Maynard, J.B., Elswick, E., Kuwahara, K., Sano, H.,
1677 2010. Changes in productivity and redox conditions in the Panthalassic Ocean during
1678 the latest Permian. *Geology* 38, 187–190.

1679 Algeo, T.J., Kuwahara, K., Sano, H., Bates, S., Lyons, T., Elswick, E., Hinnov, L.,
1680 Ellwood, B., Moser, J., Maynard, J.B., 2011b. Spatial variation in sediment fluxes,
1681 redox conditions, and productivity in the Permian–Triassic Panthalassic Ocean.
1682 *Palaeogeography, Palaeoclimatology, Palaeoecology* 308, 65–83.

1683 Ausich, W.I., Bottjer, D.J., 2002. Sessile invertebrates. In: Briggs, D.E.G., Crowther, P.R.
1684 (eds.), *Palaeobiology II*. Blackwell Science, Oxford, pp. 384–386.

1685 Baldwin, C.T., McCave, I.N., 1999. Bioturbation in an active deep-sea area: Implications
1686 for models of trace fossil tiering. *Palaios* 14, 375–388.

1687 Beatty, T.W., Zonneveld, J.-P., Henderson, C.M., 2008. Anomalously diverse Early
1688 Triassic ichnofossil assemblages in northwest Pangea: a case for a shallow-marine
1689 habitable zone. *Geology* 36, 771–774.

1690 Benner, J.S., Ekdale, A.A., 2004. Macroborings (*Gastrochaenolites*) in Lower

1691 Ordovician Hardgrounds of Utah: Sedimentologic, Paleoecologic, and Evolutionary
 1692 Implications. *Palaaios* 19, 543–550.

1693 Benton, M.J., Twitchett, R.J., 2003. How to kill (almost) all life: the end-Permian
 1694 extinction event. *Trends in Ecology and Evolution* 18, 358–365.

1695 Bond, D.P.G., Wignall, P.B., 2010. Pyrite framboid study of marine Permian–Triassic
 1696 boundary sections: a complex anoxic event and its relationship to contemporaneous
 1697 mass extinction. *Geological Society of America Bulletin* 122, 1265–1279.

1698 Bottjer, D.J., Droser, M.L., Jablonski, D., 1988. Fine-scale resolution of mass extinction
 1699 events: Trace fossil evidence from the Permian-Triassic boundary in South China.
 1700 *Geological Society of America, Abstracts with Programs* 20, p. A106.

1701 Bottjer, D.J., Clapham, M.E., Frasier, M.L., Powers, C.M., 2008. Understanding
 1702 mechanisms for the end-Permian mass extinction and the protracted Early Triassic
 1703 aftermath and recovery. *GSA Today* 18, 4–10.

1704 Bowring, S.A., Erwin, D.H., Jin, Y.G., Martin, M.W., David, E.K., Wang, W., 1998.
 1705 U/Pb zircon geochronology and tempo of the end-Permian mass extinction. *Science*
 1706 280, 1039–1045.

1707 Brennecka, G.A., Herrmann, A.D., Algeo, T.J., Anbar, A.D., 2011. Rapid expansion of

1708 oceanic anoxia immediately before the end-Permian mass extinction. Proceedings of
 1709 the National Academy of Sciences, U.S.A. 108, 17631–17634.
 1710 Bromley, R.G., 1996. Trace Fossils: Biology, Taphonomy and Applications (2nd edition).
 1711 Chapman & Hall, London, 361 pp.
 1712 Bromley, R.G., Ekdale, A.A., 1984. *Chondrites*: a trace fossil indicator of anoxia in
 1713 sediments. Science 224, 872-874.
 1714 Buatois, L.A., Mángano, M.G., 2011. Ichnology: Organism-Substrate Interactions in
 1715 Space and Time. Cambridge University Press, New York. 1–358.
 1716 Buatois, L.A., Gingras, M.K., MacEachern, J., Mangano, M.G., Zonneveld, J.P.,
 1717 Pemberton, S.G., Netto, R.G., Martin, A., 2005. Colonization of brackish-water
 1718 systems through time: Evidence from the trace-fossil record. Palaios 20, 321-347.
 1719 Burgess, S.D., Bowring, S., Shen, Z.Q., 2014. High-precision timeline for Earth's most
 1720 severe extinction. Proceedings of National Academy of Sciences, U.S.A. 111,
 1721 3316–3321.
 1722 Cao, C.Q., Shang, Q.H., 1998. Microstratigraphy of Permo-Triassic transitional sequence
 1723 of the Meishan section, Zhejiang, China. Palaeoworld 9, 147-152.
 1724 Cao, C.Q., Zheng, Q.F., 2007. High-resolution lithostratigraphy of the Changhsingian

1725 stage in Meishan section, Zhejiang. Journal of Stratigraphy 31, 14-22.

1726 Cao C Q, Zheng Q F. 2009. Geological event sequences of the Permian-Triassic

1727 transition recorded in the microfacies in Meishan section. Science China Series

1728 D-Earth Sciences 52, 1529–1536

1729 Cao, C.Q., Wang, W., Jin, Y., 2002. Carbon isotope excursions across the

1730 Permian-Triassic boundary in the Meishan section, Zhejiang Province, China.

1731 Chinese Science Bulletin 47, 1125-1129.

1732 Cao, C., Love, G.D., Hays, L.E., Wang, W., Shen, S., Summons, R.E., 2009.

1733 Biogeochemical evidence for euxinic oceans and ecological disturbance presaging

1734 the end-Permian mass extinction event. Earth and Planetary Science Letters 281,

1735 188–201.

1736 Chen, J., Chen, Z.Q., Tong, J.N., 2010b. Palaeoecology and taphonomy of two

1737 brachiopod shell beds from the Anisian (Middle Triassic) of Guizhou, Southwest

1738 China: recovery of benthic communities from the end-Permian mass extinction.

1739 Global and Planetary Change 73, 149-160.

1740 Chen, J., Chen, Z.Q., Tong, J., 2011b, Environmental determinants and ecologic

1741 selectivity of benthic faunas from nearshore to bathyal zones in the end-Permian

Formatted: Font: Times New Roman, 12 pt

Formatted: Left, Indent: Left: 0 cm, Hanging: 1.77 ch

Formatted: Font: Times New Roman, 12 pt

1742 [mass extinction: brachiopod evidence from South China. Palaeogeography,](#)
1743 [Palaeoclimatology, Palaeoecology 308, 84-97.](#)

1744 Chen, J.H., 2004. Macroevolution of bivalves after the end-Permian mass extinction in
1745 South China. In: Rong, J.Y., Fong, Z.J. (eds), Biotic mass extinction and
1746 recovery—evidence from Palaeozoic and Triassic of South China. China University
1747 of Science & Technology Press, Hefei. pp. 647–700.

1748 Chen, Z.Q., Benton, M.J., 2012. The timing and pattern of biotic recovery following the
1749 end-Permian mass extinction. Nature Geoscience 5, 375–383.

1750 Chen, Z.Q., Liao, Z.T., 2009. Brachiopod faunas across the Wuchiapingian-
1751 Changhsingian (Late Permian) boundary at the stratotype section and subsurface of
1752 Changxing area, South China. Neues Jahrbuch für Geologie und Paläontologie 254,
1753 315–335.

1754 Chen, Z.Q., McNamara, K.J., 2006. End-Permian extinction and subsequent recovery of
1755 the Ophiuroidea (Echinodermata). Palaeogeography, Palaeoclimatology,
1756 Palaeoecology 236, 321–344.

1757 Chen, Z.Q., Algeo, T.J., Bottjer, D.J., 2014^a. Global review of the Permian–Triassic mass
1758 extinction and subsequent recovery: Part I. Earth-Science Reviews [137, 1-5.](#)~~(in~~

1759 [press\), ~~http://dx.doi.org/10.1016/j.jearseirev.2014.05.007~~](http://dx.doi.org/10.1016/j.jearseirev.2014.05.007)

1760 Chen, Z.Q., Campi, M., Shi, G.R., Kaiho, K., 2005b. Post-extinction brachiopod faunas

1761 from the Late Permian Wuchiapingian coal series of South China. *Acta*

1762 *Palaeontologica Polonica* 50, 343-363.

1763 Chen, Z.Q., Fraiser, M.L., Bolton, C., 2012. Early Triassic trace fossils from Gondwana

1764 Interior Sea: Implication for ecosystem recovery following the end-Permian mass

1765 extinction in south high-latitude region. *Gondwana Research* 22, 238-255.

1766 Chen, Z.Q., Kaiho, K., George, A.D., 2005a. Survival strategies of brachiopod faunas

1767 from the end-Permian mass extinction. *Palaeogeography, Palaeoclimatology,*

1768 *Palaeoecology* 224, 232-269.

1769 Chen, Z.Q., Kaiho, K., George, A.D., Tong, J., 2006b. Survival brachiopod faunas of the

1770 end-Permian mass extinction from northern Italy and south China. *Geological*

1771 *Magazine* 143, 301-327.

1772 Chen, Z.Q., Shi, G.R., Kaiho, K., 2002. A new genus of rhynchonellid brachiopod from

1773 the Lower Triassic of South China and implications for timing the recovery of

1774 Brachiopoda after the end-Permian mass extinction. *Palaeontology* 45, 149-164.

1775 Chen, Z.Q., Shi, G.R., Yang, F.Q., Gao, Y.Q., Tong, J.N., Peng, Y.Q., 2006a. An

1776 ecologically mixed brachiopod fauna from Changhsingian deep-water basin of South
 1777 China: consequence of end-Permian global warming. *Lethaia* 39, 79–90.

1778 | Chen, Z.Q., Tong, J.N., Fraiser, M.L., 2011 [a](#). Trace fossil evidence for restoration of
 1779 marine ecosystems following the end-Permian mass extinction in the Lower Yangtze
 1780 region, South China. *Palaeogeography, Palaeoclimatology, Palaeoecology* 299,
 1781 449–474.

1782 Chen, Z.Q., Tong, J.N., Liao, Z.T., Chen, J., 2010a. Structural changes of marine
 1783 communities over the Permian–Triassic transition: ecologically assessing the
 1784 end-Permian mass extinction and its aftermath. *Global and Planetary Change* 73,
 1785 123–140.

1786 Chen, Z.Q., Tong, J., Zhang, K., Yang, H., Liao, Z., Song, H., Chen, J., 2009.
 1787 Environmental and biotic turnover across Permian–Triassic boundary from shallow
 1788 carbonate platform in western Zhejiang, South China. *Australian Journal of Earth*
 1789 *Sciences* 56, 775–797.

1790 Chen, Z.Q., Tong, J., Kaiho, K., Kawahata, H., 2007. Onset of biotic and environmental
 1791 recovery from the end-Permian mass extinction within 1–2 million years: A case
 1792 study of the Lower Triassic of the Meishan section, South China. *Palaeogeography,*

- 1793 Palaeoclimatology, Palaeoecology 252, 176-187.
- 1794 [Chen, Z.Q., Wang, J.L., Yang, H., Tu, C.Y., Polov, Y., He, W.H., 2014b. Permian-Triassic](#)
- 1795 [evolutionary dynamics of the Brachiopoda: paleobiogeography,](#)
- 1796 [extinction-survival-recovery, latitudinal diversity gradients, body size variations,](#)
- 1797 [and longevity changes. Earth-Science Reviews \(under review, in this volume\).](#)
- 1798 Claoue-Long, J.C., Zhang, Z.C., Ma, G.G. and Du, S.H., 1991. The age of the
- 1799 Permian-Triassic boundary. Earth and Planetary Science Letters 105, 182–190.
- 1800 Clapham, M., Payne, J., 2011. Acidification, anoxia, and extinction: a multiple logistic
- 1801 regression analysis of extinction selectivity during the Middle and Late Permian.
- 1802 Geology 39, 1059–1062.
- 1803 Condie, K.C., 2001. Mantle Plumes and Their Record in Earth History. Cambridge
- 1804 University Press, Cambridge. 306 pp.
- 1805 Crasquin, S., Forel, M.B., Feng, Q.L., Yuan, A.H., Baudin, F., Collin, P.Y., 2010.
- 1806 Ostracods (Crustacea) through the Permian-Triassic boundary in South China: the
- 1807 Meishan stratotype (Zhejiang Province). Journal of Systematic Palaeontology 8,
- 1808 331-370.
- 1809 Dasgupta, S., Buatois, L.A., 2012. Unusual occurrence and stratigraphic significance of

1810 the *Glossifungites* ichnofacies in a submarine paleo-canyon — Example from a

1811 Pliocene shelf-edge delta, Southeast Trinidad. *Sedimentary Geology* 269-270,

1812 69-77.

1813 Droser, M.L., Bottjer, D.J., 1986. A semiquantitative field classification of ichnofabric.

1814 *Journal of Sedimentary Petrology* 56, 558-559.

1815 Ekdale, A.A., Bromley, R.G., 2001. A day and a night in the life of a cleft-foot clam:

1816 *Protovirgularia-Lockeia-Lophoctenium*. *Lethaia* 34, 119-124.

1817 Ekdale, A.A., Bromley, R.G., 2003. Paleoethologic interpretation of complex

1818 *Thalassinoides* in shallow-marine limestone, Lower Ordovician, southern Sweden.

1819 *Palaeogeography, Palaeoclimatology, Palaeoecology* 192, 221-227.

1820 Elderfield, H., Greaves, M.J., 1982. The rare earth elements in seawater. *Nature* 296,

1821 214–219.

1822 Erwin, D.H., 2001. Lessons from the past: biotic recoveries from mass extinctions.

1823 *Proceedings of the National Academy of Sciences, U.S.A.* 98, 5399–5403.

1824 Erwin, D.H., 2006. *How Life on Earth Nearly Ended 250 Million Years Ago*. Princeton

1825 University Press, Princeton, 306 pp.

1826 Farabegoli, E., Perri, M.C., 2012. Millennial physical events and the end-Permian mass

1827 mortality in the western Palaeotethys: timing and primary causes. In: Talent, J.A.

1828 (ed.), *Earth and Life, International Year of Planet Earth*, Springer, London, pp.

1829 719-758.

1830 Flugel, E., 1982. *Microfacies Analysis of Limestone*, Springer, New York, 663 pp.

1831 Forel, M.-B., Crasquin, S., 2011. Lower Triassic ostracods (Crustacea) from the Meishan

1832 section, Permian-Triassic boundary GSSP (Zhejiang Province, South China). *Journal*

1833 *of Systematic Palaeontology* 9, 455-466.

1834 Fraiser, M.L., Bottjer, D.J., 2007. Elevated atmospheric CO₂ and the delayed biotic

1835 recovery from the end-Permian mass extinction. *Palaeogeography,*

1836 *Palaeoclimatology, Palaeoecology* 252, 164–175.

1837 Fraiser, M.L., Bottjer, D.J., 2009. Opportunistic behavior of invertebrate marine

1838 tracemakers during the Early Triassic aftermath of the end-Permian mass extinction.

1839 *Australian Journal of Earth Sciences* 56, 841–857.

1840 Gao, Q.L., Zhang, N., Xia, W.C., Feng, Q.L., Chen, Z.Q., Zheng, J.P., Griffin, W.L.,

1841 O'Reilly, S.Y., Pearson, N.J., Wang, G.Q., Wu, S., Zhong, W.L., Sun, X.F., 2013.

1842 Origin of volcanic ash beds across the Permian-Triassic boundary, Daxiakou, South

1843 China: Petrology and U-Pb age, trace elements and Hf-isotope composition of zircon.

1844 Chemical Geology 360-361, 41-53.

1845 Gao, Q.L., Chen, Z.Q., Zhang, N., Xia, W.C., Wang, G.Q., Jiang, T.F., Xia, X.F., 2014.

1846 Ages, trace elements and Hf-isotopic compositions of zircon from claystones around

1847 the Permian-Triassic boundary in the Zunyi section, South China: implications for

1848 nature and tectonic setting of the volcanism. Journal of Earth Sciences 26 (in press).

1849 Gorjan, P., Kaiho, K., Kakegawa, T., Niitsuma, S., Chen, Z.Q., Kajiwar, Y., Nicora, A.,

1850 2007. Paleoredox, biotic and sulfur-isotopic changes associated with the

1851 end-Permian mass extinction in the western Tethys. Chemical Geology 244,

1852 483-492.

1853 Gouramis, C., Webb, J.A., Warren, A.A., 2003. Fluviodeltaic sedimentology and

1854 ichnology of part of the Silurian Grampians Group, western Victoria. Australian

1855 Journal of Earth Sciences 50, 811-825.

1856 Grice, K., Cao, C., Love, G.D., Bottcher, M.E., Twitchett, R.J., Grosjean, E., Summons,

1857 R.E., Turgeon, S.C., Dunning, W., Jin, Y., 2005. Photic zone euxinia during the

1858 Permian-Triassic superanoxic event. Science 307, 706-709

1859 Hammer, O., Harper, D.A.T., Ryan, P.D., 2001. PAST: palaeontological statistics

1860 software package for education and data analysis. Palaeontologia Electronica 4, 1-9.

- 1861 Häntzschel, W., 1975. Trace fossils and problematica. In: Teichert, C. (ed.), *Treatise of*
1862 *Invertebrate Paleontology* (2nd Edition), Part W, Miscellaneous, Supp 1. University of
1863 Kansas and Geological Society of America, Lawrence, Kansas, 269 pp.
- 1864 He, J.W., 1981. Clay minerals in the Changhsingian stratotype section and the basal part
1865 of Yinkeng Formation, with reference to the Permo-Triassic boundary (in Chinese).
1866 *Journal of Stratigraphy* 5, 197–206
- 1867 He, J.W., Rui, L., Chai, Z.F., 1987. The latest Permian and earliest Triassic volcanic
1868 activities in the Meishan area of Changxing, Zhejiang. *Journal of Stratigraphy* 11,
1869 194–199.
- 1870 He, W., Feng, Q., Gu, S., Jin, Y., 2005. Changxingian (Upper Permian) Radiolarian fauna
1871 from Meishan D section, Changxing, Zhejiang, China, and its possible
1872 paleoecological significance. *Journal of Paleontology* 79, 209–218.
- 1873 Hinojosa, J.L., Brown, S.T., Chen, J., DePaolo, D.J., Paytan, A., Shen, S.Z., Payne, J.L.,
1874 2012. Evidence for end-Permian ocean acidification from calcium isotopes in
1875 biogenic apatite. *Geology* 40, 743–746.
- 1876 Huang, C.J., Tong, J.N., Hinnov, L., Chen, Z.Q., 2011. Did the great dying of life take
1877 700 ky? Evidence from global astronomical correlation of the Permian-Triassic

1878 boundary interval. *Geology* 39, 779-782.

1879 [Huang, Y.F., Tong, J.N., Fraiser, M.L., Chen, Z.Q., 2014. Extinction patterns among](#)

1880 [bivalves in South China during the Permian-Triassic crisis. *Palaeogeography,*](#)

1881 [*Palaeoclimatology, Palaeoecology* 399, 78-88.](#)

1882 Hubbard, S.M., Shultz, M.R., 2008. Deep burrows in submarine fan-channel deposits of

1883 the Cerro Toro Formation (Cretaceous), Chilean Patagonia: implications for

1884 firmground development and colonization in the deep sea. *Palaios* 23, 223–232.

1885 Jacobsen, N., Twitchett, R.J., Krystyn, L., 2011. Palaeoecological methods for assessing

1886 marine ecosystem recovery following the Late Permian mass extinction event.

1887 *Palaeogeography, Palaeoclimatology, Palaeoecology* 308, 200–212.

1888 Jiang, H.S., Lai, X., Luo, G., Aldridge, R., Zhang, K., Wignall, P.B., 2007. Restudy of

1889 conodont zonation and evolution across the P/T boundary at Meishan section,

1890 Changxing, Zhejiang, China. *Global and Planetary Change* 55, 39-55.

1891 Jiang, H.S., Aldridge, R.J., Lai, X.L., Sun, Y.D., Luo, G.M., 2008. Observations on the

1892 surface microreticulation of platform elements of *Neogondolella* (Conodonta) from

1893 the Upper Permian, Meishan, China. *Lethaia* 41, 263-274.

1894 [Jiang, H.S., Lai, X.L., Sun, Y.D., Wignall, P.B., Liu, J., Yan, C., 2014. Permian-Triassic](#)

- 1895 [conodonts from Dajiang \(Guizhou, South China\) and their implication for the age of](#)
1896 [microbialite deposition in the aftermath of the end-Permian mass extinction. Journal](#)
1897 [of Earth Science 25, 413-430.](#)
- 1898 Jiang, H.S., Lai, X.L., Yan, C.B., Aldridge, R.J., Wignall, P., Sun, Y.D., 2011. Revised
1899 conodont zonation and conodont evolution across the Permian-Triassic boundary at
1900 the Shangsi section, Guangyuan, Sichuan, South China. *Global and Planetary Change*,
1901 77, 103-115,
- 1902 Jiang, Y., Tang, Y., Dai, S., Zou, X., Qian, H., Zhou, G., 2006. Pyrites and sulfur isotopic
1903 composition near the Permian-Triassic boundary in Meishan. *Zhejiang. Acta*
1904 *Geologica Sinica* 80, 1202-1207.
- 1905 Jin, Y., Wang, Y., Wang, W., Shang, Q., Cao, C., Erwin, D.H., 2000. Pattern of marine
1906 mass extinction near the Permian-Triassic boundary in South China. *Science* 289,
1907 432-436.
- 1908 Joachimski, M.M., Lai, X., Shen, S., Jiang, H., Luo, G., Chen, B., Chen, J., Sun, Y., 2012.
1909 Climate warming in the latest Permian and the Permian-Triassic mass extinction.
1910 *Geology* 40, 195-198.
- 1911 Jost, L., 2006. Entropy and diversity. *Oikos* 113, 363-375.

- 1912 Jost, L., 2007. Partitioning diversity into independent alpha and beta components.
1913 Ecology 88, 2427–2439.
- 1914 Jumars, P.A., Wheatcroft, R.A., 1989. Responses of benthos to changing food quality and
1915 quantity with a focus of deposit feeding and bioturbation. In: Berger, W.H., Smetacek,
1916 V.S., Wefer, G., (eds.), Productivity in the Ocean: Past and Present. Wiley, Chichester,
1917 pp. 235-253.
- 1918 Kaiho, K., Chen, Z.Q., Miura, Y., Kawahata, H., Kajiwar, Y., Sato, H., 2006b. Close-up
1919 of the end-Permian mass extinction horizon recorded in the Meishan section, South
1920 China: Sedimentary, elemental, and biotic characterization with a negative shift of
1921 sulfate sulfur isotope ratio. Palaeogeography, Palaeoclimatology, Palaeoecology 239,
1922 396-405.
- 1923 Kaiho, K., Kajiwar, Y., Chen, Z.Q., Gorjan, P., 2006a. A sulfur isotope event at the end
1924 of the Permian. Chemical Geology 235, 33-47
- 1925 Kaiho, K., Chen, Z.Q., Sawada, K., 2009. Possible causes for a negative shift of stable
1926 carbon isotope ratio before, during, and after the end-Permian mass extinction in
1927 Meishan, South China. Australian Journal of Earth Sciences 56, 799-808.
- 1928 Kaiho, K., Kajiwar, Y., Nakano, T., Miura, Y., Chen, Z.Q., Shi, G.R., 2001. End-Permian

- 1929 catastrophe by a bolide impact: evidence of a gigantic release of sulfur from the
- 1930 mantle. *Geology* 29, 815-818.
- 1931 Keighley, D.G., Pickeril, P.K., 1994. The ichnogenus *Beaconites* and its distinction from
- 1932 *Ancorichnus* and *Taenidium*. *Palaeontology* 37, 305-337.
- 1933 Knaust, D., 1998. Trace fossils and ichnofabrics on the Lower Muschelkalk carbonate
- 1934 ramp (Triassic) of Germany: tool for high-resolution sequence stratigraphy.
- 1935 *Geologische Rundschau* 87, 21-31.
- 1936 Knaust, D., 2004. Cambro–Ordovician trace fossils from the SW Norwegian Caledonides.
- 1937 *Geological Journal* 39, 1–24.
- 1938 Knoll, A.H., Bambach, R.K., Oayne, J.L., Pruss, S., Fischer, W.W., 2007.
- 1939 Paleophysiology and end-Permian mass extinction. *Earth and Planetary Science*
- 1940 *Letters* 256, 295–313.
- 1941 Korte, C., Kozur, H., Joachimski, M.M., Strauss, H., Veizer, J., Schwark, L., 2004a.
- 1942 Carbon, sulfur, oxygen and strontium isotope records, organic geochemistry and
- 1943 biostratigraphy across the Permian/Triassic boundary in Abadeh, Iran. *International*
- 1944 *Journal of Earth Sciences* 93, 565–581
- 1945 Kosnik, M.A., Wagner, P.J., 2006. Effects of taxon abundance distributions on expected

- 1946 numbers of sampled taxa. *Evolutionary Ecology Research* 8, 195–211.
- 1947 Kozur, H., 2007. Biostratigraphy and event stratigraphy in Iran around the
- 1948 Permian–Triassic Boundary (PTB): Implications for the causes of the PTB biotic
- 1949 crisis. *Global and Planetary Change* 55, 155–176.
- 1950 Lea, D.W., Pak, D.K., Spero, H.J., 2000. Climate impact of late quaternary equatorial
- 1951 pacific sea surface temperature variations. *Science* 289, 1719–1724.
- 1952 Li, J., Cao, C.Q., Servais, T., Zhu, Y.H., 2004. Later Permian acritarchs from Meishan
- 1953 (SE China) in the context of Permian palaeobiogeography and palaeoecology. *Neues*
- 1954 *Jahrbuch für Geologie und Paläontologie, Monatshefte* 7, 427–448.
- 1955 Li, W.Z., Shen, S.Z., 2008. Lopingian (Late Permian) brachiopods around the
- 1956 Wuchiapingian-Changhsingian boundary at the Meishan sections C and D,
- 1957 Changxing, South China. *Geobios* 41, 307–320.
- 1958 Liang H., 2002, End-Permian catastrophic event of marine acidification by hydrated
- 1959 sulfuric acid: Mineralogical evidence from Meishan section of South China:
- 1960 *Chinese Science Bulletin* 47, 1393–1397.
- 1961 Liao, Z.T., 1984. New genera and species of Late Permian and earliest Triassic
- 1962 brachiopods from Jiangsu, Zhejiang and Anhui Provinces. *Acta Palaeontologica*

- 1963 Sinica 23, 276–285.
- 1964 Luo, G.M., Lai, X.L., Jiang, H.S., Zhang, K.X., 2006. Size variation of the end Permian
- 1965 conodont *Neogondolella* at Meishan section, Changxing, Zhejiang and its
- 1966 significance. Science in China, Series D 49, 337–347.
- 1967 Luo, G.M., Lai, X.L., Shi, G.R., Jiang, H.S., Yin, H.F., Xie, S.C., Tong, J.N., Zhang,
- 1968 K.X., He, W.H., Wignall, P.B., 2008. Size variation of conodont elements of the
- 1969 *Hindeodus-Isarcicella* clade during the Permian-Triassic transition in South China
- 1970 and its implication for mass extinction. Palaeogeography, Palaeoclimatology,
- 1971 Palaeoecology 264, 176-187.
- 1972 Luo, G.M., Huang, J.H., Xie, S.C., Wignall, P.B., Tang, X.Y., Huang, X.Y., Yin, H.F.,
- 1973 2010. Relationships between carbon isotope evolution and variation of microbes
- 1974 during the Permian-Triassic transition at Meishan section, South China. International
- 1975 Journal of Earth Sciences 99, 775-784.
- 1976 Luo, G.M., Wang, Y.B., Yang, H., Algeo, T.J., Kump, L., Huang, J.H., Xie, S.C., 2011.
- 1977 Stepwise and large-magnitude negative shift in delta C-13 (carb) preceded the main
- 1978 marine mass extinction of the Permian-Triassic crisis interval. Palaeogeography,
- 1979 Palaeoclimatology, Palaeoecology 299, 70-82.

- 1980 MacEachern, J.A., Raychaudhuri, I., Pemberton, S.G., 1992. Stratigraphic applications of
- 1981 the *Glossifungites* ichnofacies: delineating discontinuities in the rock record. In:
- 1982 Pemberton, S.G. (ed.), Applications of Ichnology to Petroleum Exploration: A Core
- 1983 Workshop: SEPM Core Workshop No. 17, pp. 169–198 Tulsa, USA.
- 1984 MacEachern, J.A., Bann, K.L., Pemberton, S.G., Gingras, M.K., 2007. The ichnofacies
- 1985 paradigm: high-resolution paleoenvironmental interpretation of the rock record. In:
- 1986 MacEachern, J.A., Bann, K.L., Gingras, M.K., Pemberton, S.G. (eds), Applied
- 1987 Ichnology: SEPM Short Course Notes No. 52, pp. 27–64. Tulsa, USA.
- 1988 Mei, S.L., Zhang, K.X., Wardlaw, B.R., 1998. A refined succession of Changhsingian and
- 1989 Griesbachian neogondolellid conodonts from the Meishan section, candidate of the
- 1990 Global Stratotype Section and Point of the Permian-Triassic boundary.
- 1991 Palaeogeography, Palaeoclimatology, Palaeoecology 143, 213–226.
- 1992 Miller, M.F., Smail, S.E., 1997. A semiquantitative method for evaluating bioturbation
- 1993 on bedding planes. Palaios 12, 391–396.
- 1994 Mundil, R., Metcalfe, I., Ludwig, K.R., Renne, P.R., Oberli, F., Nicoll, R.S., 2001.
- 1995 Timing of the Permian–Triassic biotic crisis: implications from new zircon U/Pb age
- 1996 data (and their limitations). Earth and Planetary Science Letters 187, 131–145.

- 1997 Mundil, R., Ludwig, K.R., Metcalfe, I., Renne, P.R., 2004. Age and timing of the Permian
- 1998 mass extinctions: U/Pb dating of closed-system zircons. *Science* 305, 1760–1763.
- 1999 Myrow, P.M., 1995. *Thalassinoides* and the enigma of early Paleozoic open-framework
- 2000 burrow systems. *Palaios* 10, 58–74.
- 2001 Nicoll, R.S., Metcalfe, I., Wang, C.Y., 2002. New species of the conodont genus
- 2002 *Hindeodus* and conodont biostratigraphy of the Permian–Triassic boundary interval.
- 2003 *Journal of Asian Earth Sciences* 20, 609–631.
- 2004 Olszewski, T.D., 2004. A unified mathematical framework for the measurement of
- 2005 richness and evenness within and among multiple communities. *Oikos* 104,
- 2006 377–378.
- 2007 Orchard, M.J., Krystyn, L., 1998. Conodonts of the lowermost Triassic of Spiti, and new
- 2008 zonation based on *Neogondolella* successions. *Rivista Italiana di Paleontologia e*
- 2009 *Stratigrafia* 104, 341–368.
- 2010 Orchard, M.J., Nassichuk, W.W., Rui, L., 1994. Conodonts from the Lower Griesbachian
- 2011 *Otoceras latilobatum* bed of Selong, Tibet and the position of the Permian–Triassic
- 2012 boundary. *Canadian Society of Petroleum Geologists, Proceedings of Pangea*
- 2013 Conference, Memoir 17, 823–843.

2014 Payne, J.L., Clapham, M.E., 2012. End-Permian mass extinction in the oceans: An
2015 ancient analog for the twenty-first century? *Annual Reviews of Earth and Planetary*
2016 *Sciences* 40, 89–111.

2017 Payne, J.L., Lehrmann, D.J., Wei, J.Y., Orchard, M.J., Schrag, D.P., Knoll, A.H., 2004.
2018 Large perturbations of the carbon cycle during recovery from the end-Permian
2019 extinction. *Science* 205, 505–509.

2020 Payne, J.L., Lehrmann, D.J., Wei, J., Knoll, A.H., 2006. The pattern and timing of biotic
2021 recovery from the end-Permian extinction on the Great Bank of Guizhou, Guizhou
2022 Province, China. *Palaios* 21, 63–85.

2023 Payne, J.L., Lehrmann, D.J., Follett, D., Seibel, M., Kump, L.R., Riccardi, A., Altiner, D.,
2024 Sano, H., Wei, J., 2007. Erosional truncation of uppermost Permian shallow-marine
2025 carbonates and implications for Permian–Triassic boundary events. *Geological*
2026 *Society of America, Bulletin* 119, 771–784.

2027 Pemberton, S.G., Frey, R.W., 1985. The *Glossifungites* ichnofacies: modern examples
2028 from the Georgia coast, USA. In: Curran, H.A., (ed.), *Biogenic Structures: Their Use*
2029 *in Interpreting Depositional Environments: SEPM Special Publication*, 35, pp.
2030 237–259, Tulsa, USA.

2031 Pemberton, S.G., Flach, P.D., Mossop, G.D., 1982. Trace fossils from the Athabasca Oil
 2032 Sands, Alberta, Canada. *Science* 217, 825-827.

2033 Pemberton, S.G., MacEachern, J.A., Saunders, T., 2004. Stratigraphic applications of
 2034 substratespecific ichnofacies: delineating discontinuities in the fossil record. In:
 2035 McIlroy, D. (ed.), *The Application of Ichnology to Palaeoenvironmental and*
 2036 *Stratigraphic Analysis*: Geological Society of London, Special Publication, 228,
 2037 29–62.

2038 Perri, M.C., Farabegoli, E., 2003. Conodonts across the Permian–Triassic boundary in
 2039 the Southern Alps. *Courier Forschungsinstitute Senckenberg* 245, 281–313.

2040 Pruss, S.B., Bottjer, D.J., 2004. Early Triassic fossils of the western United States and
 2041 their implications for prolonged environmental stress from the end-Permian mass
 2042 extinction. *Palaios* 19, 551-564.

2043 Reichow, M.K., Pringle, M.S., Al'Mukhamedov, A.I., Allen, M.B., Andreichev, V.L.,
 2044 Buslov, M.M., Davies, C.E., Fedoseev, G.S., Fitton, J.G., Inger, S., Medvedev, A.Y.,
 2045 Mitchell, C., Puchkov, V.N., Safanova, I.Y., Scott, R.A., Saunders, A.D., 2009. The
 2046 timing and extent of the eruption of the Siberian Traps large igneous province:
 2047 implications for the end-Permian environmental crisis. *Earth and Planetary Sciences*

2048 Letters 277, 9–20.

2049 Renne, P.R., Black, M.T., Zheng, Z.C., Richards, M.A., Basu, A.R., 1995. Synchrony
 2050 and causal relations between Permian–Triassic boundary crisis and Siberian flood
 2051 volcanism. *Science* 269, 1413–1416.

2052 Renne, P.R., Mundil, R., Balco, G., Min, K., Ludwig, K.R., 2010. Joint determination of
 2053 ^{40}K decay constants and $^{40}\text{Ar}^*/^{40}\text{K}$ for the Fish Canyon sanidine standard, and
 2054 improved accuracy for $^{40}\text{Ar}/^{39}\text{Ar}$ geochronology. *Geochimica et Cosmochimica*
 2055 *Acta* 74, 5349–5367.

2056 Riccardi, A., Arthur, M.A., Kump, L.R., 2006. Sulfur isotopic evidence for chemocline
 2057 upward excursions during the end-Permian mass extinction. *Geochimica et*
 2058 *Cosmochimica Acta* 70, 5740–5752.

2059 Rindsberg, A.K., Kopaska-Merkel, D.C., 2005. *Treptichnus* and *Arenicolites* from the
 2060 Steven C. Minkin Paleozoic footprint Site (Langsettian, Alabama, USA). In: Buta,
 2061 R.J., Rindsberg, A.K., Kopaska-Merkel, D.C., (eds.), *Pennsylvanian Footprints in*
 2062 *the Black Warrior Basin of Alabama: Monograph, 1*. Alabama Paleontological
 2063 Society, pp. 121–141.

2064 Rui, L., He, J., Chen, C., Wang, Y., 1988. Discovery of fossil animals from the basal clay

2065 of Permian–Triassic boundary in the Meishan area of Changxing, Zhejiang and its
 2066 significance. *Journal of Stratigraphy* 12, 48–52.

2067 Savrda, C.E., 1992. Trace fossils and benthic oxygenation. In: Maples, C.G., West, R.R.
 2068 (eds), *Trace Fossils, Short Courses in Paleontology* 5. University of Tennessee Press,
 2069 Knoxville pp. 172–196.

2070 Savrda, C.E., Bottjer, D.J., 1987. The exaerobic zone, a new oxygen-deficient marine
 2071 biofacies. *Nature* 327, 54–56.

2072 Savrda, C.E., Browning, J.V., Krawinkel, H., Hesselbo, S.P., 2001. Firmground
 2073 ichnofabrics in deep-water sequence stratigraphy, Tertiary clinoform-toe deposits,
 2074 New Jersey slope. *Palaaios* 16, 294–305.

2075 Seilacher, A. 1967. Bathymetry of trace fossils. *Marine Geology* 5, 413–428.

2076 Seilacher, A. 1977. Pattern analysis of *Paleodictyon* and related trace fossils. In: Crimes,
 2077 T.P., Harper, J.C. (eds.), *Trace Fossils* 2. *Geological Journal Special Issue* No. 9,
 2078 289–334.

2079 Seilacher, A., 2007. *Trace Fossil Analysis*. Springer, Berlin. 226 pp.

2080 Sephton, M.A., Looy, C.V., Brinkhuis, H., Wignall, P.B., de Leeuw, J.W., Visscher, H.,
 2081 2005. Catastrophic soil erosion during the end-Permian biotic crisis. *Geology* 33,

2082 941–944.

2083 Sepkoski Jr., J.J., 1982. A Compendium of Fossil Marine Families: Milwaukee Public

2084 Museum Contributions in Biology and Geology, 51, p. 125.

2085 Sepkoski Jr., J.J., 2002. A Compendium of Fossil Marine Animal Genera: Bulletin of

2086 American Paleontology 363, 1-563.

2087 Sheldon, N.D., 2006. Abrupt chemical weathering increase across the Permian–Triassic

2088 boundary. *Palaeogeography, Palaeoclimatology, Palaeoecology* 231, 315–321.

2089 Shen, J., Algeo, T.J., Zhou, L., Feng, Q., Yu, J., Ellwood, B., 2012. Volcanic

2090 perturbations of the marine environment in South China preceding the latest Permian

2091 mass extinction and their biotic effects. *Geobiology* 10, 82-103.

2092 Shen, S.Z., James L. Crowley, J.L., Wang, Y., Bowring, S.A., Erwin, D.H., Sadler, P.M.,

2093 Cao, C.Q., Rothman, D.H., Henderson, C.M., Ramezani, J., Zhang, H., Shen, Y.A.,

2094 Wang, X.D., Wang, W., Mu, L., Li, W.Z., Tang, Y.G., Liu, X.L., Liu, L.J., Zeng, Y.,

2095 Jiang, Y.F., Jin, Y.G., 2011b. Calibrating the end-Permian mass extinction. *Science*

2096 9, 1367-1372,

2097 Shen, W.J., Lin, Y.T., Xu, L., Li, J. F., Wu, Y.S., Sun, Y.G., 2007. Pyrite framboids in the

2098 Permian-Triassic boundary section at Meishan, China: Evidence for dysoxic

- 2099 deposition. *Palaeogeography, Palaeoclimatology, Palaeoecology* 253, 323-331.
- 2100 Shen, Y.A., Farquhar, J., Zhang, H., Masterson, A., Zhang, T., Wing, B.A., 2011a.
- 2101 Multiple S-isotopic evidence for episodic shoaling of anoxic water during Late
- 2102 Permian mass extinction. *Nature Communications* 2, 210e.
- 2103 Sheng, J., Chen, C., Wang, Y., Rui, L., Liao, Z., Bando, Y., Ishii, K., Nakazawa, K.,
- 2104 Nakamura, K., 1984. Permian–Triassic boundary in Middle and Eastern Tethys.
- 2105 *Journal of Faculty of Science, Hokkaido University* 21, 133–181.
- 2106 Sheng, J.Z., Chen, C.Z., Wang, Y.G., Rui, L., Liao, Z.T., He, J.W., Jiang, N.Y., Wang,
- 2107 C.Y., 1987. New evidence on the Permian and Triassic boundary of Jiangsu,
- 2108 Zhejiang and Anhui. In: Nanjing Institute of Geology and Palaeontology, Academia
- 2109 Sinica (ed.), *Stratigraphy and Palaeontology of Systemic Boundaries in China.*
- 2110 Permian–Triassic Boundary (1). Nanjing University Press, Nanjing, pp. 1–21
- 2111 Shi, C., Chen, D., 1987. The Changhsingian ostracodes from Meishan, Changxing,
- 2112 Zhejiang. In: Nanjing Institute of Geology and Palaeontology, Academia Sinica (Ed.),
- 2113 *Stratigraphy and Palaeontology of systemic boundaries in China. Permian-Triassic*
- 2114 *boundary (1).* Nanjing University Press, Nanjing, pp. 23-80.
- 2115 Song, H., Tong, J., Chen, Z.Q., 2009. Two episodes of foraminiferal extinction near the

2116 Permian–Triassic boundary at the Meishan section, South China. Australian Journal
2117 of Earth Sciences 56, 765–773.

2118 Song, H., Tong, J., Zhang, K., Wang, Q., Chen, Z.Q., 2007. Foraminiferal survivors from
2119 the Permian–Triassic mass extinction in the Meishan section, South China.
2120 Palaeoworld 16, 105–119.

2121 Song, H.J., Wignall, P.B., Tong, J.N., Yin, H.F., 2013^a. Two pulses of extinction during
2122 the Permian-Triassic crisis. Nature Geoscience 6, 52-56.

2123 Song, H.J., Wignall, P.B., Chu, D.L., Tong, J.N., Sun, Y.D., Song, H.Y., He, W.H., Tian,
2124 L., 2014. Anoxia/High temperature double whammy during the Permian-Triassic
2125 marine crisis and its aftermath. Scientific Reports 4, 4132,

2126 Song, H.Y., Tong, J.N., Algeo, T.J., Horacek, M., Qiu, H.O., Song, H.J., Tian, L., Chen,
2127 Z.Q., 2013^b. Large vertical $\delta^{13}\text{C}$ gradients in Early Triassic seas of the South China
2128 craton: Implications for oceanographic changes related to Siberian Traps volcanism.
2129 Global and Planetary Change 105, 7–20.

2130 Sun, Y.D., Joachimski, M.M., Wignall, P.B., Yan, C.B., Chen, Y.L., Jiang, H.S., Wang,
2131 L., Lai, X.L., 2012. Lethally hot temperatures during the Early Triassic greenhouse.
2132 Science 338, 366–370.

Formatted: Font:

2133 Tian, S.F., Chen, Z.Q., Huang, C.J., 2014. Orbital forcing and sea-level changes in the
 2134 earliest Triassic of the Meishan section, South China. *Journal of Earth Science* 25,
 2135 64-73.

2136 Tong, J.N., Yang, Y., 1998. Advance in the study of the Lower Triassic conodonts at
 2137 Meishan section, Changxing, Zhejiang Province. *Chinese Science Bulletin* 43,
 2138 1350–1353.

2139 Twitchett, R.J., 1999. Palaeoenvironments and faunal recovery after the end-Permian
 2140 mass extinction. *Palaeogeography, Palaeoclimatology, Palaeoecology* 154, 27-37.

2141 Twitchett, R.J., 2006. The palaeoclimatology, palaeoecology and palaeoenvironmental
 2142 analysis of mass extinction events. *Palaeogeography, Palaeoclimatology,*
 2143 *Palaeoecology* 232, 190-213.

2144 Twitchett, R.J., Barras, C.G., 2004. Trace fossils in the aftermath of mass extinction
 2145 events. In: McIlroy, D. (Ed.), *Application of Ichnology to Palaeoenvironmental and*
 2146 *Stratigraphic Analysis*. Geological Society of London, Special Publication 228, pp.
 2147 395-415.

2148 Twitchett, R.J., Krystyn, L., Baud, A., Wheeley, J.R., Richoz, S., 2004. Rapid marine
 2149 recovery after the end-Permian mass-extinction event in the absence of marine

2150 anoxia. *Geology* 32, 805-808.

2151 Wang, C., Visscher, H., 2007. Abundance anomalies of aromatic biomarkers in the

2152 Permian–Triassic boundary section at Meishan, China—evidence of end-Permian

2153 terrestrial ecosystem collapse. *Palaeogeography, Palaeoclimatology, Palaeoecology*

2154 252, 291–303.

2155 Wang, Y., Sadler, P.M., Shen, S.Z., Erwin, D.H., Zhang, Y.C., Wang, X.D., Wang, W.,

2156 Crowley, J.L., Henderson, C.M., 2014. Quantifying the process and abruptness of the

2157 end-Permian mass extinction. *Paleobiology* 40, 113-129.

2158 [Wignall, P.B., 2007. The end-Permian mass extinction—how bad did it get? *Geobiology*](#)

2159 [5, 303–309.](#)

2160 Wignall, P.B., Hallam, A., 1993. Griesbachian (earliest Triassic) palaeoenvironmental

2161 changes in the Salt Range, Pakistan and southeast China and their bearing on the

2162 Permo–Triassic mass extinction. *Palaeogeography, Palaeoclimatology,*

2163 *Palaeoecology* 102, 215-37.

2164 Wignall, P.B., Twitchett, R.J., 2002. Extent, duration and nature of the Permian-Triassic

2165 superanoxic event. *Geological Society of America, Special Paper* 356, 395-413.

2166 Wignall, P.B., Morante, R., Newton, R., 1998. The Permo–Triassic transition in

2167 Spitsbergen; $\delta^3\text{Corg}$ chemostratigraphy, Fe and S geochemistry, facies, fauna and
 2168 trace fossils. Geological Magazine 135, 47-62.

2169 Wignall, P.B., Newton, R., Brookfield, M.E., 2005. Pyrite framboid evidence for
 2170 oxygen-poor deposition during the Permian–Triassic crisis in Kashmir.
 2171 Palaeogeography, Palaeoclimatology, Palaeoecology 216, 183–188.

2172 Wignall, P.B., Kershaw, S., Collin, P.Y., Crasquin-Soleau, S., 2009. Comment: erosional
 2173 truncation of uppermost Permian shallow-marine carbonates and implications for
 2174 Permian–Triassic boundary events. Geological Society of America, Bulletin 121,
 2175 954–956.

2176 Williams, A., James, M.A., Emig, C.C., Mackay, S., Rhodes, M.C., Cohen, B.L.,
 2177 Gawthrop, A.B., Peck, L.S., Curry, G.B., Ansell, A.D., Cusack, M., Walton, D.,
 2178 Brunton, C.H.C., MacKinnon, D.I., Richardson, J.R., 1997. Treatise on Invertebrate
 2179 Paleontology Part H, Brachiopoda, Revised, Volume 1: Introduction. The Geological
 2180 Society of America and The University of Kansas, Boulder, Colorado and Lawrence,
 2181 Kansas, 539 pp.

2182 Wilson, M.A., Palmer, T.J., 1998. The earliest *Gastrochaenolites* (Early Pennsylvanian,
 2183 Arkansas, USA): an upper Paleozoic bivalve boring? Journal of Paleontology, 72,

2184 769–772.

2185 Wu, H.C., Zhang, S.H., Hinnov, L.A., Jiang, G.Q., Feng, Q.L., Li, H.Y., Yang, T.S., 2013.

2186 Time-calibrated Milankovitch cycles for the Late Permian. *Nature Communications*

2187 4, 2452.

2188 Xie, S.C., Pancost, R.D., Yin, H.F., Wang, H.M., Evershed, R.P., 2005. Two episodes of

2189 microbial change coupled with Permo/Triassic faunal mass extinction. *Nature* 343,

2190 494-497.

2191 Xie, S., Pancost, R.D., Huang, J., Wignall, P.B., Yu, J., Tang, X., Chen, L., Huang, X.,

2192 Lai, X., 2007. Changes in the global carbon cycle occurred as two episodes during

2193 the Permian–Triassic crisis. *Geology* 35, 1083–1086.

2194 Xu, D.Y., Yan, Z., 1993. Carbon-isotope iridium event markers near the Permian-Triassic

2195 boundary in the Meishan section, Zhejiang Province, China. *Palaeogeography,*

2196 *Palaeoclimatology, Palaeoecology* 104, 171-176.

2197 Yang, W., Jiang, N., 1981. Sedimentary features and microfacies of the Changhsing

2198 Formation and Permian-Triassic boundary. *Bulletins of the Nanjing Institute of*

2199 *Geology and Palaeontology, Academia Sinica* 2, 113-133.

2200 Yang, Z., Yin, H., Wu, S., Yang, F., Ding, M., Xu, G., 1987. Permian-Triassic boundary

- 2201 stratigraphy and fauna of South China. Ministry of Geology and Mineral Resources,
- 2202 People's Republic of China, Geological Memoirs Series 2, Number 6. Geological
- 2203 Publishing House, Beijing, 379 pp.
- 2204 Yang, Z., Wu, S., Yin, H., Xu, G., Zhang, K., Bi, X., 1993. Permo-Triassic events of South
- 2205 China. Geological Publishing House, Beijing, 153 pp.
- 2206 Yin, H., Ding, M., Zhang, K., Tong, J., Yang, F., Lai, X., 1995. Dongwuan-Indosinian
- 2207 (Late Permian-Middle Triassic) Ecostratigraphy of the Yangtze Region and its
- 2208 Margins. Science Press, Beijing, 338 pp.
- 2209 Yin, H., Zhang, K., Tong, J., Yang, Z., Wu, S., 2001. The Global Stratotype Section and
- 2210 Point (GSSP) of the Permian-Triassic Boundary. Episodes 24(2), 102-114.
- 2211 Yin, H., Sweet, W.C., Glenister, B.F., Kotlyar, G., Kozur, H., Newell, N.D., Sheng, J.,
- 2212 Yang, Z. and Zakharov, Y.D., 1996, Recommendation of the Meishan section as
- 2213 Global Stratotype Section and Point for basal boundary of Triassic System:
- 2214 Newsletter on Stratigraphy 34, 81–108.
- 2215 Yin, H.F., Feng, Q.L., Lai, X.L., Baud, A., Tong, J.N., 2007⁺. The protracted
- 2216 Permo-Triassic crisis and multi-episode extinction around the Permian-Triassic
- 2217 boundary. Global and Planetary Change 55, 1-20.

2218 Yin, H.F., Huang, S.J., Zhang, K.X., Hansen, H.J., Yang, F.Q., Ding, M.H., Bie, X.M.,
 2219 1992, The effects of volcanism on the Permo-Triassic mass extinction in South
 2220 China, *in* Sweet, W.C., Yang, Z.Y, Dickins, J.M., Yin, H.F. (eds), Permo-Triassic
 2221 Events in the Eastern Tethys. Cambridge, UK, Cambridge University Press, p.
 2222 169-174.
 2223 Yin, H.F., Xie, S., Luo, G., Algeo, T.J., Zhang, K., 2012. Two episodes of environmental
 2224 change at the Permian-Triassic boundary of the GSSP section Meishan.
 2225 Earth-Science Reviews 115, 163-172.
 2226 Yin, H.F., Jiang, H.S., Xia, W.C., Feng, Q.L., Zhang, N., Shen, J., 2014. The end-Permian
 2227 regression in South China and its implication on mass extinction. Earth-Science
 2228 Reviews [137, 19-33\(in press\)](#).
 2229 Yuan, D.X., Shen, S.Z., Henderson, C.M., Chen, J., Zhang, H., Feng, H.Z., 2014. Revised
 2230 conodont-based integrated high-resolution timescale for the Changhsingian Stage
 2231 and end-Permian extinction interval at the Meishan sections, South China. Lithos
 2232 [204, 220-245\(in press\), doi:10.1016/j.lithos.2014.03.026](#).
 2233 Zeebe, R.E., Zachos, J.C., Dickens, G.R., 2009. Carbon dioxide forcing alone insufficient
 2234 to explain Palaeocene–Eocene thermal maximum warming. Nature Geoscience 2,

- 2235 576–580.
- 2236 Zhang, H., Shen, S.Z., Cao, C.Q., Zheng, Q.F., 2014. Origins of microspherules from the
 2237 Permian-Triassic boundary event layers in South China. *Lithos* (~~in press~~)[204](#),
 2238 [246-257doi:10.1016/j.lithos.2014.02.018](#).
- 2239 Zhang, K.X., Lai, X.L., Tong, J.N., Jiang, H.S., 2009. Progresses on study of conodont
 2240 sequence for the GSSP section at Meishan, Changxing, Zhejiang Province, South
 2241 China. *Acta Palaeontologica Sinica* 48, 485–495.
- 2242 Zhang, K.X., Tong, J.N., Shi, G.R., Lai, L.X., Peng, Y.Q., Yu, J.X., He, W., Jin, Y.L.,
 2243 2007. Early Triassic conodont-palynological biostratigraphy of the Meishan D
 2244 section in Changxing, Zhejiang Province, South China. *Palaeogeography*,
 2245 *Palaeoclimatology*, *Palaeoecology* 252, 4–23
- 2246 Zhang, K.X., Tong, J.N., Yin, H.F., Wu, S.B., 1997. Sequence stratigraphy of the
 2247 Permian-Triassic boundary section of Changxing, Zhejiang, Southern China. *Acta*
 2248 *Geologica Sinica* 71, 90–103.
- 2249 Zhang, K.X., Tong, J.N., Hou, G.J., Wu, S.B., Zhu, Y.H., Lin, Q.X., 2005. Regional
 2250 Geological report, the People's Republic of China (Meishanzhen Map H50E006023,
 2251 Changxingian Map, H50E006024, Scale:1:50000). University of Geosciences Press,

- 2252 264 pp., Wuhan, China.
- 2253 Zhao, J., Sheng, J., Yao, Z., Liang, X., Chen, C., Rui, L., Liao, Z., 1981. The
- 2254 Changhsingian and Permian-Triassic boundary of South China, Bulletin of the
- 2255 Nanjing Institute of Geology and Palaeontology, Academia Sinica 2, 1-95.
- 2256 Zhao, X.M., Tong, J.N., 2010. Two episodic changes of trace fossils through the
- 2257 Permian-Triassic transition in the Meishan section cores, Zhejiang Province, Science
- 2258 China, Earth Science 40, 1241-1249.
- 2259 Zheng, Q.F., Cao, C.Q., Zhang, M.Y., 2013. Sedimentary features of the Permian-Triassic
- 2260 boundary sequence of the Meishan section in Changxing County, Zhejiang Province.
- 2261 Science China, Earth Sciences 56, 956-969.
- 2262 [Zhao, L., Chen, Y., Chen, Z.Q., Cao, L., 2013b. Uppermost Permian to Lower Triassic](#)
- 2263 [conodont zonation from Three Gorges area, South China. Palaios 28, 523-540.](#)
- 2264 Zhao, L., Chen, Z.Q., Algeo, T.J., Chen, J., Chen, Y., Tong, J., Gao, S., Zhou, L., Hu, Z.,
- 2265 Liu, Y., 2013[a](#). Rare-earth element patterns in conodont albid crowns: Evidence for
- 2266 massive inputs of volcanic ash during the latest Permian biocrisis? Global and
- 2267 Planetary Change 105, 135-151.
- 2268 Zonneveld, J.-P., Gingras, M.K., Beatty, T.W., 2010. Diverse ichnofossil assemblage

2269 following the P–T mass extinction, Lower Triassic, Alberta and British Columbia,
2270 Canada: evidence for shallow marine refugia on the northwestern coast of Pangaea.
2271 *Palaios* 25, 368–392.

2272

2273

2274 **Figure captions**

2275

2276 **Fig. 1.** The GSSP for the Permian-Triassic boundary at Meishan, Changxing county,
2277 northwestern Zhejiang Province, east China. A, location of the Meishan section. B,
2278 close-up of the white volcanic ash bed (Bed 25) in Meishan. C, geopark of the GSSP
2279 Meishan showing GSSP position at the Meishan section D. D, the P-Tr boundary beds
2280 showing biostratigraphic boundary through the mid-Bed 27 and the mass extinction
2281 horizon at the base of Bed 25. E, outcrop of the P-Tr boundary beds and Yinkeng
2282 Formation along strike on the Meishan hill from the geopark section.

2283 **Fig. 2.** Biostratigraphy of the P-Tr transition at the Meishan section with the updated
2284 conodont zones and correlations with ammonoid, bivalve, brachiopod and microfloral
2285 assemblages from Meishan as well as conodont zones from North Italy, Iran and

2286 Germany, and India. Note that the updated conodont zonation is revised from those
 2287 documented by Jiang et al. (2007) and Zhang et al. (2009) and our new observations.
 2288 White arrows indicate that conodont zones extend to horizons below Bed 22 of Meishan
 2289 and its equivalents.

2290 **Fig. 3.** P-Tr succession exposed in the GSSP Meishan showing lithology, facies types,
 2291 depositional environments, stratigraphic distributions of trace fossils, and bioturbation
 2292 levels. Ichnofabric indices (ii: Droser and Bottjer, 1986) are assessed as 1 to 6, indicating
 2293 bioturbation from lowest to highest levels. Bedding plane bioturbation index (bpbi) is
 2294 evaluated based on bedding plane coverage of burrows (Miller and Smail, 1997). Facies
 2295 symbols: om = offshore mudstone facies, bs = basinal black shale facies, ow = offshore
 2296 wackestone facies, os = offshore siltstone facies; ew = epeiric sea wackestone facies,
 2297 HCS = hummocky cross stratification, hb = horizontal bedding. Depositional
 2298 environment (DE): ns = nearshore, fw = fair-weather wave base, sw = subtidal zone to
 2299 fair-weather wave base, swb = storm wavebase.

2300 **Fig. 4.** Lithology and fossils from the exposure of the P-Tr transition in Meishan. A-B, D,
 2301 field photograph, polished surface and microphotograph showing hummocky
 2302 cross-stratified (HCS) muddy limestone (Bed 54), upper Yinkeng Formation; pen is 15

2303 cm long; scale bars are 2 cm. C, pale mudstone and calcareous mudstone (Bed 41)

2304 showing horizontal stratification, lower Yinkeng Formation; pen is 15 cm long. E, F, I,

2305 ammonoid fossils across the P-Tr boundary with large ammonoid shell (E) in Bed 24e of

2306 the Changhsing Formation contrasting to small shells (F, I) recorded in the middle and

2307 upper Yinkeng Formation; coins are 1.5 cm in diameter; scale bar is 1 cm. G, dark

2308 thin-bedded limestone interbedded with bioclastic limestone bands, Bed 24e; pen is 10

2309 cm long. H, irregular contact between Beds 24d and 24e; cross-bedding is pronounced in

2310 the uppermost Bed 24d; scale bar is 1 cm. J, vertical burrow of *Balanoglossites* in the

2311 upper part of Bed 24d; scale bar is 1.5 cm.

2312 **Fig.5.** Microfacies and fossil fragment assemblages from Beds 23-~~24~~26, upper

2313 Changhsing Formation. A, microphotograph of claystone, Bed 25. B, microphotograph

2314 showing horizontal laminae (black arrow) of black shale, Bed 26. C, bioclastic packstone

2315 of Bed 23a showing brachiopod (b), crinoids (c), and ostracods (o) fragments. D,

2316 ~~Bioclastic~~bioclastic packstone of Bed 24c showing abundant foraminifer (f), brachiopod

2317 (b), crinoids (c), ostracods (o) and other fragments.

2318 **Fig. 6.** Pie diagrams showing percentage of major components in all rocks sampled from

2319 Beds 22-60 in Meishan. Detailed fossil fragment contents (%) of each sample are

2320 tabulated in Table 3. Component symbols: 1 = foraminifers, 2 = ostracods, 3 = crinoids, 4
 2321 = echinoids, 5 = brachiopods, 6 = bryozoans, 7 = sponge spicules, 8 = calcareous sponges,
 2322 9 = gastropods, 10 = radiolarians, 11 = macroalgae, 12 = micrites, 13 = cavities, 14 =
 2323 other particles (fecal pellets, peloids, pyrites and undetermined particles).

2324 **Fig.7.** Microfacies across the boundary between Beds 24e-5 and 24e-6. A, transverse
 2325 view of one sponge spicule. B-C, cross-section view of sponge spicules. D,
 2326 microphotograph showing the laminated horizon separating bioclastic layer (Bed 24e-5)
 2327 from the overlying sponge spicule-rich layer (Bed 24e-6). E, SEM image of one isolated
 2328 specimen of a sponge spicule. B-C, scale bars are both 50 μ m; E, Scale bar is 40 μ m.

2329 **Fig. 8.** Microfacies and fossil fragment assemblages from Bed 26b, 8-10 cm above the
 2330 base of Bed 25. A, microphotograph showing foraminifer (f), bryozoan (bry), echinoid
 2331 (e), and brachiopod (bra) fragments. ~~A, microphotograph showing foraminifer (f),~~
 2332 ~~bryozoan (bry), echinoid (e), and brachiopod (bra) fragments.~~ B, microphotograph
 2333 showing ostracod (o), echinoid (e), and brachiopod (bra) fragments. C, microphotograph
 2334 showing brachiopod (bra) and echinoid (e) fragments. D, microphotograph showing
 2335 bryozoan (bry) and brachiopod (bra) fragments. E, microphotograph showing foraminifer
 2336 (f) and echinoid (e) fragments. F, microphotograph showing brachiopod (bra) and

2337 foraminifer (f) fragments. G, microphotograph showing foraminifer (f) and echinoid (e)
2338 fragments. H, microphotograph showing bryozoan (bry) and foraminifer (f) fragments. I,
2339 microphotograph showing foraminifer (f) and echinoid (e) fragments. J,
2340 microphotograph showing foraminifer (f) fragments. K, microphotograph showing
2341 bryozoan (bry) and echinoid (e) fragments. L, microphotograph showing foraminifer (f)
2342 and echinoid (e) fragments. All scale bars are all 100 μm .

2343 **Fig. 9.** Polished surface of Bed 27 and its microfacies features. A, polished surface
2344 showing the entire bed is subdivided into four parts (labelled a, b, c, d) by two sets of
2345 pronounced irregular surfaces, in which burrows (red arrows) are commonly present. B,
2346 microphotograph of the basal part of Bed 27a, 11-13 cm above the base of Bed 25,
2347 showing foraminifer (f) and brachiopod (bra) fragments. C, microphotograph of the
2348 upper part of Bed 27a, 13-15 cm above the base of Bed 25, showing foraminifers (f) and
2349 other fossil fragments. D, microphotograph of the lower part of Bed 27b, 15-17 cm above
2350 the base of Bed 25, showing claystone-dominated texture. E, microphotograph of the
2351 upper part of Bed 27b, 18-20 cm above the base of Bed 25, showing echinoid (e) and
2352 other fossil fragments. F, microphotograph of the upper part of Bed 27c, 21-23 cm above
2353 the base of Bed 25, showing abundant foraminifer (f), echinoid (e) and brachiopod (bra)

2354 fragments. G, microphotograph of Bed 27d, 23-28 cm above the base of Bed 25, showing
2355 abundant ostracods (o), foraminifers (f), echinoid (e), and other fragments. H,
2356 microphotograph of the upper part of Bed 26b, 8-10 cm above the base of Bed 25,
2357 showing abundant foraminifer (f) and other fossil fragments.

2358 **Fig. 10.** Bioclastic packstone to wackestone showing various fossil fragments from Bed
2359 27a, 13-15 cm above the base of Bed 25. A, foraminifer (f). B, brachiopod (bra) and other
2360 fragments. C, foraminifer (f), echinoid (e) and other undetermined fragments. D,
2361 foraminifer (f). E, foraminifer (f). F, foraminifer (f), brachiopod (b) and other
2362 undetermined fragments. G, I-K, foraminifer tests. H, echinoid (e) fragment. Scale bars
2363 are all 50 μ m.

2364 **Fig. 11.** Bioclastic packstone and various fossil fragments from Bed 27c, 21-23 cm above
2365 the base of Bed 25. A, foraminifer (f) and brachiopod (bra) fragments. B, foraminifer
2366 *Frodina permica* test. C, echinoid (e) and brachiopod (b) fragments; D, bryozoan (bry) ,
2367 foraminifer (f) and other undetermined fragments. E, foraminifer (f) *Nodosinelloides*
2368 *netschajewi* test and echinoid (e) fragments. F, foraminifer test of *Hemigordius* sp. G,
2369 brachiopod (bra) fragment. H, bryozoan (bry) fragment. I, foraminifer (f) *Hemigordius* sp.
2370 test. J, foraminiferal (f) fragment. K, echinoid (e) and foraminifer (f) fragments. L-M,

2371 echinoid fragments. Scale bars are all 50 μm .

2372 **Fig. 12.** Bioclastic packstone to wackestone showing various fossil fragments from Bed

2373 27d, 23-28 cm above the base of Bed 25. A, foraminifer test of *Nodosinelloides* sp. B,

2374 brachiopod (b), foraminifer (f) and echinoid (e) fragments. C-D, foraminifer tests of

2375 *Nodosinelloides* sp. and *Nodosaria* sp., respectively. E, brachiopod (bra), foraminifer (f)

2376 and other fragments. F, echinoid fragment. G, sponge spicule. H, foraminiferal fragment

2377 of *Tuberitina maljavkini*. I, echinoid fragment. J, brachiopod (bra) and sponge spicule (ss);

2378 K, foraminifer test of *Nodosinelloides* sp. L, foraminifer *Nodosinelloides aequi ampla* and

2379 brachiopod (bra) fragments. M, foraminifer (f) fragment. N, ostracod (o), foraminifer (f)

2380 and echinoid (e) fragments. O, brachiopod (bra) and echinoid (e) fragments; P,

2381 brachiopod (bra) and echinod (e) fragments. B, scale bar is 100 μm ; F-G, scale bars are

2382 20 μm ; other scale bars are all 50 μm .

2383 **Fig. 13.** Microfacies and fossil fragment assemblage from strata of Bed 29 and above. A,

2384 bioclastic wackestone with ostracod (o) and brachiopod (bra) fragments, Bed 29. B,

2385 bioclastic wackestone with brachiopod (bra) and ostracod (o) fragments, Bed 29. C,

2386 echinoid fragment, Bed 53. D, ostracods test, Bed 52. F, ostracod test, Bed 53. I, K, M,

2387 ostracods tests, Bed 54. N, ostracods test, Bed 55. P-R, ostracod tests, Beds 56, 57 and 58,

2388 respectively. E, foraminifer fragment, Bed 29. J, L, foraminifer fragments, Beds 52 and
2389 53, respectively. G, foraminifer *Nodosaria* sp., Bed 56. H, foraminifer *Nodosaria*
2390 *rostrata* Trifonova, Bed 56. O, micrite containing pyrite particles (black) and tiny tubes
2391 (t), Bed 44. Scale bars are all 50 μ m.

2392 **Fig. 14.** Fossil fragment distributions over the P-Tr transition (Beds 22-60) in Meishan.

2393 Vertical axis represents percentage of various fossil fragments in all rock.

2394 **Fig. 15.** Shell beds from the Yinkeng Formation in Meishan. A, *Claraia* concentrations
2395 (white arrows) from Bed 40; scale bar is 1 cm; B, shell concretions of *Claraia griesbachi*
2396 (c) and *Ophiceras* sp. (o) of the *O-P* community from Bed 32; coin is 1.5 cm in diameter;
2397 C, shell concretions of *Claraia griesbachi* from Bed 35; coin is 1.5 cm in diameter; D,
2398 shell concretions of *Claraia wangi* of the *C* community from Bed 40; coin is 1.5 cm in
2399 diameter; E, shell concretions of *Claraia griesbachi* from Bed 36; coin is 1.5 cm in
2400 diameter; F, shell concretions of *Meishanorhynchia* (m), *Lytophiceras* (ly) and
2401 ophiceratid (o) of the *M-L* community from Bed 55; Scale bar is 4 mm.

2402 **Fig. 16.** Trace fossils from the Changhsing Formation of the Meishan section. A, D,
2403 *Thalassinoides* sp. 1 on base of Bed 8; coin is 1.5 cm; B, *Paleophycus* isp. from Bed 9;
2404 scale bar is 1 cm; C, *Balanoglossites triadicus* from Bed 24d; coin is 1.5 cm in diameter;

2405 E, *Taenidium* isp. from upper surface of Bed 24d; coin is 1.5 cm in diameter; F, *Lockeia*

2406 isp. on the upper surface of Bed 9; coin is 1.5 cm in diameter.

2407 **Fig. 17.** Trace fossils from the Changhsing Formation (Beds 23-24) continued. A, E,

2408 horizontal burrows of *Planolites* isp. 1 from upper surface of Bed 24e-6; USB is 2 cm

2409 long; B-C, problematica from upper surface of Bed 23; Coins are 1.5 cm in diameter; D,

2410 *Taenidium* isp. from upper surface of Bed 24e; Coin is 1.5 cm in diameter; F,

2411 *Dendrorhaphie* isp. from upper surface of Bed 23; Coin is 1.5 cm in diameter.

2412 **Fig. 18.** Trace fossils from the Yinkeng Formation. A-B, F, *Planolites* from upper

2413 surfaces of Bed 36, 41, and 56, respectively; coins are 1.5 cm, 2 cm and 1.5 cm in

2414 diameter, respectively; C, *Chondrites* isp. on upper surface of Bed 52; Coin is 1.5 cm in

2415 diameter; D-E, *Thalassionoides* isp. 3 from upper surfaces of Bed 53 and 56, respectively;

2416 coins are 1.5 in diameter; G-H, sketch reconstruction and trace of *Treptichnus* isp. on

2417 upper surface of Bed 57; coin is 1.5 cm in diameter.

2418 **Fig. 19.** Polished slabs and sketches showing the successions of trace-fossil assemblages

2419 in Bed 27. A-C, vertical cross section of Bed 27 showing the ichnofabric change from a

2420 firmground ichnocoenoses of *Glossifungites* ichnofacies in the lower to a softground

2421 ichnocoenose in the upper. Note these three sample blocks (A-C) were cut from one

2422 complete sample of Bed 27. D–F, portraits of blocks A–C, respectively. Ar. = *Arenicolites*
2423 isp., Ch. = *Chondrites* isp. 1, Ga. = *Gastrochaenolites* isp., Pa. = *Planolites* isp. 2, Ps. =
2424 *Psilonichnus*; isp., Th. = *Thalassinoides* isp. 2.

2425 **Fig. 20.** Polished surface and its portrait of Bed 27 showing burrow systems in
2426 firmground of the *Glossifungites* ichnofacies and vertical colonization by ichnofaunas on
2427 different substrates. A, polished slab across the entire Bed 27 (from base to top). B, sketch
2428 reconstruction showing ichnofabrics manifested in Fig. 25A. C, cartoon reconstruction
2429 showing the generalized colonization zonation of ichnofaunas. For abbreviations of
2430 ichnotaxon names see caption of Fig. 19.

2431 **Fig. 21.** Trace fossil evolution at Meishan. A, ichnodiversity change throughout the
2432 uppermost Changhsingian to Griesbachian in Meishan. B, burrow size variations (in
2433 mean diameter and maximum diameter) over the P-Tr transition. C, tiering level change
2434 through the P-Tr transition.

2435 **Fig. 22.** Burrow sizes of selected ichnogenera through the P-Tr transition. A, burrow size
2436 variation of *Planolites* through the P-Tr transition. B, burrow size variation of
2437 *Thalassinoides* through the P-Tr transition. C, burrow sizes of both *Dendrorhaphe* and
2438 problematic trace from the upper Changhsing Formation. D, burrow sizes of

2439 *Balanoglossites*, *Taenidium*, *Chondrites*, and *Treptichnus* from the P-Tr transition in
2440 Meishan.

2441 **Fig. 23.** Pyrite framboids and crystals preserved on fossil skeletons and in sediments of
2442 Bed 27. A-C, pyrite crystals ([white arrows](#)) on brachiopod shells of *Paryphella*. D-E,
2443 pyrite crystals ([white arrows](#)) preserved in sediments and foraminiferal test; scale bars are
2444 40 μm ; F-G, pyrite crystals ([white arrows](#)) preserved in foraminiferal tests; scale bars are
2445 all 40 μm . H, L, SEM images showing pyrite framboids preserved on brachiopod shells
2446 of Bed 27; I-K, pyrite framboids preserved in sediments of Bed 27; M-N, EDS results
2447 showing mineral composition of framboids of Fig. 23L and Fig. 23J, respectively.

2448 **Fig. 24.** Sizes of pyrite framboids from 17 horizons through the P-Tr transition in
2449 Meishan. MD = mean diameter, SD = standard derivation, N = Number of framboid
2450 grains.

2451 **Fig. 25.** Redox conditions indicated by pyrite framboid sizes through the P-Tr transition
2452 at Meishan. Two SEM images show morphologies of pyrite framboids from Bed 24 (left)
2453 and Bed 39 (right). PTB = Permo-Triassic boundary; PTME = Permo-Triassic mass
2454 extinction.

2455 **Fig. 26.** Composite figure showing exceptionally increased seawater surface temperature,

2456 carbon isotopic excursion, Chemical index of alternation (CIA) and Eu/Eu* profiles,
 2457 through the P-Tr transition at Meishan. Total organic content (TOC) and Ce/Ce* profiles,
 2458 framboid size variation, specific and generic richness variations, and community
 2459 structural changes indicated by true diversity index (Exp (H)) and dominance (D) through
 2460 the P-Tr transition in Meishan. Note: seawater temperature data after Joachimski et al.
 2461 (2012) and Sun et al. (2012); CIA value is calculated using published data by Zhang et al.
 2462 (2005); Carbon isotopic excursion after Burgess et al. (2014); Eu/Eu* and Ce/Ce* values
 2463 after Zhao et al. (2013^a). TOC profile after Yin et al. (2012). Framboid size data from this
 2464 study. Detailed bioturbation data see Fig. 3; II = Ichnofabric indices; BPBI = Bedding
 2465 plane bioturbation index. Datum source of burrow diameters sees Fig. 24. More details of
 2466 fossil fragment contents see Fig. 14. Species and genus richness data after Song et al.
 2467 (2013^a). Community structure data from Chen et al. (2010a).

2468

2469 **Table captions**

2470

2471 Table 1. Radiometric ages obtained from the P-Tr succession at the GSSP Meishan (in
 2472 Ma).

2473 Table 2. Key conodont zones with their durations across the PTB in Meishan.

2474 Table 3. Percentage of major components in all rocks sampled from Beds 22-60 in

2475 Meishan.

2476 Table 4. X-ray diffraction (XRD) data of the PTB beds at Meishan (sourced from Liang,

2477 2002).

2478 Table 5. Structural indices of the latest Permian to earliest Triassic shelly communities

2479 from Meishan (Chen et al., 2010a).

2480 Table 6. Major indices showing community structural changes over the P-Tr transition in

2481 Meishan

2482 Table 7. Characteristics of major trace fossils from the uppermost Permian to lowest

2483 Triassic in Meishan

2484

Figure 1
[Click here to download high resolution image](#)

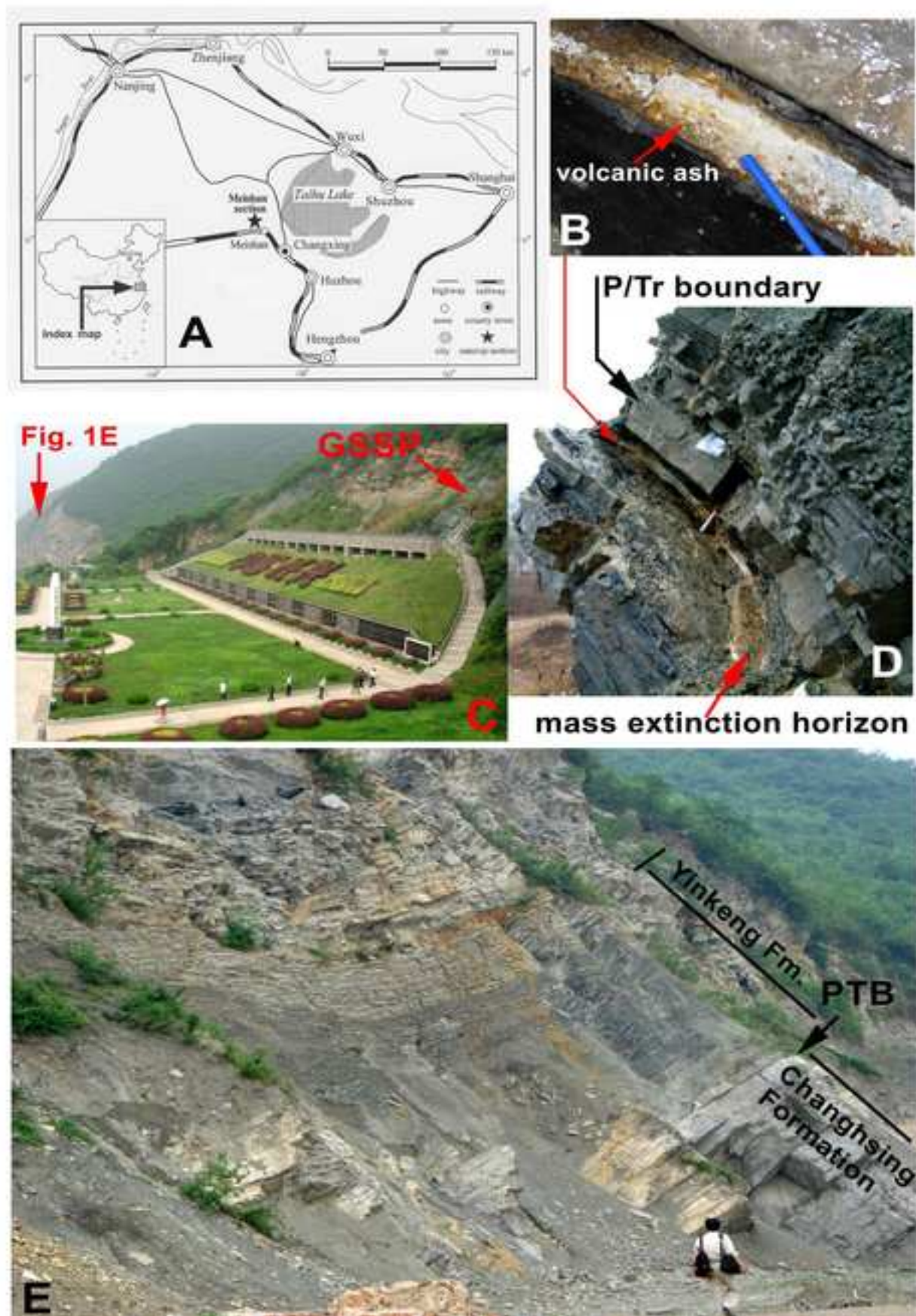


Figure 2
Click here to download high resolution image

System	Stage	Conodont zonation						Bivalves	Ammonoids	Brachiopods	Palynology	
		North Italy	Iran and Germany		Spiti		Meishan		Meishan	Meishan	Meishan	Meishan
		Farabegoli and Perri, 2012	Kozur, 2007		Orchard and Krystyn, 1998		Revised after Jiang et al. (2007) and Zhang et al. (2009)		Chen et al., 2009	Yin et al., 2001; Chen et al., 2010	Chen et al., 2010	Zhang et al., 2007
		pelagic	shallow water	gondoloid zone	hindeoid zone	Zone	Beds					
Triassic	Induan	?	?		<i>N. discreta</i>	<i>H. postparvus</i> - <i>I. isarcica</i>	<i>Nc. discreta</i>	55 and above		<i>Lytphiceras</i>	<i>Mei. meishanensis</i> (Beds 51-55)	?
		<i>I. isarcica</i>	<i>I. isarcica</i>	<i>N. krystyni</i>	<i>C. planata</i>		30-54					
		<i>I. staeschei</i>		<i>I. isarcica</i>	29b							
		<i>I. lobata</i>		<i>I. staeschei</i>	<i>I. staeschei</i>	28-29a	<i>Claraia wangi</i> - <i>C. griesbachi</i>	<i>Ophiceras</i>	<i>Paryphella triquetra</i>			
		<i>H. parvus</i>	<i>H. parvus</i>	<i>H. parvus</i>	27c-27d							
					<i>N. meishanensis</i>	<i>H. praeparvus</i>	<i>C. taylorae</i>	27a-27b	<i>Eumorphotis venetiana</i> * - <i>Towapteria scythica</i> - <i>Pteria ussurica variabilis</i>			
Permian	Changhsingian	<i>I. prisca</i>	<i>Merrilia ultima</i> - <i>Stepanov ?mostleri</i>	<i>H. praeparvus</i>	<i>N. meishanensis</i>	<i>H. praeparvus</i>	<i>H. changxingensis</i>	26	<i>Claraia huzhouensis</i> - <i>C. cf. bionii</i>	<i>Hypophiceras</i>	<i>Tethyochonetes liaoi</i>	
		<i>C. meishanensis</i> - <i>H. praeparvus</i>	<i>C. meishanensis</i>			25						
			<i>C. hauschkei</i>	<i>H. typicalis</i>	<i>N. changxingensis</i>	<i>H. latidentatus</i>	<i>C. yini</i>	24		<i>Rotodiscoceras</i>	<i>Mei. =</i> <i>Meishanorhynchia</i>	
		<i>H. praeparvus</i>	<i>C. iranica</i>									
			<i>C. zhangii</i>									
			?	<i>C. changxingensis</i> - <i>C. deflecta</i>	<i>H. julfensis</i>			<i>C. changxingensis</i>	22-23	* from the Huangzhishan section (Chen et al., 2009)		

Figure 3
[Click here to download high resolution image](#)

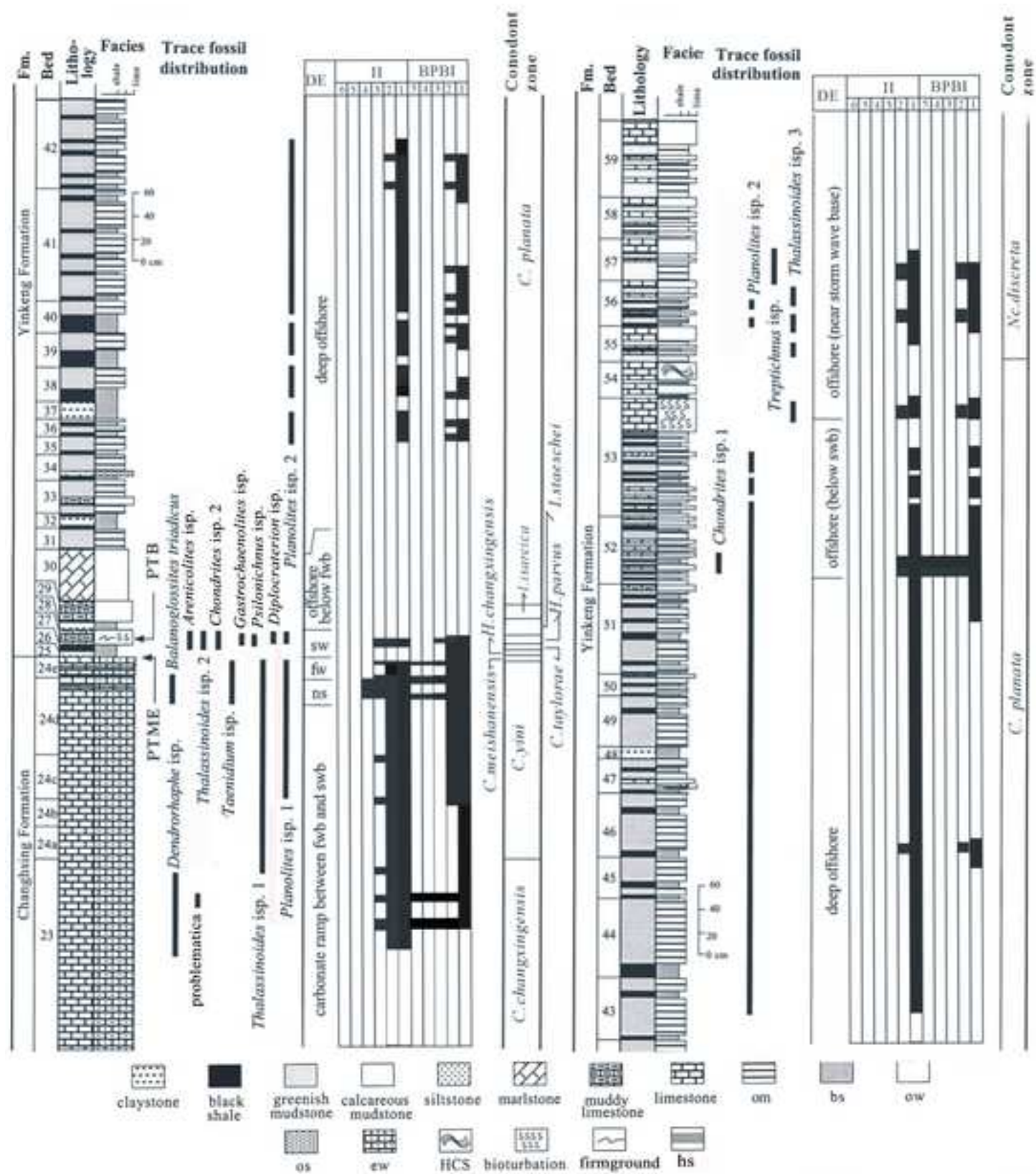


Figure 4
[Click here to download high resolution image](#)

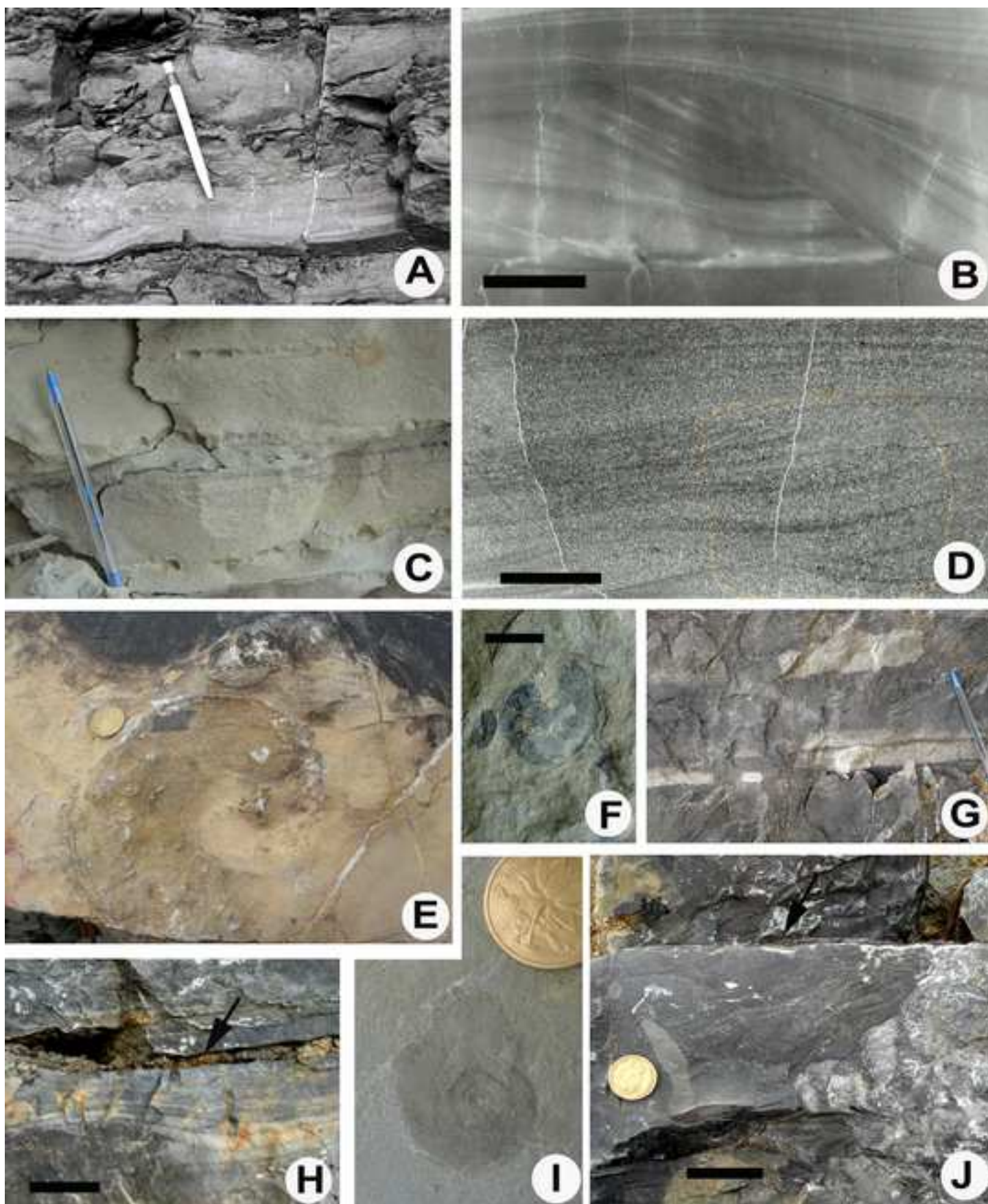


Figure 5
[Click here to download high resolution image](#)

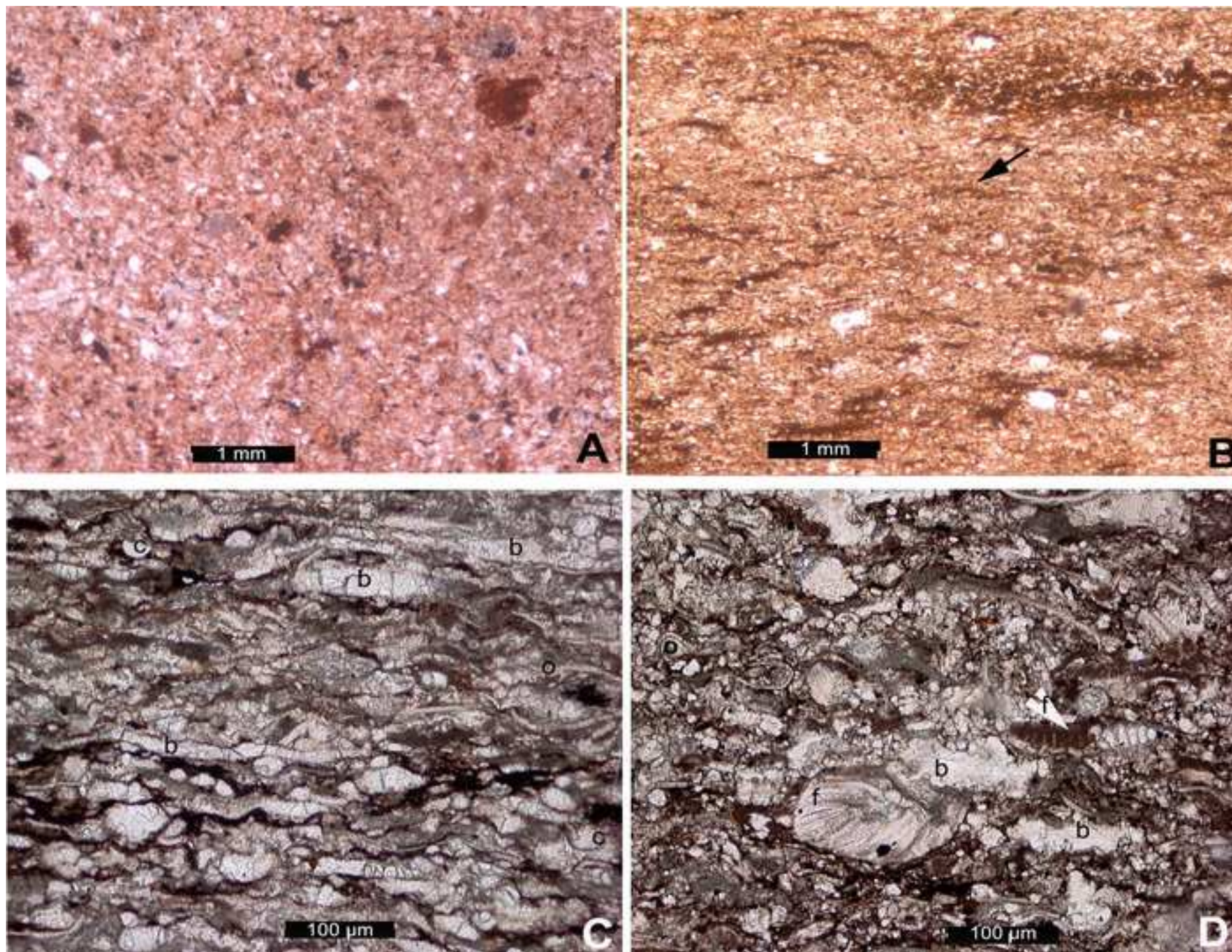


Figure 6
[Click here to download high resolution image](#)

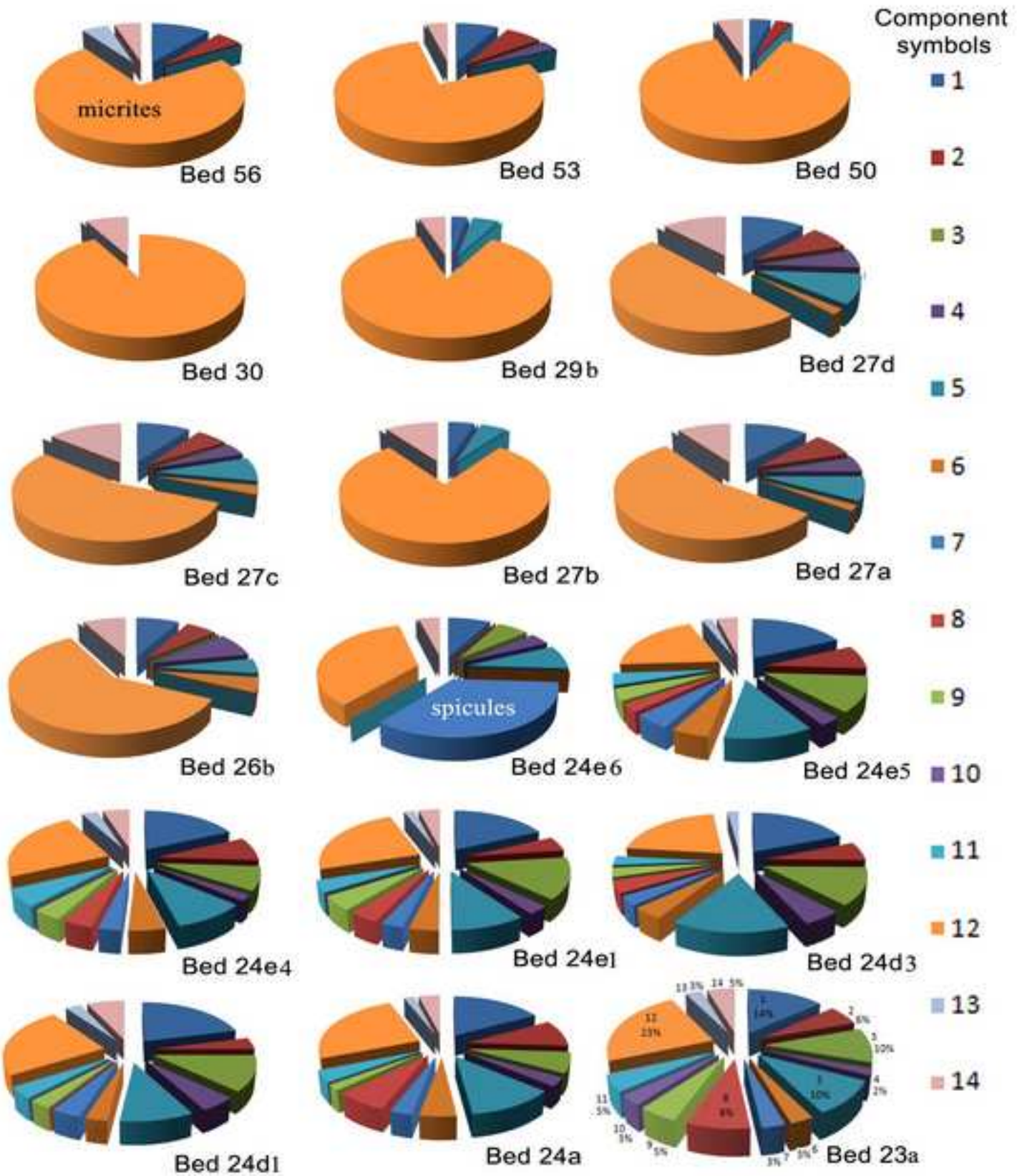


Figure 7
[Click here to download high resolution image](#)

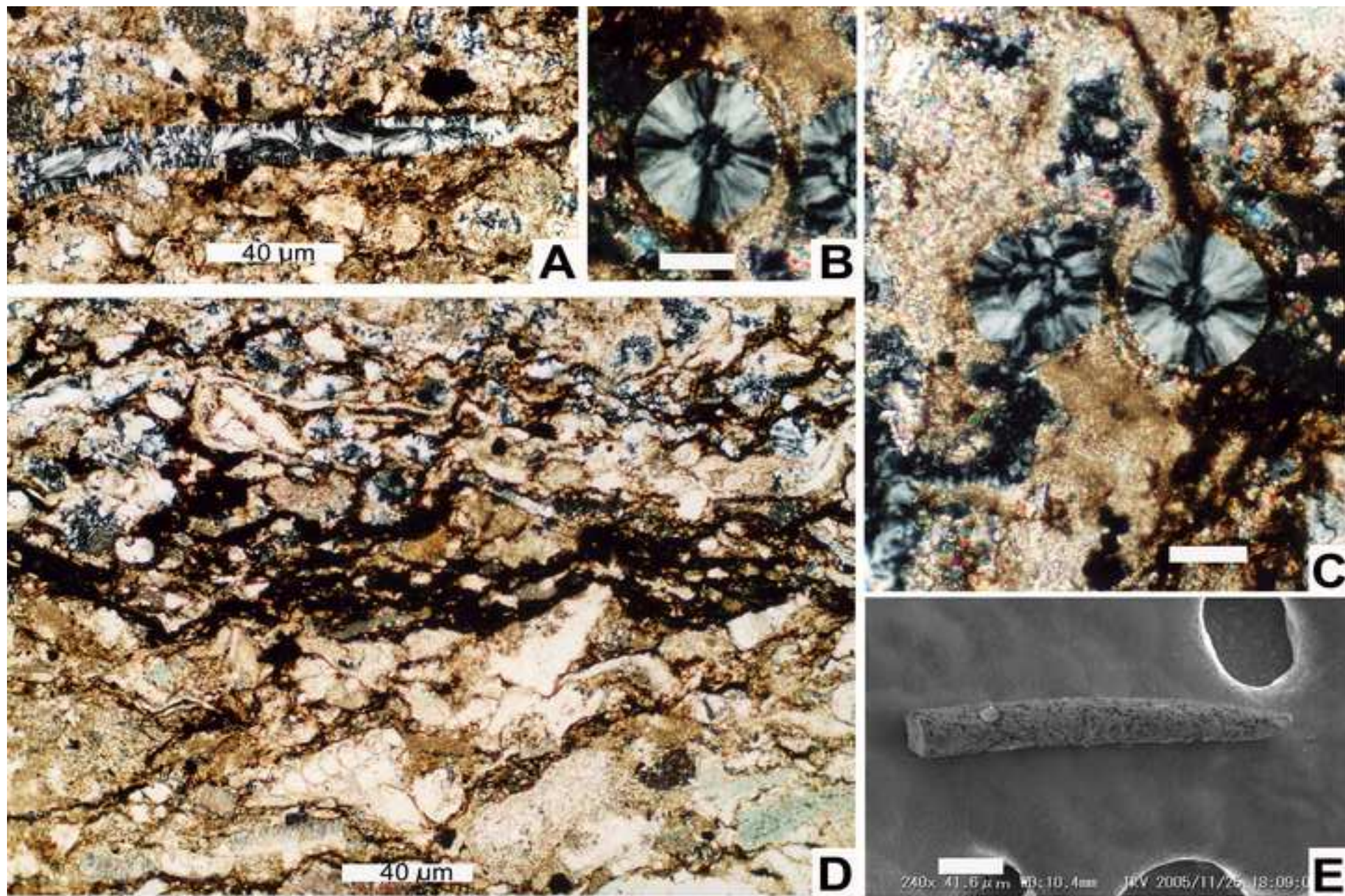


Figure 8
[Click here to download high resolution image](#)

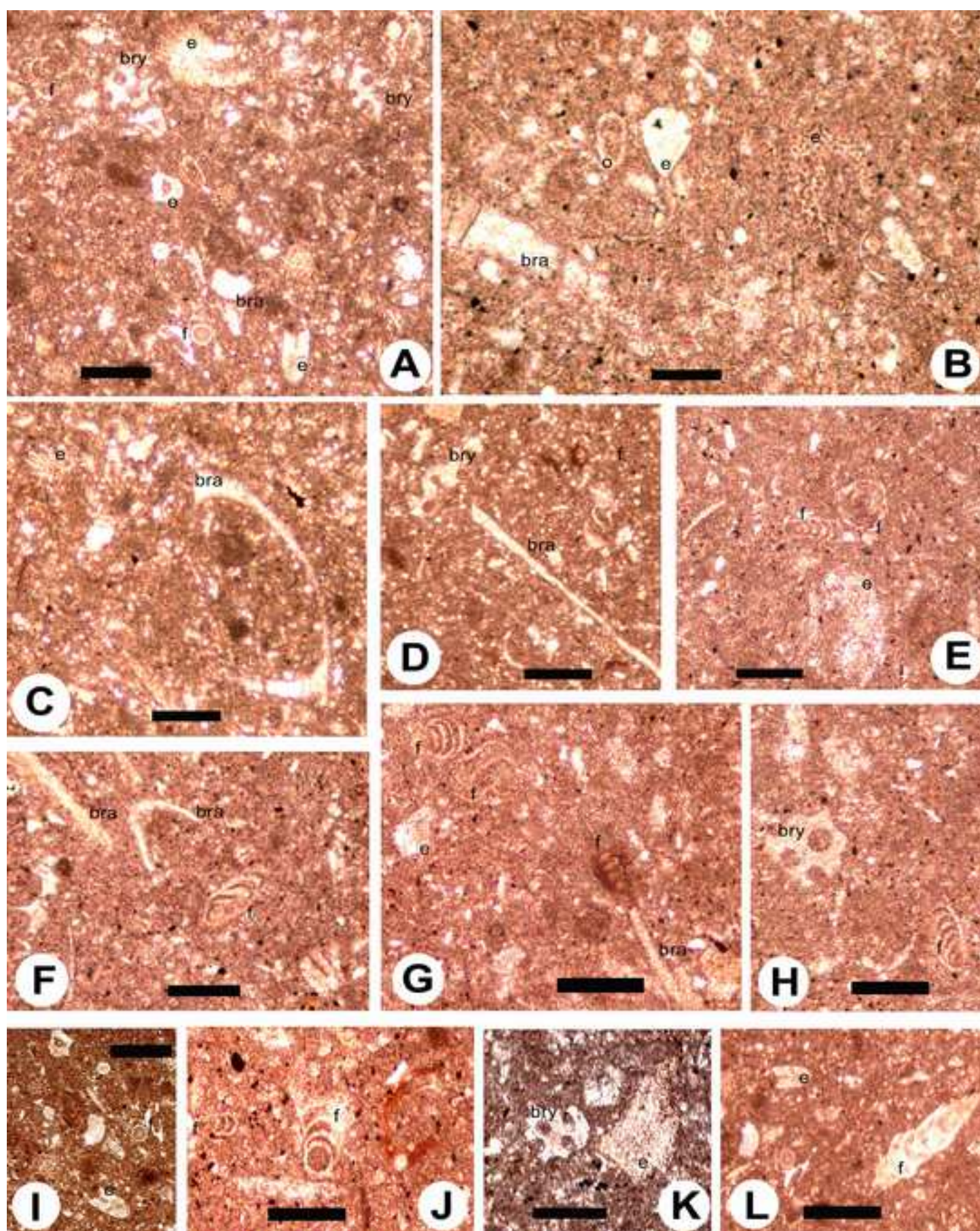


Figure 9
[Click here to download high resolution image](#)

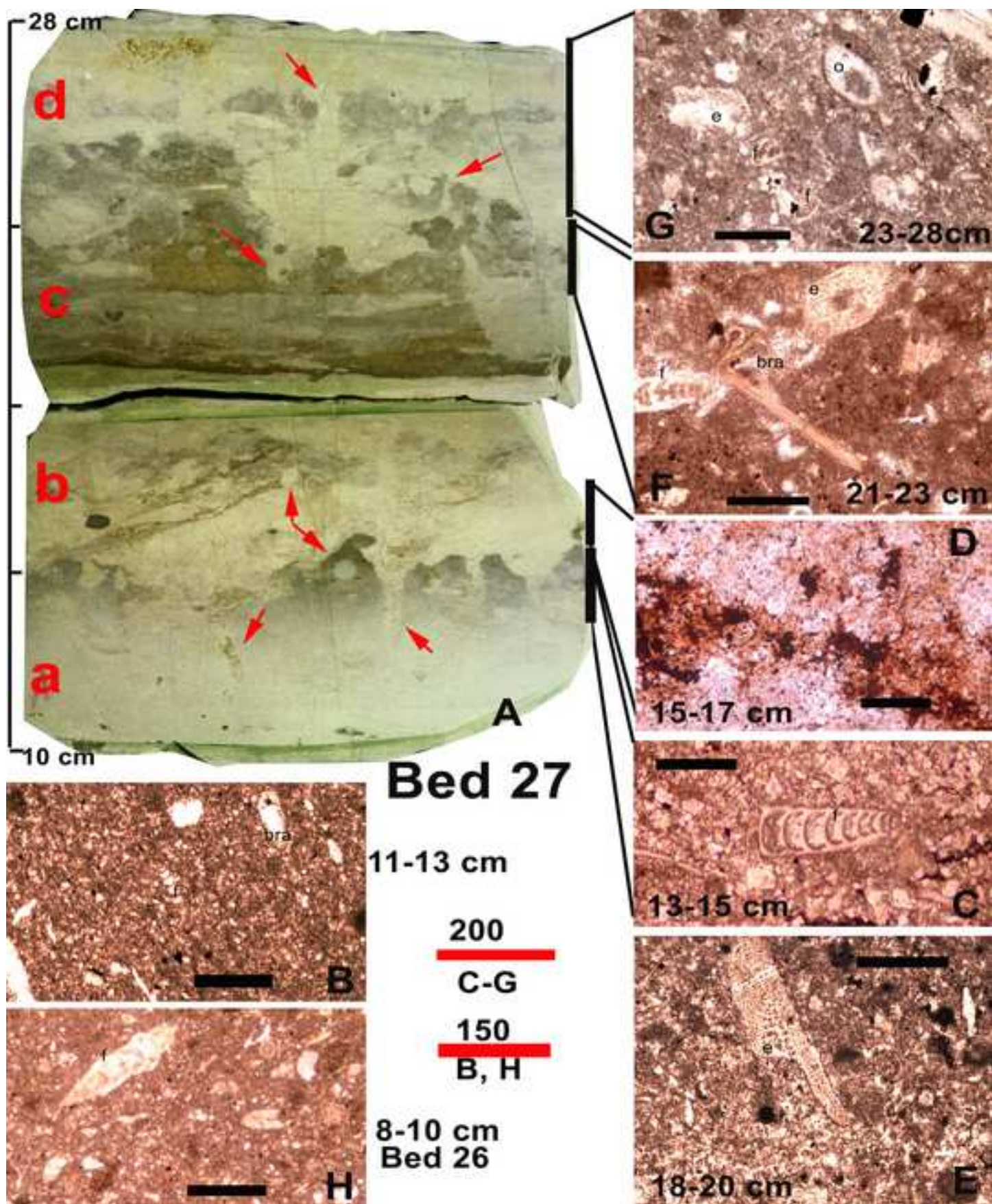


Figure 10
[Click here to download high resolution image](#)

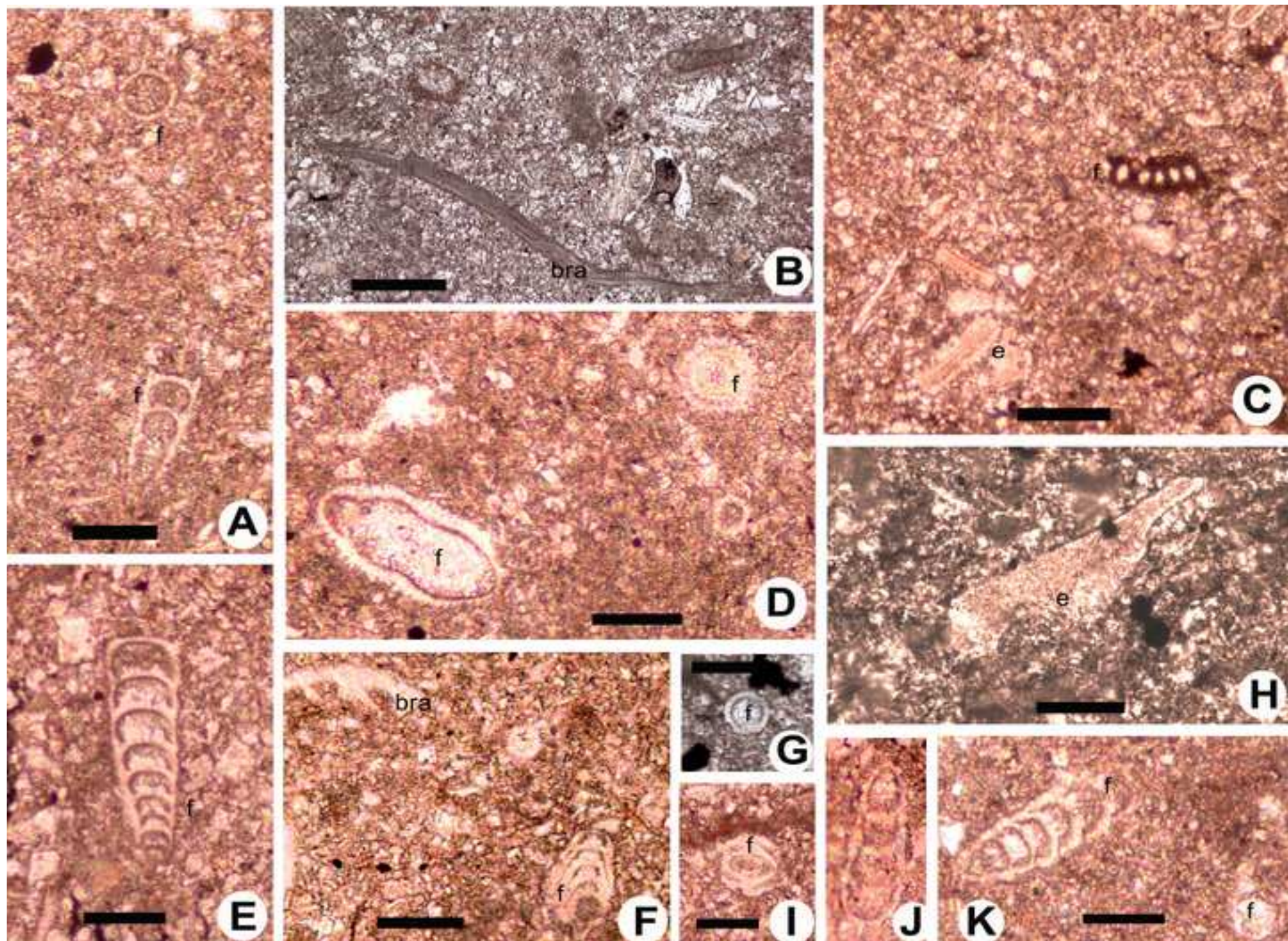


Figure 11
[Click here to download high resolution image](#)

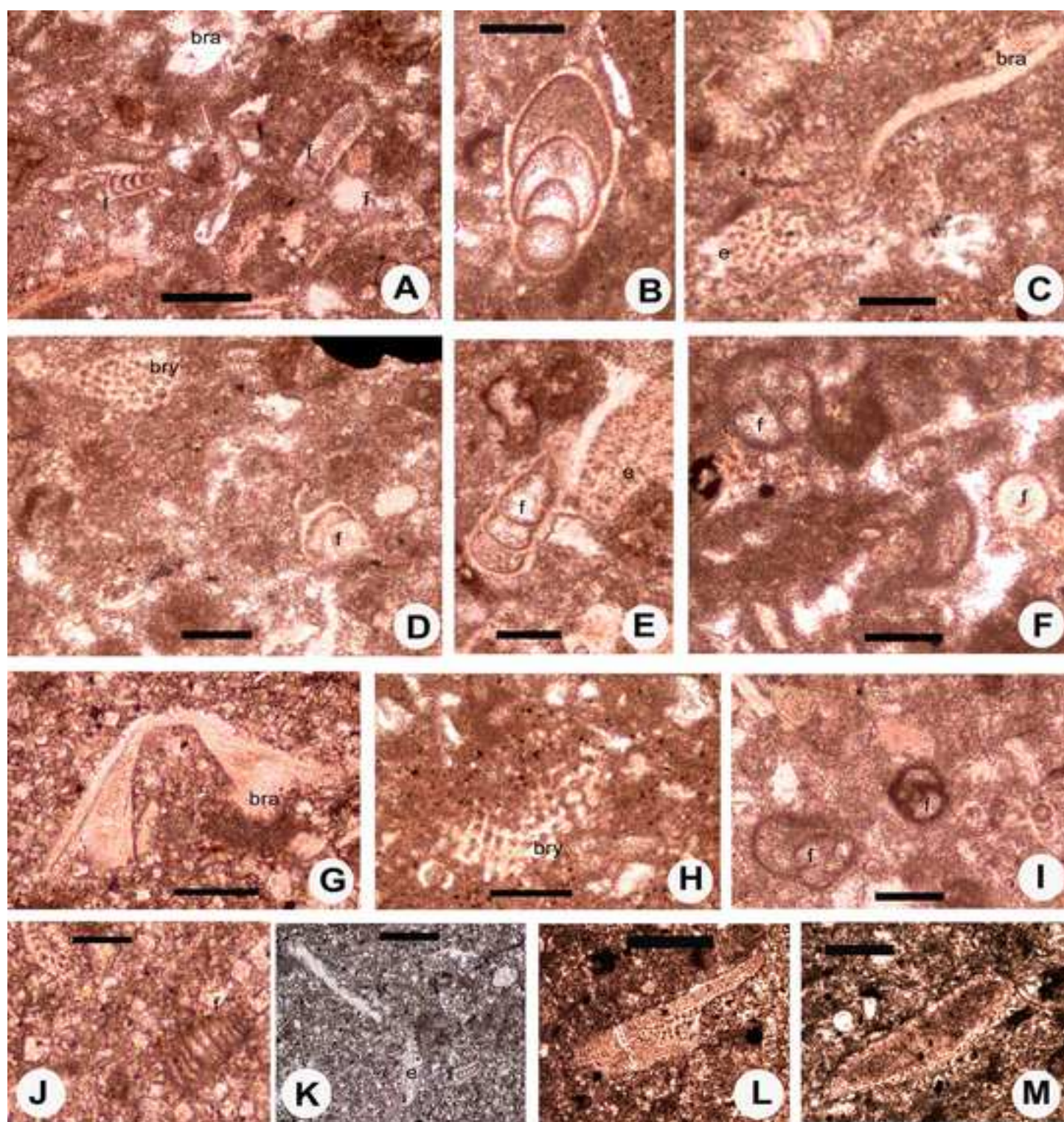


Figure 12
[Click here to download high resolution image](#)

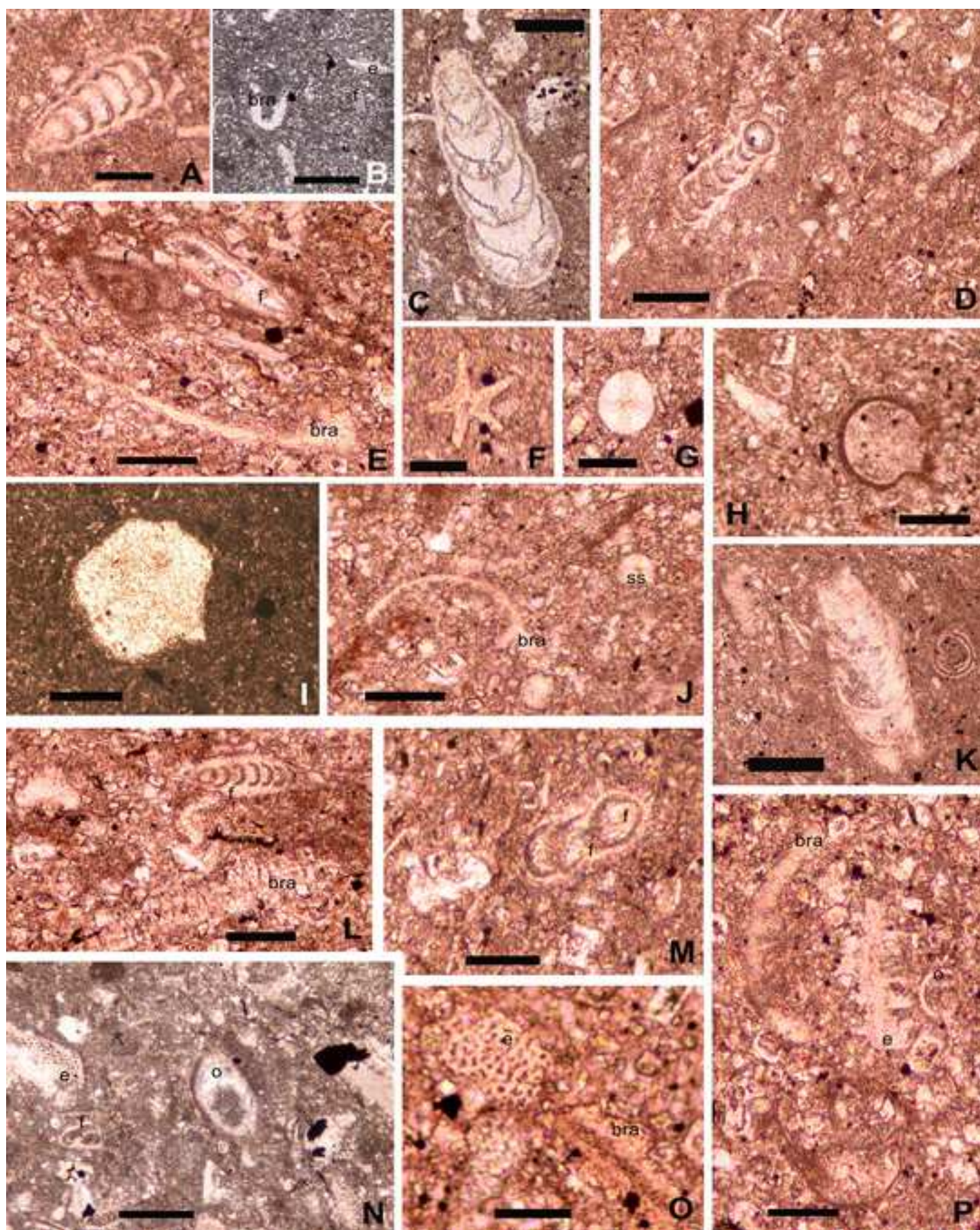


Figure 13
[Click here to download high resolution image](#)

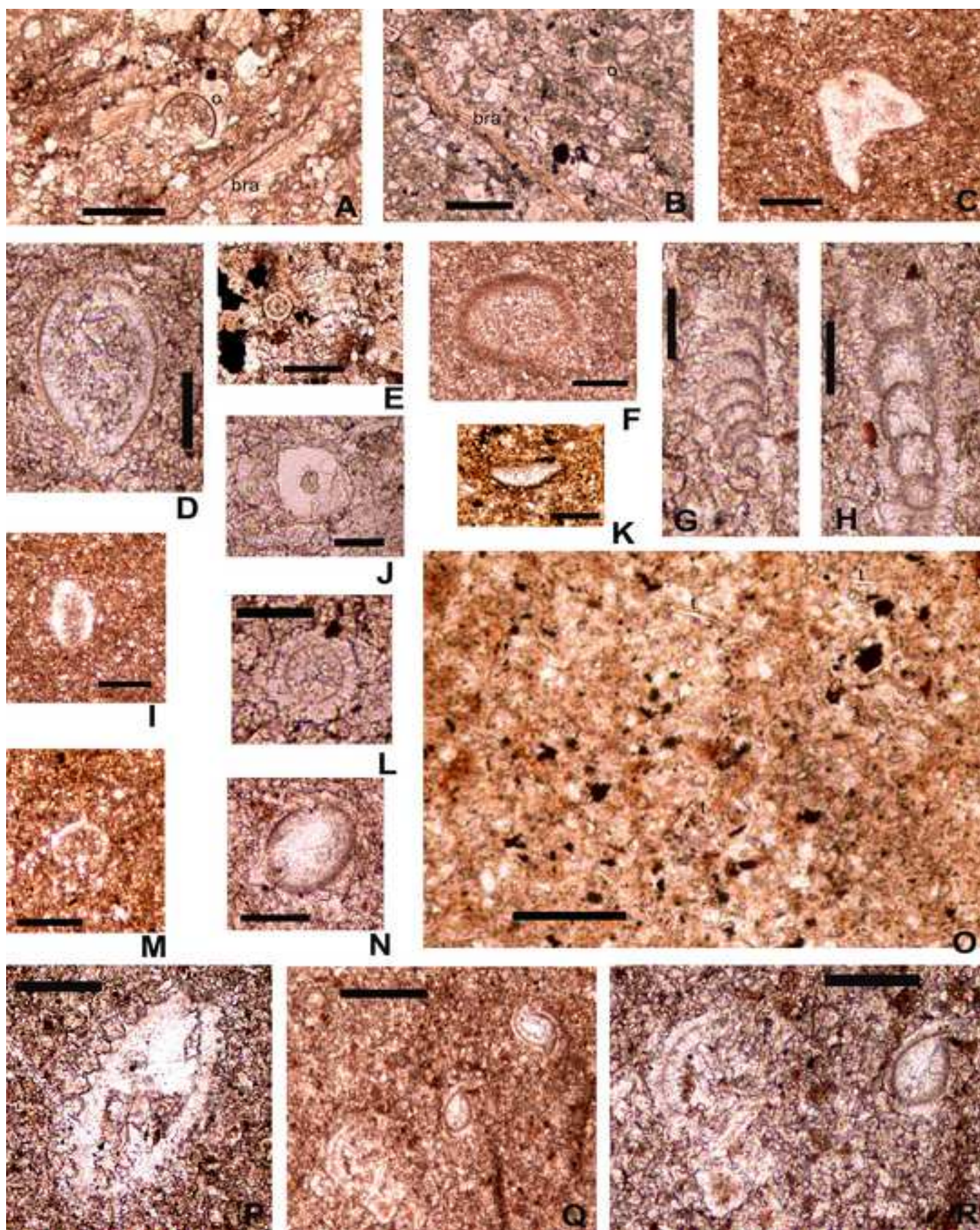


Figure 14

[Click here to download high resolution image](#)

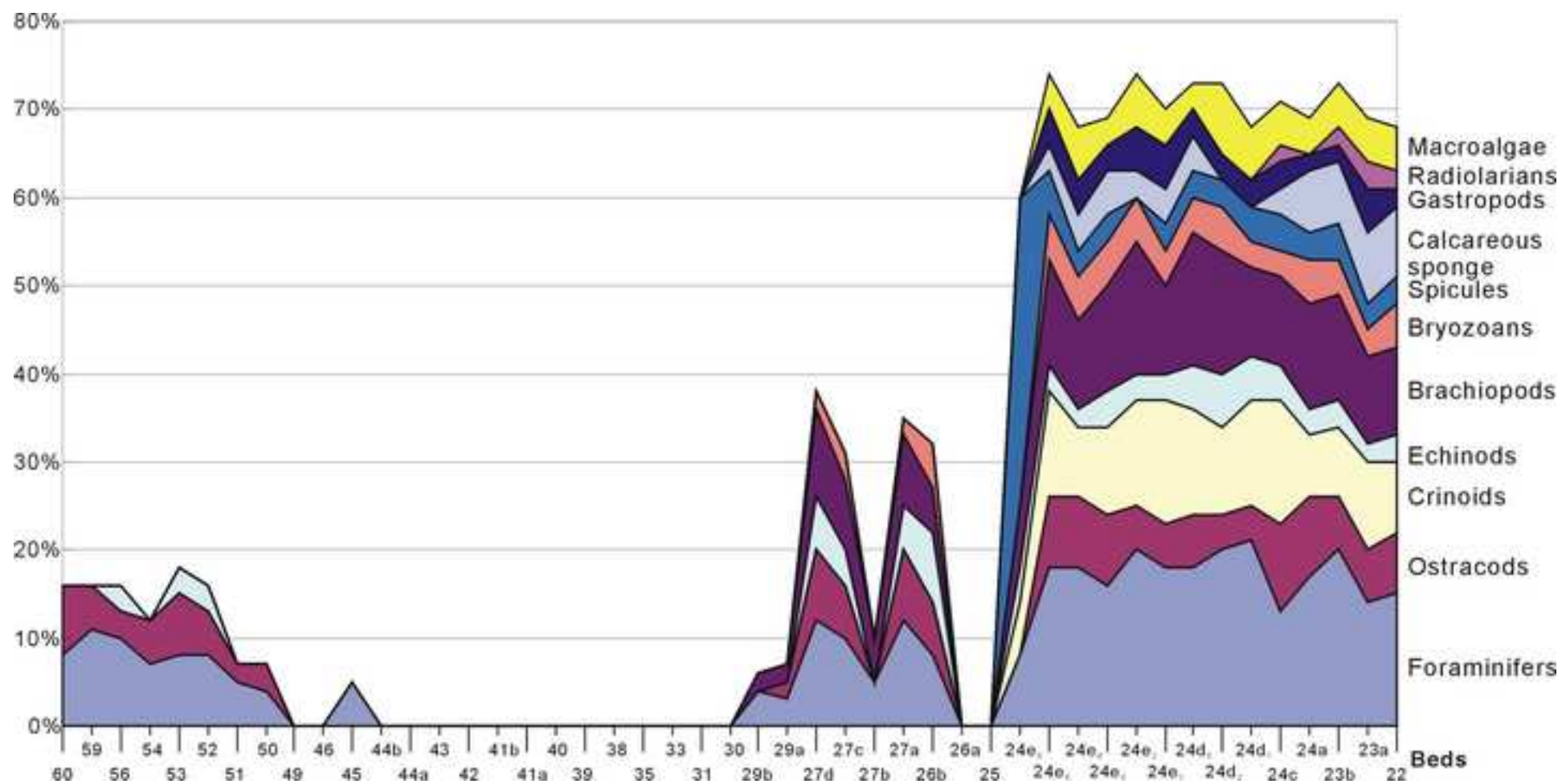


Figure 15
[Click here to download high resolution image](#)

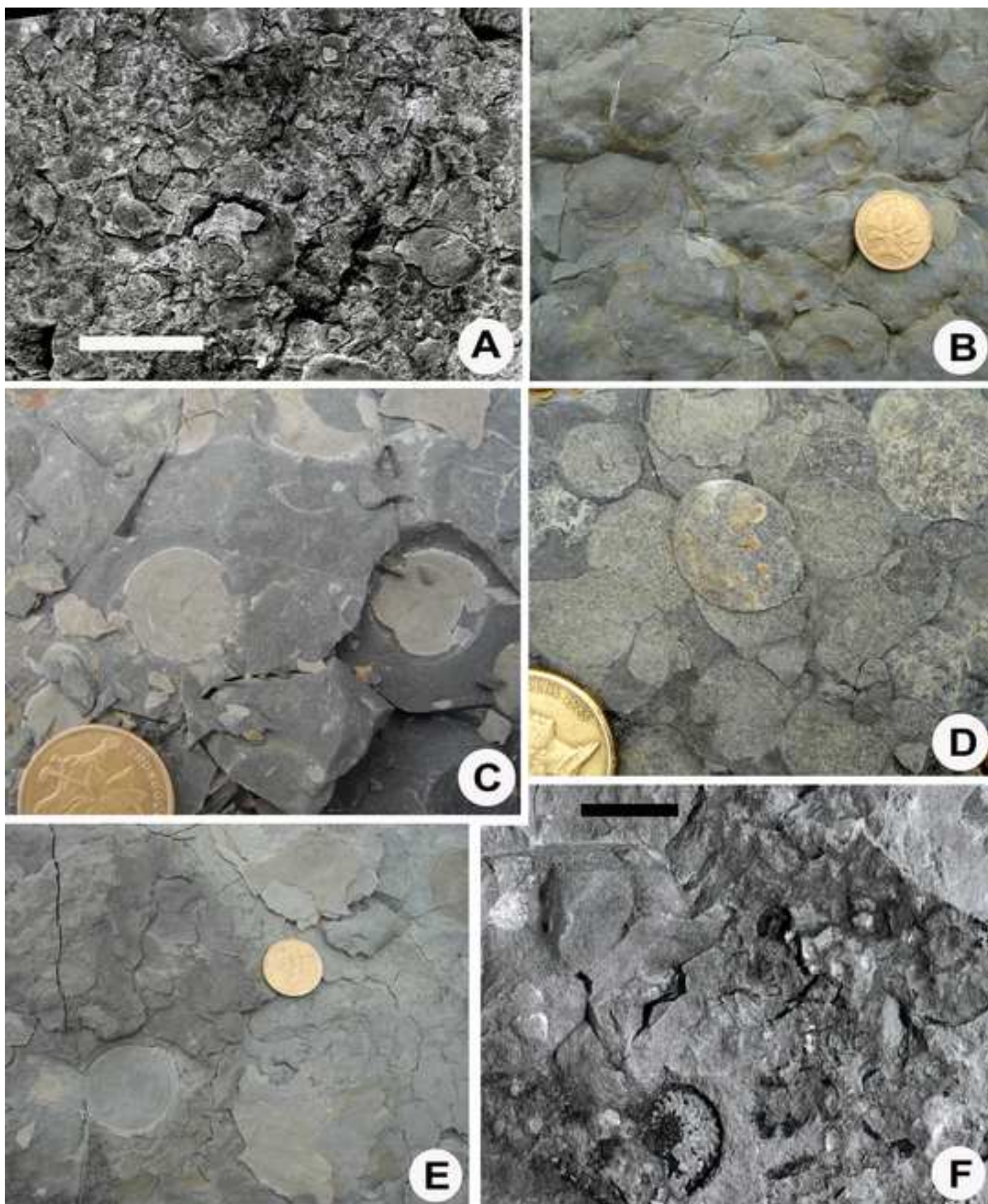


Figure 16
[Click here to download high resolution image](#)



Figure 17
[Click here to download high resolution image](#)

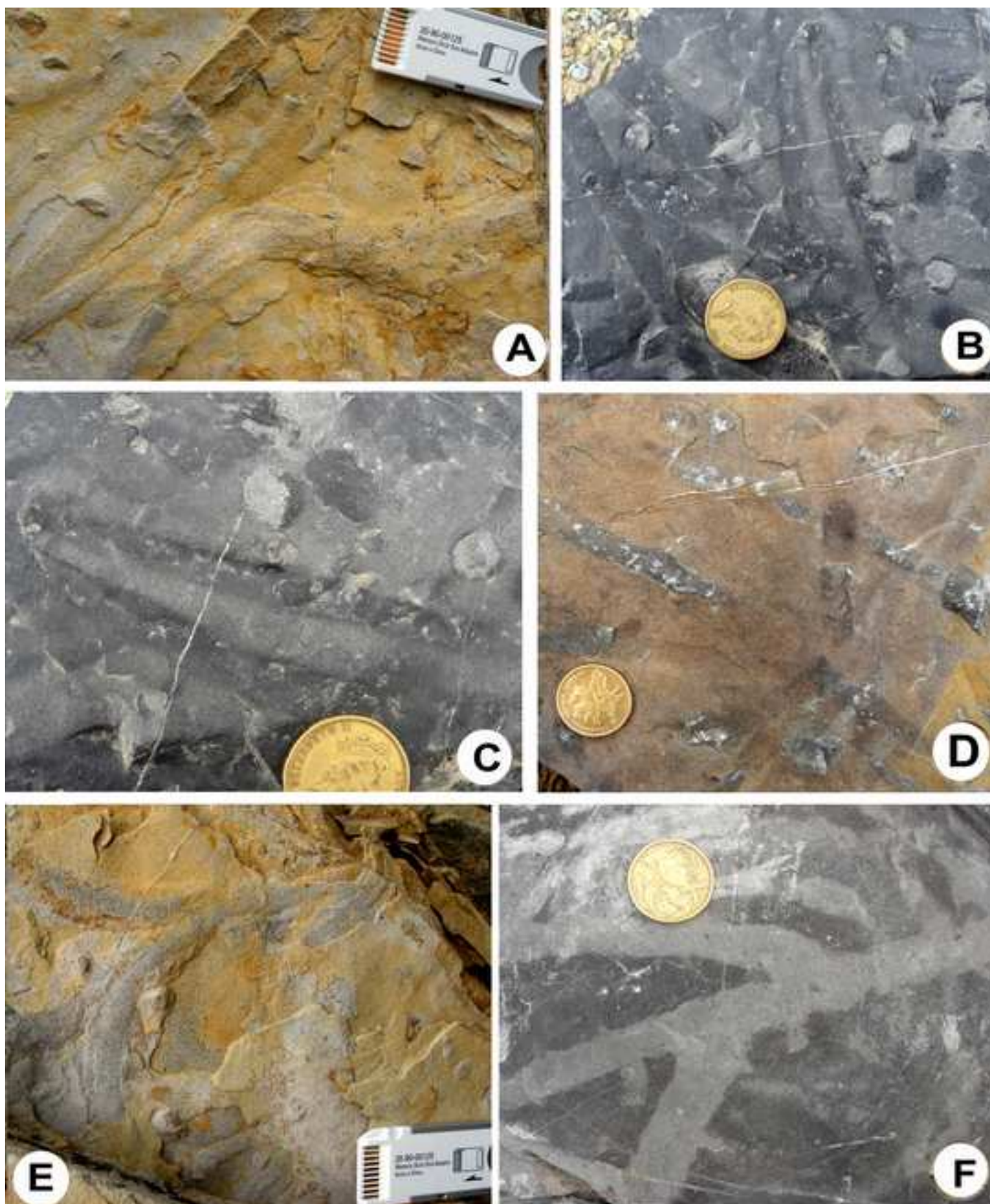


Figure 18
[Click here to download high resolution image](#)

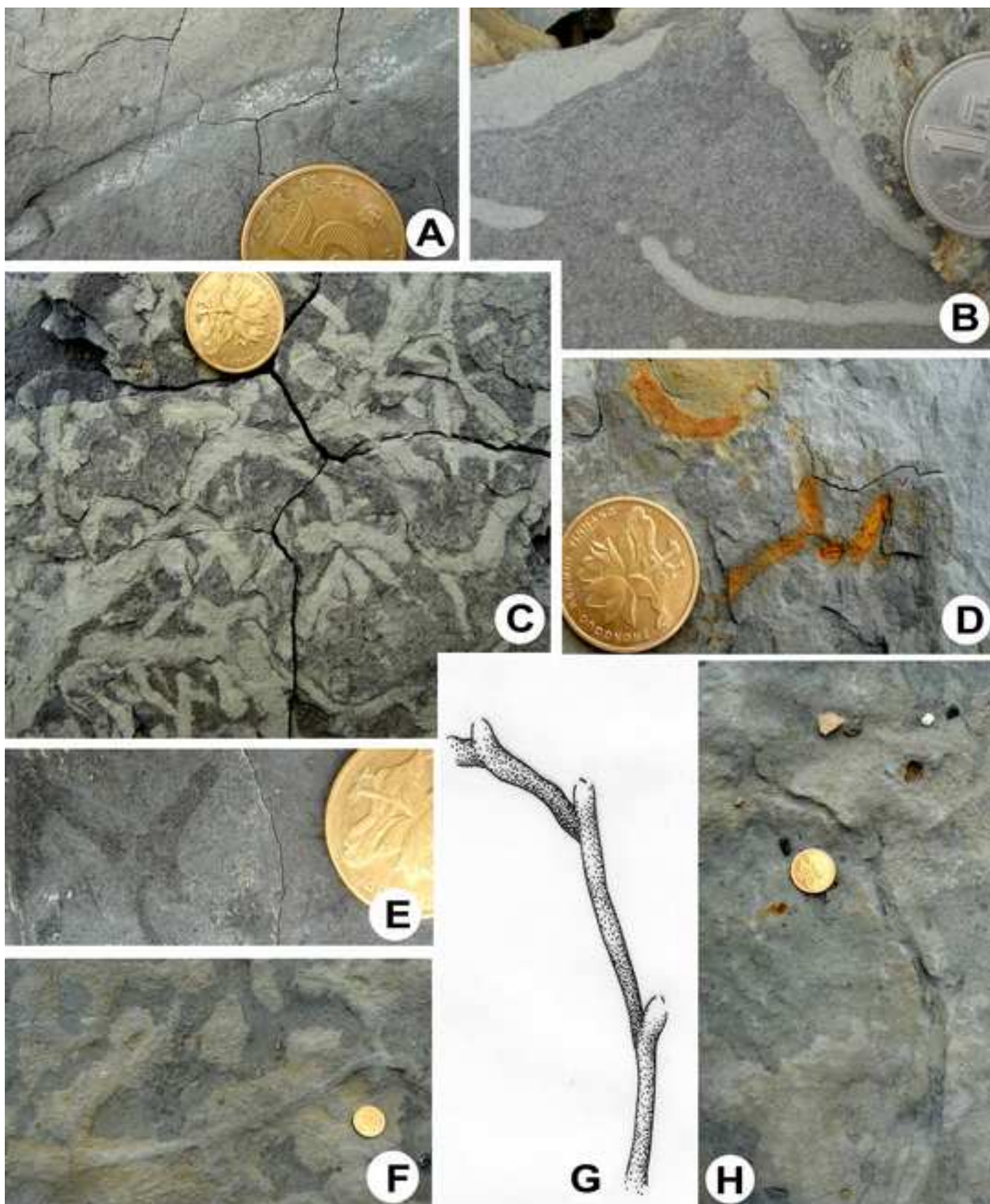


Figure 19
[Click here to download high resolution image](#)

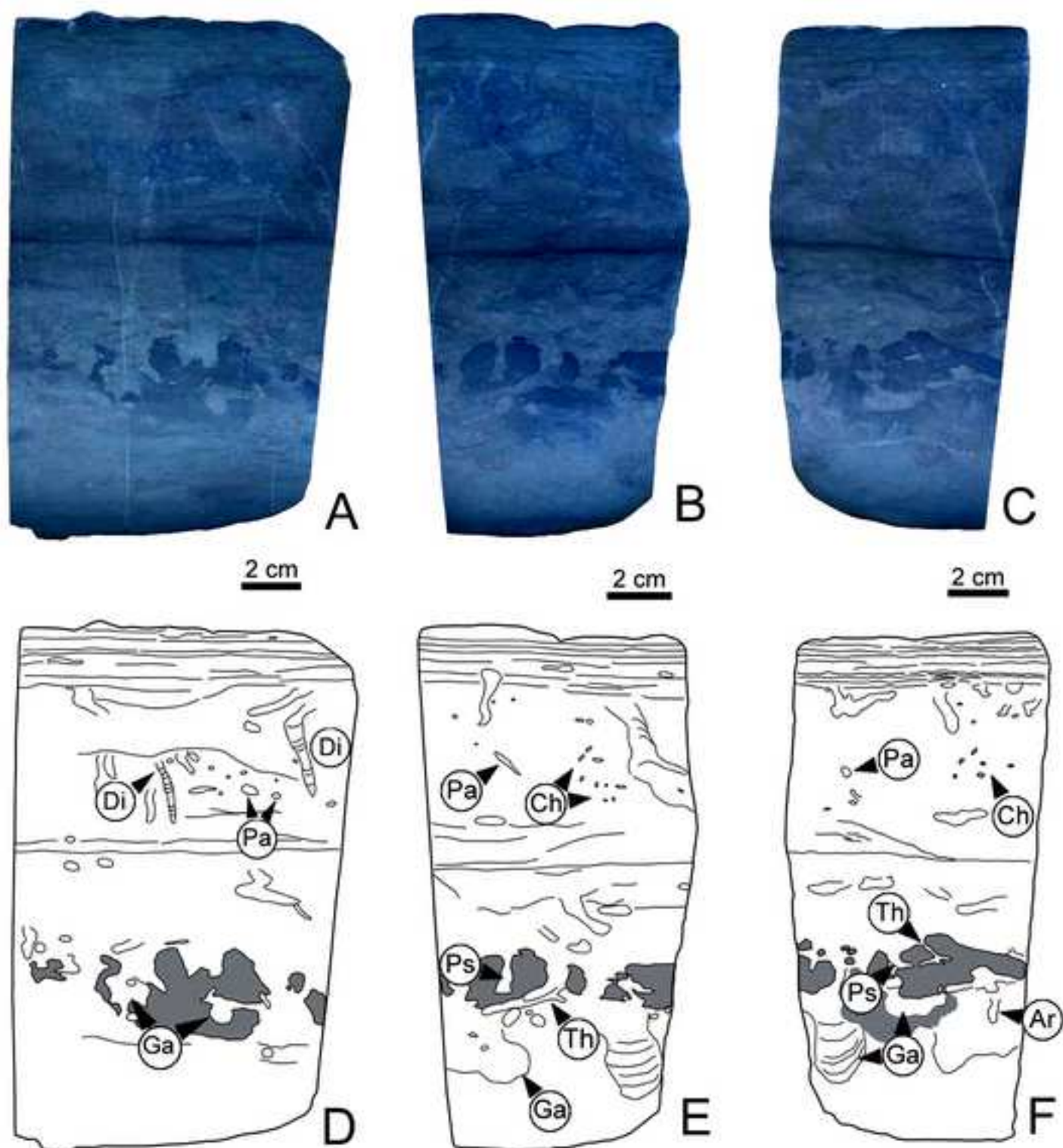


Figure 20
[Click here to download high resolution image](#)

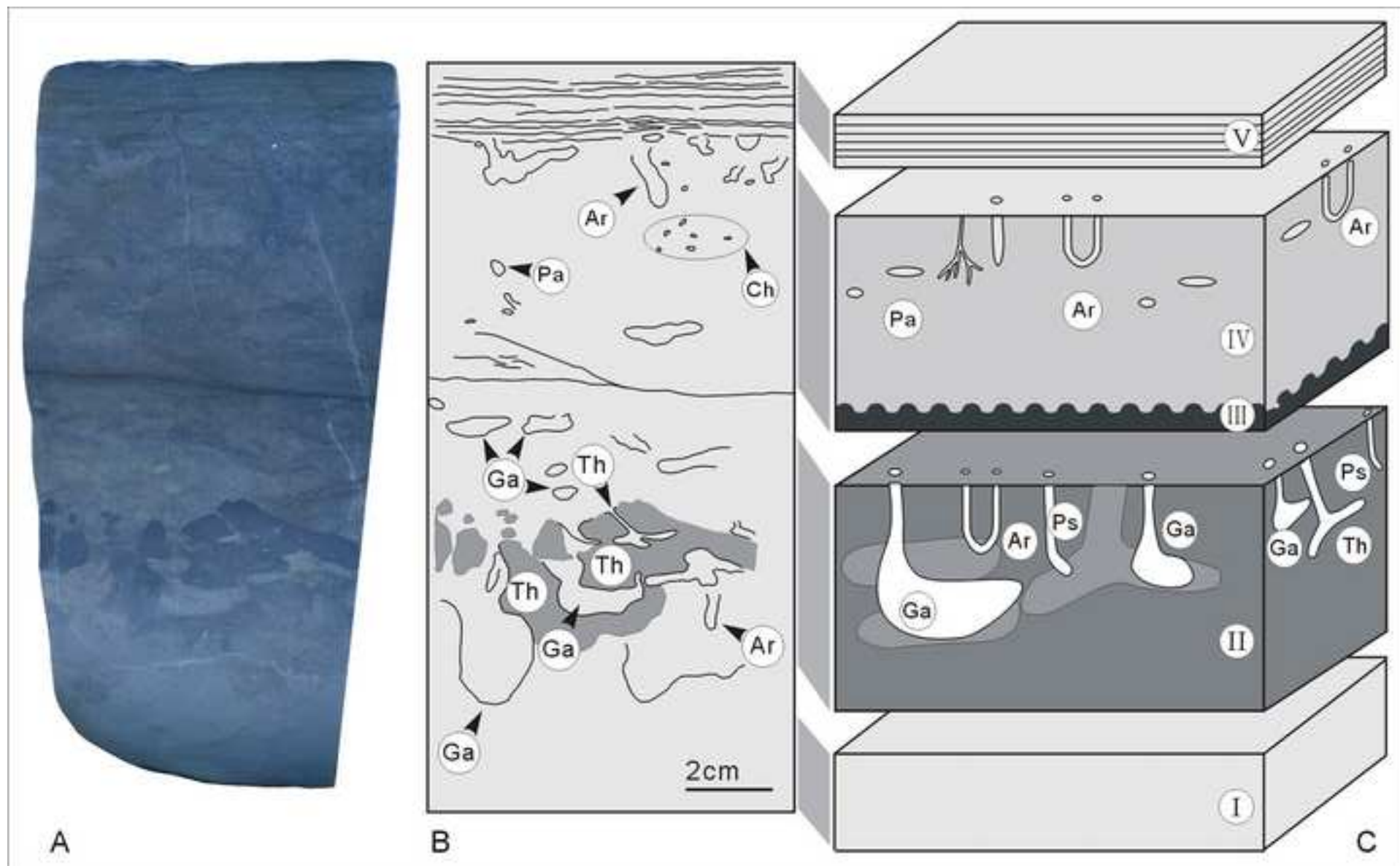


Figure 21
[Click here to download high resolution image](#)

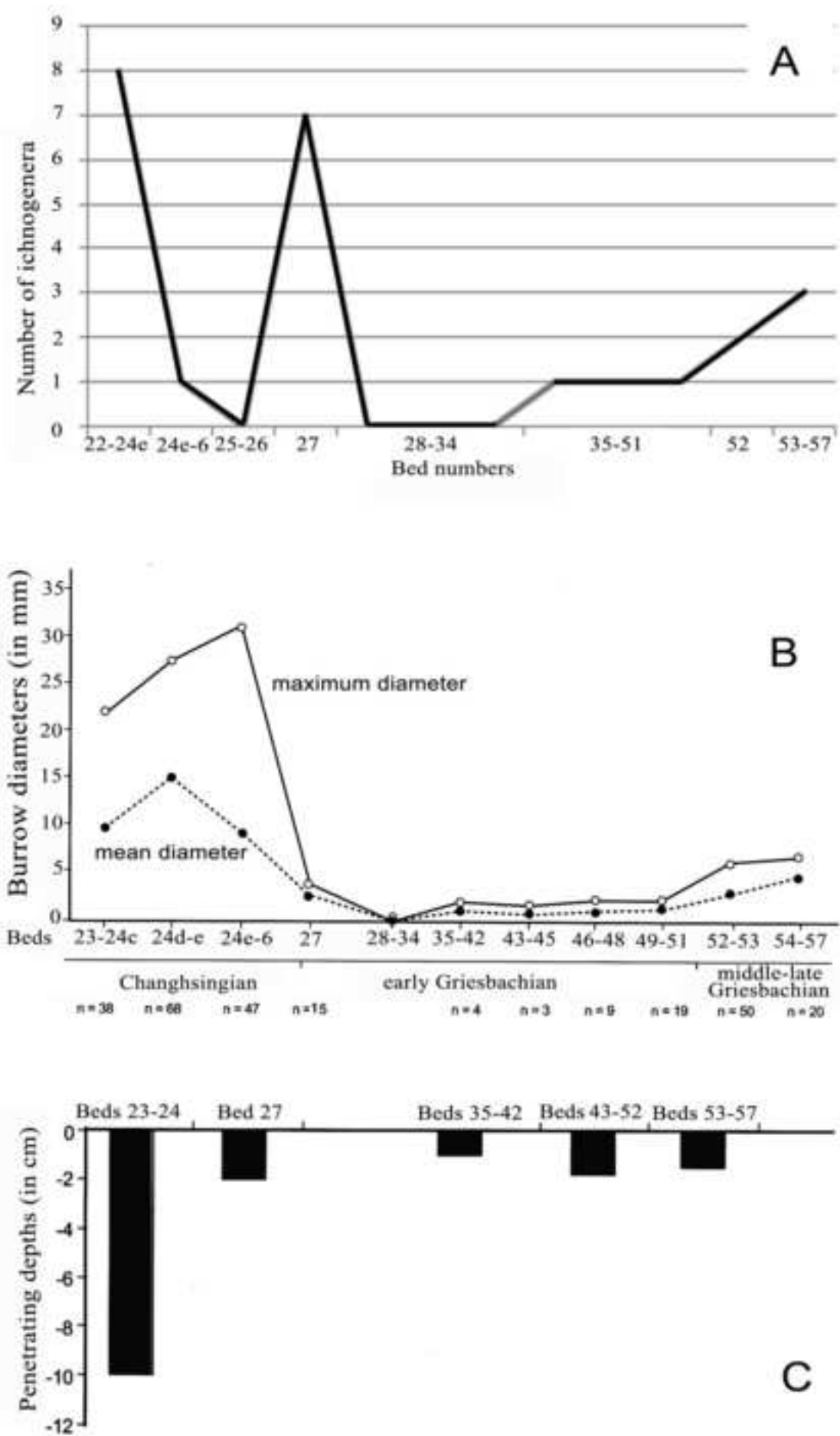


Figure 22
[Click here to download high resolution image](#)

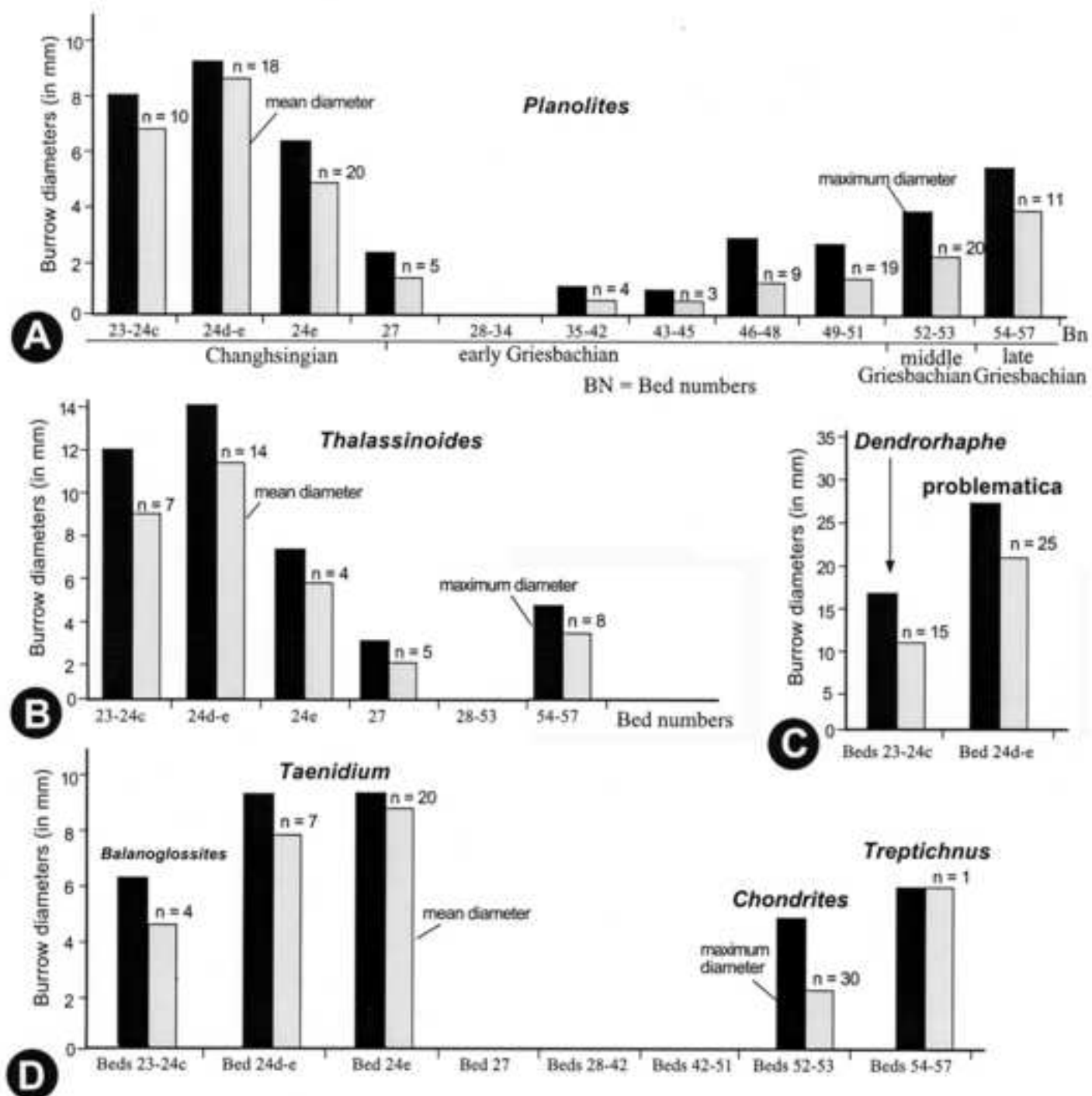


Figure 23
[Click here to download high resolution image](#)

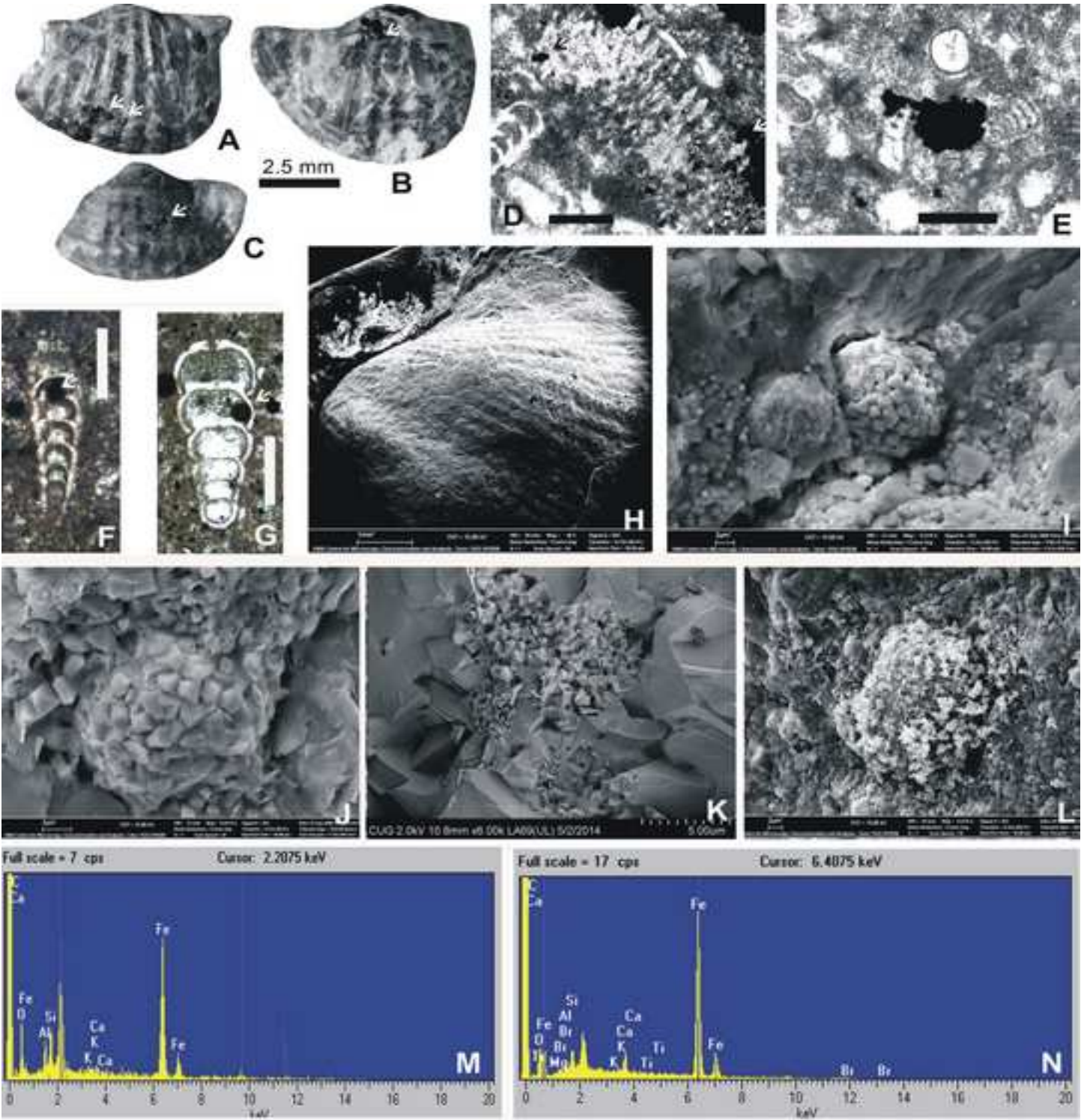


Figure 24
[Click here to download high resolution image](#)

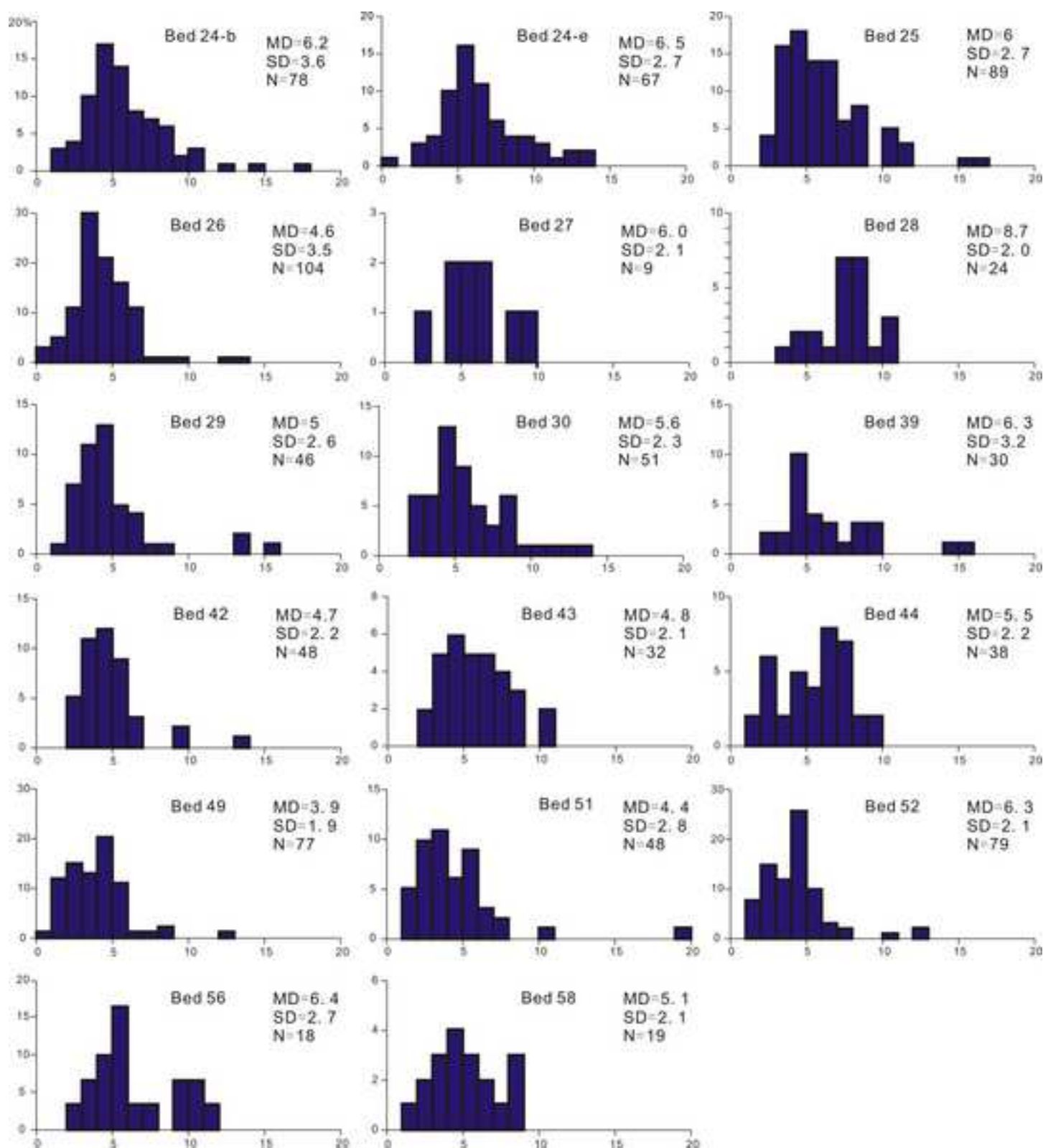


Figure 25
Click here to download high resolution image

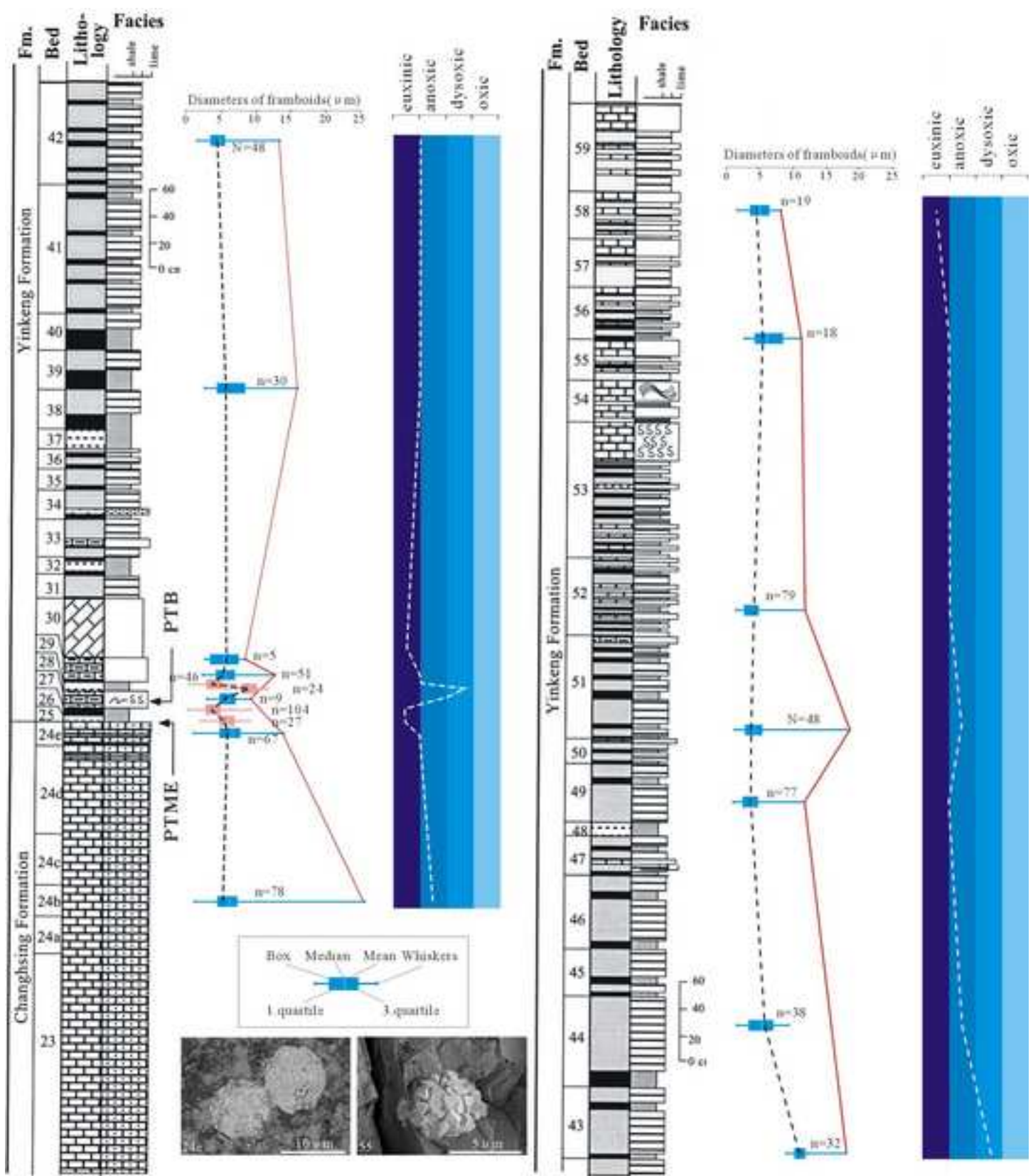


Figure 26
[Click here to download high resolution image](#)

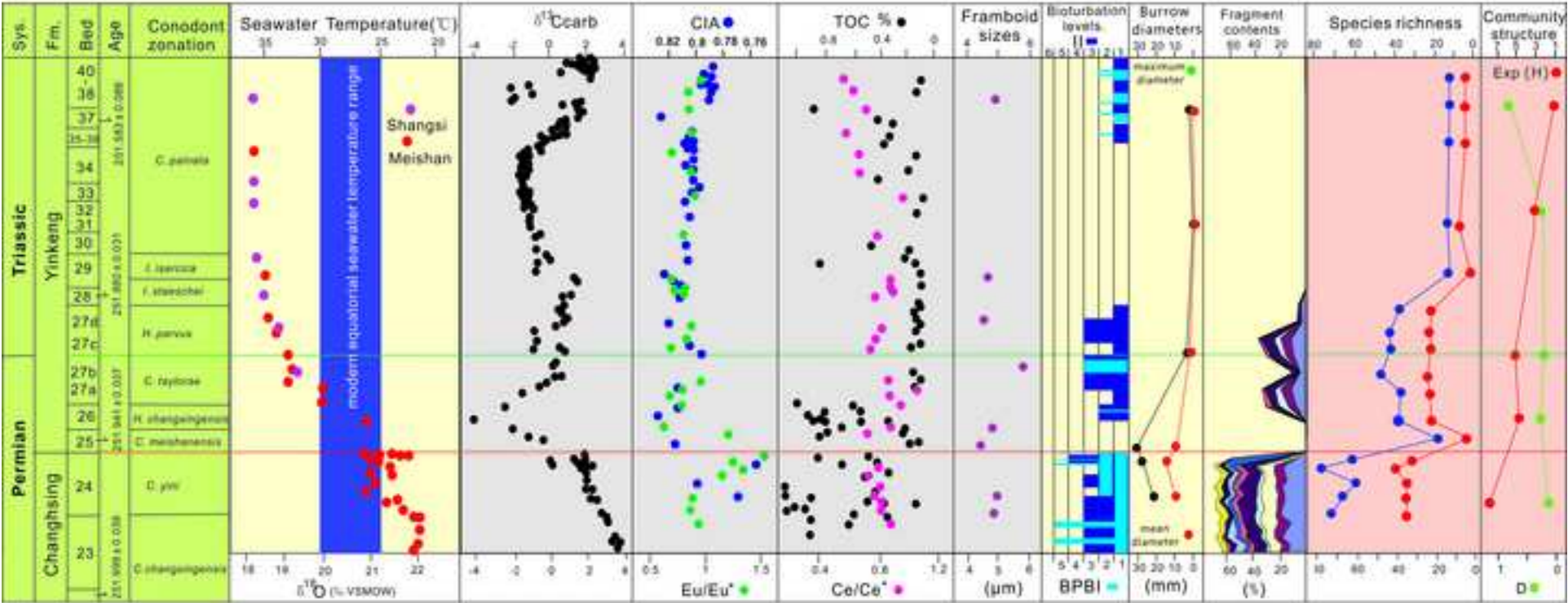


Table 1. Radiometric ages obtained from the P-Tr succession in GSSP Meishan (in Ma)

	Bed 7	Bed 22	Bed 25	Bed 28	Bed 37	Bed 48
Claoue-Long et al., 1991			251.2 ± 3.4 (SHRIMP)			
Renne et al., 1995			249.91 ± 0.15*			
Bowring et al., 1998	253.4 ± 0.2	252.3 ± 0.2	251.4 ± 0.3	250.7 ± 0.3	250.4 ± 0.5	250.2 ± 0.2
Mundil et al., 2001, 2004			252.41 ± 0.41	252.48 ± 0.3		
Reichow et al., 2009				250.98 ± 0.14 *		
Renne et al., 2010			251.63 ± 0.2*			
Shen et al., 2011	253.45 ± 0.08	252.50 ± 0.11	252.28 ± 0.08	252.10 ± 0.06		
Burgess et al., 2014		252.104 ± 0.06	251.941 ± 0.037	251.880 ± 0.031	251.583 ± 0.086	251.495 ± 0.064

* ⁴⁰Ar/³⁹Ar age; others are ²⁰⁶Pb/²³⁸U ages. Note: Beds 33 and 34 of Bowring et al. (1998), Shen et al. (2011) and Burgess et al. (2014) are equivalent to Beds 37 and 48 of this study, respectively.

Table 2. Key conodont zones with their durations across the PTB in Meishan

Conodont zones	Stratigraphic ranges	Starting dates	Duration
<i>I. isarcica</i> Zone	Bed 29b	251.845 Ma	27 ka
<i>I. staeschei</i> Zone	Beds 28-29a	251.880 Ma	35 ka
<i>H. parvus</i> Zone	Bed 27c-d	251.896 Ma	16 ka
<i>C. taylorae</i> Zone	Bed 27a-b	251.912 Ma	16 ka
<i>H. changxingensis</i> Z.	Bed 26	251.933 Ma	21 ka
<i>C. meishanensis</i> Z.	Bed 25	251.941 Ma	8 ka
<i>C. yini</i> Zone	Bed 24	251.969 Ma	28 ka
<i>C. changxingensis</i> Z.	Beds 22-23	252.104 Ma	135 ka

Table 3. Percentage of major components of rocks sampled from Beds 22-60 in Meishan

Beds	Elev.* (cm)	Foram (%)	Ostra. (%)	Crin. (%)	Echin. (%)	Brach. (%)	Bryo. (%)	Spon. (%)	Cal. sp. (%)	Gastr. (%)	Radio. (%)	Algae (%)	Micrites (%)	Cavity (%)	Particles (%)
60	1357~1363	8	8	0	0	0	0	0	0	0	0	0	72	3	9
59	1250~1255	11	5	0	0	0	0	0	0	0	0	0	74	5	5
56	1160~1165	10	3	0	3	0	0	0	0	0	0	0	80	0	4
54	1055~1060	7	5	0	0	0	0	0	0	0	0	0	80	0	8
53	1005~1010	8	7	0	3	0	0	0	0	0	0	0	78	0	4
52	950~955	8	5	0	3	0	0	0	0	0	0	0	77	0	7
51	900~910	5	2	0	0	0	0	0	0	0	0	0	88	0	5
50	850~855	4	3	0	0	0	0	0	0	0	0	0	88	0	5
49	800~810	0	0	0	0	0	0	0	0	0	0	0	90	0	10
46	750~755	0	0	0	0	0	0	0	0	0	0	0	90	0	10
45	700~705	5	0	0	0	0	0	0	0	0	0	0	90	0	5
44b	650~655	0	0	0	0	0	0	0	0	0	0	0	95	0	5
44a	600~605	0	0	0	0	0	0	0	0	0	0	0	95	0	5
43	550~556	0	0	0	0	0	0	0	0	0	0	0	95	0	5
42	500~505	0	0	0	0	0	0	0	0	0	0	0	90	0	10
41b	450~455	0	0	0	0	0	0	0	0	0	0	0	92	0	8
41a	400~405	0	0	0	0	0	0	0	0	0	0	0	92	0	8
40	350~355	0	0	0	0	0	0	0	0	0	0	0	90	0	10
39	300~305	0	0	0	0	0	0	0	0	0	0	0	95	0	5
38	250~255	0	0	0	0	0	0	0	0	0	0	0	90	0	10
35	200~205	0	0	0	0	0	0	0	0	0	0	0	92	0	8
33	160~165	0	0	0	0	0	0	0	0	0	0	0	95	0	5
31	100~110	0	0	0	0	0	0	0	0	0	0	0	90	0	10
30	60~63	0	0	0	0	0	0	0	0	0	0	0	92	0	8
29b	36~39.5	4	0	0	0	2	0	0	0	0	0	0	88	0	6
29a	30~33.5	3	2	0	0	2	0	0	0	0	0	0	88	0	5
27d	23~28	12	8	0	6	10	2	0	0	0	0	0	50	0	12
27c	21~23	10	6	0	4	8	3	0	0	0	0	0	55	0	14
27b	15~17	5	0	0	0	5	0	0	0	0	0	0	80	0	10
27a	13~15	12	8	0	5	8	2	0	0	0	0	0	55	0	10
26b	8~10	8	6	0	8	5	5	0	0	0	0	0	60	0	8
26a	4~6	0	0	0	0	0	0	0	0	0	0	0	0	0	0
25	0.3~2	0	0	0	0	0	0	0	0	0	0	0	0	0	0
24e6	-1~0	8	0	6	4	7	0	35	0	0	0	0	35	0	5
24e5	-2~-1	18	8	12	3	12	5	5	3	4	0	4	20	2	4
24e4	-3~-2	18	8	8	2	10	5	3	4	4	0	6	24	3	5
24e3	-6~-3	16	8	10	4	12	5	3	5	3	0	3	24	2	5
24e2	-9~-6	20	5	12	3	15	5	0	3	5	0	6	20	2	4

24e1	-11~-9	18	5	14	3	10	4	3	4	5	0	4	24	2	4
24d3	-14~-11	18	6	12	5	15	4	3	4	3	0	3	20	2	5
24d2	-20~-15	20	4	10	6	14	5	3	0	3	0	8	18	4	5
24d1	-45~-50	21	4	12	5	10	3	4	0	3	0	6	24	3	5
24c	-60~-55	13	10	14	4	10	3	4	3	3	2	5	22	2	5
24a	-90~-80	17	9	7	3	12	5	3	7	2	0	4	25	2	4
23b	-150~-145	20	6	8	3	12	4	4	7	2	2	5	21	3	3
23a	-205~-200	14	6	10	2	10	3	3	8	5	3	5	23	3	5
22	-255~-250	15	7	8	3	10	5	3	8	2	2	5	22	2	8

*Elev. = Elevation, referring to accumulative distance (in cm) of sampling horizon to the base of Bed 25; minus value indicates sampling horizon below Bed 25.

Component codes: Foram. = foraminifers, Ostra. = ostracods, Crin. = crinoids, Echin. = echinoids, Brach. = brachiopods, Bryo. = bryozoans, Spon. = sponge spicules, Cal. sp. = calcareous sponges, Gastr. = gastropods, Radio. = radiolarians, Algae = macroalgae, Particles = other particles (fecal pellets, peloids, pyrites and undetermined particles).

Table 4.

Beds	Samples	BT. mm	Composition and percentage	Colour	lithology
Bed 29	MD 29	260	calcite 6%, ankerite 62%, silica 15%, illite 5%, kaolinite 2%	grey	marlstone
Bed 28	MD 28	40	calcite 4%, silica 50%, illite 16%, kailinite 22%, orthoclase 5%	white	claystone
Bed 27c-d	MD 27cd	80	calcite 33%, ankerite 38%, silica 23%, illite 4%, kaolinite 2%	grey	marlstone
Bed 27a-b	MD 27ab	80	calcite 30%, ankerite 38%, silica 26%, illite 4%, kaolinite 2%	grey	marlstone
Bed 26	MD 26	60	gypsum 21%, calcite 8%, silica 36%, illite 18%, kaolinite 17%	black	shale
Beds 25-2, 25-3	MD 25	40	gypsum 34%, chlorite 9%, montm 28%, illite 10%, kaolinite 19%	white	claystone
Bed 25-1	MD 25mr	0.3	gypsum 63%, goethite 25%, chlorite 12%	red	
Bed 24e-3	MD 25 my	0.3	gypsum 76%, chlorite 6%, silica 18%	yellow	
Bed 24e-3	MD 25mb	0.3	gypsum 35%, calcite 11%, chlorite 4%, silica 50%	brown	
Beds 24e-2, 24e-1	MD 24e	200	calcite 97%, illite 0.5%, kaolinite 0.5%, silica 2%	black	packstone
Bed 24d	MD 24d	230	calcite 98%, silica 2%	black	packstone

BT. = Bed thickness

Table 5. Structural indices of the latest Permian to earliest Triassic shelly communities from Meishan (Chen et al., 2010a).

CC	Beds	Age	SR	N	H	Exp(H)	D	D'	Δ	E
<i>R-P</i>	24	Changhsingian	9	42	2.029	7.60648	0.1519	1.1791	0.15561	0.8453
<i>T</i>	26	Changhsingian	8	36	1.47	4.34942	0.3673	1.5805	0.37779	0.5439
<i>P-T</i>	27	Griesbachian	7	67	1.565	4.78267	0.2658	1.3620	0.26983	0.6836
<i>C-O</i>	32	Griesbachian	3	125	0.7559	2.12953	0.5233	2.0978	0.52752	0.7098
<i>C</i>	40	Griesbachian	1	129	0	1	1	?	1.00781	1
<i>M-L</i>	53-55	Griesbachian	8	143	1.288	3.62553	0.4379	1.7790	0.44098	0.4531

CC: Community codes; SR: species richness; N: individual number; H: Shannon entropy; Exp (H): standard diversity Shannon index; D: Dominance entropy; D': standard diversity dominance index [$1/(1-D)$]; Δ: bias-corrected Simpson's evenness [$N \times D / (N-1)$]; E: evenness index ($e^{H/S}$).

Table 6. Major indices showing community structural changes over the P-Tr transition in Meishan

Community boundary	Diversity [Exp (H)] changes	D' changes
<i>R-P/T</i>	-43.6%	+34.0%
<i>T/P-T</i>	+10%	-14.1%
<i>P-T/C-O</i>	-55.5%	+54%
<i>C-O/C</i>	-53%	?
<i>C/M-L</i>	+262.6%	?
<i>C-O/M-L</i>	+70%	-15.2%

Exp (H): standard diversity Shannon index; D': standard diversity dominance index [1/(1-D)]; - indicates decrease, while + represents increase

Table 7. Characteristics of major trace fossils from the uppermost Permian to lowest Triassic in Meishan

Ichnotaxa	Beds	Illustr.	Description	Interpretation
<i>Arenicolites</i> isp.	27	Figs. 24-25	U-shaped burrows with unbranched, parallel limbs, 0.5 to 3.0 mm in diameter, perpendicular to bedding plane, and lacking spreite; filled with light-grey, coarse sediments that are distinguished from surrounding dark, fine-grained sediments.	Domichnia with trace-makers of polychaete worms, amphipod and crustaceans (Knaust, 2004; Chen et al., 2011, 2012)
<i>Balanoglossites triadicus</i>	24d	Fig. 20C	Vertical tubes, 14-18 mm wide and 10 cm long, perpendicular to bedding, penetrating to a depth of 5-10 cm; filled with light-coloured sediments distinguished from the surrounding dark sediments.	Produced by polychaete-like or enteropneust worms (Hantzschel, 1975).
<i>Chondrites</i> isp. 1	52	Fig. 25C	Plantlike dendritic system composed of fine, branching, cylindrical ramifying burrows, parallel to bedding plane in compact groups, and filled with yellow, coarsely grained sediments distinct from surrounding dark, fine-grained sediments.	Fodinichnia, feeding structures of sediment-eating animals (Bromley and Ekdale, 1984; Chen et al., 2011).
<i>Chondrites</i> isp. 2	27	Fig. 24-25	Small branching, cylindrical burrows forming plantlike dendritic systems, penetrating into sediments, and filled with light, coarsely grained sediments and distinguished from surrounding dark, fine-grained sediments	Same as above
<i>Dendrorhaphé</i> isp.	23	Fig. 21G	Tree-like trace system comprises a rather straight main axis, along which side branches are mostly perpendicular to the main axis and given off on both sides. Minor branches also give birth to further secondary branches in same way.	Occurring in deep-water or oxygen-deficient niches; feeding structures of sediment-eating animals (Seilacher, 1977)
<i>Diplocraterion</i> isp.	27	Fig. 24	U-shaped burrows with unbranched, parallel limbs, perpendicular to bedding plane, and having spreite; filled with light-grey, coarse sediments that are distinguished from surrounding dark, fine-grained sediments.	Produced by polychaete worms, amphipod and crustaceans (Knaust, 2004)
<i>Gastrochaenolites</i> isp.	27	Figs. 24-25	Irregular, tear-shaped borings filled by light grey sediments in a dark-colored firmground lime mudstone substrate, penetrating down to the firmground layer at a maximum depth of 4 cm.	Produced by various organisms i.e., bivalves, annelids and sipunculans (Benner and Ekdale, 2004)
<i>Lockeia</i> isp.	8-9	Figs. 20F, 21B	Small, almond-shaped oblong structure, 8-18 mm long and 7-12 mm wide, tapering to sharp points at both ends; preserved in either concave impressions on the tops or convex relief on the soles.	Resting impressions of bivalves (Bromley, 1996; Ekdale and Bromley, 2001)
<i>Paleophycus</i> isp.	8-9	Fig. 20B	Branching, slightly curved, cylindrical burrows, 2–7 mm in diameter, with wall typically lined and preserved as positive reliefs on top of bed.	Rrepichnion or domichnion, produced by predaceous or suspension-feeding animals (Gouramis et al., 2003).

<i>Psilonichnus</i> isp.	27	Figs. 24-25	Vertical cylindrical burrows that are inclined with bedding in its distal end.	Trace of ocypodid ghost crabs (Buatois and Mángano, 2011).
<i>Planolites</i> isp. 1	24e	Fig. 23A-F	Simple, unbranched, unornamented, vermiform burrows that are straight and horizontally distributed on bedding tops, with some intersecting the sediment irregularly. Burrows, 3-9 mm in diameters, are occasionally densely packed.	Deposit-feeding activities of polychaetes or worm-like creatures, or feeding burrow of deposit-feeders (Bromley, 1996).
<i>Planolites</i> isp. 2	34-53, 55-56	Fig. 25A-B, F	Simple, unbranched, vermiform burrows that, 1-4 mm in diameter, are straight or curving and horizontally distributed on bedding surfaces.	Same as above
Problematic trace	23	Fig. 21A, C-D	Simple, straight, unbranched burrows, 20-27 mm in diameter, with 2-5 mm thick tube wall. Single burrow originates at a small, rounded end and extends distally to form a horn-shaped burrow with an open distal end.	Sharing the same trace-makers with <i>Planolites</i> .
<i>Taenidium</i> isp.	24d-e	Figs. 20E, 21E	Cylindrical, straight, unbranching burrows with backfilling structures; Some tubes are horizontal on tops of beds, and others are slightly oblique to bedding planes. Tube diameters are 6-9.5 mm.	Feeding behaviours of worm-like animals (Keighley and Pickerill, 1994).
<i>Thalassinoides</i> isp. 1	23-24 c	Fig. 20A, D	Large Y-shaped, branching, smooth, rounded burrows, 10-14 mm in diameter (Fig. 22), penetrating a depth of < 1 cm into sediment and forming incomplete intricate networks.	Behaviour of cerianthid sea anemones, worms and decapod crustaceans (Myrow, 1995; Bromley, 1996; Ekdale and Bromley, 2003).
<i>Thalassinoides</i> isp. 2	27	Figs. 24-25	Small Y-shaped, branching burrows, 1-2 mm in diameter, penetrating a depth of < 1 cm into sediment, filled with light coarsely grained sediments distinct from surrounding dark, fine-grained sediments.	Same as above
<i>Thalassinoides</i> isp. 3	53-56	Fig. 25D-E	Medium-sized Y-shaped, branching burrows, 3-4.5 mm in diameter, mostly horizontal on tops of beds and filled with dark, organic sediments.	Same as above
<i>Treptichnus</i> isp.	56-57	Fig. 25G-H	Meandering burrow system with one main burrow, 6 mm in width, terminates its growth after bifurcating to give a minor branch on its outer side. The minor branch ceases its growth soon after giving birth to further secondary branch.	Deposit-feeding of worm-like organism in a zigzag or other segmented pattern with older segments abandoned after use (Rindsberg and Kopaska-Merkel, 2005; Seilacher, 2007).

Illustr. = Illustration